Reconstructions of Aquatic Primary Producer Dynamics, Cyanobacteria Dominance and Cyanotoxin Concentrations in Subtropical Lake Ecosystems Throughout the Holocene and Late Pleistocene

by

Savvas Paradeisis-Stathis

A dissertation submitted to the Graduate Faculty of
Auburn University
in partial fulfillment of the
requirements for the Degree of
Doctor of Philosophy

Auburn, Alabama
August 9, 2025

Keywords: Paleolimnology, Paleoecological reconstructions, Nutrients, Photosynthetic pigments, Cyanobacteria, Microcystins, Subtropical lakes

Approved by

Matthew Waters, Chair, Associate Professor, Department of Crop, Soil and Environmental Sciences,
David Blersch, Associate Professor, Department of Biosystems Engineering
Thomas Cullen, Assistant Professor, Department of Geosciences
Richard Vachula, Assistant Professor, Department of Geosciences

Abstract

Harmful algal blooms (HABs) are intensifying globally, threatening freshwater ecosystems and public health. Although modern HABs have been extensively studied in the context of anthropogenic nutrient enrichment, the long-term ecological dynamics driving cyanobacteria dominance and cyanotoxin production remain underexplored. Lake sediments serve as natural archives of past environmental change, yet paleolimnological approaches have rarely been applied over millennial timescales in subtropical lake systems. This dissertation reconstructs the dynamics of primary producers, cyanobacteria dominance, and cyanotoxin concentrations throughout the Holocene and Late Pleistocene in four shallow lakes in the southeastern United States. By utilizing sedimentary photosynthetic pigments and cyanotoxins (total microcystins, MCs), it investigates the ecological patterns underlying long-term eutrophication and HAB development. Chapter 1 introduces the background and rationale for this research. Chapter 2 examines a ~6,900-year sediment record from Lake Wauberg, Florida, where natural phosphate geology led to millennial-scale enrichment of total phosphorus (TP) that sustained cyanobacteria. However, sharp increases in cyanobacteria and MCs only occurred once TP exceeded ~2.2 mg g^{-1} in the past ~300 years. Chapter 3 investigates the deposition of MCs in two hypereutrophic Florida lakes, Dora and Marian, with sediment records spanning approximately 7,000 years. The results indicate that MC deposition has occurred throughout the history of these lakes, with its concentration varying over time and being primarily driven by nutrient levels, particularly TP, and primary producer composition, rather than climate. Chapter 4 analyzes a ~27,500-year record from Lake Waccamaw, North Carolina, demonstrating persistent cyanobacteria dominance and MC production under natural climate variability during both glacial and interglacial periods. Abrupt shifts in aquatic and terrestrial ecosystems during Interstadial 3 (~27.8-26.4 ka BP) and the early Holocene (~11.4-7 ka BP) underscore the roles of hydroclimatic forcing and nutrient stoichiometry in shaping the dynamics of aquatic primary producers. Together, these studies demonstrate the value of millennial-scale paleolimnological records in identifying ecological thresholds, understanding the natural baseline conditions of HABs, and contextualizing modern changes in lake systems.

Acknowledgments

I want to thank my mom, Sapfo Stathi, and my dad, Nikolaos Paradeisis, for their support of my decision to attend Auburn, as well as their love and patience. My dad didn't come to see the end of this, but I know he would be proud. I'm also grateful to the friends who shared joyful moments with me during study breaks, and to the many students I had the chance to meet and work with during my PhD. Your insights enriched my research and made student life more enjoyable. Alongside my lab mates, many of you became my Auburn family. Tayler Schillerberg, Michail Katsigiannis, Minas Pantelidakis, Anet Filipova, Waad Torman, Alexandros Androutsopoulos, Aimee Jameson, Nikolia Darzenta, Dimitrios Sakkas, Vasiliki Syropoulou, and Aliki Kalpourtzidou, thank you for the support, laughter, and memories!

I want to thank all the outstanding graduate students I had the pleasure of working with at the Auburn Paleoenvironmental Lab, Troy Clift, Chloe Eggert, Jessie Curl, Savanna Wooten, and Dr. Benjamin Webster, as well as our exceptional lab technician, Kaye Bowling. You are all brilliant scientists and wonderful people with a bright future ahead. You helped me transition to life in the US, and I am grateful for the unforgettable moments we shared. It was a privilege to have you actively involved in fieldwork for this project and as dedicated collaborators in the lab.

It has been a great honor to meet and collaborate with several outstanding scientists through our lab partnerships. Dr. Mark Brenner and Dr. Jason Curtis from the University of Florida, you are a stellar coring duo, and it was truly inspiring to learn from you in the field. Dr. Debra Willard and the Palynology Laboratory at the Florence Bascom Geoscience Center of the US Geological Survey, thank you for being exceptional collaborators and producing such valuable pollen data. Dr. Richard Vachula from the Department of Geosciences at Auburn University, I greatly appreciated your valuable contribution with charcoal data, as well as your insights and support throughout this work.

Finally, my deepest gratitude goes to my PhD advisor, Dr. Matthew Waters. Dr. Waters brought me to the US to assist with research on paleo-HABs, and from day one, he has been not only the best mentor I could have hoped for but also a kind and generous scientist. You always made time for my questions, were an endless source of inspiration, and offered support at every stage of this journey. I hope to carry forward the same kindness, dedication to science, and ability to inspire others.

Table of Contents

List of Tables

List of Figures

List of Abbreviations

AMS	Accelerator Mass Spectrometry
ANOVA	Analysis of Variance
B-A	Bølling–Allerød
BP	Before Present
CE	Common Era
CHAR	Charcoal Accumulation Rate
CONISS	Constrained Incremental Sum of Squares Analysis
CRS	Constant Rate of Supply
DI	Deionized
ELISA	Enzyme-Linked Immunosorbent Assay
HAB	Harmful Algal Bloom
HPLC	High-Performance Liquid Chromatography
ICP	Inductively Coupled Plasma
ka	Thousand Years
LDO	Lake Dora
LGM	Last Glacial Maximum
LMA	Lake Marian
LOI	Loss On Ignition
LOWESS	Locally Weighted Scatterplot Smoothing
MC	Microcystin
OD	Older Dryas
PCA	Principal Component Analysis
rbacon	Bayesian Accumulation in R
TN	Total Nitrogen
TOC	Total Organic Carbon
TP	Total Phosphorus
YD	Younger Dryas

Chapter 1: Harmful Algal Bloom Research and Importance of Paleolimnological Reconstructions of Aquatic Environments in Southeastern USA

1.1. Introduction

Harmful algal blooms (HABs) are among the most urgent water quality issues impacting lake ecosystems worldwide. Cyanobacteria are prokaryotes that obtain energy through photosynthesis, rapidly metabolize nutrients from various sources, and play a crucial role in nutrient cycling (Díez and Ininbergs, 2014; Nienaber and Steinitz-Kannan, 2018). Additionally, cyanobacteria have played a vital role in the evolution of life through the Great Oxygenation Event by releasing oxygen as a byproduct through photosynthesis (Grettenberger et al., 2025). However, the overgrowth or bloom of cyanobacteria (HABs) and the production of cyanotoxins over the past century threaten ecosystem services, the economic value of aquatic systems, and the health of both animals and humans (Kaloudis et al., 2022; Paerl and Otten, 2013). The recent increase in HAB frequency in fresh waters is typically associated with cultural eutrophication (Taranu et al., 2015), defined as excessive nutrient loading resulting from human-associated inputs of nutrients, land-use changes, and hydrological modifications (Schindler et al., 2016; Smith, 2003). Consequently, monitoring efforts have significantly increased over the past few decades to identify and alleviate anthropogenic pressures on lakes. To eradicate these negative impacts, management goals and water quality standards can be developed and implemented, but success is often dependent on an understanding of nutrient baselines that predate human impacts and monitoring records (Brenner et al., 1993; Brooks et al., 2016; Smol, 1992). One successful tool in understanding historic lake trophic conditions is to utilize historical data preserved in lake sediment records. The recent development of paleolimnological tools such as photosynthetic pigment analysis and cyanotoxin measurements can provide direct measurements of increased cyanobacteria assemblages and toxin production over time (Riedinger-Whitmore et al., 2005; Waters et al., 2012; Earley et al., 2017). Therefore, to understand the long-term dynamics underlying HABs, it is crucial to complement modern observations with historical ecological conditions (Battarbee et al., 2005).

Lake ecosystems are highly sensitive to both natural and anthropogenic disturbances, and lake sediments serve as archives of physical processes, biological activity, and long-term environmental changes (Saulnier-Talbot, 2016). Paleolimnological studies focus on analyzing

aquatic sediment records to reconstruct the historical evolution of freshwater systems as well as the surrounding terrestrial environment (Smol, 1992; Brenner et al., 1993; Battarbee et al., 2005). Thus, lakes can preserve historical data, and by employing appropriate paleolimnological techniques and proxies, past environmental conditions can be inferred (Davidson and Jeppesen, 2013). With proxies such as photosynthetic pigments and sediment geochemistry, paleolimnology can identify the timing of ecological transitions and connect ecosystem thresholds with regime shifts (Saulnier-Talbot, 2016). The paleolimnological toolkit has significantly expanded in recent decades with the development of new techniques, including cyanotoxin extractions and ancient DNA analysis, alongside the ongoing application and refinement of established methods such as photosynthetic pigments and lipid biomarkers (Gregory-Eaves and Smol, 2024). These techniques have improved the reconstruction of aquatic environments by linking biotic responses, such as HABs and cyanotoxin production, to abiotic drivers, including anthropogenic nutrient enrichment and climate change. However, most studies focus on the last ~100 years, leaving greater temporal scales that are needed to understand ecosystem change prior to the onset of cultural impacts.

Modern limnology has struggled to determine the role of macronutrients, such as phosphorus (P) and nitrogen (N), and their stoichiometric balance (N/P) in driving HABs, with research often yielding conflicting results across ecosystems (Dolman et al., 2012; Paerl and Otten, 2013; Schindler et al., 2016). The role of secondary metabolites, such as cyanotoxins, in cyanobacteria ecology has also been explored, and multiple triggers have been proposed (Dolman et al., 2012; Kaplan et al., 2012). While research over the past decades has advanced our understanding of cyanobacteria and cyanotoxin ecology, establishing the primary and secondary drivers of eutrophication and cyanotoxin production over longer timescales has been problematic, leaving two pressing questions. First, the long-term roles of environmental factors, such as natural nutrient enrichment, water level fluctuations, hydroclimatic shifts, and land-cover changes, remain poorly understood in the establishment and maintenance of original eutrophic conditions. Second, although the impacts of cyanotoxins on other biota are well documented, the ecology of cyanotoxins and the triggers of cyanotoxin production under nutrient stoichiometry imbalances, primary producer community interactions, and other ecological stresses in natural environments remain unresolved.

This dissertation provides new insights into how environmental and ecological processes interact over long timescales (millennial) to influence cyanobacterial proliferation and cyanotoxin production. Thus, the three primary chapters of this dissertation will address: 1) long-term total phosphorus (TP) enrichment, 2) drivers of microcystin (MC) production, and 3) aquatic and terrestrial ecosystem responses to climate variability during the Late Quaternary. The included studies demonstrate that millennial-scale sediment records are essential for contextualizing modern ecosystem trajectories and deepening our understanding of ecological processes and the vulnerabilities of aquatic ecosystems. This research contributes to a growing body of literature illustrating the value of paleolimnology in understanding HAB ecology and guiding freshwater management under conditions of rapid global change.

1.2. Photosynthetic Pigments and Cyanotoxins as Proxies of Water Quality

The extraction of chlorophylls and carotenoids from lake sediments was first developed in the 1950s, with the earliest paleolimnological applications appearing in the late 1960s. The systematic use of sedimentary pigments to reconstruct past aquatic communities began in the 1980s and 1990s, when researchers confirmed the preservation potential of organic signals for hundreds to thousands of years after the disintegration of the most apparent morphological structures (Leavitt and Carpenter, 1990; Leavitt and Hodgson, 2001; Swain, 1985). Since 2015, pigment-based paleolimnological research has expanded rapidly, averaging over eleven publications per year (Fig. 1.1). Despite the early analytical limitations, sedimentary pigment analysis has become a widely accepted and powerful proxy for reconstructing historical aquatic community composition and the relative abundance of primary producers once specific pigments were identified as being better suited for preservation and ecological reconstruction (McGowan, 2013; Waters et al., 2005, 2021). In addition to photosynthetic pigments, recent advancements in cyanotoxin extraction techniques from sediments enable the quantification of cyanotoxin concentrations, providing further insights into past water quality (Waters, 2016; Zastepa et al., 2017; Waters et al., 2021). By applying paleolimnological techniques, including the analysis of photosynthetic pigments and cyanotoxin extraction, along with analyses of nutrients, charcoal, and pollen, to ^{210}Pb- and ^{14}C-dated sediment cores, this work addresses fundamental questions regarding the natural and anthropogenic drivers of eutrophication and HABs.

1.3. Aquatic Ecosystems in the Southeastern USA

The widespread hypereutrophic conditions across the southeastern USA present a compelling region for this research. For instance, Florida has a high abundance of shallow lakes with naturally nutrient-rich conditions, and when combined with warm temperatures, frequent hydrologic fluctuations, and extensive human landscape modifications, many lakes experience an almost year-round occurrence of HABs (Bachmann et al., 2012; Kosten et al., 2012). While rapid environmental changes and high lake densities in higher latitudes have received significant attention, the southeastern United States and the subtropics remain relatively unexplored. Despite their ecological importance and vulnerability, few millennial-scale sediment records are available from this region (Earley et al., 2017; Waters, 2016; Waters et al., 2005, 2012), creating a significant gap in our understanding of long-term lake dynamics under subtropical conditions.

1.4. Scientific Significance

Despite extensive research over the past few decades on the drivers of cyanobacteria dominance and the environmental conditions under which they release cyanotoxins, many uncertainties remain (Henao et al., 2020; Rastogi et al., 2014; Shingai et al., 2023; Waters, 2016; Waters et al., 2021; Zastepa et al., 2017). Most analyses have concentrated on short-term in vitro and in vivo experiments, which may not accurately reflect the dynamic conditions of the natural environment. Additionally, most monitoring studies begin after ecosystem disturbance and HAB development, and previous paleolimnological studies typically depict the past few centuries, preceding the onset of cultural eutrophication. However, high cyanobacteria abundance and cyanotoxins have also posed hazards for ecosystem degradation prior to modern cultural eutrophication (Huisman et al., 2018). Therefore, longer records are necessary to understand the mechanisms driving shifts in aquatic community assemblages and cyanotoxin release, and paleolimnological techniques can provide valuable insights (Saulnier-Talbot, 2016). Incorporating paleolimnology can help reconstruct the history of these systems and offer a more analytical perspective on the evolutionary stages in lakes. This can inform current decisions regarding past drivers of change and assist in assessing the feasibility and expectations of current management strategies. Lastly, it also offers guidelines for the potential effects of climate warming and the gradual increase in human pressure in higher latitudes.

1.5. Ph.D. Dissertation Overview

The purpose of this Ph.D. dissertation is to investigate the paleolimnology of four lakes in the southeastern United States, three of which are located in Florida and one in North Carolina. The goal is to identify the long-term drivers that lead to cyanobacteria dominance and cyanotoxin production over millennial timescales. The dissertation consists of four chapters. The first chapter serves as an introduction and statement of purpose for this research, while chapters 2-4 present the main scientific contributions. The contents of the subsequent chapters are summarized below:

- Chapter 2: "Linking Phosphorus Dynamics with Hypereutrophic Conditions on the Millennial Scale: The Paleolimnology of Shallow and Subtropical Lake Wauberg, Florida, USA" investigates a hypereutrophic lake where sedimentary TP increased over a millennial timescale and shows the response of primary producers and cyanotoxin production to different TP thresholds.
- Chapter 3: "Microcystin Deposition on the Millennial Scale: A Paleolimnological Investigation of Two Subtropical Lakes in Central Florida, USA" investigates two hypereutrophic lakes, linking millennial-scale MC production to nutrient dynamics and shifts in primary producer community composition.
- Chapter 4: "Abrupt Earth, Water, and Fire Transitions and Sustained Cyanobacteria Dominance over the last 27,500 Years in the North American Subtropics" examines a 27,500-year sediment record identifying abrupt changes in aquatic primary producers, terrestrial vegetation, and fire activity in relation to major climate transitions.

The integration of these four chapters demonstrates how long-term ecological and nutrient dynamics shape cyanobacteria dominance and cyanotoxin production in shallow, subtropical lakes. This research provides context for modern ecological changes and advances our understanding of aquatic processes in both natural and human-dominated ecosystems. Collectively, these studies highlight the importance of millennial-scale paleolimnological records in elucidating the drivers of ecological change within the Earth System and addressing the pressing issue of modern HABs.

1.6 References

Bachmann, R.W., Bigham, D.L., Hoyer, M.V., Canfield, D.E., 2012. Factors determining the distributions of total phosphorus, total nitrogen, and chlorophyll a in Florida lakes. Lake and Reservoir Management 28, 10-26. https://doi.org/10.1080/07438141.2011.646458.

Battarbee, R.W., John Anderson, N., Jeppesen, E., Leavitt, P.R., 2005. Combining palaeolimnological and limnological approaches in assessing lake ecosystem response to nutrient reduction. Freshwater Biology 50, 1772-1780. https://doi.org/10.1111/j.1365-2427.2005.01427.x.

Brenner, M., Whitmore, T.J., Flannery, M.S., Binford, M.W., 1993. Paleolimnological methods for defining target conditions in lake restoration: Florida case studies. Lake and Reservoir Management 7, 209-217. https://doi.org/10.1080/07438149309354272.

Brooks, B.W., Lazorchak, J.M., Howard, M.D.A., Johnson, M.-V.V., Morton, S.L., Perkins, D.A.K., Reavie, E.D., Scott, G.I., Smith, S.A., Steevens, J.A., 2016. Are harmful algal blooms becoming the greatest inland water quality threat to public health and aquatic ecosystems? Environmental Toxicology and Chemistry 35, 6-13. https://doi.org/10.1002/etc.3220.

Davidson, T.A., Jeppesen, E., 2013. The role of palaeolimnology in assessing eutrophication and its impact on lakes. Journal of Paleolimnology 49, 391-410. https://doi.org/10.1007/s10933-012-9651-0.

Díez, B., Ininbergs, K., 2014. Ecological importance of cyanobacteria. In: Sharma, N.K., Rai, A.K. and Stal, L.J. (eds), Cyanobacteria, pp. 41-63. https://doi.org/10.1002/9781118402238.ch3.

Dolman, A.M., Rücker, J., Pick, F.R., Fastner, J., Rohrlack, T., Mischke, U., Wiedner, C., 2012. Cyanobacteria and cyanotoxins: The influence of nitrogen versus phosphorus. PLOS ONE 7(6), e38757. https://doi.org/10.1371/journal.pone.0038757.

Earley, S.M., Waters, M.N., Thieme, D., Smoak, J.M., 2017. Linking biogeochemical processes and historic primary producer communities in a SE USA sinkhole lake from the mid-Holocene to present. Journal of Paleolimnology 57, 295-306. https://doi.org/10.1007/s10933-017-9948-0.

Gregory-Eaves, I., Smol, J.P., 2024. Chapter 30 - Paleolimnology: Approaches and Applications, in: Jones, I.D., Smol, J.P. (Eds.), Wetzel's Limnology (Fourth Edition). Academic Press, San Diego, pp. 1015-1043. https://doi.org/10.1016/B978-0-12-822701-5.00030-6.

Grettenberger, C., Gold, D.A., Brown, C.T., 2025. Distribution of early-branching Cyanobacteriia and the potential habitats that gave rise to the earliest oxygenic phototrophs. mSphere, e0101324. https://doi.org/10.1128/msphere.01013-24.

Henao, E., Rzymski, P., Waters, M.N., 2020. A Review on the study of cyanotoxins in paleolimnological research: Current knowledge and future needs. Toxins 12, 6. https://doi.org/10.3390/toxins12010006.

Huisman, J., Codd, G.A., Paerl, H.W., Ibelings, B.W., Verspagen, J.M.H., Visser, P.M., 2018. Cyanobacterial blooms. Nature Reviews Microbiology 16, 471-483. https://doi.org/10.1038/s41579-018-0040-1.

Kaloudis, T., Hiskia, A., Triantis, T.M., 2022. Cyanotoxins in bloom: Ever-increasing occurrence and global distribution of freshwater cyanotoxins from planktic and benthic cyanobacteria. Toxins 14, 264. https://doi.org/10.3390/toxins14040264.

Kaplan, A., Harel, M., Kaplan-Levy, R.N., Hadas, O., Sukenik, A., Dittmann, E., 2012. The languages spoken in the water body (or the biological role of cyanobacterial toxins). Frontiers in Microbiology 3, 138. https://doi.org/10.3389/fmicb.2012.00138.

Kosten, S., Huszar, V.L., Bécares, E., Costa, L.S., van Donk, E., Hansson, L.A., Jeppesen, E., Kruk, C., Lacerot, G., Mazzeo, N., 2012. Warmer climates boost cyanobacterial dominance in shallow lakes. Global Change Biology 18, 118-126. https://doi.org/10.1111/j.1365-2486.2011.02488.x.

Leavitt, P.R., Carpenter, S.R., 1990. Aphotic pigment degradation in the hypolimnion: Implications for sedimentation studies and paleolimnology. Limnology and Oceanography 35, 520-534. https://doi.org/10.4319/lo.1990.35.2.0520.

Leavitt, P., Hodgson, D., 2001. Sedimentary pigments. In: Smol, J.P., Birks, H.J.B., Last, W.M., Bradley, R.S., Alverson, K. (eds), Tracking environmental change using lake sediments. Springer, pp. 295–325. https://doi.org/10.1007/0-306-47668-1_15.

McGowan, S., 2013. Paleolimnology; pigment studies. In: Elias, S.A., Mock, C.J. (eds), Encyclopedia of Quaternary Science (Second Edition). Elsevier, pp. 326–338. https://doi.org/10.1016/b978-0-444-53643-3.00235-1.

Nienaber, M.A., Steinitz-Kannan, M., 2018. A Guide to cyanobacteria identification and impact. University Press of Kentucky. https://doi.org/10.2307/j.ctv8j70z.

Paerl, H.W., Otten, T.G., 2013. Harmful cyanobacterial blooms: Causes, consequences, and controls. Microbial Ecology 65, 995-1010. https://doi.org/10.1007/s00248-012-0159-y.

Rastogi, R.P., Sinha, R.P., Incharoensakdi, A., 2014. The cyanotoxin-microcystins: Current overview. Reviews in Environmental Science and Bio/Technology 13, 215-249. https://doi.org/10.1007/s11157-014-9334-6.

Riedinger-Whitmore, M.A., Whitmore, T.J., Smoak, J.M., Brenner, M., Moore, A., Curtis, J., Schelske, C.L., 2005. Cyanobacterial proliferation is a recent response to eutrophication in many Florida lakes: A paleolimnological assessment. Lake and Reservoir Management 21, 423-435. https://doi.org/10.1080/07438140509354447.

Saulnier-Talbot, É., 2016. Paleolimnology as a tool to achieve environmental sustainability in the Anthropocene: An overview. Geosciences 6, 26. https://doi.org/10.3390/geosciences6020026.

Schindler, D.W., Carpenter, S.R., Chapra, S.C., Hecky, R.E., Orihel, D.M., 2016. Reducing phosphorus to curb lake eutrophication is a success. Environmental Science & Technology 50, 8923-8929. https://doi.org/10.1021/acs.est.6b02204.

Shingai, Q.K., Wilkinson, G.M., 2023. Microcystin as a biogeochemical cycle: Pools, fluxes, and fates of the cyanotoxin in inland waters. Limnology and Oceanography Letters 8, 406-418. https://doi.org/10.1002/lol2.10300.

Smith, V.H., 2003. Eutrophication of freshwater and coastal marine ecosystems a global problem. Environmental Science and Pollution Research 10, 126-139. https://doi.org/10.1065/espr2002.12.142.

Smol, J.P., 1992. Paleolimnology: an important tool for effective ecosystem management. Journal of Aquatic Ecosystem Health 1, 49-58. https://doi.org/10.1007/BF00044408.

Swain, E.B., 1985. Measurement and interpretation of sedimentary pigments. Freshwater Biology 15, 53-75. https://doi.org/10.1111/j.1365-2427.1985.tb00696.x.

Taranu, Z.E., Gregory-Eaves, I., Leavitt, P.R., Bunting, L., Buchaca, T., Catalan, J., Domaizon, I., Guilizzoni, P., Lami, A., McGowan, S., Moorhouse, H., Morabito, G., Pick, F.R., Stevenson, M.A., Thompson, P.L., Vinebrooke, R.D., 2015. Acceleration of cyanobacterial dominance in north temperate-subarctic lakes during the Anthropocene. Ecology Letters 18, 375-384. https://doi.org/10.1111/ele.12420.

Waters, M.N., 2016. A 4700-year history of cyanobacteria toxin production in a shallow subtropical lake. Ecosystems 19, 426-436. https://doi.org/10.1007/s10021-015-9943-0.

Waters, M.N., Brenner, M., Curtis, J.H., Romero-Oliva, C.S., Dix, M., Cano, M., 2021. Harmful algal blooms and cyanotoxins in Lake Amatitlán, Guatemala, coincided with ancient Maya occupation in the watershed. Proceedings of the National Academy of Sciences 118, e2109919118. https://doi.org/10.1073/pnas.2109919118.

Waters, M.N., Piehler, Michael F., Smoak, Joseph M., Bianchi, T.S., 2012. Algal community responses to shallow lake dystrophication. Canadian Journal of Fisheries and Aquatic Sciences 69, 1433-1443. https://doi.org/10.1139/f2012-021.

Waters, M.N., Schelske, C.L., Kenney, W.F., Chapman, A.D., 2005. The use of sedimentary algal pigments to infer historic algal communities in Lake Apopka, Florida. Journal of Paleolimnology 33, 53-71. https://doi.org/10.1007/s10933-004-1691-7.

Zastepa, A., Taranu, Z.E., Kimpe, L.E., Blais, J.M., Gregory-Eaves, I., Zurawell, R.W., Pick, F.R., 2017. Reconstructing a long-term record of microcystins from the analysis of lake sediments. Science of The Total Environment 579, 893-901. https://doi.org/10.1016/j.scitotenv.2016.10.211.

1.7 Figures

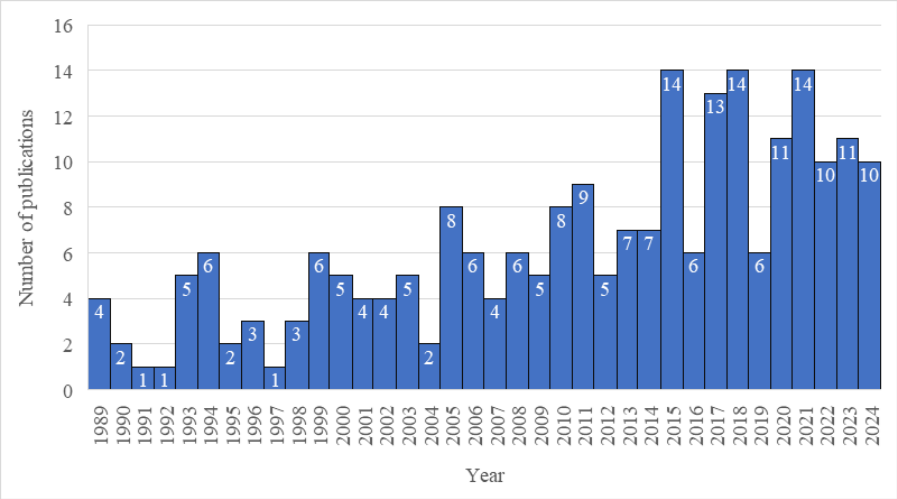

Figure 1.1 Publications applying photosynthetic pigment analysis in paleolimnological investigations from 1989 to 2024.

Chapter 2: Linking Phosphorus Dynamics with Hypereutrophic Conditions on the Millennial Scale: The Paleolimnology of Shallow and Subtropical Lake Wauberg, Florida, USA

2.1 Abstract

Eutrophication and harmful algal blooms pose a global challenge to water quality and ecosystem services. Whereas eutrophication has been linked to nutrient additions in conjunction with human activities, much less is known about water quality trends when nutrient additions persist for centuries or millennia. Here, we used paleolimnological techniques to reconstruct eutrophication and cyanobacteria dynamics in Lake Wauberg, FL, USA, a lake that has experienced millennial-scale nutrient additions from natural phosphate geology. We measured photosynthetic pigments, cyanotoxins, and nutrient concentrations on a sediment core spanning the last ~6,900 years. Our primary hypothesis is that the long-term total phosphorus (TP) additions caused constant cyanobacteria dominance throughout the entire history of the lake. Focusing on the last 5 ka BP with constant lake conditions, photosynthetic pigments and cyanotoxins demonstrated a strong positive relationship with TP over other nutrients. By dividing TP inputs into three levels, primary producers positively increased with low TP inputs but showed no change under moderate levels. Under high (2.2-3 mg g^{-1}) and extreme (>3 mg g^{-1}) TP sedimentary concentrations over the last 0.3 ka BP, substantial increases in cyanobacteria abundance, rapid production of microcystins (MCs), and a possible shift to N-fixation occurred. These data show that chronic and additive TP inputs can produce asynchronous responses in the primary producer community and MC concentrations with substantial increases occurring at higher TP thresholds. Linking the historic ecological response to TP periods with current limnological conditions could provide new directions in forecasting and managing aquatic ecosystems that experience chronic TP inputs.

2.2 Graphical Abstract

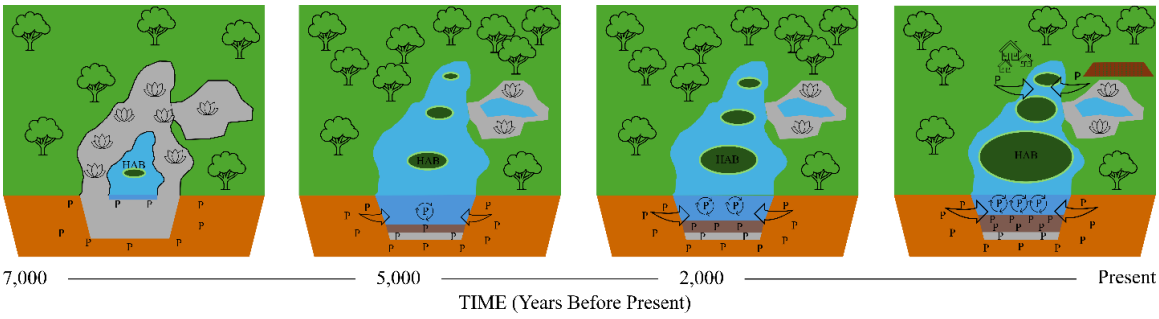

2.3 Introduction

Eutrophication and cyanobacteria proliferation are impacting aquatic systems worldwide, with the combined threats of nutrient enrichment and climate change as primary drivers of ecosystem degradation and biogeochemical change (Huang et al., 2022; Meerhoff et al., 2022; Moss et al., 2011). Many eutrophied systems coincide with the growth of dense cyanobacteria communities called harmful algal blooms (HABs), which can produce toxins and promote adverse effects on water quality, aquatic life, and animal and human health (Rastogi et al., 2014). The recent rise in HAB events, accompanied by the increased concentration of a variety of cyanotoxins, challenges the future ecological health and services of aquatic environments.

The importance of phosphorus (P) as the most essential driver of eutrophication has been established by research including whole-lake experiments in the Experimental Lakes Area in Ontario, Canada (Schindler, 1974; Schindler et al., 2008), paleolimnological records from shallow lakes in Florida, USA (Kenney et al., 2002; Waters et al., 2015), and the dual nutrient reduction policy in Danish lakes (Kronvang et al., 2005). However, increased inputs of other nutrients from anthropogenic activities, such as nitrogen (N), have also been decisive for eutrophication and cyanobacteria dominance (Burford et al., 2023). Reducing the inputs of both P and N is often necessary to restrain eutrophication (Conley et al., 2009; Finlay et al., 2013) because they may develop a synergistic relationship or individual limitation depending on parameters such as N/P stoichiometry, trophic state, temperature, the primary producer community, and lake depth (Filstrup and Downing, 2017; Liang et al., 2020; Quinlan et al., 2021). Nevertheless, the relationship between primary producer community growth and P and N dynamics has rarely been considered over longer timescales, such as centuries or millennia. Hence, the initiation of eutrophication and the establishment of permanent, resilient eutrophic conditions are often obscured (Carpenter et al., 1999).

While monitoring data can provide information on the trajectories of future conditions and management practices, many eutrophic systems developed HABs well before monitoring efforts began (Brenner et al., 1993; Nisbeth et al., 2019). Besides human disturbance, eutrophication is also driven by increased nutrient inputs under natural conditions, such as changes in precipitation (Battarbee et al., 2005) and modifications to groundwater hydrology (Waters et al., 2015). Likewise, alterations to lake depth can increase or decrease stratification, thereby transforming oxygen dynamics, biogeochemical processes, and nutrient availability

(Zhou et al., 2022). However, natural eutrophication is often overlooked in favor of modern trends and recent pre-disturbance conditions of polluted systems (McGowan et al., 1999). Unlike elements like N, the biogeochemical cycle of P primarily consists of solid and liquid phases, lacking a gaseous component that can escape from the system. As a result of prolonged external P inputs, P accumulates in lake sediments, becoming available for biological production through internal loading (Kirol et al., 2024; Missimer et al., 2021; Søndergaard et al., 2003). Hence, investigating the long-term occurrence of HABs in lakes where P is naturally abundant can identify the biological response to natural drivers of eutrophication and historical HAB occurrence preceding human impacts.

The subtropical region of Florida, USA, is one area containing both natural P deposits and natural lake systems where millennial-scale nutrient inputs could occur. Natural factors from Florida geology have played a significant role in developing the current nutrient conditions and trophic states (Bachmann et al., 2012). Additionally, Florida lakes are subtropical and generally shallow, thus promoting eutrophication from internal nutrient loading and cyanobacteria dominance due to warming (Kosten et al., 2012). The shallow and hypereutrophic Lake Wauberg in Alachua County in north-central Florida has minimal human development in the catchment area and is naturally rich in P from local geology (Canfield and Hoyer, 1988). Physical geography and geology make this lake a natural experiment of the drivers of long-term nutrient additions on primary producer abundance throughout the Holocene. We applied paleolimnological measurements of nutrients, N stable isotopes, phytoplankton pigments, and cyanotoxins to a sediment core spanning the last ~6,900 years to investigate two primary research questions: 1) have the naturally high P levels contributed to a high cyanobacteria abundance throughout the lake's existence? and 2) how do changes in cyanobacteria abundance over millennia relate to shifts in aquatic communities and the production of cyanotoxins?

2.4 Material and Methods

2.4.1 Study Site

Lake Wauberg (29°31'42" N, 82°18'08" W) is a small (1.5 km^2) and shallow (~3.6 m mean depth and ~4.2 m max depth) subtropical lake in the Paynes Prairie Preserve in Alachua County in north-central Florida, USA (Fig. 2.1). The elevation is 21 m a.s.l. and the topography has flat to gentle slope. The geologic substrate is characterized by limestone and poorly consolidated phosphatic sands and clays of the Hawthorn Group (Coosawhatchie Formation)

deposited during the Miocene (Scott, 1992). Lake Wauberg developed in a gradually formed, shallow solution sinkhole in a natural phosphate geological setting (Kindinger et al., 1999) and was infilled with Holocene gyttja.

The lake's catchment comprises hardwood pine and oak forests and wetlands, and 5% of the watershed features minimal residential development on the northwestern side and recreational facilities on the eastern side (Florida Department of Environmental Protection, 2013). Rainfall and P-rich groundwater are the main hydrologic inputs to the lake, and a small outflow to the east side discharges water to Sawgrass Pond during high water levels (Arnold et al., 2019). Fluctuations in groundwater levels have historically impacted the surrounding wetlands. The most notable recorded event occurred in 1873 CE when heavy rainfall clogged the Alachua Sink on the northern side of the prairie and inundated previous wetlands to form Alachua Lake, which rapidly disappeared in 1891 CE (A Florida Lake Gone, 1891, August 23). However, Lake Wauberg's sub-basin was likely separated from Alachua Lake even during periods of high-water levels, as indicated by historical maps (Matheson & McMillan Publishers, 1880). In addition, the impermeable bottom of Lake Wauberg and the seepage of groundwater from surrounding higher elevations help to mitigate water level fluctuations, even during dry conditions (Florida Department of Environmental Protection, 2013). The response of Lake Wauberg to the shallow and orthophosphate-rich groundwater can be exacerbated by the increased regional risk of P leaching from the surface soils (Liao et al., 2019).

The lake's water quality has been monitored by Florida Lakewatch since 1990 and is classified as a softwater hypereutrophic lake with a mean Secchi depth of 0.5 m, mean chlorophyll 91 μg L^{-1}, mean TP 123 μg L^{-1} and mean TN 2,005 μg L^{-1} (Hoyer et al., 2014). The surface sediments have a high abundance of cyanobacteria pigments, including canthaxanthin and aphanizophyll, as well as cyanotoxin MCs (Lamb, 2021). Light limitation is a constraint for aquatic macrophytes, and phytoplankton and cyanobacteria have been the primary sources of productivity in the lake since the early 20th century (Gu et al., 2006) and even before intense human impacts (Riedinger-Whitmore et al., 2005).

2.4.2 Fieldwork and Core Sampling

A sediment core was collected on January 4th, 2022 with the coring location selected after an in-situ sediment mapping survey and consultation with previous studies (Whitmore et al., 1996). A piston corer (7 cm diameter tubes) designed to collect undisturbed mud/water

interface sediments (Fisher et al., 1992) was used to extract the uppermost 137 cm of sediments, while deeper sediments were collected using a modified Livingstone corer (5.5 cm diameter tubes). Each extracted sediment core aimed to have a 20 cm overlapping section with the previous. Removing the overlapping sections through stratigraphic analysis yielded approximately 380 cm of continuous sediments. Based on previous paleolimnological research in Florida, the mud-water interface core was subsampled in 4 cm sections in the field (Kenney et al., 2016; Waters et al., 2015), packed in labeled Whirl-pak bags, and stored in coolers with ice. The more consolidated sections were kept in their labeled polycarbonate core barrels and transported in coolers back to the laboratory at Auburn University, where they were cut in half lengthwise, photographed, and described using a Geoteck Core-logger. One half was stored as an archive, and the second was subsampled every 2 cm. After subsampling, the wet sediments were processed for gravimetric analysis and then freeze-dried, ground, and stored in labeled scintillation vials for further analyses.

2.4.3 Laboratory Analysis

2.4.3.1 Organic Matter, Nutrients and Elements

Wet samples were weighed into crucibles, dried in an oven at 60°C for 24 h, weighed at room temperature, and the dried weight was divided by the volume of the sediment used, 4.929 cm^3 (for 5 mL scoops of sample) to calculate bulk density as represented by g dry cm^{-3} wet (Dean, 1974). For LOI, the dried samples were weighed and burned in a muffle furnace at 550°C for 3 h. The ash from the samples was reweighed, and the weight difference was used to calculate percent organic matter. Total nitrogen (TN) and organic carbon (TOC) were measured using a Costech ECS 4010 elemental analyzer at Auburn University. The TN analysis was performed after weighing freeze-dried samples into tin capsules. The TOC analysis was conducted after weighing the samples in silver capsules and placing them in an acid vapor bath with hydrochloric acid (HCl) for 24 h to fumigate the inorganic C fraction. The capsules were folded and placed in tin capsules before analysis to aid in the total combustion of the sample. The TOC/TN ratios (here on known as C/N) were reported in atomic ratios after dividing each element by its corresponding atomic weight. The samples for the N isotopic analysis were prepared similarly to TN, and the analysis was carried out at the Light Stable Isotope Mass Spec Lab of the University of Florida with a Thermo Electron DeltaV Advantage isotope ratio mass spectrometer coupled with a ConFlo II interface linked to a Carlo Erba NA 1500 CNHS

Elemental Analyzer. Inductively Coupled Plasma (ICP) Spectroscopy, with 90-minute nitric acid digestion on a heated block (EPA 6010B) at Waters Agricultural Laboratories in Camilla, GA, USA, was used to measure total P, S, Fe, and Mn, as well as other elements, in the sediments.

2.4.3.2 Photosynthetic Pigments

Photosynthetic pigments (chlorophylls and carotenoids) were extracted from dried sediment samples using a solvent mixture of 80% acetone, 15% methanol, and 5% HPLC-grade water containing an internal standard (Apocarotenal or trans-β-apo-8'-carotenal; Sigma-Aldrich Chemical Corp.). The analysis was performed using High-Performance Liquid Chromatography (HPLC) following the methods designed for pigment extraction from sediments (Leavitt and Hodgson, 2001; Waters et al., 2012).

The samples were injected into a Shimadzu HPLC system following the mobile phase and the time sequence of Leavitt and Hodgson (2001). The separation of chlorophylls and carotenoids was performed by passing through a Phenomenex Luna 3 μm C18 long column (200 x 4.6 mm), and measurement was carried out using a photodiode array detector for carotenoids coupled to a fluorescence detector for chlorophylls. Pigment identification was performed using retention times and pigment-specific spectra of known standards (DHI Lab Products, Denmark). Pigment concentration was calculated by comparing peak areas against standards of known concentration and was expressed in nmol per gram of organic matter.

2.4.3.3 Microcystins Analysis

The extraction of MCs from the sediment core samples was based on previous investigations of sediment cyanotoxins (Waters, 2016; Waters et al., 2021; Zastepa et al., 2017). Cyanotoxins were measured as total MCs using the microcystin/nodularin ADDA OH enzyme-linked immunosorbent assay (ELISA) kit by Abraxis, purchased from Gold Standard Diagnostics. This biochemical method can measure the MC congeners containing the ADDA amino acid, which is present in 220 of the 279 identified MC congeners, yielding a total sedimentary microcystin measurement (Bouaïcha et al., 2019). The samples were extracted from dried sediments for each subsampled section of the core, following Abraxis instructions for extracting MCs from soils, as well as the methods described by Zastepa et al. (2017) and Waters et al. (2021).

The samples were mixed with 10 mL solvent of 75% methanol, 25% deionized (DI) water, and 0.05% trifluoroacetic acid, then sonicated, centrifuged, and the supernatant was

transferred to a labeled scintillation vial. The process was repeated with another 5 mL of solvent, and the combined supernatant was evaporated in a heated water bath at 60ºC under a stream of nitrogen gas until the total sample volume was about 1.5 mL. A total of 6 mL HPLC-grade water was added to each vial, which was sonicated and vortexed until all contents were dissolved. Then, the extract was cleaned using solid-phase extraction. The content of each vial was passed through a conditioned Strata X column, rinsed with 2 mL of 5% methanol, and eluted with 9 mL of 90% acetonitrile solution. The 9 mL sample was collected in a clean and labeled scintillation vial and evaporated to dryness in a heated water bath at 60ºC under a stream of nitrogen. The dry samples were reconstituted with 1.5 mL HPLC-grade water, sonicated, vortexed, and passed through a 0.2 μm syringe filter to a labeled amber vial before analysis. Samples exceeding the high detection limit, especially at the top of the cores, were diluted with the provided sample diluent in the ELISA kit. Total MCs were reported as ng toxin per gram of organic matter, and due to their large value range, they were converted to a base-10 logarithmic scale.

2.4.3.4 ^{210}Pb Dating, ^{14}C Dating and the Age-Depth Model

Dried samples from the upper layers of the mud-water interface core were weighed into polystyrene tubes filled to approximately 30 mm height and sealed with epoxy for at least 19 days to achieve secular equilibrium between the atmospheric sourced ^{226}Ra and the daughter product ^{222}Rn (3.8 days half-life) (Brenner et al., 2004). The samples were dated using gamma spectroscopy to measure the ^{210}Pb total activity and ^{226}Ra (supported ^{210}Pb) and then calculate the excess ^{210}Pb (Appleby et al., 1986; Schelske et al., 1994). The analysis was done with an ORTEC Intrinsic Germanium Detector connected to a 4096-channel multichannel analyzer at Auburn University. The dates were calculated using the constant rate of supply (CRS) model that assumes a continuous supply rate of excess ^{210}Pb in the system (Appleby and Oldfield, 1983) (Fig. S2.1). This model is well-suited for measuring the excess ^{210}Pb in Florida due to human-induced variations in sedimentation rate and dilution effects from organic matter accumulation (Brenner et al., 2004).

For the dates below the CRS-modeled dates, one twig and five charcoal macrofossil samples were measured for AMS ^{14}C ages (Table S2.1) at the National Ocean Sciences Accelerator Mass Spectrometry (NOSAMS) facility at the Woods Hole Oceanographic Institution in Massachusetts, USA. The wood macrofossil was collected from wet sediments, rinsed with DI water, and put in the oven at 60ºC to dry. The charcoal samples were collected

from a petri dish under a microscope after adding 10 mL of 5% potassium hydroxide (KOH) to 5 mL of wet sediments for 24 h, removing the supernatant, adding 10 mL of 5% hydrogen peroxide (H_2O_2) for 24 h, and then sieving through a 125 μm mesh sieve.

The ^{14}C-dated ages were calibrated with the IntCal20 calibration curve (Reimer et al., 2020) and combined with the excess ^{210}Pb calculated ages to create an age-depth model (Fig. S2.2) using the Bacon package in R (Blaauw and Christen, 2011), with 4 cm thickness sections and a 30 cm accumulation rate.

2.4.3.5 Data Visualization and Analysis

The map for Lake Wauberg was created in ESRI ArcGIS Pro v. 3.4.2 using an online service layer for basemap, land cover data from the Florida Department of Environmental Protection Geospatial Open Data (2022) (https://geodata.dep.state.fl.us/), bathymetric data from St. Johns River Water Management District Open Data (2015) (https://mapdirect-fdep.opendata.arcgis.com/), and a digital elevation model based on USGS lidar data (2018-2020) from National Oceanic and Atmospheric Administration (NOAA) data access viewer (https://coast.noaa.gov/dataviewer/#/). The paleoecological time plots were created in Tilia v. 3.0.3 (Williams et al., 2018). Additionally, in Tilia, the core was divided into zones based on total phosphorus (TP) concentration using a dendrogram produced by constrained incremental sum of squares (CONISS) clustering. Principal components analysis (PCA) was performed using the built-in prcomp function in R v. 4.4.1 (R Core Team, 2024) and the autoplot function in the ggfortify package (Tang et al., 2016). Correlation and scatter plots were generated in R using log10-normalized pigment and cyanotoxin data and the ggcorrmat function with the Pearson correlation method in the ggstatsplot package (Patil, 2021) and the built-in plot function in R, respectively. The locally weighted scatter plot smooth (LOWESS) function in R, with a smoothing parameter (f=0.45), was used to visualize the smoothed dataset in the scatterplots. The change between consecutive smoothed data points along the x and y axes was calculated using the diff function in R. The ratio of these changes was then computed to perform the slope analysis and highlight the rate of change in the relationships between the independent (TP) and the dependent (photosynthetic pigments and cyanotoxins) variables. To detect breakpoints in slope, hierarchical clustering of the dependent variables using Ward's method and a predefined number of clusters was performed in IBM SPSS statistics v.28.

2.5 Results

2.5.1 Sediment Description and Chronology

The sediment core collected from Lake Wauberg, FL contained homogeneous dark brown organic sediments with some silty pockets and sparse macrofossils. As it reached the bottom (~350 cm), the color turned to greyish black sediments with more silt and macrofossils.

Excess ^{210}Pb reached supported levels at 88 cm, which yielded the date of 1892 CE per the CRS model (Fig. S2.1). The supported ^{210}Pb demarcation was assigned when the excess ^{210}Pb activity crossed the parent radionuclide ^{226}Ra activity and reached radioactive secular equilibrium (Appleby and Oldfield, 1983). When combined with radiocarbon dates (Table S2.1), the age-depth model indicated a bottom date of ~6,900 years (Fig. S2.2). The rBacon default suggested setting the sedimentation rate prior to 20 yr cm^{-1}, excluding the bottom radiocarbon date. However, the prior was set to 30 yr cm^{-1} because the accuracy of the date was supported by the high abundance of charcoal particles, which aligns with increased wildfire activity in the region reconstructed from nearby lake systems (Mendieta et al., 2018).

2.5.2 Sediment geochemistry and aquatic community composition and abundance

The deposition of TP varied throughout the record, showing a notable increase after 3.7 ka BP, rising from 0.5 to 4 mg g^{-1} in the top of the core. To analyze paleolimnological changes based on TP concentration, a dendrogram generated from CONISS cluster analysis was utilized to divide the core into four zones representing one wetland (Zone Ø) and three lacustrine (Zones I, II, III) periods of the lake (Fig. 2.2), with analysis of variance (ANOVA) and subsequent Tukey's post-hoc test indicating significant ($p<0.05$) difference between the successive zones (Table S2.2).

Zone Ø (6.9 to 5 ka BP; 380 to 350 cm) was characterized by high bulk density and a more significant contribution of terrestrial elements and low organic matter content (Fig. S2.3). However, the bulk density gradually decreased with increased organic matter content (TOC, LOI). Throughout Zone Ø, all other nutrients, elements, and ratios either remained constant (TP, δ^{15}N) or increased (TN, C/N, TS, N/P) (Fig. 2.2A). Chlorophyll-a and pheophytin-a were partially present in the sedimentary interval before 5 ka BP (Fig. 2.2B). The pigment concentrations remained low, with a continuous presence of lutein+zeaxanthin, canthaxanthin, alloxanthin, diatoxanthin, and detectable MCs concentration.

In Zone I (5 to 2.2 ka BP; 350 to 260 cm), TP levels slightly decreased initially, and after

3.7 ka BP, TP gradually increased to an average of 0.8 mg g^{-1} (±0.2) (Fig. 2.2A, Table 2.1). Total OC, TN, and N/P recorded their highest values early in Zone I but declined as TP concentrations increased. Despite the changes in TOC and TN, C/N showed minor fluctuations in Zone I, averaging 13.3 (±0.4). Sulfur levels increased steadily over this interval, with a brief decrease occurring near the end of the zone. The $\delta^{15}N$ ratio initially had a remarkable decrease from 2.2 to 0.7‰, but after 3.7 ka BP, it increased again, reaching high values (2.6‰) similar to Zone Ø. Photosynthetic pigment abundance increased, with canthaxanthin and echinenone showing the highest concentrations among non-generalized pigment markers like beta-carotene (Fig. 2.2B, Table 2.1). Most measured pigments maintained constant concentrations without significant fluctuations, and after 3.1 ka BP, they slightly increased. The concentration of MCs initially decreased but began to rise again after 2.6 ka BP, averaging at 5 ng g^{-1} org (±3.3).

In Zone II (2.2 to 0.3 ka BP; 260 to 104 cm), TP concentrations gradually increased until 1.4 ka BP and reached an average of 1.9 mg g^{-1} (±0.3) (Fig. 2.2A, Table 2.1). Total OC and TN decreased following ~3.7 ka BP and started more frequent fluctuations after 2 ka BP. Despite a notable drop in C/N at ~0.8 ka BP, the overall variations were minor, and the values averaged around 13.6 (±1.4). Sulfur reached the highest values in the zone but showed several fluctuations and decreased after 1.4 ka BP. The N/P ratio decreased (Fig. 2.2A), P/Fe increased, and Fe/Mn reached the highest values and decreased after 1.4 ka BP (Fig. S2.3). While the $\delta^{15}N$ ratio fluctuated, the average only slightly decreased from 1.7‰ (±0.7) in Zone I to 1.6‰ (±0.4) in Zone II, reaching the lowest values (~1.3‰) of the zone after 0.8 ka BP. The photosynthetic pigment concentrations continued to increase, and Zone II demonstrated higher averages than Zone I (Fig. 2.2B, Table 2.1). Echinenone and canthaxanthin increased, but diatoxanthin and okenone, proxies for diatoms and purple sulfur bacteria, respectively, had the most notable increase, with a more than five- and two-fold increase, respectively. The average concentration of cyanotoxins also increased by almost 77% to 8.9 ng g^{-1}org (±5.7). Despite the overall increase in pigment and cyanotoxin concentration and the appearance of oscillaxanthin and aphanizophyll (Fig. S2.3), many notable fluctuations occurred.

Zone III (0.3 ka BP to present; 104 cm to top) contained multiple abrupt changes to all paleolimnological proxies measured (Fig. 2.2, S2.3). Total P continued to increase throughout the interval, reaching the highest values and an average of 2.8 mg g^{-1} (±0.7), signifying a 1.5-fold increase from the average concentration of Zone II or 3.5-fold increase from Zone I (Fig. 2.2A,

Table 2.1). Total OC and TN reached higher values only in the top of the core, representing the last few decades. However, C/N fluctuated significantly, and the average value slightly decreased to 12.9 (±2). Despite the overall decrease in N/P following 3.7 ka BP, it decreased further, reaching the lowest average value after Zone Ø. The $\delta^{15}N$ ratio showed a notable decrease, reaching the lowest average value of the record (~1.1‰, ±0.3). Photosynthetic pigment abundance and MCs concentration increased, reaching maximum values (Fig. 2.2B, Table 2.1). Alloxanthin had a dramatic 14-fold increase in concentration, echinenone a 7-fold, canthaxanthin a 5.5-fold, and MCs a 44-fold increase. However, okenone was mostly undetectable over the last century, and diatoxanthin decreased significantly and increased only during the last decade, coinciding with higher pigment preservation, as inferred from Chl-a/Pheo-a. Dramatic increases also occurred in oscillaxanthin, aphanizophyll, and pyropheophorbide, which had a continuously high abundance in the top zone (Fig. S2.3, Table S2.4).

2.5.3 Planktonic Community and Cyanotoxins Response to Phosphorus Concentration

The PCA for the lake stages with limnological conditions (Zone I, II, III) produced PC1 (65.4%) and PC2 (14.5%), which accounted for 79.9% of the dataset variance (Fig. 2.3A), while PC3 (6.5%) and PC4 (5.6%) accounted for an additional 12% (Fig. S2.4). Most eigenvectors, including most photosynthetic pigments, MCs, and TP, were ordinated along the PC1 axis. In contrast, other elements (TS, TN, TOC) showed a stronger alignment with PC2, with okenone and diatoxanthin exhibiting an opposite orientation to these elements. Nevertheless, in PC4, okenone and diatoxanthin exhibited a strong ordination with all elements (TP, TS, TN, TOC) (Fig. S2.4). The eigenvectors in PC1 indicated a strong relationship among alloxanthin, canthaxanthin, echinenone, and MCs with TP and beta-carotene while demonstrating an inverse relationship with TOC and TN and no relationship with TS (Fig. 2.3A, S2.4). However, MCs also showed a strong positive and negative ordination with TN and TS and a moderate positive and negative ordination with TOC and TP, respectively, in PC3. The distribution of the samples within 68% confidence intervals (1σ of Gaussian distribution) on the PC1 and PC2 biplot revealed a chronologically concise clustering (Fig. 2.3A). Zone I (5-2.2 ka BP) ordinated more with TOC and TN eigenvectors. Low ordination characterized Zone II (2.2-0.3 ka BP), with only diatoxanthin and okenone vectors in proximity. Zone III (0.3 ka BP-pres.) exhibited a strong ordination with several eigenvectors, such as TP, cyanobacteria pigments, alloxanthin, and MCs, while showing an opposite ordination with Zone I. The PC1 scores, reflecting the direction and

variability of individual samples driven by the loadings of all variables but TS in PC1 (Fig. S2.4), indicated that significant changes ($p<0.05$) occurred more frequently after 2.2 ka BP, culminating in an abrupt shift over the last 300 years BP (Fig. S2.5).

The strong ordination between photosynthetic pigments and TP in the PCA was also reflected by strong positive correlations (Fig. 2.3B). While other measured nutrients and elements had an insignificant correlation, TP showed a significant ($p<0.05$) Pearson correlation (r) ranging from 0.69 to 0.85 with all photosynthetic pigments except okenone. The concentration of MCs in the sediments had a significant ($p<0.05$) positive correlation (r) with all photosynthetic pigments (0.59-0.88) and TP (0.73) except okenone.

To identify primary producer abundance and cyanotoxins response to TP concentrations during the lake phases of Lake Wauberg's limnological history (Z I, II, III), TP was compared to photosynthetic pigments and MCs (Fig. 2.4). The LOWESS smoother indicated that the responses of photosynthetic pigments and MCs varied depending on TP concentration thresholds (TP I, II, IIIa, IIIb) (Fig. 2.4A-C). The slope change estimates from the smoothed dataset and their hierarchical clustering highlighted four TP concentration zones of low (TP I, <1.6 m g^{-1}), moderate (TP II, 1.6-2.2 mg g^{-1}), high (TP IIIa, 2.2-3 mg g^{-1}), and extreme (TP IIIb, >3 mg g^{-1}) TP which roughly corresponded to the chronological Zones I (TP I), II (TP II) and III (TP IIIa and TP IIIb) (Fig. 2.4D-J).

The concentration of photosynthetic pigments increased in response to TP concentration up to 1.6 mg g^{-1} (low) (Fig. 2.4). Notably, the levels of beta-carotene, diatoxanthin, and lutein+zeaxanthin (Fig. 2.4D, E, I) increased with a high rate of change (calculated as slope), but cyanobacteria pigments and alloxanthin had a weaker response to low TP concentrations (Fig. 2.4F-H). However, the initial concentration of echinenone and canthaxanthin (Fig. 2.4B) at the lowest TP concentrations was higher than non-cyanobacteria pigments (Fig. 2.4A). As the TP concentration ranged from 1.6 to 2.2 mg g^{-1} (moderate), photosynthetic pigments and cyanotoxins concentration remained largely stable, with a notable decrease in the rate of change (Fig. 2.4D-J). The change in slope for beta-carotene and lutein+zeaxanthin sharply decreased, while diatoxanthin had an equal magnitude gradual change. When TP concentration exceeded 2.2 mg g^{-1} (high), there was a pronounced increase in photosynthetic pigments and cyanotoxin concentrations, marked by an abrupt change in slope. However, diatoxanthin exhibited a moderate increase and maintained a low slope. Despite the increased photosynthetic pigment

concentrations, the rate of increase flattened out, stabilizing at extreme TP concentrations (>3 mg g^{-1}). Only the rate of change in MCs increased in a stepwise fashion from high to extreme TP concentrations.

2.6 Discussion

The phosphorus record from Lake Wauberg provides a novel long-term archive of TP dynamics in a shallow subtropical lake ecosystem spanning the last 6,900 years. The presence of phosphate rocks in the local geology was apparent early in the lake's geochemical history, with TP inputs occurring on a millennial scale contributing to the natural accumulation of TP in the sediments (Fig. 2.2A). The average TP concentration of 1.9 mg g^{-1} (±0.9) in lacustrine sediments over the last 5 ka BP is remarkably higher than that found in other shallow subtropical lakes experiencing persistent HABs in Florida and beyond (Clift and Waters, 2024; Kenney et al., 2002; Lin et al., 2023; Waters et al., 2021).

2.6.1 Phosphorus and Paleolimnological Development of Lake Wauberg

2.6.1.1 Lake Prehistory – Zone Ø (6.9 to 5 ka BP)

Phosphorus inputs were consistently high prior to the modern lake period (6.9 to 5 ka BP), maintaining an average concentration of around 1.8 mg g^{-1} (±0.4). These elevated TP values occurred during the transition from a wetland with low organic matter and high bulk density to a lacustrine environment, which has also been seen in other Florida lake systems (Kenney et al., 2016; Waters et al., 2015). Although wetlands in this area lack constant inundation, N isotope sources were consistent, C/N levels were the lowest, and green algae and colonial cyanobacteria pigments were present. However, the low pigment concentration and the absence of chl-a and pheo-a (Fig. 2.2B) reflect lower pigment preservation (Leavitt, 1993), likely attributable to the lower water levels and lack of constant anoxia from inundation necessary for optimal pigment preservation. As a result, most of the discussion will focus on the modern lake period, which includes paleolimnological zones I, II, and III, and all TP zones (I, II, IIIa/b) used in Fig. 2.4.

2.6.1.2 Paleolimnological Adjustments – Zone I (5 to 2.2 ka BP)

The TP concentrations from 5 to 2.2 ka BP were the lowest in the paleolimnological record, with average values around 0.8 mg g^{-1} (±0.2) (Fig. 2.2A, Table 2.1). Despite this being the lowest TP value for any zone recorded in the sediment core from Lake Wauberg, the level of TP in these sediments is comparable to modern hypereutrophic lakes experiencing continual HABs, such as Lake Taihu, China (0.5 mg g^{-1}, Lin et al., 2023) and Lake Amatitlan, Guatemala

(1.2 mg g^{-1}, Waters et al., 2021). This period also coincided with the establishment of permanent lake conditions, linked to increased groundwater levels known to have begun in Florida around 5 ka BP (Filley et al., 2001; Kenney et al., 2016; Willard, 2023). The C/N values during this period suggest that organic matter was largely autochthonous (Meyers and Ishiwatari, 1993). As the system accumulated organic matter, the N/P load increased due to lower P deposition and consistent N inputs to the sediments, peaking at 3.7 ka BP. During this period, pigment abundance increased, and most primary producer groups were represented (Fig. 2.2B, S2.3). The increase in TS and the appearance of purple sulfur bacteria, measured as okenone (Fig. 2.2), indicate the establishment of limnological conditions with stratification occurring in the water column (Bjorndahl et al., 2022; Karmakar et al., 2015) as well as an increase in organic matter accumulation (Brenner and Binford, 1986), trophic conditions (Urban et al., 1999), and groundwater inputs (Bates et al., 1995). Despite cyanobacteria and other algal producers driving productivity, the trophic state of the lake was much lower than the hypereutrophic conditions observed today.

2.6.1.3 Accelerated Phosphorus Deposition – Zone II (2.2 to 0.3 ka BP)

Zone II was characterized by a remarkable increase in TP to more than double the concentration in Zone I, and coincided with an overall increase in most primary producer biomarkers (pigments) and cyanotoxins (Fig. 2.2, Table 2.1). The Fe/Mn ratio peaked (Fig. S2.3), indicating reduced oxygen levels in the benthic zone (Davies et al., 2015), which could increase P availability during resuspension events (Clift, 2022). Despite periods of constant nutrient deposition, photosynthetic pigments demonstrated a dynamic primary producer community. The accelerated increase in TP at 2.2 ka BP brought an instant increase in photosynthetic pigments indicative of the broader primary producer community composition (B-car and lut+zea) (Fig. 2.2B, S2.3). Cryptophytes and cyanobacteria remained relatively constant, and only diatom abundance showed a more gradual increasing trend from 1.8 ka BP. Most measured pigments spiked around 1.4 ka BP, with some of the highest increases in diatoms (diato), colonial cyanobacteria (canth), and purple-sulfur bacteria (oke), with the latter suggesting lake stratification while light reached the anoxic hypolimnion. While TP fluctuated at high values (2.1±0.3 mg g^{-1}) from 1.3 to 0.3 ka BP, most photosynthetic pigment concentrations decreased for the remainder of the zone, except for general cyanobacteria (ech) from 1.2 to 0.7 ka BP and diatoms from 0.8 to 0.3 ka BP. As a result, this period of Lake Wauberg appears to

have had a varied primary producer response to accelerated P deposition, with an overall increase in pigment abundance, while maintaining a trophic level that allowed light to reach the hypolimnion.

2.6.1.4 Establishment of Hypereutrophic Conditions – Zone III (0.3 ka BP to Present)

The increase in TP reached an unprecedented level, with an average of 2.8 mg g^{-1} (±0.7) and a minimum/maximum of 1.8/4.3 mg g^{-1}. During this period of extreme P in the system, the concentrations were notably higher than in Lake Apopka, USA (1.9 mg g^{-1}, Schelske et al., 2005), other hypereutrophic systems in Florida (Kenney et al., 2002), and hypereutrophic systems in Guatemala (Waters et al., 2021) and China (Lin et al., 2023). All cyanobacteria pigments increased abruptly (Fig. 2.2B), and two new cyanobacteria pigments have a constant presence (osc & aphani) (Fig. S2.3). The presence of new cyanobacteria pigments indicates an alteration in the primary producer community, as well as an increase in overall cyanobacteria abundance. Furthermore, the absence of purple sulfur bacteria (oke), combined with the increase in phytoplankton markers, indicates a deterioration in benthic photic levels. The shift towards higher planktonic production could reduce water clarity, limiting benthic production and exacerbating internal P loading (Genkai-Kato et al., 2012).

While the establishment of La Chua Ranch in the area, one of the biggest cattle ranches in mid-17th century Florida (Arnade, 1961), may have influenced TP inputs and aquatic community composition, earlier changes were independent of human presence (Fig. S2.6). The private status of the lake since the second half of the 19th century (Matheson & Mcmillan Publishers, 1880) coincided with an increase in TP aligned with rapid shifts in Zn and B, which had previously followed different trends than TP (Fig. S2.6). Similar to other lakes in Florida (Clift and Waters, 2024; Kenney et al., 2016; Waters et al., 2015), the period after 1892 CE marks the early anthropogenic impacts that preceded the significant deterioration of lake environments resulting from demographic growth in Florida in the 1950s. However, apart from the increasing human pressure, TP concentrations have also been in concert with recorded hydroclimatic fluctuations over the last century (Fig. S2.7). Whereas previous research has suggested increased macrophyte coverage during this time (Arnold et al., 2019), our C/N data and pigment markers indicate that Lake Wauberg maintained a hypereutrophic cyanobacteria-dominated lake during this period.

2.6.2 Natural Phosphorus Loading, Thresholds, Sediment Biogeochemistry and Ecosystem Response

The availability of phosphate rocks in the local geology of Lake Wauberg constituted the primary source of P, with groundwater inputs serving as the delivery mechanism of P into the system (Lisboa et al., 2024; Meinikmann et al., 2015; Nisbeth et al., 2019). The constant external P inputs built up in the sediments, creating a P pool enhanced by high levels of autochthonous production and organic matter decomposition. At the same time, the biochemical conditions in the sediment-water interface determined the amount of available P for biological productivity in the water column. Hence, the shallow Lake Wauberg constitutes a natural, millennial-scale P experiment preceding human-induced nutrient inputs.

Even though lakes with significantly lower sedimentary P concentrations are currently hypereutrophic in Florida, the TP concentration levels in Lake Wauberg can only be compared with lakes exhibiting extremely high sedimentary P levels. Historically, many lakes in Florida had TP values around 0.5 mg g^{-1} and transitioned to phytoplankton dominance when TP levels exceeded 1 mg g^{-1} (Clift and Waters, 2024; Kenney et al., 2002; Kenney et al., 2016; Schelske et al., 2005; Waters, 2016). Only a few lake systems, like Newmans Lake, Little Lake Jackson (Kenney et al., 2002), Clear Lake, Lake Hollingsworth, and Lake Parker (Brenner et al., 1999), have shown similarly high TP concentrations to Lake Wauberg, with concentration exceeding modern phytoplankton transition thresholds (~1 mg g^{-1} TP) of several systems (Kenney et al., 2002) during the past 2.2 ka.

Our paleolimnological analysis indicates that primary producers responded to the different TP thresholds (Fig. 2.4), with photosynthetic pigments indicative of the broader aquatic community (B-car, lut+zea) demonstrating the most distinct trends (Fig. 2.4C, D, I). Diatoms exhibited heightened sensitivity to TP at lower concentrations (TP I, <1.6 mg g^{-1}) (Fig. 2.4A, E) compared to other primary producers. After 2 ka BP, TP reached 1.6 to 2.2 mg g^{-1} (TP II, moderate) and acted as a transition zone, with primary producers exhibiting a decreased response compared to higher and lower TP concentration thresholds, as shown by the lack of slope change in the threshold comparison (Fig. 2.4). When TP levels in the sediments ranged from 2.2 to 3 mg g^{-1} (TP IIIa, high), cyanobacteria abundance rapidly increased (Fig. 2.4B, G, H), potentially leading to a prolonged presence of high cyanobacteria biomass, indicating the shift to a constant hypereutrophic state. The extreme P period (TP IIIb, >3 mg g^{-1}) sustained a high pigment

concentration but with a restrained increase. Overall, the established TP thresholds reveal alterations in the phytoplankton communities to the varying amounts of P in the ecosystem. This shows that P was historically the primary driver of cyanobacteria. However, as P increased, the ecosystem experienced limitation periods from additional nutrients and potentially from increased light attenuation.

Despite the historic P increase, TN concentrations are inferred to have influenced the current hypereutrophic state of the lake. While the system showed a strong linear response to low (TP I) and high (TP IIIa) TP concentrations, primary producer abundance was restrained at moderate (TP II) and, to a lesser extent, extreme TP (IIIb) levels (Fig. 2.4), possibly due to N-limitation or overall nutrient availability discrepancy between the benthic and pelagic zones (Elser et al., 2007). Eutrophic conditions can amplify the stoichiometric imbalance between N and P because N removal through denitrification is more efficient in eutrophic systems with high P levels, favoring cyanobacteria growth (Finlay et al., 2013). Nitrogen biogeochemical dynamics can follow multiple pathways during high P events, such as N internal inputs from organic matter degradation, N-fixation, denitrification, or ammonification in benthic areas. Although natural P occurrence is a determinant in this system, N transformations under different trophic levels must also have constituted a limitation (Scott et al., 2019).

As indicated by decreases in $\delta^{15}N$ at high and extreme TP concentrations (TP IIIa/b) and the sudden appearance of the N-fixing-associated pigment aphanizophyll (Fig. S2.3) (Cottingham et al., 2000; Leavitt and Hodgson, 2001), N limitation may have occurred in Lake Wauberg, thereby favoring N-fixing cyanobacteria. Whereas an increase in $\delta^{15}N$ would manifest the dominance of denitrification in the N cycle, the decrease in $\delta^{15}N$ (Fig. 2.2A) indicates a period of N-fixation in the cyanobacteria community where cyanobacteria sequester N_2 from the air, which has a $\delta^{15}N$ signature of 0‰ (Brenner et al., 1999). The altering responses to nutrient concentrations and stoichiometric balances by cyanobacteria suggest management strategies based on reducing both P and N. However, the paleolimnological record in Lake Wauberg indicates a potentially more biodiverse environment with less cyanobacteria biomass with sedimentary TP levels below 1.6 mg g^{-1}.

Like N dynamics, hydroclimatic alterations could be a secondary driver of P dynamics and cyanobacteria dominance in Lake Wauberg. After the Holocene Thermal Maximum, Florida's temperature remained relatively stable. However, the mid-Holocene decrease in

insolation triggered shifts in the Intertropical Convergence Zone in teleconnection with other climate indices (Pollock et al., 2017), causing significant hydroclimatic variations capable of influencing P delivery in the system. While relatively drier hydroclimatic conditions during the middle Holocene in Florida maintained TP levels, wetter conditions after 2.2 ka BP (Pollock et al., 2017; Soto, 2005), accelerated delivery and increased TP concentration, indirectly influencing the aquatic community composition, as has been shown in other Florida lakes (Clift and Waters, 2024; Waters et al., 2015). Similarly, TP concentrations exhibited sensitivity to modern hydroclimatic fluctuations (Fig. S2.7) while the system was subjected to increased anthropogenic influence (Fig. S2.6). However, the increased abundance of primary producers and cyanobacteria dominance were also determined by biogeochemical processes, affecting nutrient availability. For instance, in conjunction with purple-sulfur bacteria, the Fe/Mn ratio (Fig. S2.3) indicates deteriorated oxygen levels in benthic areas from 3.7 to 1.4 ka BP. This decline may have impacted other biogeochemical processes and benthic ecology, ultimately influencing the overall availability of P in the water column, as also suggested by the rising P/Fe ratio (Jensen et al., 1992) (Fig. S2.3). While caution is needed when using the Fe/Mn ratio, as well as other elemental ratios because diagenetic processes and landscape erosion affect element speciation (Makri et al., 2021), extended periods with severe anoxia that can intensify diagenetic processes are unlikely in shallow lakes, and surface runoff is minor in most Florida lakes (Brenner et al., 1990).

2.6.3 Eutrophication and Microcystins

Microcystin concentration levels are influenced by diverse abiotic and biotic factors, including nutrient availability, light intensity, high temperatures, increased primary production, and the presence of toxic cyanobacteria strains (Rastogi et al., 2014). In several sedimentary records, cyanotoxins were often detected prior to anthropogenic impacts, while modern increases tracked P additions (Clift and Waters, 2024; Efting et al., 2011; Waters, 2016; Waters et al., 2021; Zastepa et al., 2017). Surface sediments from a 47-lake dataset in Florida, USA, revealed a strong relationship between TP and MC concentrations (Lamb, 2021). In Lake Amatitlán, Guatemala, MC spikes coincided with increases in diatom markers, while high cyanobacteria abundance during the Maya prehistory was associated with low MC concentrations (Waters et al., 2021). In this study, MC concentrations were ordinated and closely correlated with general and colonial cyanobacteria, non-cyanobacteria producers, total primary producer abundance, and

TP (Fig. 2.3), perhaps with slightly less sensitivity to the exact timing of changes (Fig. 2.2).

Microcystins were detected throughout the record, with concentrations ranging from a minimum of 2.2 ng g org^{-1} at 2.8 ka BP to a maximum of 3,106 ng g org^{-1} in the top of the core. Interestingly, MC concentrations were at moderate levels in the bottom of the core, where average TP was close to moderate (Zone II/TP II), and pigments were absent or present in very low abundance (Fig. 2.2, Table 2.1). Microcystins are known to be robust molecules and could show higher levels of preservation as cellular components than pigments during the wetland period of Lake Wauberg. Around 2.4 ka BP, MCs concentration increased while only diatoms and total primary producer abundance (B-car) changed to higher concentrations (Fig. 2.2B). Afterward, MC concentrations increased dramatically, displaying earlier and more persistent peaks than cyanobacteria and exhibiting a 44-fold increase at the top zone compared to the period before 0.3 ka BP. While historic eutrophication helped sustain MCs production, moderate TP levels (TP II) decelerated their increase (Fig. 2.4C, J). In high and extreme TP (IIIa/b) levels, MCs exhibited a gradual increase, contrary to the decelerated increase in cyanobacteria pigments at extreme TP (IIIb) levels. Overall, MCs increased more prominently during accelerated nutrient additions (Fig. 2.4J) than cyanobacteria pigments (Fig. 2.4G-I), a pattern observed in other sedimentary records (Zastepa et al., 2017) and epilimnetic studies (Dolman et al., 2012). The observations from Lake Wauberg at high and extreme TP (IIIa/b) levels over the last 300 years are indicative of independent cyanotoxin concentrations from cyanobacteria abundance (Lawson et al., 2025) due to the increased presence of toxic cyanobacteria strains under P- and N-rich conditions (Vézie et al., 2002). Nevertheless, the relatively higher P to N enrichment, depicted by the decreasing N/P ratio during high MCs intervals, must have also been essential, as observed in tropical (Waters et al., 2021) and higher latitude lakes (Orihel et al., 2012).

The continuous presence of MCs and increased concentration over time are additional concerns to the high cyanobacteria abundance. The subtropical climate in Florida has provided optimal water temperatures for MCs production (Walls et al., 2018), and especially under the recent climate warming, with increasing minimum temperatures (Bachmann and Canfield, 2024), MCs can have a year-round occurrence. High nutrient availability can sustain the energy-intensive process of cyanotoxin synthesis, and oxidative stress resulting from increased biomass production can favor the dominance of toxic cyanobacteria strains (Wei et al., 2024). Additionally, the ongoing effects of climate change, with more frequent hydroclimatic extremes,

can alter the biogeochemical cycles in lakes (Jeppesen et al., 2021) and favor the production of cyanotoxins. Hence, including cyanotoxins in environmental lake assessments is crucial for developing comprehensive management practices and addressing health concerns for both humans and aquatic biota. The intracellular nature of MCs and the high resistance of toxin-potent resting cells after sediment deposition necessitates a holistic approach involving both water column and sediment studies. Especially in shallow lakes, resuspension events could potentially constitute another pathway of cyanotoxin loading (Clift, 2022; Waters, 2016), which can be exacerbated by reduced MC degradation under increased light attenuation in eutrophic conditions (Welker and Steinberg, 2000). Despite the relatively short half-life of extracellular MCs (Zhang et al., 2023), the bursting of MC cells at bottom sediments and the water solubility of extracellular MCs can become hazardous without warning by visible surface scum.

2.7 Conclusions

The long-term P enrichment in Lake Wauberg, Florida, has coincided with alterations in the primary producer community, producing persistent and toxic hypereutrophic conditions over the last millennia. High TP levels and an adequate supply of other macro- and micronutrients in the shallow subtropical setting promoted algal growth and cyanobacteria proliferation throughout the paleolimnological record. However, primary producer abundance and cyanotoxin concentration demonstrated a strong relationship only with TP. In contrast to low TP levels, moderate TP concentration produced a reduced response, suggesting alterations to the biogeochemical drivers and pathways associated with the primary producer community through time. Cyanobacteria and cyanotoxins increased remarkably once TP exceeded 2.2 mg g^{-1} around 0.3 ka BP. Despite the limited human development and agricultural activities in the catchment area, a more significant increase in TP since ~1892 CE indicates additional pollution from anthropogenic sources, leading to extreme TP levels exceeding 3 mg g^{-1} and a dramatic increase in MCs. It is inferred that the high TP worked in concert with altering N dynamics and hydrological conditions to maintain HAB conditions in the ecosystem.

2.8 References

A Florida Lake Gone. (1891, August 23) The Sun, p. 4. Retrieved from the NYS Historic Newspapers, https://www.nyshistoricnewspapers.org/?a=d&d=sun18910823-01.1.4.

Appleby PG, Oldfield F. (1983) The assessment of 210Pb data from sites with varying sediment accumulation rates. Hydrobiologia 103:29-35. https://doi.org/10.1007/BF00028424.

Appleby PG, Nolan PJ, Gifford DW, Godfrey MJ, Oldfield F, Anderson NJ, Battarbee RW. (1986) 210Pb dating by low background gamma counting. Hydrobiologia 143:21-27. https://doi.org/10.1007/BF00026640.

Arnade CW. (1961) Cattle raising in Spanish Florida, 1513-1763. Agricultural History 35:116-124. http://www.jstor.org/stable/3740622.

Arnold TE, Brenner M, Kenney WF, Bianchi TS. (2019) Recent trophic state changes of selected Florida lakes inferred from bulk sediment geochemical variables and biomarkers. Journal of Paleolimnology 62:409-423. https://doi.org/10.1007/s10933-019-00096-y.

Bachmann RW, Bigham DL, Hoyer MV, Canfield DE. (2012) Factors determining the distributions of total phosphorus, total nitrogen, and chlorophyll a in Florida lakes. Lake and Reservoir Management 28:10-26. https://doi.org/10.1080/07438141.2011.646458.

Bachmann RW, Canfield DE. (2024) An assessment of air and lake water temperatures (1981–2020) in Florida with a hindcast to 1895. Florida scientist 87: 38-60.

Bates AL, Spiker EC, Hatcher PG, Stout SA, Weintraub VC. (1995) Sulfur geochemistry of organic-rich sediments from Mud Lake, Florida, U.S.A. Chemical Geology 121:245-262. https://doi.org/10.1016/0009-2541(94)00122-O.

Battarbee RW, John Anderson N, Jeppesen E, Leavitt PR. (2005) Combining palaeolimnological and limnological approaches in assessing lake ecosystem response to nutrient reduction. Freshwater Biology 50:1772-1780. https://doi.org/10.1111/j.1365-2427.2005.01427.x.

Bjorndahl JA, Gushulak CAC, Mezzini S, Simpson GL, Haig HA, Leavitt PR, Finlay K. (2022) Abrupt changes in the physical and biological structure of endorheic upland lakes due to 8-m lake-level variation during the 20th century. Limnolology and Oceanography 67:1022-1039. https://doi.org/10.1002/lno.12054.

Blaauw M, Christen JA. (2011) Flexible paleoclimate age-depth models using an autoregressive gamma process. Bayesian Analysis 6:457-474, 418. https://doi.org/10.1214/11-BA618.

Bouaïcha N, Miles CO, Beach DG, Labidi Z, Djabri A, Benayache NY, Nguyen-Quang T. (2019) Structural diversity, characterization and toxicology of microcystins. Toxins (Basel) 11. https://doi.org/10.3390/toxins11120714.

Brenner M, Binford MW. (1986) Material transfer from water to sediment in Florida lakes. Hydrobiologia 143:55-61. https://doi.org/10.1007/BF00026645.

Brenner M, Binford MW, Deevey ES. (1990) Lakes. In: Myers RL, Ewel JJ (eds), Ecosystems of Florida. University of Central Florida Press, Orlando, pp 364-391.

Brenner M, Whitmore TJ, Flannery MS, Binford MW. (1993) Paleolimnological methods for defining target conditions in lake restoration: Florida case studies. Lake and Reservoir Management 7:209-217. https://doi.org/10.1080/07438149309354272.

Brenner M, Whitmore TJ, Curtis JH, Hodell DA, Schelske CL. (1999) Stable isotope (δ13C and δ15N) signatures of sedimented organic matter as indicators of historic lake trophic state. Journal of Paleolimnology 22:205-221. https://doi.org/10.1023/A:1008078222806.

Brenner M, Schelske CL, Kenney WF. (2004) Inputs of dissolved and particulate 226Ra to lakes and implications for 210Pb dating recent sediments. J Paleolimnol 32:53-66. https://doi.org/10.1023/B:JOPL.0000025281.54969.03
Burford MA, Willis A, Xiao M, Prentice MJ, Hamilton DP. (2023) Understanding the relationship between nutrient availability and freshwater cyanobacterial growth and abundance. Inland Waters 13:143-152. https://doi.org/10.1080/20442041.2023.2204050.

Canfield Jr DE, Hoyer MV. (1988) Regional geology and the chemical and trophic state characteristics of Florida lakes. Lake and Reservoir Management 4:21-31. https://doi.org/10.1080/07438148809354375.

Carpenter SR, Ludwig D, Brock WA. (1999) Management of eutrophication for lakes subject to potentially irreversible change. Ecological Applications 9:751-771. https://doi.org/10.2307/2641327.

Clift TL. (2022) Cyanotoxin production in subtropical lakes over the last 150 years with implications for human and ecosystem health. Master's thesis, Crop, Soil and Environmental Sciences. Auburn University, Auburn, Alabama.

Clift TL, Waters MN. (2024) Paleolimnological evidence for primary producer change linked to hydrologic connectivity and human impacts in Lake Carlton, Florida, USA. Journal of Paleolimnology 72:35-48. https://doi.org/10.1007/s10933-024-00318-y.

Conley DJ, Paerl HW, Howarth RW, Boesch DF, Seitzinger SP, Havens KE, Lancelot C, Likens GE. (2009) Controlling eutrophication: nitrogen and phosphorus. Science 323:1014-1015. https://doi.org/10.1126/science.1167755.

Cottingham KL, Rusak JA, Leavitt PR. (2000) Increased ecosystem variability and reduced predictability following fertilisation: Evidence from palaeolimnology. Ecology Letters 3:340-348. https://doi.org/10.1046/j.1461-0248.2000.00158.x.

Davies SJ, Lamb HF, Roberts SJ. (2015) Micro-XRF core scanning in palaeolimnology: recent developments. In: Croudace IW, Rothwell RG (eds), Micro-XRF Studies of Sediment Cores: Applications of a Non-Destructive Tool for the Environmental Sciences. Springer Netherlands, Dordrecht, pp 189-226. https://doi.org/10.1007/978-94-017-9849-5_7.

Dean WE. (1974) Determination of carbonate and organic matter in calcareous sediments and sedimentary rocks by loss on ignition; comparison with other methods. Journal of Sediment Research 44:242-248. https://doi.org/10.1306/74D729D2-2B21-11D7-8648000102C1865D.

Dolman AM, Rücker J, Pick FR, Fastner J, Rohrlack T, Mischke U, Wiedner C. (2012) Cyanobacteria and cyanotoxins: The influence of nitrogen versus phosphorus. PLOS ONE 2012; 7: e38757. https://doi.org/10.1371/journal.pone.0038757.

Efting AA, Snow DD, Fritz SC. (2011) Cyanobacteria and microcystin in the Nebraska (USA) Sand Hills Lakes before and after modern agriculture. Journal of Paleolimnology 46:17-27. https://doi.org/10.1007/s10933-011-9511-3.

Elser JJ, Bracken MES, Cleland EE, Gruner DS, Harpole WS, Hillebrand H, Ngai JT, Seabloom EW, Shurin JB, Smith JE. (2007) Global analysis of nitrogen and phosphorus limitation of primary producers in freshwater, marine and terrestrial ecosystems. Ecology Letters 10:1135-1142. https://doi.org/10.1111/j.1461-0248.2007.01113.x.

Filley TR, Freeman KH, Bianchi TS, Baskaran M, Colarusso LA, Hatcher PG. (2001) An isotopic biogeochemical assessment of shifts in organic matter input to Holocene sediments from Mud Lake, Florida. Organic Geochemistry 32:1153-1167. https://doi.org/10.1016/S0146-6380(01)00063-8.

Filstrup CT, Downing JA. (2017) Relationship of chlorophyll to phosphorus and nitrogen in nutrient-rich lakes. Inland Waters 7:385-400. https://doi.org/10.1080/20442041.2017.1375176.

Finlay JC, Small GE, Sterner RW. (2013) Human influences on nitrogen removal in lakes. Science 342:247-250. https://www.science.org/doi/abs/10.1126/science.1242575.

Fisher MM, Brenner M, Reddy KR. (1992) A simple, inexpensive piston corer for collecting undisturbed sediment/water interface profiles. Journal of Paleolimnology 7:157-161. https://doi.org/10.1007/BF00196870

Florida Department of Environmental Protection. (2013). Paynes Prairie Preserve State Park. Unit Management Plan. Retrieved from the Florida Department of Environmental Protection, https://floridadep.gov/parks/parks-office-park-planning/documents/paynes-prairie-preserve-state-park.

Genkai-Kato M, Vadeboncoeur Y, Liboriussen L, Jeppesen E. (2012) Benthic–planktonic coupling, regime shifts, and whole-lake primary production in shallow lakes. Ecology 93:619-631. https://doi.org/10.1890/10-2126.1.

Gu B, Chapman AD, Schelske CL. (2006) Factors controlling seasonal variations in stable isotope composition of particulate organic matter in a softwater eutrophic lake. Limnology and Oceanography 51:2837-2848. https://doi.org/10.4319/lo.2006.51.6.2837.

Hoyer MV, Bigham DL, Bachmann RW, Canfield DE. (2014) Florida LAKEWATCH: Citizen scientists protecting Florida's aquatic systems. Florida Scientist 77:184-197. http://www.jstor.org/stable/24321923.

Huang S, Zhang K, Lin Q, Liu J, Shen J. (2022) Abrupt ecological shifts of lakes during the Anthropocene. Earth-Science Reviews 227:103981. https://doi.org/10.1016/j.earscirev.2022.103981.

Jensen HS, Kristensen P, Jeppesen E, Skytthe A. (1992) Iron:phosphorus ratio in surface sediment as an indicator of phosphate release from aerobic sediments in shallow lakes. In: Hart BT, Sly PG (eds), Sediment/Water Interactions. Springer Netherlands, Dordrecht, pp 731-743. https://doi.org/10.1007/BF00026261.

Jeppesen E, Pierson D, Jennings E. (2021) Effect of extreme climate events on lake ecosystems. Water 13: 282. https://doi.org/10.3390/w13030282.

Karmakar M, Leavitt PR, Cumming BF. (2015) Enhanced algal abundance in northwest Ontario (Canada) lakes during the warmer early-to mid-Holocene period. Quaternary Science Reviews 123:168-179. https://doi.org/10.1016/j.quascirev.2015.06.025.

Kenney WF, Waters MN, Schelske CL, Brenner M. (2002) Sediment records of phosphorus-driven shifts to phytoplanktondominance in shallow Florida lakes. Journal of Paleolimnology 27:367-377. https://doi.org/10.1371/journal.pone.0147331.

Kenney WF, Brenner M, Curtis JH, Arnold TE, Schelske CL. (2016) A Holocene Sediment Record of Phosphorus Accumulation in Shallow Lake Harris, Florida (USA) Offers New Perspectives on Recent Cultural Eutrophication. PLOS ONE 11:e0147331. https://doi.org/10.1023/A:1016075012581.

Kindinger JL, Davis JB, Flocks JG. (1999) Geology and evolution of lakes in north-central Florida. Environmental Geology 38:301-321. https://doi.org/10.1007/s002540050428.

Kirol AP, Morales-Williams AM, Braun DC, Marti CL, Pierson OE, Wagner KJ, Schroth AW. (2024) Linking sediment and water column phosphorus dynamics to oxygen, temperature, and aeration in shallow eutrophic lakes. Water Resources Research 60: e2023WR034813. https://doi.org/10.1029/2023WR034813.

Kosten S, Huszar VL, Bécares E, Costa LS, van Donk E, Hansson LA, Jeppesen E, Kruk C, Lacerot G, Mazzeo N. (2012) Warmer climates boost cyanobacterial dominance in shallow lakes. Global Change Biology 18:118-126. https://doi.org/10.1111/j.1365-2486.2011.02488.x.

Kronvang B, Jeppesen E, Conley DJ, Søndergaard M, Larsen SE, Ovesen NB, Carstensen J. (2005) Nutrient pressures and ecological responses to nutrient loading reductions in Danish streams, lakes and coastal waters. Journal of Hydrology 304:274-288. https://doi.org/10.1016/j.jhydrol.2004.07.035.

Lamb A. (2021) Using Sediments to Identify Drivers of Cyanobacteria, Cyanotoxins, and Eutrophication in the Shallow, Subtropical Lakes of Florida, USA. Master's thesis, Crop Soils and Environmental Sciences, Auburn University, Auburn, Alabama.

Lawson GM, Young JL, Aanderud ZT, Jones EF, Bratsman S, Daniels J, Malmfeldt MP, Baker MA, Abbott BW, Daly S, Paerl HW, Carling G, Brown B, Lee R, Wood RL. (2025) Nutrient limitation and seasonality associated with phytoplankton communities and cyanotoxin production in a large, hypereutrophic lake. Harmful Algae 143:102809. https://doi.org/10.1016/j.hal.2025.102809.

Leavitt PR. (1993) A review of factors that regulate carotenoid and chlorophyll deposition and fossil pigment abundance. Journal of Paleolimnology 9:109-127. https://doi.org/10.1007/BF00677513.

Leavitt, P., Hodgson, D., 2001. Sedimentary pigments. In: Smol, J.P., Birks, H.J.B., Last, W.M., Bradley, R.S., Alverson, K. (eds), Tracking environmental change using lake sediments. Springer, pp. 295–325. https://doi.org/10.1007/0-306-47668-1_15.

Liang Z, Soranno PA, Wagner T. (2020) The role of phosphorus and nitrogen on chlorophyll a: Evidence from hundreds of lakes. Water Research 185:116236. https://doi.org/10.1016/j.watres.2020.116236.

Liao X, Nair VD, Canion A, Dobberfuhl DR, Foster DK, Inglett PW. (2019) Subsurface transport and potential risk of phosphorus to groundwater across different land uses in a karst springs basin, Florida, USA. Geoderma 338: 97-106. https://doi.org/10.1016/j.geoderma.2018.11.005

Lin Q, Zhang K, McGowan S, Huang S, Xue Q, Capo E, Zhang C, Zhao C, Shen J. (2023) Characterization of lacustrine harmful algal blooms using multiple biomarkers: Historical processes, driving synergy, and ecological shifts. Water Research 235:119916. https://doi.org/10.1016/j.watres.2023.119916.

Lisboa MS, Schneider RL, Rudstam LG, Walter MT. (2024) Groundwater inputs could be a significant but often overlooked source of phosphorus in lake ecosystems. Scientific Reports 14:16269. https://doi.org/10.1038/s41598-024-66985-z.

Makri S, Wienhues G, Bigalke M, Gilli A, Rey F, Tinner W, Vogel H, Grosjean M. (2021) Variations of sedimentary Fe and Mn fractions under changing lake mixing regimes, oxygenation and land surface processes during Late-glacial and Holocene times. Science of the Total Environment 755:143418. https://doi.org/10.1016/j.scitotenv.2020.143418.

Matheson & Mcmillan Publishers. (1880) Map of Alachua County, Florida. Gainesville, Florida: Matheson & McMillan Publishers. Retrieved from the Library of Congress, https://www.loc.gov/item/2012592398/.

McGowan S, Britton G, Haworth E, Moss B. (1999) Ancient blue-green blooms. Limnology and Oceanography 44:436-439. https://doi.org/10.4319/lo.1999.44.2.0436.

Meerhoff M, Audet J, Davidson TA, De Meester L, Hilt S, Kosten S, Liu Z, Mazzeo N, Paerl H, Scheffer M, Jeppesen E. (2022) Feedback between climate change and eutrophication: revisiting the allied attack concept and how to strike back. Inland Waters 12:187-204. https://doi.org/10.1080/20442041.2022.2029317.

Meinikmann K, Hupfer M, Lewandowski J. (2015) Phosphorus in groundwater discharge – A potential source for lake eutrophication. Journal of Hydrology 524:214-226. https://doi.org/10.1016/j.jhydrol.2015.02.031.

Mendieta KL, Gerber S, Brenner M. (2018) Florida wildfires during the Holocene Climatic Optimum (9000–5000 cal yr BP). Journal of Paleolimnology 60:51-66. https://doi.org/10.1007/s10933-018-0023-2.

Meyers PA, Ishiwatari R. (1993) Lacustrine organic geochemistry—an overview of indicators of organic matter sources and diagenesis in lake sediments. Organic Geochemistry 20:867-900. https://doi.org/10.1016/0146-6380(93)90100-P.

Missimer TM, Thomas S, Rosen BH. (2021) Legacy phosphorus in Lake Okeechobee (Florida, USA) sediments: A review and new perspective. Water 13: 39. https://doi.org/10.3390/w13010039.

Moss B, Kosten S, Meerhoff M, Battarbee RW, Jeppesen E, Mazzeo N, Havens K, Lacerot G, Liu Z, De Meester L, Paerl H, Scheffer M. (2011) Allied attack: climate change and eutrophication. Inland Waters 1:101-105. https://doi.org/10.5268/IW-1.2.359.

Nisbeth CS, Kidmose J, Weckström K, Reitzel K, Odgaard BV, Bennike O, Thorling L, McGowan S, Schomacker A, Kristensen DLJ, Jessen S. (2019) Dissolved inorganic geogenic phosphorus load to a groundwater-fed lake: Implications of terrestrial phosphorus cycling by groundwater. Water 11: 2213. https://doi.org/10.3390/w11112213.

Orihel DM, Bird DF, Brylinsky M, Chen H, Donald DB, Huang DY, Giani A, Kinniburgh D, Kling H, Kotak BG, Leavitt PR, Nielsen CC, Reedyk S, Rooney RC, Watson SB, Zurawell RW, Vinebrooke RD. (2012) High microcystin concentrations occur only at low nitrogen-to-phosphorus ratios in nutrient-rich Canadian lakes. Canadian Journal of Fisheries and Aquatic Sciences 69: 1457-1462. https://doi.org/10.1139/f2012-088.

Patil I. (2021) Visualizations with statistical details: The 'ggstatsplot' approach. Journal of Open Source Software 6:3167. https://doi.org/10.21105/joss.03167.

Pollock AL, van Beynen PE, DeLong KL, Polyak V, Asmerom Y. (2017) A speleothem-based mid-Holocene precipitation reconstruction for West-Central Florida. Holocene 27:987-996. https://doi.org/10.1177/0959683616678463.

Quinlan R, Filazzola A, Mahdiyan O, Shuvo A, Blagrave K, Ewins C, Moslenko L, Gray DK, O'Reilly CM, Sharma S. (2021) Relationships of total phosphorus and chlorophyll in lakes worldwide. Limnology and Oceanography 66:392-404. https://doi.org/10.1002/lno.11611.

R Core Team (2024) R: A language and environment for statistical computing. R Foundation for Statistical Computing, Vienna, Austria. https://www.R-project.org/.

Rastogi RP, Sinha RP, Incharoensakdi A. (2014) The cyanotoxin-microcystins: current overview. Reviews in Environmental Science and Bio/Technology 13:215-249. https://doi.org/10.1007/s11157-014-9334-6.

Reimer PJ, Austin WEN, Bard E, Bayliss A, Blackwell PG, Bronk Ramsey C, Butzin M, Cheng H, Edwards RL, Friedrich M, Grootes PM, Guilderson TP, Hajdas I, Heaton TJ, Hogg AG, Hughen KA, Kromer B, Manning SW, Muscheler R, Palmer JG, Pearson C, van der Plicht J, Reimer RW, Richards DA, Scott EM, Southon JR, Turney CSM, Wacker L, Adolphi F, Büntgen U, Capano M, Fahrni SM, Fogtmann-Schulz A, Friedrich R, Köhler P, Kudsk S, Miyake F, Olsen J, Reinig F, Sakamoto M, Sookdeo A, Talamo S. (2020) The IntCal20 Northern Hemisphere radiocarbon age calibration curve (0–55 cal kBP). Radiocarbon 62:725-757. https://doi.org/10.1017/RDC.2020.41.

Riedinger-Whitmore MA, Whitmore TJ, Smoak JM, Brenner M, Moore A, Curtis J, Schelske CL. (2005) Cyanobacterial proliferation is a recent response to eutrophication in many Florida lakes: A paleolimnological assessment. Lake and Reservoir Management 21:423-435. https://doi.org/10.1080/07438140509354447.

Schelske CL, Peplow A, Brenner M, Spencer CN. (1994) Low-background gamma counting: applications for 210Pb dating of sediments. Journal of Paleolimnology 10:115-128. https://doi.org/10.1007/BF00682508.

Schelske CL, Lowe EF, Battoe LE, Brenner M, Coveney MF, Kenney WF. (2005) Abrupt biological response to hydrologic and land-use changes in Lake Apopka, Florida, USA. Ambio 34:192-198, 197. https://doi.org/10.1579/0044-7447-34.3.192.

Schindler DW. (1974) Eutrophication and recovery in Experimental Lakes: implications for lake management. Science 184:897-899. https://doi.org/10.1126/science.184.4139.897.

Schindler DW, Hecky RE, Findlay DL, Stainton MP, Parker BR, Paterson MJ, Beaty KG, Lyng M, Kasian SEM. (2008) Eutrophication of lakes cannot be controlled by reducing nitrogen input: Results of a 37-year whole-ecosystem experiment. PNAS 105:11254-11258. https://doi.org/10.1073/pnas.0805108105.

Scott JT, McCarthy MJ, Paerl HW. (2019) Nitrogen transformations differentially affect nutrient-limited primary production in lakes of varying trophic state. Limnology & Oceanography Letters 4:96-104. https://doi.org/10.1002/lol2.10109.

Scott TM. (1992) A geological overview of Florida. Florida Geological Survey. Accessed online Oct. 7, 2024, https://doi.org/10.35256/OFR50.

Soto LR. (2005) Reconstruction of late Holocene precipitation for Central Florida as derived from isotopes in speleothems. USF Tampa Graduate Theses and Dissertations. https://digitalcommons.usf.edu/etd/872/.

Søndergaard M, Jensen JP, Jeppesen E. (2003) Role of sediment and internal loading of phosphorus in shallow lakes. Hydrobiologia 506:135-145. https://doi.org/10.1023/B:HYDR.0000008611.12704.dd.

Tang Y, Horikoshi M, Li W. (2016) ggfortify: Unified interface to visualize statistical result of popular R packages. The R Journal 8:474–485. https://doi.org/10.32614/RJ-2016-060.

Urban NR, Ernst K, Bernasconi S. (1999) Addition of sulfur to organic matter during early diagenesis of lake sediments. Geochimica et Cosmochimica Acta 63:837-853. https://doi.org/10.1016/S0016-7037(98)00306-8.

Vézie C, Rapala J, Vaitomaa J, Seitsonen J, Sivonen K. (2002) Effect of nitrogen and phosphorus on growth of toxic and nontoxic Microcystis strains and on intracellular microcystin concentrations. Microbial Ecology 43:443-454. https://doi.org/10.1007/s00248-001-0041-9.

Walls JT, Wyatt KH, Doll JC, Rubenstein EM, Rober AR. (2018) Hot and toxic: Temperature regulates microcystin release from cyanobacteria. Science of the Total Environment 610-611: 786-795. https://doi.org/10.1016/j.scitotenv.2017.08.149.

Waters MN, Piehler M F, Smoak JM, Bianchi TS. (2012) Algal community responses to shallow lake dystrophication. Canadian lakes. Canadian Journal of Fisheries and Aquatic Sciences 69:1433-1443. https://doi.org/10.1139/f2012-021.

Waters MN, Schelske CL, Brenner M. (2015) Cyanobacterial dynamics in shallow Lake Apopka (Florida, U.S.A.) before and after the shift from a macrophyte-dominated to a phytoplankton-dominated state. Freshwater Biology 60:1571-1580. https://doi.org/10.1111/fwb.12589.

Waters MN. (2016) A 4700-year history of cyanobacteria toxin production in a shallow subtropical lake. Ecosystems 19:426-436. https://doi.org/10.1007/s10021-015-9943-0.

Waters MN, Brenner M, Curtis JH, Romero-Oliva CS, Dix M, Cano M. (2021) Harmful algal blooms and cyanotoxins in Lake Amatitlán, Guatemala, coincided with ancient Maya occupation in the watershed. PNAS 118:e2109919118. https://doi.org/10.1073/pnas.2109919118.

Wei N, Hu C, Dittmann E, Song L, Gan N. (2024) The biological functions of microcystins. Water Research 262:122119. https://doi.org/10.1016/j.watres.2024.122119.

Welker M, Steinberg C. (2000) Rates of humic substance photosensitized degradation of Microcystin-LR in natural waters. Environmental Science & Technology 34: 3415-3419. https://doi.org/10.1021/es991274t.

Whitmore TJ, Brenner M, Schelske CL. (1996) Highly variable sediment distribution in shallow, wind-stressed lakes: a case for sediment-mapping surveys in paleolimnological studies. Journal of Paleolimnology 15:207-221. https://doi.org/10.1007/BF00213041.

Willard DA. (2023) Pollen records, postglacial-Southeastern North America. In: Elias SA, Mock CJ (eds) Encyclopedia of Quaternary Science (Third Edition), Elsevier, pp 553–563. https://doi.org/10.1016/B978-0-323-99931-1.00030-1.

Williams JW, Grimm EC, Blois JL, Charles DF, Davis EB, Goring SJ, Graham RW, Smith AJ, Anderson M, Arroyo-Cabrales J, Ashworth AC, Betancourt JL, Bills BW, Booth RK, Buckland PI, Curry BB, Giesecke T, Jackson ST, Latorre C, Nichols J, Purdum T, Roth RE, Stryker M, Takahara H. (2018) The Neotoma Paleoecology Database, a multiproxy, international, community-curated data resource. Quaternary Research 89:156-177. https://doi.org/10.1017/qua.2017.105.

Zastepa A, Taranu ZE, Kimpe LE, Blais JM, Gregory-Eaves I, Zurawell RW, Pick FR. (2017) Reconstructing a long-term record of microcystins from the analysis of lake sediments. Science of the Total Environment 579:893-901. https://doi.org/10.1016/j.scitotenv.2016.10.211.

Zhang Y, Whalen JK, Cai C, Shan K, Zhou H. (2023) Harmful cyanobacteria-diatom/dinoflagellate blooms and their cyanotoxins in freshwaters: A nonnegligible chronic health and ecological hazard. Water Research 233:119807. https://doi.org/10.1016/j.watres.2023.119807.

Zhou J, Leavitt PR, Zhang Y, Qin B. (2022) Anthropogenic eutrophication of shallow lakes: Is it occasional? Water Research 221:118728. https://doi.org/10.1016/j.watres.2022.118728.

2.9 Tables

Table 2.1 The average concentrations and standard deviations for the analyzed variables are distributed in the four chronological TP-defined sediment zones with significant ($p<0.05$) differences (Table S2.2). The nitrogen isotope analysis was performed on 43 instead of 96 samples, which were 4, 10, 15, and 14 samples in each zone, respectively.

Variable	Unit	Zone Ø 6.9-5 ka BP (n=8)	Zone I 5-2.2 ka BP (n=23)	Zone II 2.2-0.3 ka BP (n=38)	Zone III 0.3 ka BP-pres. (n=27)
TP	mg g^{-1}	1.78 (±0.4)	0.81 (±0.2)	1.93 (±0.3)	2.82 (±0.7)
TOC	%	5.51 (±5.2)	41.64 (±2.5)	35.82 (±3.5)	32.05 (±4.5)
TN	%	0.53 (±0.4)	3.65 (±0.3)	3.09 (±0.3)	2.94 (±0.4)
TOC / TN	-	11.14 (±1.9)	13.34 (±0.4)	13.6 (±1.4)	12.89 (±2)
TN / TP	-	6.53 (±4.3)	107.72 (±37.2)	36.35 (±6.8)	24.05 (±5.6)
TS	mg g^{-1}	0.58 (±0.6)	5.63 (±0.8)	5.3 (±1.3)	5.64 (±1.1)
$\delta^{15}N$	‰ AIR	2.22 (±0.35)	1.67 (±0.73)	1.57 (±0.35)	1.07 (±0.29)
Beta-carotene	nmol g^{-1} org	1.18 (±2.3)	25.79 (±7.4)	68.32 (±26.3)	266.76 (±135.6)
Diatoxanthin	nmol g^{-1} org	0.31 (±0.2)	3.58 (±2.5)	18.36 (±13.3)	28.64 (±12.8)
Alloxanthin	nmol g^{-1} org	0.45 (±0.5)	3.11 (±1)	5.21 (±2.3)	73.53 (±57)
Echinenone	nmol g^{-1} org	0.32 (±0.6)	5.71 (±1.8)	6.95 (±3.1)	49.58 (±31)
Canthaxanthin	nmol g^{-1} org	0.95 (±0.9)	7.51 (±1.8)	9.65 (±4)	53.29 (±21.6)
Okenone	nmol g^{-1} org	-	1.44 (±0.7)	3.85 (±1.6)	1.23 (±3.1)
Microcystins	ng g^{-1} org	6.25 (±4.1)	5.04 (±3.3)	8.92 (±5.7)	329.7 (±723.7)

2.10 Figures

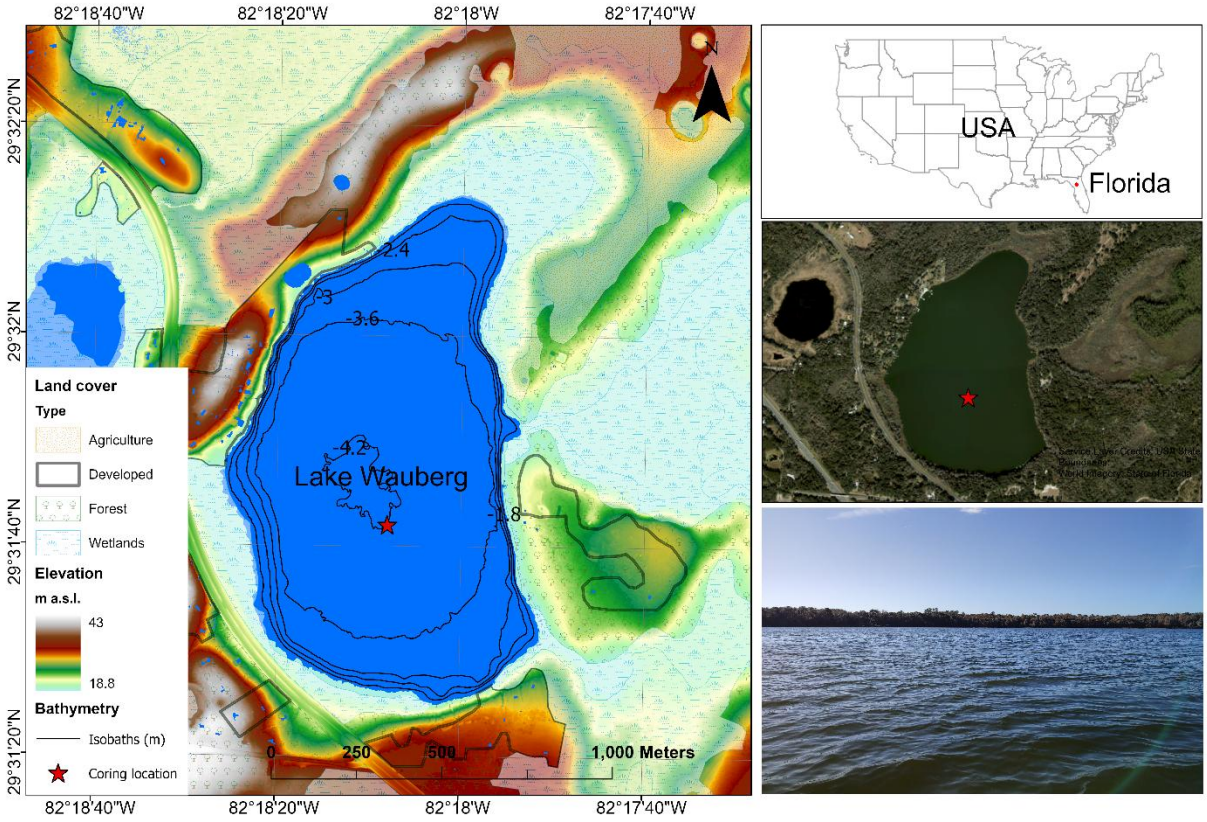

Figure 2.1 Location, elevation, bathymetry, and land use/cover maps of Lake Wauberg. The surrounding landscape is primarily composed of wetlands and forestland. The most notable human-made structure is US-441. The picture was taken from the anchor point at the coring site. GIS layer sources: section 2.3.5.

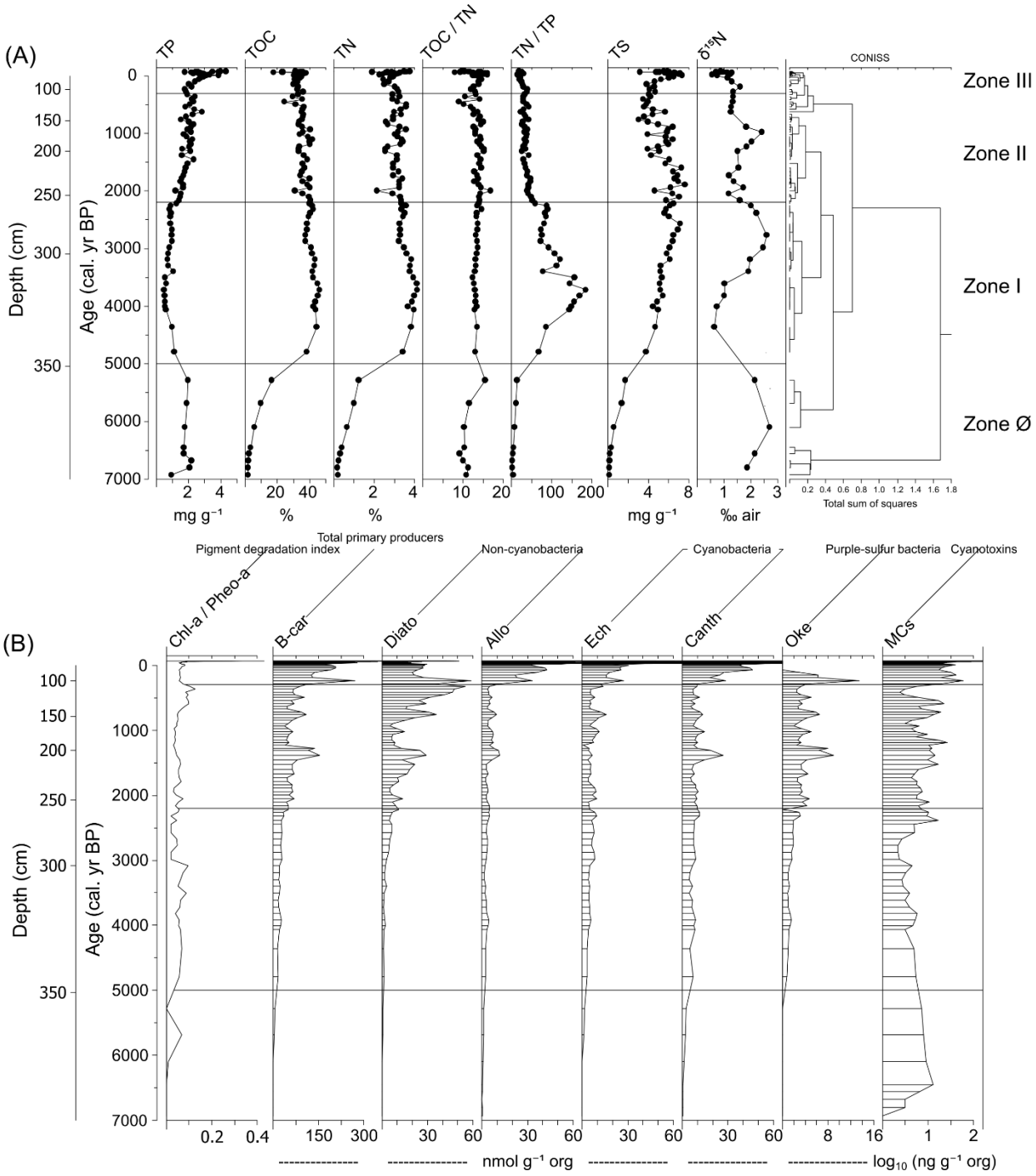

Figure 2.2 Time plots of (A) nutrients, elemental ratios, and ratio of stable N isotopes and (B) photosynthetic pigments and cyanotoxins. The solid lines delineate the zones (Ø, I, II, III) based on the dendrogram of changes in TP concentration. The pigment degradation index is the chlorophyll-a (chl-a) ratio to pheophytin-a (pheo-a). The photosynthetic pigments are beta-carotene (B-car), diatoxanthin (Diato), alloxanthin (Allo), echinenone (Ech), canthaxanthin (Canth), and okenone (Oke). An analytical description of each photosynthetic pigment is presented in Table S2.3. Cyanotoxin concentration measures total microcystins (MCs) on a $\log_{10}$ scale. Apart from diato, the photosynthetic pigment and cyanotoxin concentrations over the period with increased pigment preservation (high chl-a / pheo-a over the last ~10 years) have been truncated.

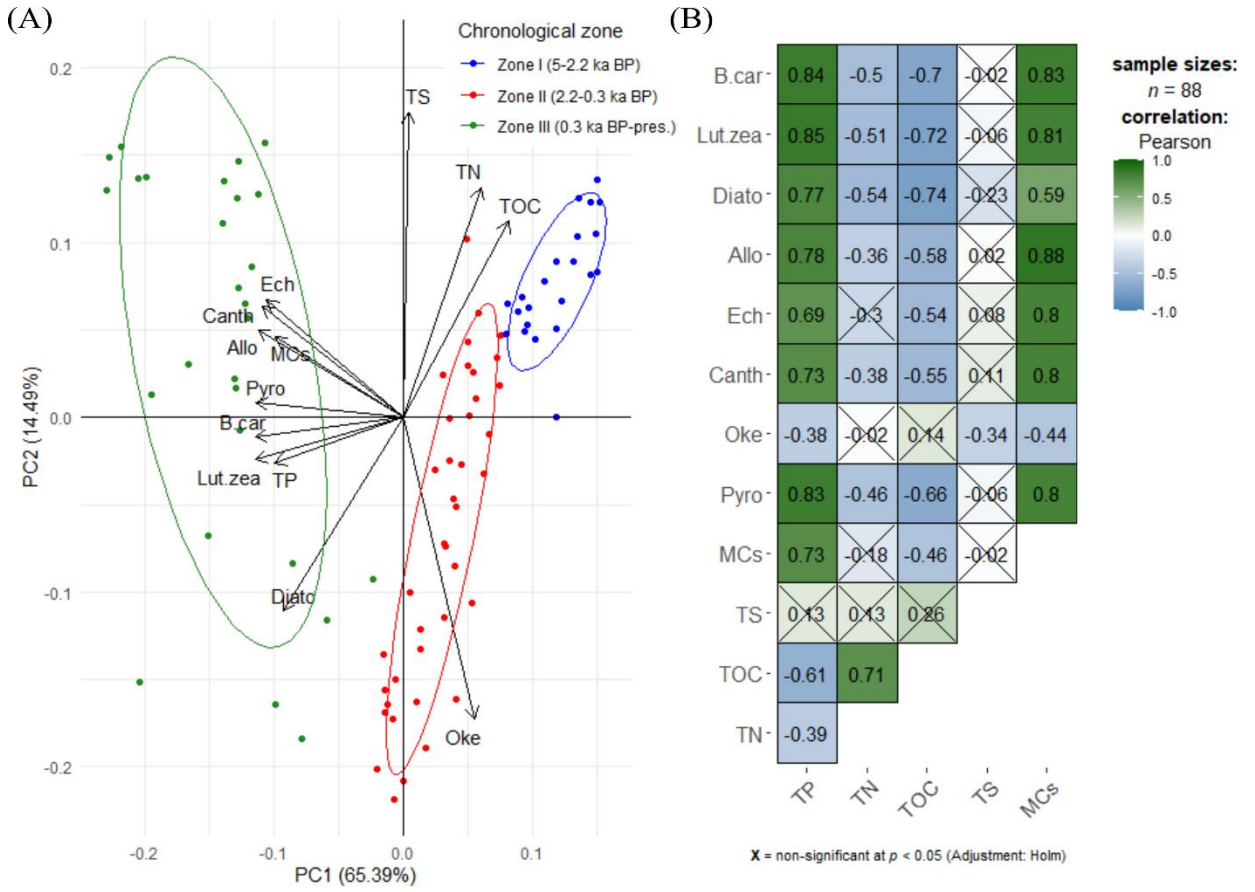

Figure 2.3 Data exploration through (A) Principal component analysis (PCA) and (B) Pearson correlation analysis. The photosynthetic pigments used in both analyses are beta-carotene (B.car), lutein+zeaxanthin (Lut.zea), diatoxanthin (Diato), alloxanthin (Allo), echinenone (Ech), canthaxanthin (Canth), okenone (Oke), and pyropheophorbide (Pyro). (A) Dimensionality reduction using PCA. The plot presents the variance in the dataset using PC1 (65.39%) and PC2 (14.49%) while grouping the data points into the three chronological zones (I-III) with limnological conditions over the last 5 ka BP. The oval shapes represent 68% confidence intervals. (B) Correlation matrices with photosynthetic pigments, MCs, TP, and elemental ratios with samples spanning the last 5 ka BP.

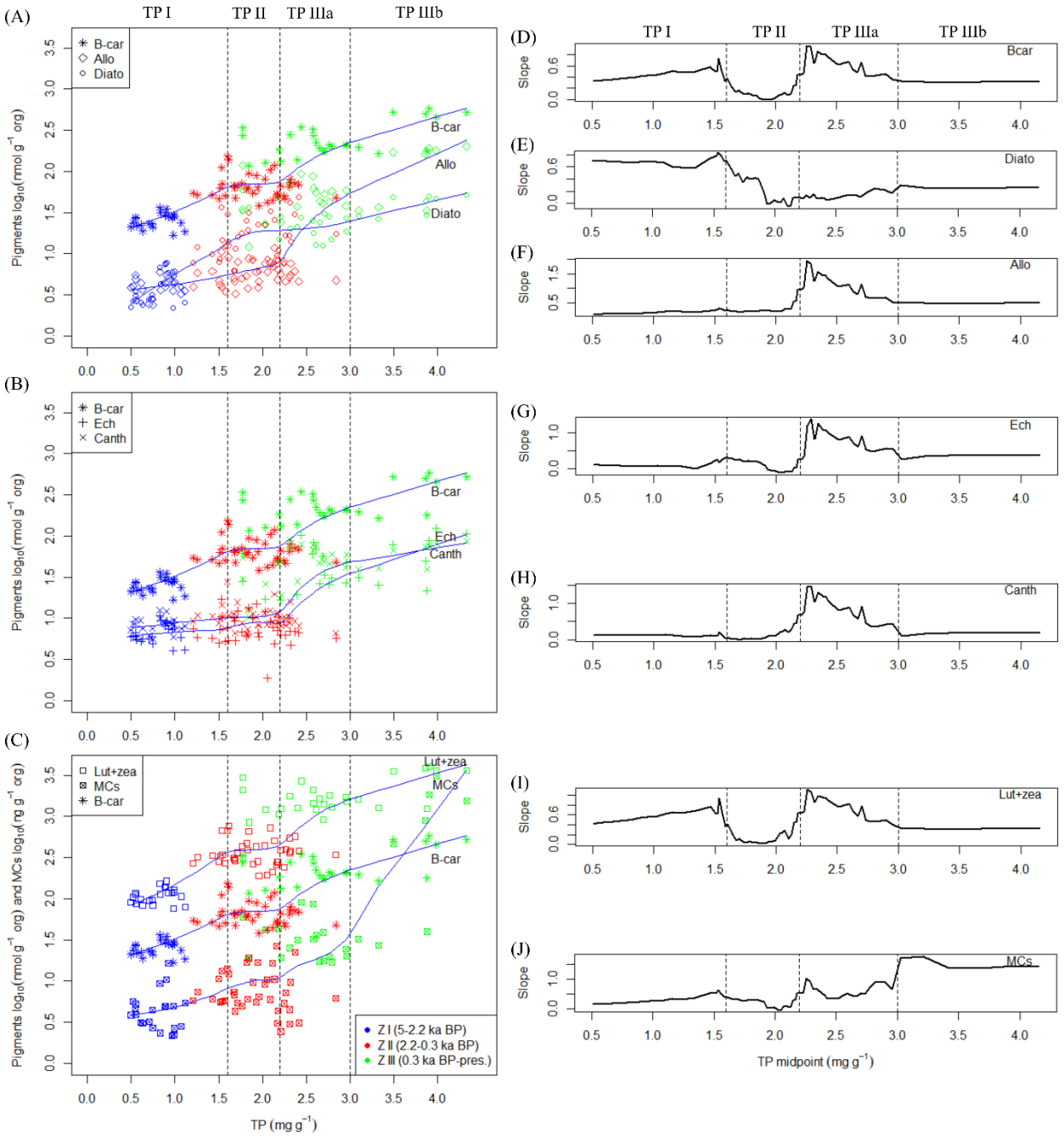

Figure 2.4 Scatter plots (A-C) with LOWESS smoother depicting the relationship between log scale photosynthetic pigments and cyanotoxins with TP (mg g^{-1}). Each panel includes total primary producer abundance (B-car) and (A) non-cyanobacteria pigments (allo and diato), (B) cyanobacteria pigments (canth and ech), and (C) green algae with cyanobacteria (lut+zea), and cyanotoxins (MCs) with samples spanning over the last 5 ka BP. Line plots (D-J) depicting the slope change of the LOWESS curves in (D) beta-carotene, (E) diatoxanthin, (F) alloxanthin, (G) echinenone, (H) canthaxanthin, (I) lutein+zeaxanthin, and (J) microcystins. Based on the hierarchical clustering of slope change values, the dashed lines delineate four TP (I, II, IIIa, IIIb) concentration intervals (<1.6, 1.6-2.2, 2.2-3, and >3 mg g^{-1}) that roughly correspond to the chronological zones (I-III).

2.11 Supplemental Tables

Table S2.1 List of radiocarbon-dated samples. The calibrated dates were estimated online by Calib 8.2 (http://calib.org/calib/calib.html) using IntCal20.

Laboratory no.	Depth (cm)	Material	Age ^{14}C BP ± error	Calibrated years BP (2 sigma median)
OS-170575	200	charcoal	1,380 ± 30	1,299
OS-168302	220	charcoal	1,830 ± 40	1,734
OS-168303	276	charcoal	1,970 ± 35	1,901
OS-168304	336	charcoal	3,730 ± 45	4,079
OS-168095	340	twig	3,670 ± 25	4,009
OS-168305	364	charcoal	5,700 ± 25	6,475

Table S2.2 The analysis of variance (ANOVA) indicated significant differences between the TP zones (Ø-III) ($p<<2e^{-16}$), and ANOVA was followed by Tukey's post-hoc test to determine the significance between the successive zones.

Zone	Difference	Lower bound	Upper bound	Adjusted p-value
Zone Ø – Zone I	0.9898200	0.4893540	1.4902860	0.0000079
Zone I – Zone II	-1.1212927	-1.4445077	-0.7980776	0.0000000
Zone II – Zone III	-0.9039460	-1.2074246	-0.6004674	0.0000000

Table S2.3 List of photosynthetic pigments, their preservation ranging from high (1) to low (3), and their role as markers of aquatic community composition. The table is adapted from Leavitt and Hodgson (2001) and Waters (2016).

Photosynthetic pigment	Abbreviation	Preservation	Aquatic marker
Beta-carotene	B-car	1	Total primary producer abundance
Chlorophyll-a	Chl-a	3	Total primary producer abundance
Pheophytin-a	Pheo-a	1	Chl-a derivative
Chlorophyll-b	Chl-b	2	Total primary producer abundance
Pheophytin-b	Pheo-b	2	Chl-b derivative
Pyropheophorbide	Pyro	2	Zooplankton grazing
Alloxanthin	Allo	1	Cryptophyta
Diatoxanthin	Diato	2	Diatoms
Lutein + zeaxanthin	Lut+zea	1	Green algae and cyanobacteria
Aphanizophyll	Aphani	2	N_2-fixing cyanobacteria
Echinenone	Ech	1	Cyanobacteria
Oscillaxanthin	Osc	2	Cyanobacteria
Canthaxanthin	Canth	1	Colonial cyanobacteria
Okenone	Oke	1	Purple-sulfur bacteria

Table S2.4 The average concentrations and standard deviations for the analyzed variables distributed in the four chronological TP-defined sediment zones.

Variable	Unit	Zone Ø 6.9-5 ka BP (n=8)	Zone I 5-2.2 ka BP (n=23)	Zone II 2.2-0.3 ka BP (n=38)	Zone III 0.3 ka BP-pres. (n=27)
Bulk Density	g cm^{-3}	0.70 (±0.34)	0.07 (±0.00)	0.07 (±0.01)	0.05 (±0.02)
Loss-on-ignition	%	11.64 (±8.5)	74.18 (±4.9)	61.54 (±28.4)	56.08 (±9.2)
P / Fe	-	0.91 (±0.3)	0.18 (±0.1)	0.74 (±0.3)	1.02 (±0.1)
Fe / Mn	-	48.57 (±9.6)	41.41 (±6.9)	51.16 (±4.7)	33.94 (±6)
Lutein+zeaxanthin	nmol g^{-1} org	7.96 (±8.7)	118.19 (±49.5)	390.7 (±152.6)	1968.13 (±993.3)
Aphanizophyll	nmol g^{-1} org	-	-	0.24 (±0.4)	22.03 (±17.3)
Oscilloxanthin	nmol g^{-1} org	-	-	10.29 (±10.3)	167.19 (±102.8)
Pyropheophorbide	nmol g^{-1} org	0.58 (±0.93)	9.57 (±3.2)	26.26 (±13)	281.97 (±104.8)

2.12 Supplemental Figures

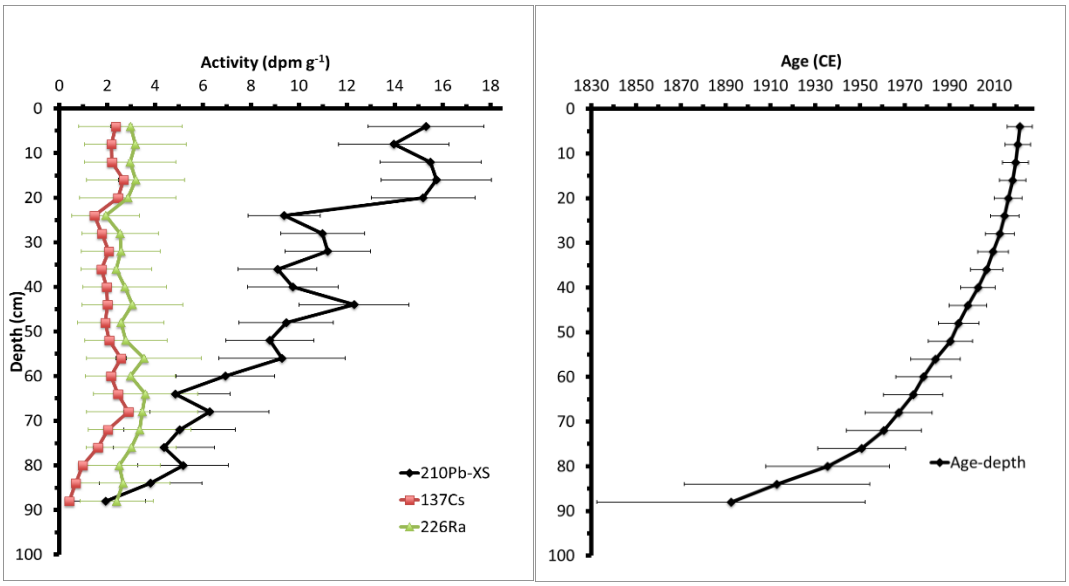

Figure S2.1 Excess ^{210}Pb, ^{137}Cs and ^{226}Ra activities (left) and age-depth relationship determined by the CRS model (right).

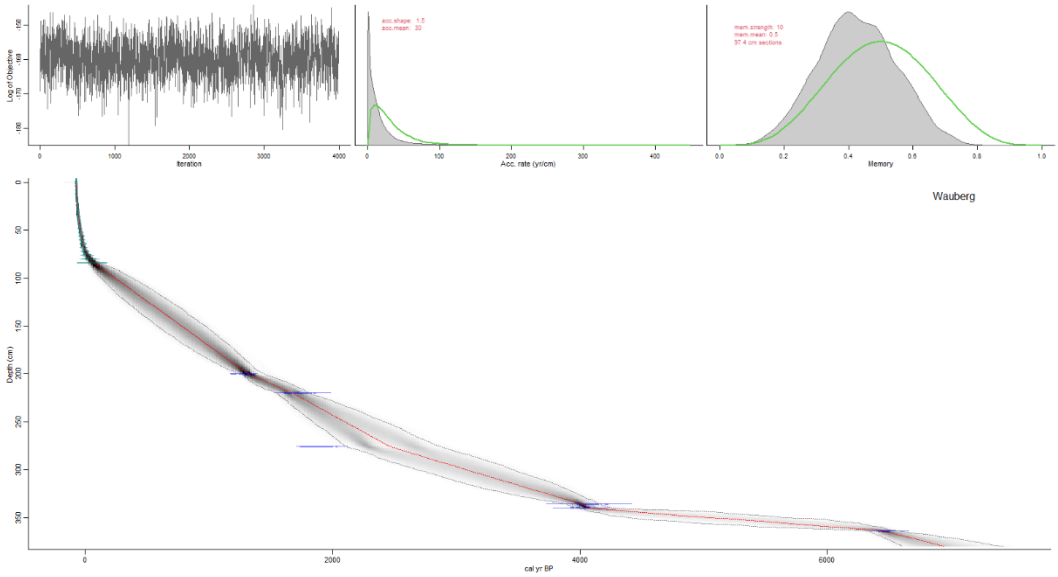

Figure S2.2 Age-depth model. The age-depth relationship was established with the rBACON package with dates from the ^{210}Pb CRS model (Fig. S2.1) and uncalibrated radiocarbon dates (Table S2.1).

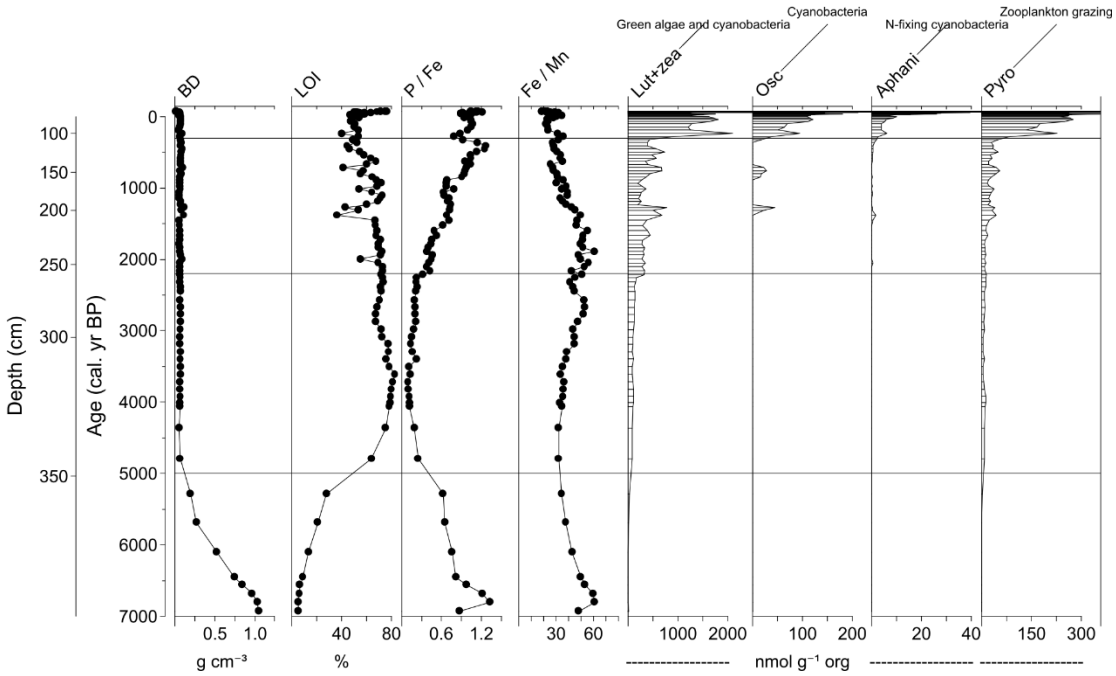

Figure S2.3 Summary time plot of bulk density (BD), loss-on-ignition (LOI), elemental ratios, and photosynthetic pigments. The delineated zones (solid lines) (Zones Ø to III) are based on the dendrogram of changes in TP concentration (Fig. 2.2A). The photosynthetic pigments are lutein+zeaxanthin (Lut+zea), oscilloxanthin (Osc), aphanizophyll (Aphani), and pyropheophorbide (Pyro). An analytical description of each photosynthetic pigment is presented in Table S2.3. Photosynthetic pigment concentrations with increased pigment preservation (high chl-a / pheo-a over the last ~10 years) have been truncated.

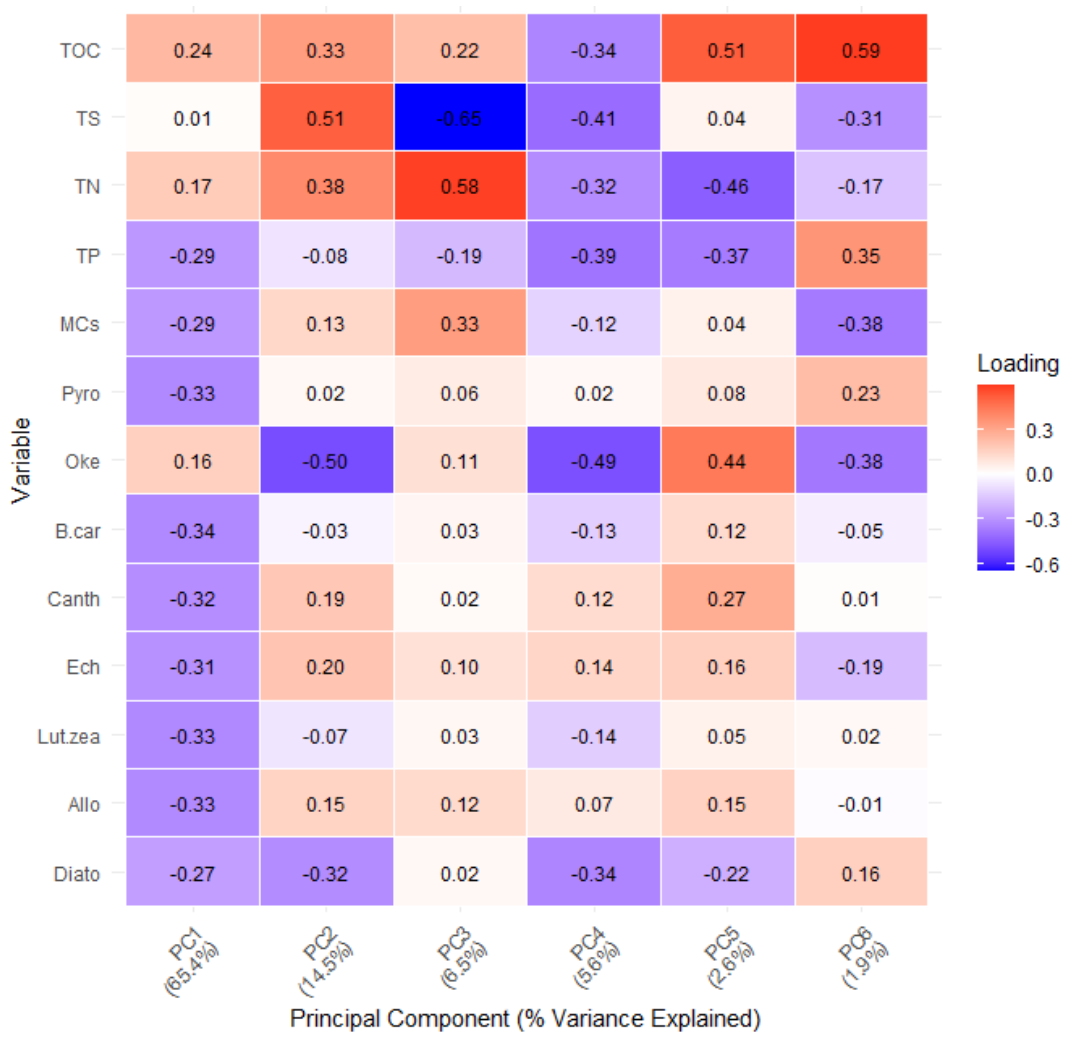

Figure S2.4 Heatmap of the principal components (PC1-6) derived from the analyzed paleolimnological variables. Each value in the heatmap represents the loading of the variable for the respective PC. The percentage of variance explained by each PC is shown in parentheses.

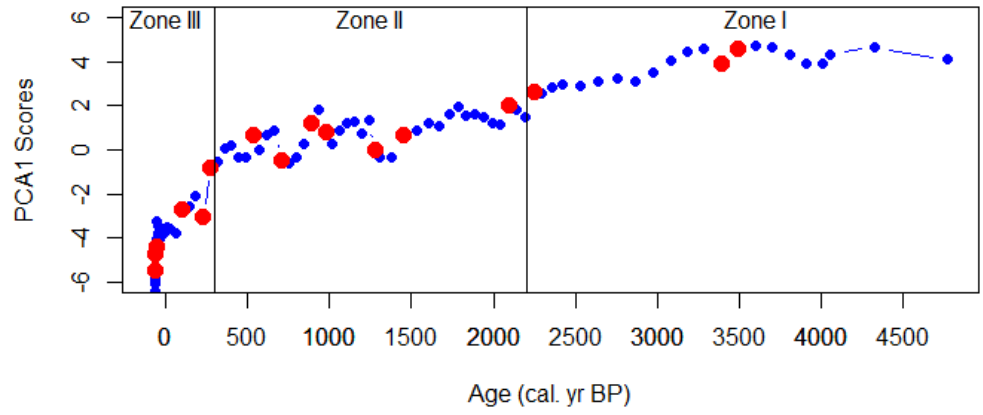

Figure S2.5 PCA1 scores plotted with time. The vertical solid lines delineate the established chronological zones based on TP (Zones I, II, and III). Based on a sequential T-test, the red dots depict data points with significant ($p<0.05$) t-statistic changes (-2>t-stat>2).

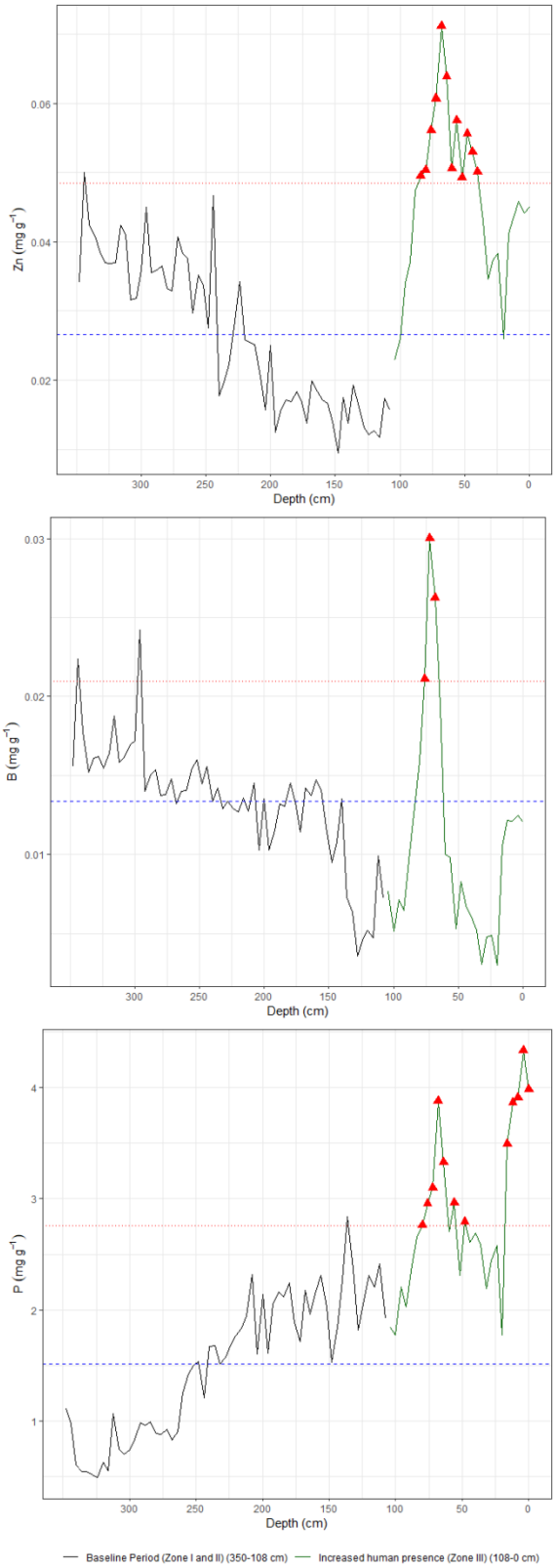

Figure S2.6 Sedimentary concentrations of zinc (up), boron (center), and phosphorus (low) plotted with depth. The blue dashed line indicates the mean concentrations under baseline conditions (black solid line) in Zones I and II. Hence, the mean excludes the period with increased human presence in Zone III (green solid line). The dashed red line indicates two standard deviations (SDs) above the mean, and the red triangles are data points higher than two SDs. An increase in Zn is observed at the start of Zone III (104-108 cm), while the concentrations exceed two SDs after 84-88 cm (1892 CE). A rapid increase in B is observed after 84-88 cm (1892 CE), while the concentrations exceed two SDs after 76-80 cm (1936 CE). Phosphorus follows a similar trend to Zn and B from 88-92 cm and above (~1850 CE), exceeding two SDs after 80-84 cm (1913 CE). All elements decreased after 64-68 cm (1964 CE) and then increased again at present (0-20 cm). The State of Florida acquired the land and established Paynes Prairie Preserve State Park in 1971 CE.

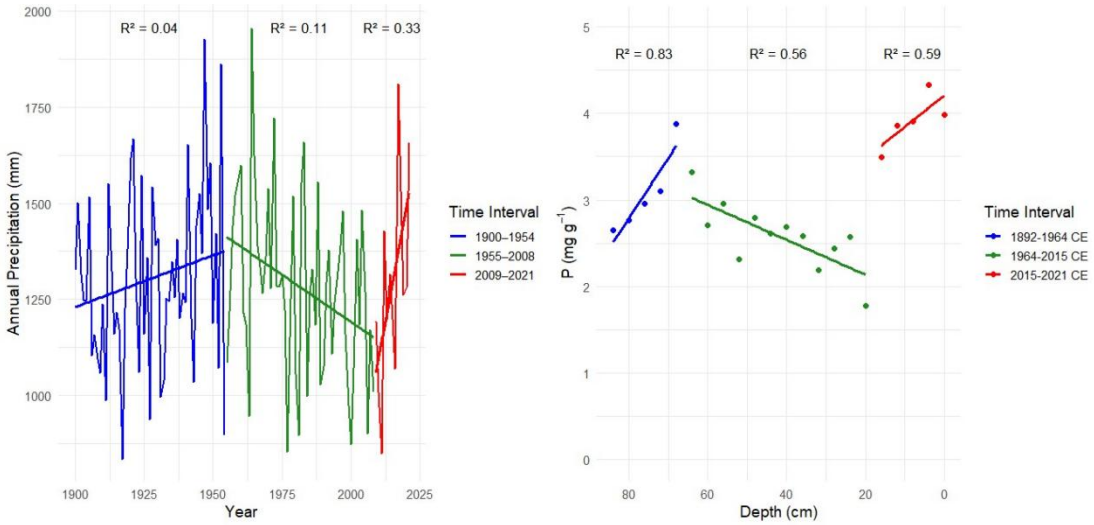

Figure S2.7 Annual precipitation in Gainesville, FL, from 1900 to 2021 CE (left) and TP concentration in Lake Wauberg plotted with depth (0-88cm; 1892 to 2021 CE) (right). Both records show an increasing trend until the mid-20th century, a decrease until the early 21st century, and an increase to the present time. The precipitation record was obtained from the Florida Climate Center. Data source: https://climatecenter.fsu.edu/products-services/data/precipitation/gainesville

Chapter 3: Microcystin Deposition on the Millennial Scale: A Paleolimnological Investigation of Two Subtropical Lakes in Central Florida, USA

3.1 Abstract

Increased cyanotoxin concentrations from harmful algal blooms (HABs) in lake systems pose a great challenge to water quality. Although remarkable progress has been made in monitoring cyanotoxins in modern environments over the past few decades, identifying the triggers of cyanotoxin release by cyanobacteria has yielded mixed results from experimental and analytical studies. Paleolimnological reconstructions can reveal whole-lake long-term changes, but few studies have directly measured paleocyanotoxins alongside other water quality proxies. Here, we investigated the drivers of sedimentary total microcystin (MC) concentrations on the millennial scale in hypereutrophic Lakes Dora and Marian in central Florida, USA. We analyzed dated sediment records using paleolimnological techniques to reconstruct nutrient deposition, cyanobacteria abundance (photosynthetic pigments), and cyanotoxins (total MCs). The objective was to investigate the linkage between MC concentrations in the sediments with both biotic (cyanobacteria and other primary producers) and abiotic factors (nutrients and climate). We found that MC production occurred throughout the ~7,000-year period, progressing from periods of moderate to low and then to high concentrations in both lakes. Statistical analyses showed that historical MC concentrations were related to sedimentary measurements of total phosphorus (TP), cyanobacteria abundance, and other primary producer groups, such as cryptophytes. However, there was only a minimal relationship with climate proxies such as charcoal and pollen. Our study demonstrates that cyanotoxins have occurred for millennia in both lakes with maintained relationships to nutrients and other environmental factors that existed both in historic and modern limnological conditions.

3.2 Introduction

Cyanotoxins associated with hypereutrophic conditions and high cyanobacteria abundance are becoming a growing problem in water bodies worldwide (Bhateria and Jain, 2016; Brooks et al., 2016). Despite cyanobacteria's crucial role in the evolution of life through the Great Oxygenation Event (Grettenberger et al., 2025), their proliferation in modern harmful algal blooms (HABs) threatens aquatic communities by diminishing their ecological health and ecosystem services (Kaloudis et al., 2022; Pick, 2016). Once released into the water, cyanotoxins

pose a threat to both wildlife and human health by contaminating drinking water resources, accumulating in food sources, and causing exposure during recreational activities, as well as being inhaled through air transport (Zhang et al., 2023).

Cyanotoxins are classified as hepatotoxins (microcystin, cylidrospermopsin), neurotoxins (anatoxin, saxitoxin), and dermatoxins (lyngbyatoxin), with potential effects on other organs (Merel et al., 2013). The cyclic peptide microcystin (MC) is the most common cyanotoxin, which is highly stable, can persist in the absence of microbes under typical water treatment processes, and causes liver failure and other health issues by inhibiting protein phosphatase (Rastogi et al., 2014). Many studies have documented HAB impacts on humans and other mammals. For example, cyanotoxins in Lake Erie, located on the border between the USA and Canada, led to the closure of the water distribution system throughout the entire city of Toledo, OH, USA, which has a population of almost 300,000 (Steffen et al., 2017). While annual reports of HAB-caused pet and livestock deaths are increasing globally, HABs have also been linked to massive deaths of megafauna in Africa (Wang et al., 2021). Likewise, the state of Florida, USA spent around $10 billion (2010) US dollars on water quality improvements in response to cyanotoxin issues (Stanton and Taylor, 2012).

High MC concentrations have been observed under various biogeochemical conditions, such as increasing total phosphorus (TP) and total nitrogen (TN) levels (Dolman et al., 2012; Vézie et al., 2002), increased TN availability following TP-targeted reductions (Schampera and Hellweger, 2024), and low N/P ratios (Harris et al., 2014). Specifically, TP levels have been linked to MC production in the water (MacKeigan et al., 2023), surface sediments (Lamb, 2021), and sediment cores (Paradeisis-Stathis and Waters, 2025; Waters et al., 2021). Other studies link toxin production to trace metals (Facey et al., 2019), suggesting an iron (Fe)-uptake stimulation mechanism in response to Fe-limited conditions (Ghio and Hilborn, 2023; Lukač and Aegerter, 1993) or Fe-stimulated toxin production (Utkilen and Gjølme, 1995). Additionally, MC concentrations have been found to increase irrespective of cyanobacteria cell densities (Lawson et al., 2025), as well as with high cyanobacteria biomass and zooplankton grazing (MacKeigan et al., 2023). While the purpose of cyanotoxins can be multifaceted, directly aiding the survival of cyanobacteria in adverse conditions and indirectly inhibiting the growth of other organisms (Wei et al., 2024), the exact triggering mechanisms are not yet fully understood, and their role in the ecology of cyanobacteria remains to be determined (Neilan et al., 2013).

One way to investigate whole-lake changes associated with cyanotoxin production and the proposed triggers for cyanotoxin release is through the application of paleolimnological proxies over millennial timescales. Paleolimnological studies comparing past and present conditions have shown clear links between cyanotoxin production, water quality degradation, and cultural eutrophication (Gregersen et al., 2022; Heathcote et al., 2023; Waters et al., 2021), as well as cyanobacteria proliferation in response to past climate changes (Bjerring et al., 2013; McGowan et al., 2018). However, knowledge of past lake changes remains limited, particularly in subtropical regions, and longer sediment records are needed to understand the baseline conditions and ecological states of lacustrine systems over time (Randsalu-Wendrup et al., 2016), as well as the history of cyanotoxin production (Henao et al., 2020). Despite the necessity for increased long-term knowledge of cyanotoxin ecology, most studies on cyanobacteria abundance in relation to MC production have been conducted in laboratory settings with predefined conditions that may not reflect the dynamic nature of physical lake environments (Dai et al., 2016). Few studies have attempted to link paleolimnological reconstructions of primary producers with paleocyanotoxin concentrations, even though intracellular cyanotoxins can be detected at concentrations from centennial (Clift, 2022; Efting et al., 2011; Pawlik-Skowrońska et al., 2010; Zastepa et al., 2017) to millennial scales (Paradeisis-Stathis and Waters, 2025; Waters, 2016; Waters et al., 2021). Even though intracellular MCs can become toxically active once cyanobacteria cells rupture, they are more resistant to degradation than other molecules (Wu et al., 2015), and the measured ADDA amino acid promotes hydrophobic binding, which is less responsive to sediment interactions (Schmidt et al., 2014). While most cyanotoxin management strategies rely on water-column data, the persistence of MCs in sediments poses a significant ecological hazard (Song et al., 2015).

The shallow subtropical region of Florida, USA is particularly vulnerable to MC accumulation (Williams et al., 2007), due to warm temperatures (Bachmann and Canfield, 2024; Walls et al., 2018), naturally nutrient-rich conditions (Canfield and Hoyer, 1988; Bachmann et al., 2012), high organic matter content from autochthonous sources (Waters et al., 2019), and frequent internal loading from resuspension (Bachmann et al., 2000). Here, we investigated the drivers of millennial-scale hypereutrophic conditions on MC production in two lakes, Lake Dora and Lake Marian, located in central Florida, USA, using dated sediment records and paleolimnological tools, focusing on historical alterations to nutrient inputs, cyanobacteria

abundance, and cyanotoxins. Our primary research objectives were 1) to determine the onset of MC production in each lake and trace changes in MC throughout the Holocene, and 2) to link stratigraphic changes in MC with changes in nutrient deposition and the primary producer community. Furthermore, we analyzed pollen and charcoal records to investigate the role of climate, given that hydroclimatic fluctuations throughout their existence might have affected nutrient inputs, leading to dynamic responses in primary producers. We hypothesized that 1) periods with abundant P and low sedimentary N/P ratios would enhance cyanobacteria abundance, and 2) MC concentrations would be driven by the abundance of cyanobacteria and other primary producers (biotic factors) and nutrient concentrations, with increased sensitivity to TP and hydroclimatic conditions (abiotic factors) over time.

3.3 Material and Methods

3.3.1 Study Sites

Lake Dora (LDO) (28°47'16" N, 81°41'09" W) is a large (18.1 km²) and shallow (~2.4 m mean depth and ~4.2 m max depth) hypereutrophic lake (Table S3.1, S3.2) located next to the town of Mount Dora (18,261 population) in Lake County, FL, USA (Fig. 3.1). The lake is situated at a low elevation (17 m a.s.l.) with a flat to gentle slope and is filled with gyttja and sediments derived from the regional geology, primarily consisting of Cypresshead Formation sands and clays from the Pliocene epoch (Florida Department of Environmental Protection Geospatial Open Data, 2023). The catchment area encompasses various land uses, such as residential, commercial, industrial, and agricultural areas, as well as wetlands (Magly, 2003). The lake is part of the upper Ocklawaha River basin, where canals connect nine lakes to form the Harris Chain of Lakes (Whitmore et al., 2018). The lake's headwaters originate from the culturally eutrophied Lake Apopka, dating back to the construction of the Apopka-Beauclair canal in 1887 (Schelske et al., 1999). Lake Dora's discharge occurs through an outflow canal to the northwest, leading to Lake Eustis (Magley, 2003). The lake's water quality was monitored by Florida Lakewatch from 1990 to 2022 and is classified as a softwater hypereutrophic lake with a mean Secchi depth of 0.4 m, mean chlorophyll of 101 μg L^{-1}, mean TP of 54 μg L^{-1}, and mean TN of 2,787 μg L^{-1} (Hoyer et al., 2014). Surface sediment measurements yielded high concentrations of cyanobacteria pigments, as well as MC concentrations at 64 ng g^{-1} org (Table S3.2) (Lamb, 2021).

Lake Marian (LMA) (27°52'55" N, 81°06'19" W) is a large (23.2 km²) and shallow (~4.3 m mean depth and ~4.6 m max depth) hypereutrophic lake (Table S3.1, S3.2) located in the Three Lakes Wildlife Management Area in Osceola County, FL (Fig. 3.1). The lake is situated on a plain (17 m a.s.l.) and is filled with gyttja and sediments derived from the regional geology, primarily consisting of undifferentiated sands and clays from the Pleistocene to the Holocene epochs (Florida Department of Environmental Protection Geospatial Open Data, 2023). While the historical land cover consisted of marshes, wet prairies, and flatwood pines (Whitmore et al., 2020), the lake's catchment is currently dominated by agriculture, wetlands, pasturelands, rangelands, and forests. The Kissimmee Chain of Lakes, of which LMA is a part, was previously connected through an extensive network of wetlands and creeks that depended on seasonal hydrological fluctuations. However, in the 1880s, canals were constructed to control flooding and drain wetlands for agriculture, resulting in a water level decline of approximately 1.8 m and significant landscape changes (Whitmore et al., 2020). The lake's water quality was monitored by Florida Lakewatch from 2007 to 2017 and is classified as a softwater hypereutrophic lake with a mean Secchi depth of 0.5 m, mean chlorophyll concentration of 104 μg L^{-1}, mean TP of 122 μg L^{-1}, and mean TN of 2,366 μg L^{-1} (Hoyer et al., 2014). An earlier study measuring MC concentrations in the top sediments of 47 Florida lakes reported the highest value of 674 ng g^{-1} org for LMA in the dataset (Lamb, 2021). While many livestock animals graze along the shore and in the lake (Fig. S3.1), MC in the water was recorded almost monthly from May 2022 to April 2025 (Florida Department of Environmental Protection, 2025), averaging 3.2 ppb throughout this period, which is double the US Environmental Protection Agency limit and more than triple the World Health Organization limit for human consumption (Fig. S3.2).

3.3.2 Sediment Coring and Subsampling

The Auburn Paleoenvironmental Lab cored LDO and LMA on January 6th and 7th, 2022, respectively. The coring locations were chosen based on previous sediment coring and in situ soft sediment surveys (Whitmore et al., 1996) conducted in the deep, central areas of the lakes. Undisturbed mud/water interface sediments were collected using a piston corer (7 cm diameter) (Fisher et al., 1992) to a depth of approximately 150 cm, while deeper sediments were gathered with a modified Livingstone corer (5.5 cm diameter). The coring process aimed to have sediment overlaps of 20 cm for each core section to create a continuous sediment record. The mud-water interface cores were subsampled in 4 cm sections in the field, packed in labeled sample bags, and

stored in coolers with ice. The deeper core sections were kept in labeled polycarbonate core barrels and transported in coolers to the laboratory at Auburn University, where they were cut in half lengthwise, photographed, and described. One half was subsampled in 2 cm sections, while the second half was archived in cold storage. A portion of the subsampled wet sediments was processed using gravimetric techniques. The remaining samples were lyophilized, ground with a mortar and pestle, and stored in labeled scintillation vials under refrigerated conditions for further analyses.

3.3.3 Sediment Dating

Continuous sediment intervals from the mud/water interface cores (top ~100 cm) were dated at Auburn University using gamma spectroscopy with an ORTEC Intrinsic Germanium Detector connected to a 4096-channel multichannel analyzer. Polystyrene tubes were filled to approximately 30 mm in height, weighed, and sealed with epoxy for at least 19 days to achieve secular equilibrium between the parent ^{226}Ra and daughter ^{222}Rn (half-life = 3.8 days) (Brenner et al., 2004). The samples were measured for ^{210}Pb total activity and ^{226}Ra (supported ^{210}Pb) to calculate excess ^{210}Pb (Appleby et al., 1986; Schelske et al., 1994). The constant rate of supply (CRS) model was used to calculate excess ^{210}Pb, assuming a continuous supply rate (Appleby and Oldfield, 1983). This model is well-suited for Florida lakes due to variations in sedimentation rates and dilution effects from high organic sediments (Brenner et al., 2004). Sediment intervals beneath the excess ^{210}Pb measured portion were dated by measuring AMS ^{14}C on charcoal fragments at the National Ocean Sciences Accelerator Mass Spectrometry (NOSAMS) facility of the Woods Hole Oceanographic Institution in Massachusetts, USA. To collect charcoal, wet sediments from the archives (5 mL) were processed with 10 mL of 5% potassium hydroxide (KOH) overnight, and after removing the supernatant, they were treated with 10 mL of 5% hydrogen peroxide (H_2O_2) overnight. The samples were sieved through a 125 μm mesh sieve, and charcoal was collected from a petri dish under a microscope. Carbon-14 dates were measured in seven samples from Lake Dora and four samples from Lake Marian. The ^{14}C-dated ages were calibrated with the IntCal20 calibration curve (Reimer et al., 2020) using the rbacon package in R (Blaauw and Christen, 2011) and combined with the excess ^{210}Pb-calculated ages to create an age-depth model in rbacon, with sections of 4 cm thickness and a 20 cm accumulation rate.

3.3.4 Paleolimnological Analyses

The wet sediment samples were measured for bulk density and organic matter content (loss-on-ignition; LOI) after drying at 60°C for 24 h and combusting at 550°C for 3 h, respectively (Dean, 1974). Bulk density was calculated as g dry cm^{-3} wet and LOI was calculated as a percentage. Total organic carbon (TOC) and total nitrogen (TN) were measured with a Costech ECS 4010 elemental analyzer at Auburn University. The samples for TOC were weighed in silver capsules and fumigated in an acid bath with hydrochloric acid (HCl) for 24 h to remove inorganic C. The silver capsules were then folded and placed in tin capsules. Samples for TN were weighed in tin capsules. The C/N ratios used the TOC and TN in atomic weights. Additional elements (TP, Fe, S) were measured using Inductively Coupled Plasma (ICP) Spectroscopy, with 90-minute nitric acid digestion on a heated block (EPA 6010B) at Waters Agricultural Laboratories in Camila, Georgia.

Photosynthetic pigment analysis was performed using High-Performance Liquid Chromatography (HPLC) following the methods for pigment analysis from sediments (Leavitt and Hodgson, 2001; Waters et al., 2012). Chlorophylls and carotenoids were extracted from dried sediment samples using a solvent mixture of 80% acetone, 15% methanol, and 5% HPLC-grade water containing an internal standard (Apocarotenal or trans-β-apo-8'-carotenal; Sigma-Aldrich Chemical Corp.). The samples were injected into a Shimadzu HPLC system with a Phenomenex Luna 3 μm C18 column (200 x 4.6 mm), following the mobile phase and the time sequence of Leavitt and Hodgson (2001). Carotenoids and chlorophylls were measured using a photodiode array detector coupled with a fluorescence detector, respectively. Pigment identification was performed using retention times and pigment-specific spectra of known standards (DHI Lab Products, Denmark). Pigment concentrations were calculated by comparing peak areas against standards of known concentration and were expressed in nmol per gram of organic matter.

Cyanotoxins were measured as total MCs using the microcystin/nodularin ADDA OH enzyme-linked immunosorbent assay (ELISA) kit by Abraxis, purchased from Gold Standard Diagnostics as described in Waters et al. (2021). The ADDA amino acid is present in almost 80% of the 279 identified MC congeners (Bouaïcha et al., 2019) and is found in variants commonly encountered in aquatic environments, such as MC-LR and MC-LA (Foss and Aubel, 2015). Cyanotoxins were extracted from dried sediments following Abraxis instructions applied

to soils and Zastepa et al. (2017). Briefly, the samples were mixed in two cycles with 10 mL and 5 mL solvent of 75% methanol, 25% deionized (DI) water, and 0.05% trifluoroacetic acid, then sonicated and centrifuged, and the supernatants were transferred to a labeled scintillation vial. The supernatants were evaporated in a heated water bath at 60°C under a stream of nitrogen gas until a total volume of 1.5 mL was reached. Each vial received 6 mL of HPLC-grade water, and the content was sonicated and vortexed. The extract in each vial was purified with solid-phase extraction in a conditioned Strata X column, rinsed with 2 mL of 5% methanol, and eluted with 9 mL of 90% acetonitrile solution. The 9 mL sample was collected in a clean and labeled scintillation vial and evaporated to dryness in a heated water bath at 60°C under a stream of nitrogen. The dried samples were reconstituted with 1.5 mL HPLC-grade water, sonicated, vortexed, and passed through a 0.2 μm syringe filter to a labeled amber vial before analysis. Samples exceeding the high detection limit were diluted with the sample diluent in the ELISA kit. Total MCs were reported as ng toxin g^{-1} of organic matter and were normalized to a base-10 logarithmic scale.

Pollen analysis was performed in 85 out of a total of 132 samples in LDO by Dr. Debra Willard and the Palynology Laboratory at the Florence Bascom Geoscience Center of the US Geological Survey. Each sample was dried and weighed before adding one Lycopodium marker tablet (batch 3862, 9666 ±212 spores/tablet) for the calculation of absolute pollen concentration (Stockmarr, 1971). Following standard techniques (Traverse, 2007; Willard et al., 2011), samples were demineralized with HCl and HF, acetolyzed using 1 part sulfuric acid to 9 parts acetic anhydride, treated with 10% KOH in a boiling water bath to remove humic material, and sieved with 150 μm and 10 μm mesh to remove sands and clays, respectively. After staining with Bismarck Brown, pollen residues were mounted on microscope slides with glycerin jelly. Residues are stored in ethanol and curated in the working collections of the U.S. Geological Survey Florence Bascom Geoscience Center in Reston, Virginia. At least 300 palynomorphs were counted from each slide using 400X magnification on a Nikon Eclipse microscope with Nomarski optics.

Charcoal analysis of the LMA record was performed on a cubic centimeter of wet sediments subsampled in 15 mL plastic tubes. A total of 103 samples were analyzed, of which 17 were duplicates (Foliano, 2024). Out of the 82 sediment intervals of LMA, 78 intervals were analyzed for charcoal. The samples were treated with 5 mL of 1 M sodium hexametaphosphate

($Na_6[(PO_3)_6]$) and 5 mL of 3.75% bleach for 24 h. The samples were sieved through a 125 µm mesh, rinsed with DI water, and transferred into lined counting trays (Vachula et al., 2019). Charcoal particles were identified under a microscope attached to a Nikon DS-Fi3 camera. The free open-source Charcoal Quantification Tool (CharTool) in ImageJ was used to quantify and classify charcoal particles (Snitker, 2020). The charcoal accumulation rate (CHAR) was calculated for each sample in particles per cubic centimeter per year based on the volumetric concentration and the age-depth model following the formula of Vachula et al. (2019):

$$\text{CHAR} = \frac{\text{\# of Particles}}{\text{Volume}} \times \frac{(\text{Top Depth} - \text{Bottom Depth})}{(\text{Top Age} - \text{Bottom age})}$$

3.3.5 Data Visualization and Analysis

The location maps for Lake Dora and Lake Marian were created in ESRI ArcGIS Pro v. 3.4.2 using an online service layer for basemap, land cover data from the Florida Department of Environmental Protection Geospatial Open Data (2022) (https://geodata.dep.state.fl.us/), and a digital elevation model based on USGS lidar data (2018-2020) from National Oceanic and Atmospheric Administration (NOAA) data access viewer (https://coast.noaa.gov/dataviewer/#/). Time plots with paleoenvironmental data were created in Tilia (version 3.0.3) (Williams et al., 2018). The cores were divided into three zones based on MC concentrations using IBM SPSS Statistics v.28, with Ward's hierarchical clustering method and a predefined number of clusters. Principal components analysis (PCA) was performed in R (version 4.4.1, R Core Team, 2024) using log-normalized element, pigment, and cyanotoxin data in the built-in prcomp function and the autoplot function in the ggfortify package (Tang and Li, 2016). Correlation plots were generated in R using the ggcorrmat function with the Pearson correlation method in the ggstatsplot package (Patil, 2021).

3.4 Results

3.4.1 Stratigraphy and Chronology

The sediment cores from LDO and LMA yielded continuous 520 cm and 322 cm records, respectively. The sediment core of LDO contained homogeneous black-brown organic sediments with pockets of silt, and the color abruptly turned to grey at the bottom of the core (500 to 520 cm). The sediment core from LMA consisted of homogeneous black-brown organic sediments in the top 215 cm, silty-sand layers from 215 to 250 cm, and a thick silty-sand layer from 250 to 260 cm. Below 260 cm, 2 to 5 cm thick bands of reddish-brown, brown, and black-brown

organic sediments, rich in gastropods, were interchanged down to 306 cm, and then the core transitioned to dark grey minerogenic sediments down to 322 cm.

Excess ^{210}Pb reached supported levels at 80 cm (LDO) and 52 cm (LMA), which yielded 1849 and 1860 CE per the CRS model, respectively (Fig. S3.3, S3.4). The parent radionuclide of ^{210}Pb, ^{226}Ra, had relatively constant activity in both lakes. Hence, the supported ^{210}Pb demarcations were assigned when the excess ^{210}Pb and ^{226}Ra activities reached radioactive secular equilibrium (Appleby and Oldfield, 1983). The radiocarbon dates of the charcoal material were continuous and without anomalies (Table S3.3). However, the bulk sediment radiocarbon date from the bottom of LMA, being unreasonably older than the expected range, was treated as an outlier. The Bayesian dating model rbacon combined the CRS dates and the radiocarbon dates to produce age-depth models (Fig. S3.5, S3.6) with constant sedimentation, indicating bottom dates of ~6,800 (LDO) and ~7,600 (LMA) years BP, and a temporal resolution of approximately 30 and 60 years per sample, respectively.

3.4.2 Sediment Geochemistry, Photosynthetic Pigments, and Cyanotoxins

The concentrations of MCs in both lakes displayed a consistent chronological pattern. The sediment records were divided into three zones of low, moderate, and high MC levels using hierarchical clustering (Fig. 3.2), which yielded a statistically significant difference between the clusters (Table S3.4, S3.5). Both lakes exhibited moderate MC levels in the bottom sediment zone, while the highest levels were observed in the top zone. However, the chronological spans of the MC zones varied between the investigated lakes. Microcystins were low or absent in LDO prior to 6.4 ka BP (500 cm), while MCs were almost constantly present in LMA throughout the 7,600-year record.

In LDO, the moderate MC concentrations extended from 6.4 to 5.1 ka BP (500 to 424 cm), averaging 5.6 ng g^{-1} org (±1.6) (Table 3.1). During this interval, the bulk density was relatively high but interchanged with increases in organic matter (Fig. S3.7, Table S3.7). Apart from a brief increase from 6.4 to 6 ka BP, nutrient levels remained low (Fig. 3.3A, Table 3.1). The nutrient stoichiometry (C/N & N/P) gradually increased without notable fluctuations. Photosynthetic pigment identification became constant primarily after 6.4 ka BP, exhibiting an abrupt transition to high abundances in all pigments that persisted almost throughout the entire zone (Fig. 3.3B, S3.7).

The low MCs concentration interval in LDO extended from 5.1 ka BP to 1942 CE (424 to 64 cm). Despite sporadic increases, MCs averaged 2.8 ng g^{-1} org (±0.9). Most nutrient and element concentrations were higher than in the previous zone (Fig. 3.3A, Table 3.1). However, TP remained low and increased gradually only after 2.5 ka BP, resulting in an average concentration similar to the previous zone at 0.24 mg g^{-1} (±0.1). The average C/N gradually decreased to 15.7 (±1.1), while the N/P ratio initially increased and then declined after 2.5 ka BP. Around the same time, the increasing trend in S and Fe halted and began to decrease. The average abundance of photosynthetic pigments decreased during this period (Table 3.1, S3.7). Diatoxanthin decreased at the start of the interval (Fig. 3.3B). Meanwhile, beta-carotene and canthaxanthin exhibited a more gradual pattern after an initial decrease, and echinenone fluctuated before decreasing around 3.4 ka BP. Then, most photosynthetic pigments maintained low abundances until 1.5 ka BP, when a gradual increase commenced, particularly for diatoxanthin and myxoxanthophyll (Fig. 3.3B, S3.7).

The high MCs concentration zone in LDO after 1942 CE (64 cm) averaged 165 ng g^{-1} org (±263), which is more than 30- and 60-fold higher than the previous averages in the other zones, respectively. During this period, TOC levels remained consistent, while TN levels increased, resulting in a notable decrease in the C/N ratio to approximately 12 (±1.2). The deposition of TP accelerated dramatically (Fig. 3.3A), reaching an average concentration eight times higher than previously (Table 3.1), resulting in a notable decrease in N/P. The concentrations increased from 1940 CE to the present by 133%, rising from 1.2 to 2.8 mg g^{-1}. The average Fe concentration decreased, while S levels increased slightly. The pigment preservation index (chl-a/pheo-a) was highest in the top MCs zone, particularly during the last 10 years (20 cm) (Fig. 3.3B). Overall, the abundance of photosynthetic pigments increased dramatically. However, diatoxanthin and canthaxanthin peaked from 1942 to 1974 CE and then decreased. In contrast, alloxanthin, echinenone, myxoxanthophyll, and aphanizophyll peaked after 1974 CE, with only the latter two pigments showing continuous increases up to the present.

In LMA, prior to 7.2 ka BP (306 cm), pigment identification and preservation were low (Fig. 3.4B). Therefore, the moderate MC section incorporated the period spanning from 7.2 to 2.3 ka BP (306 to 144 cm), with an average of 7 ng g^{-1} org (±2.4) (Table 3.2). Geochemical variables demonstrated notable fluctuations during this interval (Fig. 3.4A). The sediments transitioned to a low bulk density and high organic matter content between 7.1 and 6 ka BP and

again after 4.3 ka BP (Fig. S3.8). Total OC and TN increased from 7.1 to 6 ka BP but reached their highest value after 4.3 ka BP (32% and 2%, respectively). The C/N ratio decreased from values higher than 30 to less than 15. Total P fluctuated at values higher than 1 mg g^{-1} from 7.1 to 6 ka BP and then decreased to stabilize at values around 0.3 mg g^{-1} after 4.3 ka BP. In conjunction with TN, the N/P ratio exhibited an overall increase. Iron and S maintained high values from 7.1 to 6 ka BP and after 4.3 ka BP. Photosynthetic pigments exhibited frequent fluctuations but maintained high abundances from 7.1 to 6 ka BP and after 4.7 ka BP (Fig. 3.4B). Despite some peaks, the ratio of chlorophyll-a to pheophytin-a remained relatively stable. Beta-carotene, echinenone, and canthaxanthin were high during both intervals. The concentration of other pigments, like okenone and scytonemin (Fig. S3.8), was highest in the first interval, while diatoxanthin and aphanizophyll increased more noticeably after 4.7 ka BP (Fig. 3.4B, S3.8).

The low MCs concentration interval in LMA extended from 2.3 ka BP to 1800 CE (144 to 52 cm), averaging 3.2 ng g^{-1} org (±1.2). Total OC and TN in this period maintained a similar range to the period after 4.3 ka BP (Fig. 3.4A) and reached slightly higher average values than the previous zone (Table 3.2). However, after 1.6 ka BP, TOC and TN fluctuated with a decreasing trend. The C/N ratio averaged around 14 (±1.5) but fluctuated after 1.6 ka BP. Even though TP was low at 0.19 mg g^{-1} (±0.02), the N/P ratio fluctuated in tandem with changes in TN and gradually decreased (Fig. 3.4A). The concentrations of Fe and S also decreased, reaching lower average values. Although the abundance of photosynthetic pigments fluctuated, no pronounced changes were observed, but in most cases, the average concentrations decreased slightly (Table 3.2). However, echinenone, canthaxanthin, and aphanizophyll demonstrated a notable decrease after 1.6 ka BP (Fig. 3.4B, S3.8).

The high MCs concentration zone in LMA after 1800 CE (52 cm) averaged 1,427 ng g^{-1} org (±1,694), more than 205- and almost 442-fold higher than the previous averages, respectively. Most geochemical variables increased rapidly, especially after the 1950s CE, and only the average S slightly decreased (Fig. 3.4A). The C/N ratio decreased to 12.4 (±1.6). Total P demonstrated the most pronounced change, with an almost sixfold increase, resulting in a notable decrease in the N/P ratio. The concentration increased by ~50% from 0.19 to 0.32 mg g^{-1} in 1860 CE, to 0.55 mg g^{-1} in 1930 CE, and then to 0.91 mg g^{-1} in 1974 CE, before increasing by 103% to 1.85 mg g^{-1} in the top of the core. The pigment preservation index (chl-a/pheo-a) increased, and most photosynthetic pigments reached the highest concentrations (Fig. 3.4B, S3.6).

Alloxanthin and aphanizophyll showed the most pronounced increases (Table 3.2, S3.8), but oscillaxanthin and canthaxanthin exhibited the highest average concentrations among the individual pigment markers.

3.4.3 Environmental Drivers Concerning Primary Producers and Microcystin Production

The PCA in LDO's dataset produced PC1 (46.8%) and PC2 (24.8%), which accounted for 71.6% of the dataset variance (Fig. 3.5A), and an additional 24.5% was explained by PC3-PC6 (Fig. S3.9). Most eigenvectors of photosynthetic pigments, MCs, and TP were ordinated along the PC1 axis. In contrast, a stronger alignment with PC2 demonstrated most nutrients (TOC, TN, S, Fe) while having an opposite ordination with a few photosynthetic pigments (canth & oke). However, the eigenvectors in PC1 indicated a stronger relationship among beta-carotene, lutein+zeaxanthin, alloxanthin, diatoxanthin, echinenone, aphanizophyll, MCs, and TP. These variables also showed significant ($p<0.05$) strong positive Pearson correlations (r) with MCs, with aphanizophyll (.92), TP (.9), and alloxanthin (.84) having the strongest relationship (Fig. 3.5B). The samples representing Zone I (moderate MCs - 6.4 to 5.1 ka BP) on the biplot (68% confidence intervals; 1σ of Gaussian distribution) showed a wide distribution range and better alignment with PC2 components and the eigenvectors of canthaxanthin and okenone (Fig. 3.5A). Additionally, Zone I demonstrated a negative ordination with TOC, TN, S, and Fe. Low ordination with PC1 and PC2 characterized Zone II samples (low MCs - 5.1 to 0.01 ka BP). Zone III (high MCs - 0.01 ka BP to pres.) exhibited a strong ordination with the primary eigenvectors of PC1. The direction and variability of individual samples driven by the loading scores of the variables in PC1 (Fig. S3.9) yielded more intervals with significant changes ($p<0.05$) in PC1 scores in Zones I (moderate MCs) and III (high MCs) and an abrupt change since 1942 CE (Fig. S3.10).

The PCA in LMA's dataset produced PC1 (47.5%) and PC2 (21.6%), which accounted for 69.1% of the dataset variance (Fig. 3.6A), and an additional 27.3% was explained by PC3-PC6 (Fig. S3.11). The eigenvectors of all variables were ordinated within PC1, but the relationship of okenone and S with PC1 was weak. Microcystins had a slightly stronger relationship with PC2 and were ordinated positively with lutein+zeaxanthin, beta-carotene, alloxanthin, and TP and negatively with S, Fe, TOC, and TN. Microcystins showed the strongest significant ($p<0.05$) positive Pearson correlations (r) with alloxanthin (.83), aphanizophyll (.77),

beta-carotene (.73), and TP (.71) (Fig. 3.6B). Although most photosynthetic pigments had a positive correlation (r) with TP, for echinenone and diatoxanthin the correlation was insignificant and several pigments (diato, aphani, canth, allo, ech) showed a stronger positive correlation (r) with TN as well as with TOC (canth) and Fe (canth and ech) than TP. The samples representing Zone I (moderate MCs - 7.2 to 2.3 ka BP) on the biplot (68% confidence intervals; 1σ of Gaussian distribution) showed a wide distribution range and overlapped with PC1 and PC2 axes (Fig. 3.6A). The samples representing Zone II (low MCs - 2.3 to 0.15 ka BP) were confined and ordinated more with PC2 and the eigenvector of okenone. Zone III (high MCs - 0.15 ka BP to pres.) overlapped with the PC1 and PC2 axis and exhibited strong ordination with the eigenvectors of TP, MCs, beta-carotene, alloxanthin, aphanizophyll, and lutein+zeaxanthin. The direction and variability of individual samples driven by the loading scores of the variables in PC1 (Fig. S3.11) yielded more intervals with significant changes ($p<0.05$) in PC1 scores in Zones I (moderate MCs) and III (high MCs) and an abrupt change since 0.15 ka BP (Fig. S3.12).

3.4.4 Terrestrial Signal from Pollen and Charcoal

The palynological analysis of the LDO record (Fig. 3.7, S3.13) found the highest abundances in *Pinus* and *Quercus* pollen, along with a wide range of grains from other species. The sediment interval prior to 5.1 ka BP was characterized by an increase in *Pinus* pollen from 34% to 77% and a decrease in *Quercus* pollen from 34% to 14%. Pollen grains from other tree taxa, such as *Cupressaceae* and *Carya*, as well as large shrubs like *Myrica*, were also present in low abundances (<2%). Additionally, marsh taxa such as *Poaceae*, *Amaranthaceae*, *Asteraceae*, *Cyperaceae*, and *Typha* exhibited relatively high pollen counts. However, the total abundance of marsh taxa decreased from 31% to 5%. A notable change occurred around 2.5 ka BP, marked by a slight increase in *Cupressaceae*, followed by a slight decrease in *Pinus* and an increase in *Quercus*, *Carya*, and *Myrica*. After 1900 CE, there was a notable decrease (~30%) in *Pinus*, accompanied by an increase in *Quercus*, *Ambrosia*, and marsh taxa, along with the frequent observation of *Casuarina* pollen.

The charcoal analysis of the LMA record (Fig. 3.8) revealed two distinct periods with high charcoal content. The first period spanned from 7.3 to 6 ka BP, during which charcoal particles increased from an average of 0.2 (±0.1) to 2.3 (±1.7) cm^{-2} yr^{-1}. The second period refers to the time after 2.9 ka BP, when charcoal particles increased from an average of 0.6 (±0.3) to 3.3 (±3.2) cm^{-2} yr^{-1} until the present. Although charcoal accumulation remained relatively

consistent after 2.9 ka BP, it decreased during the Little Ice Age, from ~0.7 to 0.3 ka BP, before peaking after ~1800 CE.

3.5 Discussion

3.5.1 Microcystin Production on the Millennial Scale

The paleolimnological investigation of subtropical and hypereutrophic Lakes Dora and Marian revealed a dynamic nutrient environment, cyanobacteria dominance, and MC production throughout the multi-millennial records. Although historical linkages between cyanotoxin production and ecological conditions are still limited, MCs and other cyanotoxins have been detected in paleolimnological records of tropical (Waters et al., 2021) and subtropical (Paradeisis-Stathis and Waters, 2025; Waters, 2016) lakes over similar timescales. Here, our study added two additional lakes demonstrating long-term production of cyanotoxins, showing three historical periods with different MC concentrations. Regardless of temporal discrepancies between the LDO and LMA cyanotoxin records, both lakes developed high cyanobacteria abundances with moderate MC concentrations during early limnological stages, followed by a period of low cyanotoxin production (Fig. 3.3B, 3.4B). In more recent time periods, both lakes transitioned relatively abruptly to dramatically high MC concentrations (Fig. 3.2). Similar transitions in cyanotoxin concentrations were observed in the millennial-scale records of MC in Lake Amatitlán, Guatemala (Waters et al., 2021), and cylindrospermopsin (CYN) in Lake Griffin, FL, USA (Waters, 2016). Pronounced modern increases in MCs were also observed in Lake Carlton, Florida, USA, although the record was only a few centuries long (Clift and Waters, 2024).

The subtropical climate in Florida, combined with its natural nutrient-rich baseline conditions, is ideal for high trophic levels with increased presence of cyanobacteria (Bachmann et al., 2012; Brenner et al., 1993). Nevertheless, in concert with this research, other paleolimnological records have shown that the current hypereutrophic states occurred after crossing the baseline nutrient conditions due to human activities during the past few centuries (Clift and Waters, 2024; Kenney et al., 2016; Riedinger-Whitmore et al., 2005; Waters et al., 2015; Whitmore et al., 2018; Whitmore et al., 2020). Similarly, cyanotoxin records from different latitudes have shown modern increases in MC production (Clift and Waters, 2024; Efting et al., 2011; Filatova et al., 2020; Henao et al., 2020; Pawlik-Skowrońska et al., 2010; Waters et al., 2021; Zastepa et al., 2017). Considering the paleolimnological records of several

lakes across different geographic regions, hydrologic modifications and land cover changes constituted the primary source of nutrients by determining their availability, cycling, and distribution (Gushulak et al., 2024; Heathcote et al., 2023; Huang et al., 2022; Kong et al., 2017; Waters et al., 2013).

While warm, subtropical temperatures sustained cyanobacteria abundance and MC production (Kosten et al., 2012; Walls et al., 2018), analyses of both sediment records identified shifts in biogeochemical and primary producer community structure. Changes in TP deposition and N/P stoichiometry, along with cyanobacteria and non-cyanobacteria pigment abundance, aligned with the transitions in MC levels. Phosphorus is a known driver of eutrophication (Schindler et al., 2016), with higher P enrichment over N (low N/P) in the sediments previously observed during increases in MC (Paradeisis-Stathis and Waters, 2025; Waters et al., 2021) and CYN production (Waters, 2016). Nitrogen-fixing cyanobacteria (aphani), cryptophytes (allo), green algae and cyanobacteria (lut+zea), and total primary producer abundance (b-car) also increased in concentration along with high MC values. These were also identified by the correlation matrices and ordination with MC in the PCA (Fig. 3.5, 3.6). Hence, MC production was determined by the availability of nutrients and interactions between cyanobacteria and non-cyanobacteria producers (Xue et al., 2018), as suggested by the strong positive correlations of MCs with cryptophytes (Fig. 3.5B, 3.6B). At high MC concentrations, a notable change in the cyanobacteria community to a greater presence of cyanobacteria pigments linked to N-fixation (aphani) (Cottingham et al., 2000; Leavitt and Hodgson, 2001) indicates a potential connection between MCs and nutrient stress conditions (Pimentel and Giani, 2014) due to the overall increase in primary producer abundance.

3.5.2 The Role of Nutrients and Primary Producer Community Composition in Microcystin Production

Microcystin concentrations in both LDO and LMA showed the strongest relationship with TP both in the PCA and correlation matrices (Fig. 3.5, 3.6). The lowest MC levels corresponded to the lowest TP concentrations, while the highest MC levels coincided with modern hypereutrophic conditions characterized by increased TP concentrations and primary producer abundances, such as N-fixing cyanobacteria (aphani) and cryptophytes (allo) (Table 3.1, 3.2). Phosphorus is widely recognized as the key nutrient driving the growth of cyanobacteria and promoting toxin production in many freshwater systems (Orihel et al., 2012;

Schindler et al., 2016), with internal P loading contributing to eutrophication and environmental stress conditions that favor MC production (Boopathi and Ki, 2014; Wu et al., 2017).

Although TP played a dominant role, a growing body of research also emphasizes the significance of N in shaping cyanobacteria dynamics and MC production (Conley et al., 2009; Dolman et al., 2012; Elser et al., 2007; Paerl et al., 2016). Cyanobacteria are well-adapted to P scarcity due to their ability to obtain P from various sources and utilize luxury uptake mechanisms (Xiao et al., 2022), while N loading can support cyanobacteria growth and indirectly affect MC production (Gobler et al., 2016). In both lakes, the moderate MC production during low TP deposition, alongside the sustained concentration of cyanobacteria and other primary producer pigments, suggests a role for MCs in coping with oxidative stress under P-limiting conditions (Zilliges et al., 2011). Although correlations of primary producers and MCs with nutrients other than TP were weak in LDO (Fig. 3.5B), the persistence of pigment and cyanotoxin concentrations during the moderate MC period may reflect the complexity of ecological competition for nutrients and the indirect reliance on increasing TN (Paerl et al., 2016; Wagner et al., 2019, 2021). Considering the paleolimnological records of several lakes across different geographic regions, hydrologic modifications and land cover changes constituted the primary source of nutrients by determining their availability, cycling, and distribution (Gushulak et al., 2024; Heathcote et al., 2023; Huang et al., 2022; Kong et al., 2017; Waters et al., 2013).

While the reduction in non-cyanobacteria producers can be attributed to lower TP levels (Whitmore et al., 2018), the delayed response of cyanobacteria to TP reduction in LDO and LMA (Fig. 3.3A, 3.4A), along with the lower MCs, could signal a potential shift in the cyanobacteria community toward non-toxic strains that have lower demands for P and N than toxic cyanobacteria strains (Vézie et al., 2002). During periods of low MC levels, the reduced presence of non-cyanobacteria primary producers, coupled with stable nutrient conditions, minimized the ecological necessity for cyanobacteria to maintain an energy-intensive process for regulating photosynthesis and other cell and colony processes (Zhang et al., 2023). These observations suggest a decrease in MC-potent cyanobacteria strains, along with a reduction in TP and non-cyanobacteria primary producers, despite an increase in other nutrients (TOC, TN) to baseline levels. Although a gradual increase in TP was initiated after ~2.5 ka BP in LDO (Fig. 3.3A), the system could maintain its ecological state with a gradual nutrient enrichment, taking

longer to exceed TP concentration thresholds that favor cyanobacteria proliferation (Paradeisis-Stathis and Waters, 2025).

Although changes in MC levels in LDO and LMA were associated with nutrient-rich conditions characterized by a relative enrichment of TP over TN, linkages to aquatic community composition and high pigment concentrations were also influential (Fig. 3.5, 3.6). In both systems, moderate MC levels during the middle Holocene coincided with shallow lake conditions after wetland inundation, supported by high C/N ratios (Meyers and Ishiwatari, 1993) and increased concentrations of scytonemin in LMA (Fig. S3.8), a UV-protecting pigment found in benthic colonial cyanobacteria (Leavitt and Hodgson, 2001; Rastogi et al., 2015). Benthic cyanobacteria proliferations in shallow, low-flow aquatic environments can produce MCs, and although they are less common than planktonic HABs, they have been reported under different trophic levels worldwide (Wood et al., 2020). However, while the subsequent deepening in LMA limited benthic colonial cyanobacteria, it altered the cyanobacteria community and maintained MC production.

Similar to other studies, MC concentrations in our record were positively correlated with the concentration of cryptophytes (Clift and Waters, 2024; Paradeisis-Stathis and Waters, 2025; Xue et al., 2018), as well as with the generalized aquatic community indicators (lut+zea, b-car) (Fig. 3.5B, 3.6B). In contrast, their relationship with cyanobacteria pigments (ech, canth) was more variable. Cryptophytes can overcome light attenuation by regulating their position in the water column, thereby increasing nutrient competition for cyanobacteria (Litchman and de Tezanos Pinto, 2024). This suggests that MCs may not always reflect cyanobacteria biomass (Dolman et al., 2012) but may instead relate to the multifunctional role of secondary metabolites, like MCs, in primary community interactions and ecological stress conditions (Wei et al., 2024).

The 1942 CE (LDO) and 1860 CE (LMA) increase in TP triggered a notable increase in photosynthetic pigment concentrations, leading to shifts in primary producer and cyanobacteria communities, characterized by an increased presence of cryptophytes (allo) (Fig. 3.3, 3.4), N-fixing (aphani) (Fig. S3.7, S3.8) and colonial cyanobacteria (myxo, LDO; canth, LMA) (Fig. S3.7, 3.4), and resulting in the highest MC concentrations. These observations indicate that the abundance, shifts, and interactions within the primary producer community under nutrient-rich conditions promote MC production through ecological stressors and that MC production is ecologically modulated by nutrient and competitive pressures (Pimentel and Giani, 2014).

Human activities played a central role through the hydrologic connectivity of LDO with the P-enriched Lake Apopka since 1887 CE, and through the water-level regulation of LMA via canalization in 1867 CE. These changes had tremendous impacts on primary producer communities and water quality by altering nutrient cycling, leading to a rapid departure from the earlier baseline nutrient conditions (Clift and Waters, 2024; Kenney et al., 2016; Schelske et al., 2005; Waters et al., 2015; Whitmore et al., 2020). Additionally, the dramatic increase in CHAR in LMA over the last two centuries (Fig. 3.8), in combination with similar trends in nutrients and cyanobacteria, can be attributed to an amalgam of human-driven land cover changes due to the early burning practices related to the widespread mid-19th century cattle-ranching in the area (Otto, 1985) and later extensive prescribed fire practices that may be linked to pyroeutrophication (Foliano, 2024; Waters et al., 2023).

3.5.3 Hydroclimate as a Driver of Microcystin Production

Although hydroclimatic conditions influenced nutrient delivery, the measured climatic proxies of pollen (Fig. 3.7, S3.13) and charcoal (Fig. 3.8) showed no direct relationship with MCs production. While warmer conditions generally favor cyanobacteria and MCs (Merder et al., 2023; Paerl and Huisman, 2008; Wood et al., 2017), the complex interactions between climate and aquatic ecosystem responses in the warm subtropics complicate the establishment of a direct connection. For instance, moderate MC levels in LDO from 6.4 to 6 ka BP (Fig. 3.3) and in LMA from 7.3 to 6 ka BP (Fig. 3.4) coincided respectively with wetland expansion and warm, dry conditions, as inferred from the *Quercus* to *Pinus* vegetation shift (Fig. 3.7) (Grimm et al., 2006; Willard, 2023) and higher fire activity and dry conditions as inferred by the charcoal record (Fig. 3.8). Elevated cyanobacteria pigment concentrations during the early to middle Holocene have also been reported in temperate lakes (Karmakar et al., 2015). Positive hydroclimatic conditions during the Late Holocene (Lammertsma et al., 2015), as indicated by the increase in *Cupressaceae* and *Carya* pollen in LDO after ~2.5 ka BP (Fig. 3.7), were accompanied by a gradual increase in TP and only minor changes in primary producers, suggesting that nutrient thresholds were not surpassed. Likewise, increased fire activity in LMA after 2.9 ka BP (Fig. 3.8), possibly linked to climate or Native American fire practices (Foliano, 2024), had no synchronous MC shifts. Overall, late Holocene trends in both lakes reflect ecological stability and slow-paced lake responses, even under varying hydroclimatic regimes.

3.5.4 Microcystin Measurements in Paleolimnological Records

The records from Lake Dora and Lake Marian contribute to an increasing body of evidence showing MC deposition over millennial timescales. In previous paleolimnological investigations of MCs in lake sediments (Clift and Waters, 2024; Paradeisis-Stathis and Waters, 2025; Waters et al., 2021; Zastepa et al., 2017), as well as in our research, the most extreme values were found in the top sediments (~10 years). While the modern increase in HABs justifies high MC measurements, more recently deposited sediments contain a blend of intracellular and undegraded extracellular cyanotoxins, with the latter being water-soluble and toxically active. Much like comparing photosynthetic pigments in modern and ancient sediments (Leavitt, 1993; Waters et al., 2005), interpreting MC concentrations also requires accounting for their degradation (Tsuji et al., 2001; Zastepa et al., 2014). Environmental conditions such as sunlight intensity, water clarity, lake depth, sediment resuspension, organic matter availability, and the presence of bacteria influence MC preservation (Chen et al., 2008; Welker and Steinberg, 2000; Wu et al., 2011; Zhang et al., 2023). Further paleolimnological research is needed to better understand the post-depositional mechanisms of MC degradation. Regardless, MCs are recalcitrant molecules compared to other proxies such as pigments and ancient DNA (Pal et al., 2015; Picard et al., 2022), and the application of MCs as a paleolimnological tool is both needed and growing in application (Clift and Waters, 2024; Paradeisis-Stathis and Waters, 2025; Waters, 2016; Waters et al., 2021). Our data show that MCs can be recovered in millennial sediment records. Nevertheless, further studies are necessary to expand and enhance our understanding of MC ecology both spatially and temporally.

3.6 Conclusions

The millennial deposition of MCs in the sediments of two subtropical lakes in Florida was related to TP and primary producer pigment concentrations. While various cyanobacteria pigments were found related to MCs production, the aquatic community composition of the two lakes at the different MC levels also suggests a linkage with increased abundance of cryptophytes, as well as overall primary producer pigment abundance. Ecological stabilization from wetland to lake transitions was a millennia-scale process for both lakes, initially leading to a decrease in MCs to the lowest concentrations and subsequently to reduced cyanobacteria pigment concentrations. While periods with distinct hydroclimatic conditions coincided with changes in nutrient concentrations, there is no evidence that hydroclimatic fluctuations directly

influenced MCs throughout the Holocene. The hypereutrophication of both systems corresponded to human-induced landscape and hydrological modifications, leading to accelerated TP deposition, increased cyanobacteria pigments, and the highest MC concentrations.

3.7 References

Appleby, P.G., Nolan, P.J., Gifford, D.W., Godfrey, M.J., Oldfield, F., Anderson, N.J., Battarbee, R.W., 1986. 210Pb dating by low background gamma counting. Hydrobiologia 143(1), 21-27. https://doi.org/10.1007/BF00026640.

Appleby, P.G., Oldfieldz, F., 1983. The assessment of 210Pb data from sites with varying sediment accumulation rates. Hydrobiologia 103(1), 29-35. https://doi.org/10.1007/BF00028424.

Bachmann, R.W., Bigham, D.L., Hoyer, M.V., Canfield, D.E., 2012. Factors determining the distributions of total phosphorus, total nitrogen, and chlorophyll a in Florida lakes. Lake and Reservoir Management 28(1), 10-26. https://doi.org/10.1080/07438141.2011.646458.

Bachmann, R.W., Canfield, D.E., 2024. An assessment of air and lake water temperatures (1981–2020) in Florida with a hindcast to 1895. Florida scientist 87(1), 38-60. https://www.taylorfrancis.com/chapters/edit/10.4324/9781032707648-4/taking-international-criminal-justice-seriously-klaus-bachmann.

Bachmann, R.W., Hoyer, M.V., and Canfield Jr, D.E., 2000. The potential for wave disturbance in shallow Florida lakes. Lake and Reservoir Management 16(4), 281-291. https://doi.org/10.1080/07438140009354236.

Bhateria, R., Jain, D., 2016. Water quality assessment of lake water: a review. Sustainable Water Resources Management 2(2), 161-173. https://doi.org/10.1007/s40899-015-0014-7.

Bjerring, R., Olsen, J., Jeppesen, E., Buchardt, B., Heinemeier, J., McGowan, S., Leavitt, P.R., Enevold, R., Odgaard, B.V., 2013. Climate-driven changes in water level: a decadal scale multi-proxy study recording the 8.2-ka event and ecosystem responses in Lake Sarup (Denmark). Journal of Paleolimnology 49(2), 267-285. https://doi.org/10.1007/s10933-012-9673-7.

Blaauw, M., Christen, J.A., 2011. Flexible paleoclimate age-depth models using an autoregressive gamma process. Bayesian Analysis 6(3), 457-474, 418. https://doi.org/10.1214/11-BA618.

Boopathi, T., Ki, J.-S., 2014. Impact of environmental factors on the regulation of cyanotoxin production. Toxins 6(7), 1951-1978. https://doi.org/10.3390/toxins6071951.

Bouaïcha, N., Miles, C.O., Beach, D.G., Labidi, Z., Djabri, A., Benayache, N.Y., Nguyen-Quang, T., 2019. Structural Diversity, Characterization and Toxicology of Microcystins. Toxins (Basel) 11(12). https://doi.org/10.3390/toxins11120714.

Brenner, M., Schelske, C.L., Kenney, W.F., 2004. Inputs of dissolved and particulate 226Ra to lakes and implications for 210Pb dating recent sediments. Journal of Paleolimnology 32(1), 53-66. https://doi.org/10.1023/B:JOPL.0000025281.54969.03.

Brenner, M., Whitmore, T.J., Flannery, M.S., Binford, M.W., 1993. Paleolimnological methods for defining target conditions in lake restoration: Florida case studies. Lake and Reservoir Management 7(2), 209-217. https://doi.org/10.1080/07438149309354272.

Brooks, B.W., Lazorchak, J.M., Howard, M.D.A., Johnson, M.-V.V., Morton, S.L., Perkins, D.A.K., Reavie, E.D., Scott, G.I., Smith, S.A., Steevens, J.A., 2016. Are harmful algal blooms becoming the greatest inland water quality threat to public health and aquatic ecosystems? Environmental Toxicology and Chemistry 35(1), 6-13. https://doi.org/10.1002/etc.3220.

Canfield Jr, D.E., Hoyer, M.V., 1988. Regional geology and the chemical and trophic state characteristics of Florida Lakes. Lake and Reservoir Management 4(1), 21-31. https://doi.org/10.1080/07438148809354375.

Chen, W., Song, L., Peng, L., Wan, N., Zhang, X., Gan, N., 2008. Reduction in microcystin concentrations in large and shallow lakes: Water and sediment-interface contributions. Water Research 42(3), 763-773. https://doi.org/10.1016/j.watres.2007.08.007.

Clift, T.L., 2022. Cyanotoxin Production in Subtropical Lakes over the Last 150 Years with Implications for Human and Ecosystem Health, Crop, Soil and Environmental Sciences. Auburn University, Auburn, Alabama. https://etd.auburn.edu//handle/10415/8491.

Clift, T.L., Waters, M.N., 2024. Paleolimnological evidence for primary producer change linked to hydrologic connectivity and human impacts in Lake Carlton, Florida, USA. Journal of Paleolimnology 72(1), 35-48. https://doi.org/10.1007/s10933-024-00318-y.

Cottingham, K.L., Rusak, J.A., Leavitt, P.R., 2000. Increased ecosystem variability and reduced predictability following fertilisation: Evidence from palaeolimnology. Ecology Letters 3(4), 340-348. https://doi.org/10.1046/j.1461-0248.2000.00158.x.

Dean WE. (1974) Determination of carbonate and organic matter in calcareous sediments and sedimentary rocks by loss on ignition; comparison with other methods. Journal of Sediment Research 44:242-248. https://doi.org/10.1306/74D729D2-2B21-11D7-8648000102C1865D.

Dolman, A.M., Rücker, J., Pick, F.R., Fastner, J., Rohrlack, T., Mischke, U., Wiedner, C., 2012. Cyanobacteria and cyanotoxins: The influence of nitrogen versus phosphorus. PLOS ONE 7(6), e38757. https://doi.org/10.1371/journal.pone.0038757.

Efting, A.A., Snow, D.D., Fritz, S.C., 2011. Cyanobacteria and microcystin in the Nebraska (USA) Sand Hills Lakes before and after modern agriculture. Journal of Paleolimnology 46(1), 17-27. https://doi.org/10.1007/s10933-011-9511-3.

Elser, J.J., Bracken, M.E.S., Cleland, E.E., Gruner, D.S., Harpole, W.S., Hillebrand, H., Ngai, J.T., Seabloom, E.W., Shurin, J.B., Smith, J.E., 2007. Global analysis of nitrogen and phosphorus limitation of primary producers in freshwater, marine and terrestrial ecosystems. Ecology Letters 10(12), 1135-1142. https://doi.org/10.1111/j.1461-0248.2007.01113.x.

Facey, J.A., Apte, S.C., Mitrovic, S.M., 2019. A review of the effect of trace metals on freshwater cyanobacterial growth and toxin production. Toxins 11(11), 643. https://doi.org/10.3390/toxins11110643.

Filatova, D., Picardo, M., Núñez, O., Farré, M., 2020. Analysis, levels and seasonal variation of cyanotoxins in freshwater ecosystems. Trends in Environmental Analytical Chemistry 26, e00091. https://doi.org/10.1016/j.teac.2020.e00091.

Fisher, M.M., Brenner, M., Reddy, K.R., 1992. A simple, inexpensive piston corer for collecting undisturbed sediment/water interface profiles. Journal of Paleolimnology 7(2), 157-161. https://doi.org/10.1007/BF00196870.

Florida Department of Environmental Protection Geospatial Open Data, 2023. Surficial geology of Florida. Florida Department of Environmental Protection. Accessed in May 2025, from: https://geodata.dep.state.fl.us/datasets/FDEP::surficial-geology-of-florida/about.

Florida Department of Environmental Protection, 2025. Blue-green algal bloom weekly update. Florida Department of Environmental Protection. Accessed in May 2025, from: https://floridadep.gov/sec/sec/content/weekly-updates-and-subscription.

Foss, A.J., Aubel, M.T., 2015. Using the MMPB technique to confirm microcystin concentrations in water measured by ELISA and HPLC (UV, MS, MS/MS). Toxicon 104, 91-101. https://doi.org/10.1016/j.toxicon.2015.07.332.

Ghio, A.J., Hilborn, E.D., 2023. Cyanobacterial blooms, iron, and environmental pollutants. Biometals. https://doi.org/10.1007/s10534-023-00553-2.

Gobler, C.J., Burkholder, J.M., Davis, T.W., Harke, M.J., Johengen, T., Stow, C.A., Van de Waal, D.B., 2016. The dual role of nitrogen supply in controlling the growth and toxicity of cyanobacterial blooms. Harmful Algae 54, 87-97. https://doi.org/10.1016/j.hal.2016.01.010.

Gregersen, R., Howarth, J.D., Wood, S.A., Vandergoes, M.J., Puddick, J., Moy, C., Li, X., Pearman, J.K., Moody, A., Simon, K.S., 2022. Resolving 500 years of anthropogenic impacts in a mesotrophic lake: Nutrients outweigh other drivers of lake change. Environmental Science & Technology 56(23), 16940-16951. https://doi.org/10.1021/acs.est.2c06835.

Grettenberger, C., Gold, D.A., Brown, C.T., 2025. Distribution of early-branching Cyanobacteriia and the potential habitats that gave rise to the earliest oxygenic phototrophs. mSphere, e0101324. https://doi.org/10.1128/msphere.01013-24.

Grimm, E.C., Watts, W.A., Jacobson, G.L., Hansen, B.C., Almquist, H., Dieffenbacher-Krall, A.C., 2006. Evidence for warm wet Heinrich events in Florida. Quaternary Science Reviews. https://doi.org/10.1016/j.quascirev.2006.04.008.

Gushulak, C.A.C., Chegoonian, A.M., Wolfe, J., Gray, K., Mezzini, S., Wissel, B., Hann, B., Baulch, H.M., Finlay, K., Leavitt, P.R., 2024. Impacts of hydrologic management on the eutrophication of shallow lakes in an intensive agricultural landscape (Saskatchewan, Canada). Freshwater Biology 69(7), 984-1000. https://doi.org/10.1111/fwb.14260.

Harris, T.D., M., W.F., L., G.J., and Loftin, K.A., 2014. Experimental manipulation of TN:TP ratios suppress cyanobacterial biovolume and microcystin concentration in large-scale in situ mesocosms. Lake and Reservoir Management 30(1), 72-83. https://doi.org/10.1080/10402381.2013.876131.

Heathcote, A.J., Taranu, Z.E., Tromas, N., MacIntyre-Newell, M., Leavitt, P.R., Pick, F.R., 2023. Sedimentary DNA and pigments show increasing abundance and toxicity of cyanoHABs during the Anthropocene. Freshwater Biology 68(11), 1859-1874. https://doi.org/10.1111/fwb.14069.

Henao, E., Rzymski, P., Waters, M.N., 2020. A review on the study of cyanotoxins in paleolimnological research: Current knowledge and future needs. Toxins 12(1), 6. https://doi.org/10.3390/toxins12010006.

Hoyer, M.V., Bigham, D.L., Bachmann, R.W., Canfield, D.E., 2014. Florida LAKEWATCH: Citizen scientists protecting Florida's aquatic systems. Florida Scientist 77:184-197. http://www.jstor.org/stable/24321923.

Huang, S., Zhang, K., Lin, Q., Liu, J., Shen, J., 2022. Abrupt ecological shifts of lakes during the Anthropocene. Earth-Science Reviews 227, 103981. https://doi.org/10.1016/j.earscirev.2022.103981.

Kaloudis, T., Hiskia, A., Triantis, T.M., 2022. Cyanotoxins in bloom: Ever-increasing occurrence and global distribution of freshwater cyanotoxins from planktic and benthic cyanobacteria. Toxins 14(4), 264. https://doi.org/10.3390/toxins14040264.

Karmakar, M., Leavitt, P.R., Cumming, B.F., 2015. Enhanced algal abundance in northwest Ontario (Canada) lakes during the warmer early-to mid-Holocene period. Quaternary Science Reviews 123, 168-179. https://doi.org/10.1016/j.quascirev.2015.06.025.

Kenney, W.F., Brenner, M., Curtis, J.H., Arnold, T.E., Schelske, C.L., 2016. A Holocene sediment record of phosphorus accumulation in shallow Lake Harris, Florida (USA) offers new perspectives on recent cultural eutrophication. PLOS ONE 11(1), e0147331. https://doi.org/10.1371/journal.pone.0147331.

Kong, X.Z., He, Q.S., Yang, B., He, W., Xu, F.L., Janssen, A.B.G., Kuiper, J.J., van Gerven, L.P.A., Qin, N., Jiang, Y.J., Liu, W.X., Yang, C., Bai, Z.L., Zhang, M., Kong, F.X., Janse, J.H., Mooij, W.M., 2017. Hydrological regulation drives regime shifts: evidence from paleolimnology and ecosystem modeling of a large shallow Chinese lake. Global Change Biology 23(2), 737-754. https://doi.org/10.1111/gcb.13416.

Kosten, S., Huszar, V.L., Bécares, E., Costa, L.S., van Donk, E., Hansson, L.A., Jeppesen, E., Kruk, C., Lacerot, G., Mazzeo, N., 2012. Warmer climates boost cyanobacterial dominance in shallow lakes. Global Change Biology 18(1), 118-126. https://doi.org/10.1111/j.1365-2486.2011.02488.x.

Lamb, A., 2021. Using Sediments to Identify Drivers of Cyanobacteria, Cyanotoxins, and Eutrophication in the Shallow, Subtropical Lakes of Florida, USA, Crop Soils and Environmental Sciences. Auburn University, Auburn. https://etd.auburn.edu//handle/10415/7901.

Lammertsma, E.I., Donders, T.H., Pearce, C., Cremer, H., Gaiser, E.E., Wagner-Cremer, F., 2015. Sensitivity of wetland hydrology to external climate forcing in central Florida. Quaternary Research. https://doi.org/10.1016/J.YQRES.2015.09.003.

Lawson, G.M., Young, J.L., Aanderud, Z.T., Jones, E.F., Bratsman, S., Daniels, J., Malmfeldt, M.P., Baker, M.A., Abbott, B.W., Daly, S., Paerl, H.W., Carling, G., Brown, B., Lee, R., Wood, R.L., 2025. Nutrient limitation and seasonality associated with phytoplankton communities and cyanotoxin production in a large, hypereutrophic lake. Harmful Algae 143, 102809. https://doi.org/10.1016/j.hal.2025.102809.

Leavitt, P.R., 1993. A review of factors that regulate carotenoid and chlorophyll deposition and fossil pigment abundance. Journal of Paleolimnology 9, 109-127. https://doi.org/10.1007/BF00677513.

Leavitt, P., Hodgson, D., 2001. Sedimentary pigments. In: Smol, J.P., Birks, H.J.B., Last, W.M., Bradley, R.S., Alverson, K. (eds), Tracking environmental change using lake sediments. Springer, pp. 295–325. https://doi.org/10.1007/0-306-47668-1_15.

Litchman, E., de Tezanos Pinto, P., 2024. Chapter 18 - Ecology of algae and cyanobacteria (Phytoplankton), in: Jones, I.D., Smol, J.P. (Eds.), Wetzel's Limnology (Fourth Edition). Academic Press, San Diego, pp. 511-538. https://doi.org/10.1016/B978-0-12-822701-5.00018-5.

Lukač, M., Aegerter, R., 1993. Influence of trace metals on growth and toxin production of Microcystis aeruginosa. Toxicon 31(3), 293-305. https://doi.org/10.1016/0041-0101(93)90147-B.

MacKeigan, P.W., Zastepa, A., Taranu, Z.E., Westrick, J.A., Liang, A., Pick, F.R., Beisner, B.E., Gregory-Eaves, I., 2023. Microcystin concentrations and congener composition in relation to environmental variables across 440 north-temperate and boreal lakes. Science of The Total Environment 884, 163811. https://doi.org/10.1016/j.scitotenv.2023.163811.

Magley, W., 2003. Total Maximum Daily Load for Total Phosphorus For Lake Dora and Dora Canal Lake County, Florida. Florida Department of Environmental Protection Watershed Assessment Section. https://floridadep.gov/sites/default/files/dora_canal-tp-tmdl.pdf.

McGowan, S., Anderson, N.J., Edwards, M.E., Hopla, E., Jones, V., Langdon, P.G., Law, A., Soloveiva, N., Turner, S., van Hardenbroek, M., Whiteford, E.J., Wiik, E., 2018. Vegetation transitions drive the autotrophy-heterotrophy balance in Arctic lakes. Limnology and Oceanography Letters 3(3), 246-255. https://doi.org/10.1002/lol2.10086.

Merder, J., Harris, T., Zhao, G., Stasinopoulos, D.M., Rigby, R.A., Michalak, A.M., 2023. Geographic redistribution of microcystin hotspots in response to climate warming. Nature Water 1, 844-854. https://doi.org/10.1038/s44221-023-00138-w.

Merel, S., Walker, D., Chicana, R., Snyder, S., Baurès, E., Thomas, O., 2013. State of knowledge and concerns on cyanobacterial blooms and cyanotoxins. Environment International 59, 303-327. https://doi.org/10.1016/j.envint.2013.06.013.

Meyers, P.A., Ishiwatari, R., 1993. Lacustrine organic geochemistry—an overview of indicators of organic matter sources and diagenesis in lake sediments. Organic Geochemistry 20(7), 867-900. https://doi.org/10.1016/0146-6380(93)90100-P.

Neilan, B.A., Pearson, L.A., Muenchhoff, J., Moffitt, M.C., Dittmann, E., 2013. Environmental conditions that influence toxin biosynthesis in cyanobacteria. Environmental Microbiology 15(5), 1239-1253. https://doi.org/10.1111/j.1462-2920.2012.02729.x.

Orihel, Diane M., Bird, David F., Brylinsky, M., Chen, H., Donald, Derek B., Huang, Dorothy Y., Giani, A., Kinniburgh, D., Kling, H., Kotak, Brian G., Leavitt, Peter R., Nielsen, Charlene C., Reedyk, S., Rooney, Rebecca C., Watson, Sue B., Zurawell, Ron W., Vinebrooke, Rolf D., 2012. High microcystin concentrations occur only at low nitrogen-to-phosphorus ratios in nutrient-rich Canadian lakes. Canadian Journal of Fisheries and Aquatic Sciences 69, 1457-1462. https://doi.org/10.1139/f2012-088.

Otto, J.S., 1985. Florida's cattle-ranching frontier: Manatee and Brevard Counties (1860). The Florida Historical Quarterly 64(1), 48-61. http://www.jstor.org/stable/30149906.

Paerl, H.W., Huisman, J., 2008. Blooms like it hot. Science 320(5872), 57-58. https://doi.org/10.1126/science.1155398.

Paerl, H.W., Scott, J.T., McCarthy, M.J., Newell, S.E., Gardner, W.S., Havens, K.E., Hoffman, D.K., Wilhelm, S.W., Wurtsbaugh, W.A., 2016. It takes two to tango: When and where dual nutrient (N & P) reductions are needed to protect lakes and downstream ecosystems. Environmental Science & Technology 50(20), 10805-10813. https://doi.org/10.1111/1462-2920.13035.

Pal, S., Gregory-Eaves, I., Pick, F.R., 2015. Temporal trends in cyanobacteria revealed through DNA and pigment analyses of temperate lake sediment cores. Journal of Paleolimnology 54(1), 87-101. https://doi.org/10.1007/s10933-015-9839-1.

Paradeisis-Stathis, S., Waters, M.N., 2025. Linking phosphorus dynamics with hypereutrophic conditions on the millennial scale: The paleolimnology of shallow and subtropical Lake Wauberg, Florida, USA. Science of The Total Environment 982, 179625. https://doi.org/10.1016/j.scitotenv.2025.179625.

Patil, I., 2021. Visualizations with statistical details: The 'ggstatsplot' approach. Journal of Open Source Software 6(61), 3167. https://doi.org/10.21105/joss.03167.

Pawlik-Skowrońska, B., Kornijów, R., Pirszel, J., 2010. Sedimentary imprint of cyanobacterial blooms - a new tool for insight into recent history of lakes. Polish Journal of Ecology 58, 663-670.

Picard, M., Wood, S.A., Pochon, X., Vandergoes, M.J., Reyes, L., Howarth, J.D., Hawes, I., Puddick, J., 2022. Molecular and pigment analyses provide comparative results when reconstructing historic cyanobacterial abundances from lake sediment cores. Microorganisms 10(2), 279. https://doi.org/10.3390/microorganisms10020279.

Pick, F.R., 2016. Blooming algae: a Canadian perspective on the rise of toxic cyanobacteria. Canadian Journal of Fisheries and Aquatic Sciences 73(7), 1149-1158. https://doi.org/10.1139/cjfas-2015-0470.

Pimentel, J.S.M., Giani, A., 2014. Microcystin production and regulation under nutrient stress conditions in toxic *Microcystis* strains. Applied and Environmental Microbiology 80(18), 5836-5843. https://doi.org/10.1128/aem.01009-14.

Randsalu-Wendrup, L., Conley, D.J., Carstensen, J., Fritz, S.C., 2016. Paleolimnological records of regime shifts in lakes in response to climate change and anthropogenic activities. Journal of Paleolimnology 56(1), 1-14. https://doi.org/10.1007/s10933-016-9884-4.

Rastogi, R.P., Sinha, R.P., Incharoensakdi, A., 2014. The cyanotoxin-microcystins: current overview. Reviews in Environmental Science and Bio/Technology 13(2), 215-249. https://doi.org/10.1007/s11157-014-9334-6.

Rastogi, R.P., Sonani, R.R., Madamwar, D., 2015. Cyanobacterial sunscreen scytonemin: Role in photoprotection and biomedical research. Appl Biochem Biotechnol 176(6), 1551-1563. https://doi.org/10.1007/s12010-015-1676-1.

Schampera, C., Hellweger, F.L., 2024. Nitrogen availability controls response of microcystin concentration to phosphorus reduction: Evidence from model application to multiple lakes. Harmful Algae 139, 102711. https://doi.org/10.1016/j.hal.2024.102711.

Schelske, CL, Kenney, W.F., Hansen, PS, Whitmore, T.J., Waters, M.N., 1999. Sediment and Nutrient Deposition in Lake Dora and Lake Eustis. Department of Fisheries and Aquatic Sciences University of Florida.

Schelske, C.L., Lowe, E.F., Battoe, L.E., Brenner, M., Coveney, M.F., Kenney, W.F., 2005. Abrupt biological response to hydrologic and land-use changes in Lake Apopka, Florida, USA. AMBIO: A Journal of the Human Environment 34(3), 192-198, 197. https://doi.org/10.1579/0044-7447-34.3.192.

Schelske, C.L., Peplow, A., Brenner, M., Spencer, C.N., 1994. Low-background gamma counting: applications for210Pb dating of sediments. Journal of Paleolimnology 10(2), 115-128. https://doi.org/10.1007/BF00682508.

Schindler, D.W., Carpenter, S.R., Chapra, S.C., Hecky, R.E., Orihel, D.M., 2016. Reducing phosphorus to curb lake eutrophication is a success. Environmental Science & Technology 50(17), 8923-8929. https://doi.org/10.1021/acs.est.6b02204.

Schmidt, J.R., Wilhelm, S.W., Boyer, G.L., 2014. The fate of microcystins in the environment and challenges for monitoring. Toxins (Basel) 6(12), 3354-3387. https://doi.org/10.3390/toxins6123354.

Scott, J.T., McCarthy, M.J., Paerl, H.W., 2019. Nitrogen transformations differentially affect nutrient-limited primary production in lakes of varying trophic state. Limnology and Oceanography Letters 4, 96-104. https://doi.org/10.1002/lol2.10109.

Snitker, G., 2020. The Charcoal Quantification Tool (CharTool): A suite of open-source tools for quantifying charcoal fragments and sediment properties in archaeological and paleoecological analysis. Ethnobiology Letters 11(1). https://doi.org/10.14237/ebl.11.1.2020.1653.

Song, H., Coggins, L.X., Reichwaldt, E.S., Ghadouani, A., 2015. The importance of lake sediments as a pathway for microcystin dynamics in shallow eutrophic lakes. Toxins 7(3), 900-918. https://doi.org/10.3390/toxins7030900.

Stanton, E.A., Taylor, M., 2012. Valuing Florida's clean waters. Stockholm Environment Institute–US Center. https://www.infrastructureusa.org/wp-content/uploads/2012/11/ValuingFloridasCleanWaters.pdf.

Steffen, M.M., Davis, T.W., McKay, R.M.L., Bullerjahn, G.S., Krausfeldt, L.E., Stough, J.M., Neitzey, M.L., Gilbert, N.E., Boyer, G.L., Johengen, T.H., 2017. Ecophysiological examination of the Lake Erie Microcystis bloom in 2014: linkages between biology and the water supply shutdown of Toledo, OH. Environmental science & technology 51(12), 6745-6755. https://doi.org/10.1021/acs.est.7b00856.

Stockmarr, J., 1971. Tablets with Spores used in Absolute Pollen Analysis. Pollen et Spores 13, 615-621.
Tang Y, H.M., Li W, 2016. ggfortify: Unified interface to visualize statistical result of popular R packages. The R Journal 8(2), 474–485. https://doi.org/10.32614/RJ-2016-060.

Traverse, A., 2007. Paleopalynology, 2nd ed. Springer, Dordrecht.

Tsuji, K., Masui, H., Uemura, H., Mori, Y., Harada, K.-i., 2001. Analysis of microcystins in sediments using MMPB method. Toxicon 39(5), 687-692. https://doi.org/10.1016/S0041-0101(00)00196-3.

Utkilen, H., Gjølme, N., 1995. Iron-stimulated toxin production in Microcystis aeruginosa. Appl Environ Microbiol 61(2), 797-800. https://doi.org/10.1128/aem.61.2.797-800.1995.

Vachula, R.S., Russell, J.M., Huang, Y., 2019. Climate exceeded human management as the dominant control of fire at the regional scale in California's Sierra Nevada. Environmental Research Letters 14(10), 104011. https://dx.doi.org/10.1088/1748-9326/ab4669.

Vézie, C., Rapala, J., Vaitomaa, J., Seitsonen, J., Sivonen, K., 2002. Effect of nitrogen and phosphorus on growth of toxic and nontoxic Microcystis strains and on intracellular microcystin concentrations. Microb Ecol 43(4), 443-454. https://doi.org/10.1007/s00248-001-0041-9.

Wagner, N.D., Osburn, F.S., Wang, J., Taylor, R.B., Boedecker, A.R., Chambliss, C.K., Brooks, B.W., Scott, J.T., 2019. Biological stoichiometry regulates toxin production in *Microcystis aeruginosa* (UTEX 2385), Toxins. https://doi.org/10.3390/toxins11100601.

Wagner, N.D., Quach, E., Buscho, S., Ricciardelli, A., Kannan, A., Naung, S.W., Phillip, G., Sheppard, B., Ferguson, L., Allen, A., Sharon, C., Duke, J.R., Taylor, R.B., Austin, B.J., Stovall, J.K., Haggard, B.E., Chambliss, C.K., Brooks, B.W., Scott, J.T., 2021. Nitrogen form, concentration, and micronutrient availability affect microcystin production in cyanobacterial blooms. Harmful Algae 103, 102002. https://doi.org/10.1016/j.hal.2021.102002.

Walls, J.T., Wyatt, K.H., Doll, J.C., Rubenstein, E.M., Rober, A.R., 2018. Hot and toxic: Temperature regulates microcystin release from cyanobacteria. Science of The Total Environment 610-611, 786-795. https://doi.org/10.1016/j.scitotenv.2017.08.149.

Wang, H., Xu, C., Liu, Y., Jeppesen, E., Svenning, J.-C., Wu, J., Zhang, W., Zhou, T., Wang, P., Nangombe, S., Ma, J., Duan, H., Fang, J., Xie, P., 2021. From unusual suspect to serial killer: Cyanotoxins boosted by climate change may jeopardize megafauna. The Innovation 2(2). https://doi.org/10.1016/j.xinn.2021.100092.

Waters, M.N., 2016. A 4700-year history of cyanobacteria toxin production in a shallow subtropical lake. Ecosystems 19(3), 426-436. https://doi.org/10.1007/s10021-015-9943-0.

Waters, M.N., Brenner, M., Curtis, J.H., Romero-Oliva, C.S., Dix, M., Cano, M., 2021. Harmful algal blooms and cyanotoxins in Lake Amatitlán, Guatemala, coincided with ancient Maya occupation in the watershed. Proceedings of the National Academy of Sciences 118(48), e2109919118. https://doi.org/10.1073/pnas.2109919118.

Waters, M.N., Kenney, W.F., Brenner, M., Webster, B.C., 2019. Organic carbon sequestration in sediments of subtropical Florida lakes. PLOS ONE 14(12), e0226273. https://doi.org/10.1371/journal.pone.0226273.

Waters, M.N., Piehler, M.F., Smoak, J.M., Bianchi, T.S., 2012. Algal community responses to shallow lake dystrophication. Canadian Journal of Fisheries and Aquatic Sciences 69(8), 1433-1443. https://doi.org/10.1139/f2012-021.

Waters, M.N., Schelske, C.L., Brenner, M., 2015. Cyanobacterial dynamics in shallow Lake Apopka (Florida, U.S.A.) before and after the shift from a macrophyte-dominated to a phytoplankton-dominated state. Freshwater Biology 60(8), 1571-1580. https://doi.org/10.1111/fwb.12589.

Waters, M.N., Smoak, J.M., Saunders, C.J., 2013. Historic primary producer communities linked to water quality and hydrologic changes in the northern Everglades. Journal of Paleolimnology 49(1), 67-81. https://doi.org/10.1007/s10933-011-9569-y.

Waters, M.N., Smoak, J.M., Vachula, R.S., 2023. Linking prescribed fire, nutrient deposition and cyanobacteria dominance through pyroeutrophication in a subtropical lake ecosystem from the mid Holocene to present. Anthropocene 44, 100420. https://doi.org/10.1016/j.ancene.2023.100420.

Wei, N., Hu, C., Dittmann, E., Song, L., Gan, N., 2024. The biological functions of microcystins. Water Research 262, 122119. https://doi.org/10.1016/j.watres.2024.122119.

Welker, M., Steinberg, C., 2000. Rates of humic substance photosensitized degradation of Microcystin-LR in natural waters. Environmental Science & Technology 34(16), 3415-3419. https://doi.org/10.1021/es991274t.

Whitmore, T.J., Brenner, M., Schelske, C.L., 1996. Highly variable sediment distribution in shallow, wind-stressed lakes: a case for sediment-mapping surveys in paleolimnological studies. Journal of Paleolimnology 15(3), 207-221. https://doi.org/10.1007/BF00213041.

Whitmore, T.J., Riedinger-Whitmore, M.A., Lauterman, F.M., Curtis, J.H., 2018. Cyanobacterial influence on diatom community lifeform dynamics in shallow subtropical lakes of Florida USA. Journal of Paleolimnology 60(2), 223-246. https://doi.org/10.1007/s10933-018-0018-z.

Whitmore, T.J., Riedinger-Whitmore, M.A., Reed, Z.E., Curtis, J.H., Yang, H., Evans, D.E., Cropper, N.R., Alvarado, K.S., Lauterman, F.M., Scott, A., Leonard, C.R., Franklin, D.L., 2020. Paleolimnological assessment of six lakes on the Kissimmee Chain, with implications for restoration of the Kissimmee–Okeechobee–Everglades system, Florida, USA. Lake and Reservoir Management 36(3), 218-242. https://doi.org/10.1080/10402381.2020.1785064.

Willard, D., Bernhardt, C., Brown, R., Landacre, B., Townsend, P., 2011. Development and application of a pollen-based paleohydrologic reconstruction from the Lower Roanoke River Basin, North Carolina, USA. The Holocene 21(2), 305-317. https://doi.org/10.1177/0959683610378876.

Willard, D.A., 2023. Pollen records, postglacial—Southeastern North America☆, Reference Module in Earth Systems and Environmental Sciences. Elsevier. https://doi.org/10.1016/B978-0-323-99931-1.00030-1.

Williams, C.D., Aubel, M.T., Chapman, A.D., D'Aiuto, P.E., 2007. Identification of cyanobacterial toxins in Florida's freshwater systems. Lake and Reservoir Management 23(2), 144-152. https://doi.org/10.1080/07438140709353917.

Williams, J.W., Grimm, E.C., Blois, J.L., Charles, D.F., Davis, E.B., Goring, S.J., Graham, R.W., Smith, A.J., Anderson, M., Arroyo-Cabrales, J., Ashworth, A.C., Betancourt, J.L., Bills, B.W., Booth, R.K., Buckland, P.I., Curry, B.B., Giesecke, T., Jackson, S.T., Latorre, C., Nichols, J., Purdum, T., Roth, R.E., Stryker, M., Takahara, H., 2018. The Neotoma Paleoecology Database, a multiproxy, international, community-curated data resource. Quaternary Research 89(1), 156-177. https://doi.org/10.1017/qua.2017.105.

Wood, S.A., Borges, H., Puddick, J., Biessy, L., Atalah, J., Hawes, I., Dietrich, D.R., Hamilton, D.P., 2017. Contrasting cyanobacterial communities and microcystin concentrations in summers with extreme weather events: insights into potential effects of climate change. Hydrobiologia 785, 71-89. https://doi.org/10.1007/s10750-016-2904-6.

Wood, S.A., Kelly, L., Bouma-Gregson, K., Humbert, J.F., Laughinghouse, H.D.t., Lazorchak, J., McAllister, T., McQueen, A., Pokrzywinski, K., Puddick, J., Quiblier, C., Reitz, L.A., Ryan, K., Vadeboncoeur, Y., Zastepa, A., Davis, T.W., 2020. Toxic benthic freshwater cyanobacterial proliferations: Challenges and solutions for enhancing knowledge and improving monitoring and mitigation. Freshw Biol 65(10), 1824-1842. https://doi.org/10.1111/fwb.13532.

Wu, Z., Liu, Y., Liang, Z., Wu, S., Guo, H., 2017. Internal cycling, not external loading, decides the nutrient limitation in eutrophic lake: A dynamic model with temporal Bayesian hierarchical inference. Water Research 116, 231-240. https://doi.org/10.1016/j.watres.2017.03.039.

Wu, X., Wang, C., Tian, C., Xiao, B., Song, L., 2015. Evaluation of the potential of anoxic biodegradation of intracellular and dissolved microcystins in lake sediments. Journal of Hazardous Materials 286, 395-401. https://doi.org/10.1016/j.jhazmat.2015.01.015.

Wu, X., Xiao, B., Li, R., Wang, C., Huang, J., Wang, Z., 2011. Mechanisms and factors affecting sorption of microcystins onto natural sediments. Environmental Science & Technology 45(7), 2641-2647. https://doi.org/10.1021/es103729m.

Xiao, M., Burford, M.A., Wood, S.A., Aubriot, L., Ibelings, B.W., Prentice, M.J., Galvanese, E.F., Harris, T.D., Hamilton, D.P., 2022. Schindler's legacy: from eutrophic lakes to the phosphorus utilization strategies of cyanobacteria. FEMS Microbiology Reviews 46. https://doi.org/10.1093/femsre/fuac029.

Xue, Q., Rediske, R.R., Gong, Z., Su, X., Xu, H., Cai, Y., Zhao, Y., Xie, L., 2018. Spatio-temporal variation of microcystins and its relationship to biotic and abiotic factors in Hongze Lake, China. Journal of Great Lakes Research 44(2), 253-262. https://doi.org/10.1016/j.jglr.2017.12.004.

Zastepa, A., Pick, F.R., Blais, J.M., 2014. Fate and persistence of particulate and dissolved Microcystin-LA from microcystis blooms. Human and Ecological Risk Assessment: An International Journal 20(6), 1670-1686. https://doi.org/10.1080/10807039.2013.854138.

Zastepa, A., Taranu, Z.E., Kimpe, L.E., Blais, J.M., Gregory-Eaves, I., Zurawell, R.W., Pick, F.R., 2017. Reconstructing a long-term record of microcystins from the analysis of lake sediments. Science of The Total Environment 579, 893-901. https://doi.org/10.1016/j.scitotenv.2016.10.211.

Zhang, Y., Whalen, J.K., Cai, C., Shan, K., Zhou, H., 2023. Harmful cyanobacteria-diatom/dinoflagellate blooms and their cyanotoxins in freshwaters: A nonnegligible chronic health and ecological hazard. Water Research 233, 119807. https://doi.org/10.1016/j.jes.2022.03.038.

Zilliges, Y., Kehr, J.-C., Meissner, S., Ishida, K., Mikkat, S., Hagemann, M., Kaplan, A., Börner, T., Dittmann, E., 2011. The cyanobacterial hepatotoxin microcystin binds to proteins and increases the fitness of Microcystis under oxidative stress conditions. PLoS ONE 6, e17615. https://dx.doi.org/10.1371/journal.pone.0017615.

3.8 Tables

Table 3.1 Average concentrations and standard deviations for the analyzed variables in LDO (Fig. 3.3) distributed in the three chronologically sorted MC zones.

Variable	Unit	6.4-5.1 ka BP (n=21)	5.1-0.02 ka BP (n=89)	1930 CE to pres. (n=17)
MC Zone		Moderate	Low	High
TOC	%	21.13 (±7.78)	34.72 (±2.16)	33.23 (±4.9)
TN	%	1.45 (±0.58)	2.68 (±0.32)	3.35 (±0.81)
TOC / TN	-	17.9 (±1.79)	15.67 (±1.06)	11.95 (±1.15)
TP	mg g^{-1}	0.25 (±0.13)	0.24 (±0.1)	1.93 (±0.57)
TN / TP	-	140.14 (±52.39)	270.11 (±64.6)	39.82 (±8.94)
Fe	mg g^{-1}	6.11 (±1.56)	8.63 (±2.21)	6.83 (±2.04)
TS	mg g^{-1}	11.75 (±3.49)	13.40 (±2.03)	14.86 (±1.79)
B-car	nmol g^{-1} org	78.84 (±29.45)	24.57 (±9)	98.8 (±34.67)
Diato	nmol g^{-1} org	2.6 (±1.32)	2.32 (±2.13)	56.08 (±42.88)
Allo	nmol g^{-1} org	2.07 (±0.75)	0.86 (±0.59)	8.57 (±2.8)
Ech	nmol g^{-1} org	10.46 (±3.65)	7.39 (±4.11)	37.92 (±21.18)
Canth	nmol g^{-1} org	9.28 (±5.55)	4.19 (±2.07)	7.98 (±7.8)
Oke	nmol g^{-1} org	2.27 (±2.45)	0.27 (±0.19)	-
MCs	ng g^{-1} org	5.58 (±1.57)	2.76 (±0.91)	164.82 (±262.93)

Table 3.2 Average concentrations and standard deviations for the analyzed variables in LMA (Fig. 3.4) distributed in the three chronologically sorted MC zones.

Variable	Unit	7.2-2.3 ka BP (n=42)	2.3-0.15 ka BP (n=23)	1800 CE to pres. (n=13)
MC Zone		Moderate	Low	High
TOC	%	15.76 (±9.68)	22.42 (±5.4)	27.34 (±7.51)
TN	%	1.21 (±0.84)	1.85 (±0.45)	2.66 (±0.92)
TOC / TN	-	16.94 (±5.1)	14.24 (±1.54)	12.4 (±1.56)
TP	mg g^{-1}	0.47 (±0.49)	0.19 (±0.02)	1.1 (±0.54)
TN / TP	-	163.76 (±198.84)	255.43 (±53.05)	70.91 (±28.59)
Fe	mg g^{-1}	8.36 (±4.38)	7.03 (±0.91)	7.89 (±1.41)
TS	mg g^{-1}	6.75 (±3.27)	4.49 (±0.73)	3.36 (±0.42)
B-car	nmol g^{-1} org	37.23 (±16.84)	30.28 (±8.16)	92.17 (±57.95)
Diato	nmol g^{-1} org	13.4 (±12.16)	16.97 (±4.07)	24.44 (±10.67)
Allo	nmol g^{-1} org	1.68 (±1.93)	2.45 (±0.64)	20.37 (±15.65)
Ech	nmol g^{-1} org	15.42 (±9.05)	14.69 (±8.92)	20.84 (±16.61)
Canth	nmol g^{-1} org	19.54 (±12.11)	16.29 (±7.81)	34.72 (±20.93)
Oke	nmol g^{-1} org	3.02 (±3.16)	1.68 (±0.57)	0.16 (±0.56)
MCs	ng g^{-1} org	6.97 (±2.4)	3.23 (±1.16)	1,427.24 (±1693.62)

3.9 Figures

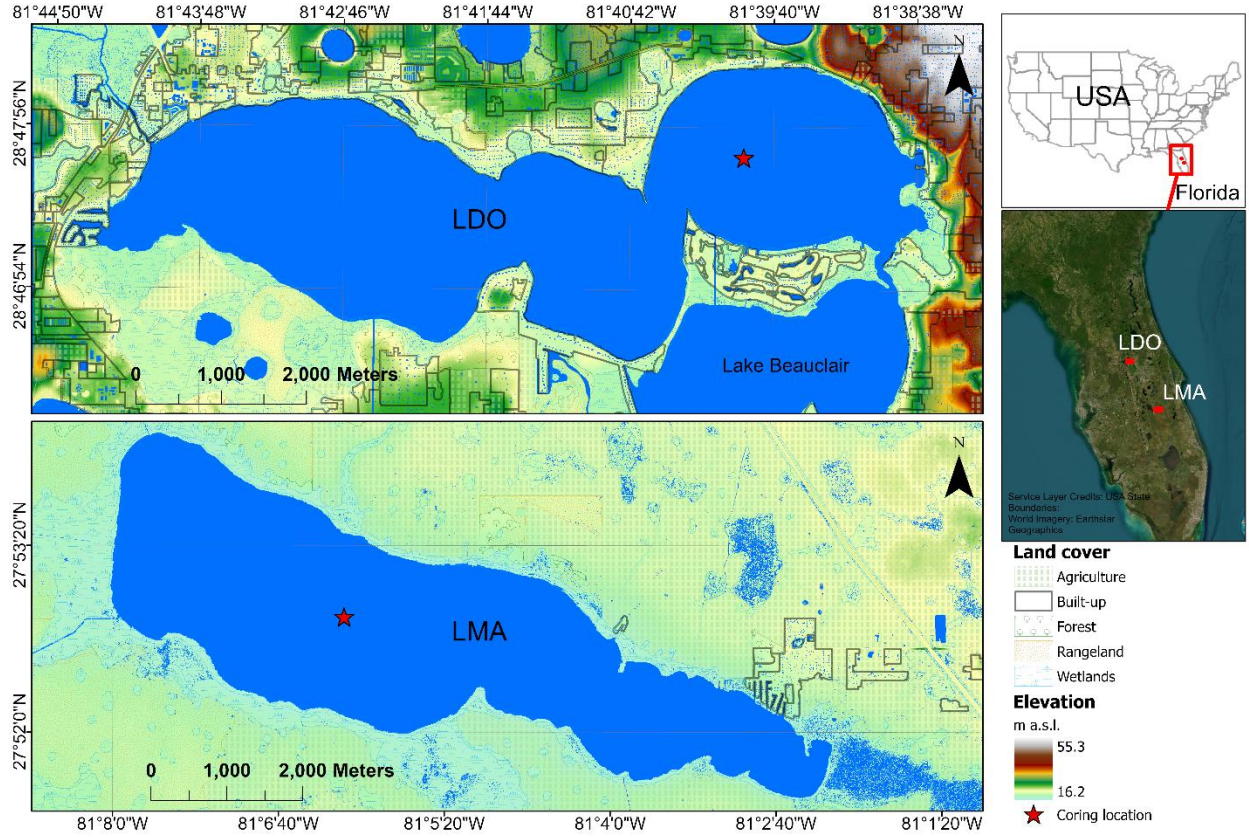

Figure 3.1 Location, elevation, land cover, and coring site maps of LDO and LMA. Elevation changes at LMA are minor, while a more distinct change is observed at the NW side of LDO. The build-up environment and agriculture characterize LDO and LMA, respectively. GIS layers source: section 3.3.5.

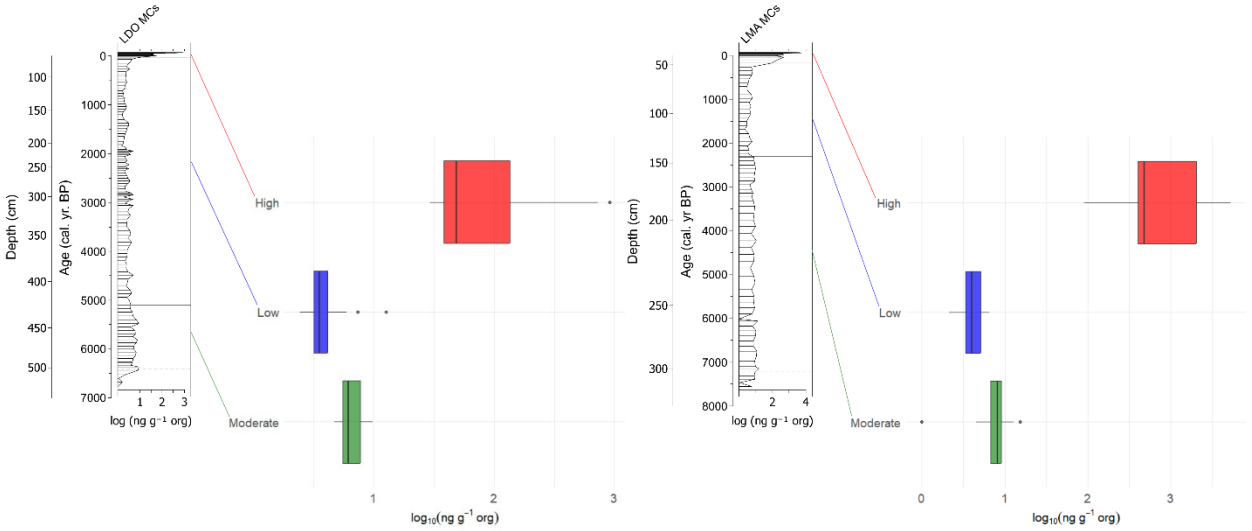

Figure 3.2 Microcystin concentrations for LDO and LMA presented over time and in box plots per MC zone. In the time plots, the dashed lines delineate the initiation of continuous limnological conditions, and the solid lines delineate the three zones of low, moderate, and high MCs.

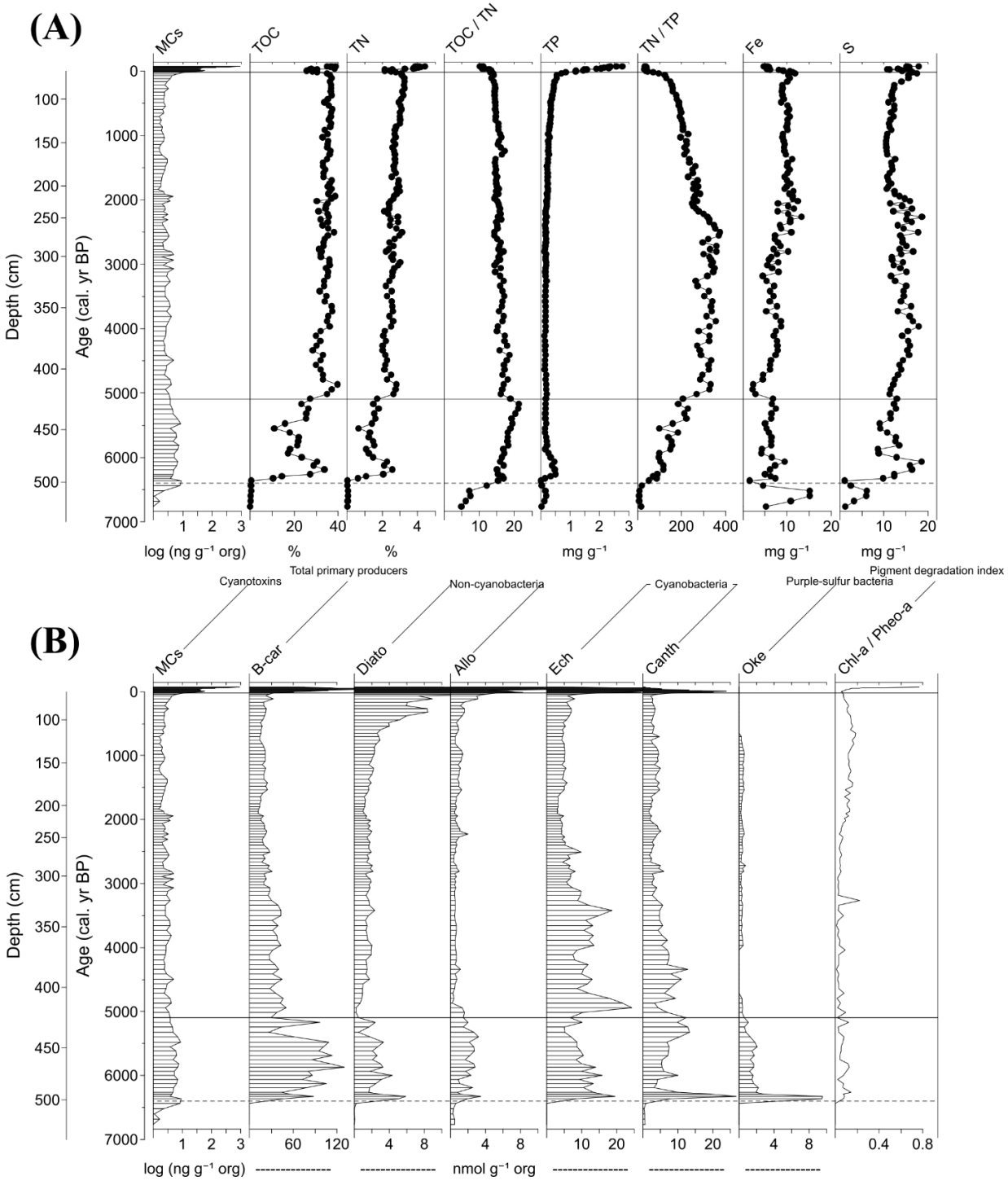

Figure 3.3 Time plots for LDO of (A) nutrients, elements, and ratios and (B) photosynthetic pigments and cyanotoxins. The dashed lines delineate the initiation of continuous limnological conditions. The solid lines delineate the MC concentration zones. The photosynthetic pigments are beta-carotene (B-car), diatoxanthin (Diato), alloxanthin (Allo), echinenone (Ech), canthaxanthin (Canth), and okenone (Oke). The pigment degradation index is the chlorophyll-a (chl-a) ratio to pheophytin-a (pheo-a). An analytical description of each photosynthetic pigment is presented in Table S3.6. The photosynthetic pigment abundances of b-car, diato, and ech in the top zone have been truncated. Cyanotoxin concentration measures total MCs on a log scale.

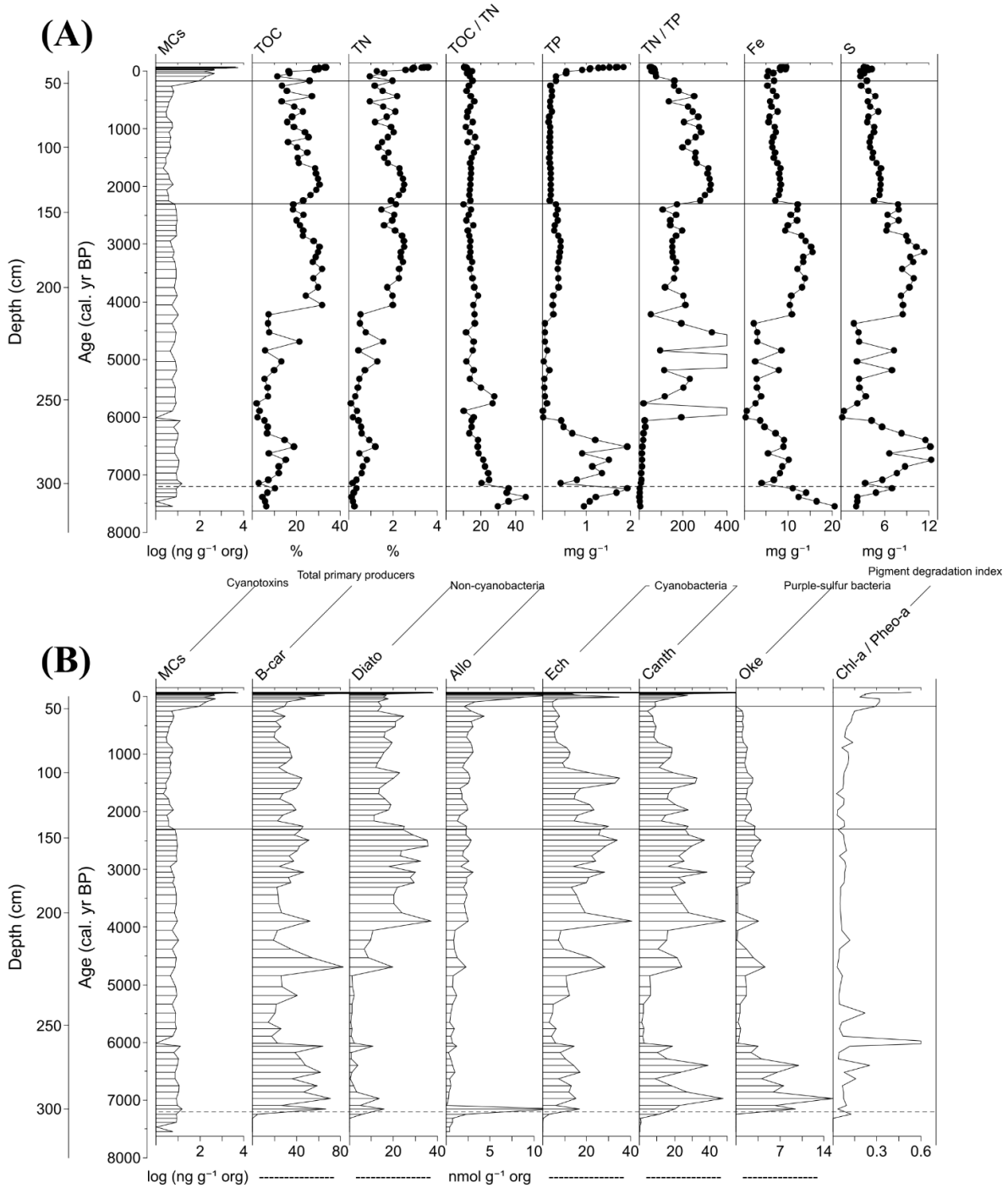

Figure 3.4 Time plots for LMA of (A) nutrients, elements, and ratios and (B) photosynthetic pigments and cyanotoxins. The dashed lines delineate the initiation of continuous limnological conditions. The solid lines delineate the MC concentration zones. The photosynthetic pigments are beta-carotene (B-car), diatoxanthin (Diato), alloxanthin (Allo), echinenone (Ech), canthaxanthin (Canth), and okenone (Oke). The pigment degradation index is the chlorophyll-a (chl-a) ratio to pheophytin-a (pheo-a). An analytical description of each photosynthetic pigment is presented in Table S3.6. The photosynthetic pigment abundances of b-car, allo, ech, and canth over the period with increased pigment preservation (high chl-a/pheo-a over the last ~10 years) have been truncated. Cyanotoxin concentration measures total MCs on a log scale.

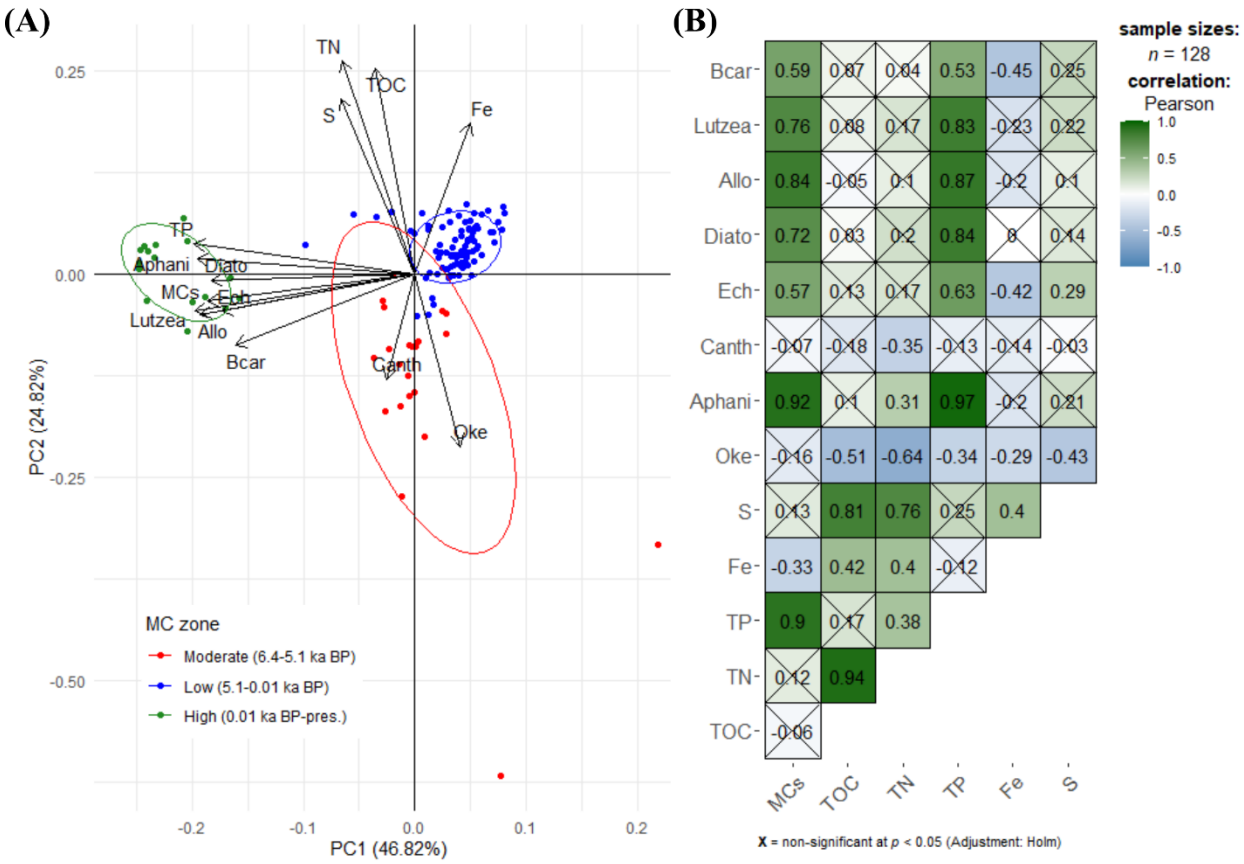

Figure 3.5 Data exploration of the LDO dataset through (A) Principal component analysis (PCA) and (B) Pearson correlation analysis. The photosynthetic pigments are beta-carotene (B-car), lutein+zeaxanthin (Lutzea), alloxanthin (Allo), diatoxanthin (Diato), echinenone (Ech), canthaxanthin (Canth), aphanizophyll (Aphani), and okenone (Oke). (A) Dimensionality reduction using PCA. The plot presents the variance in the dataset using PC1 (46.82%) and PC2 (24.82%) while grouping the data points into the three MCs-defined chronological zones (I, II, and III) with limnological conditions over the last 6.4 ka BP. The oval shapes represent 68% confidence intervals. (B) Correlation matrices with MCs, elements, and photosynthetic pigments with samples spanning the last 6.4 ka BP.

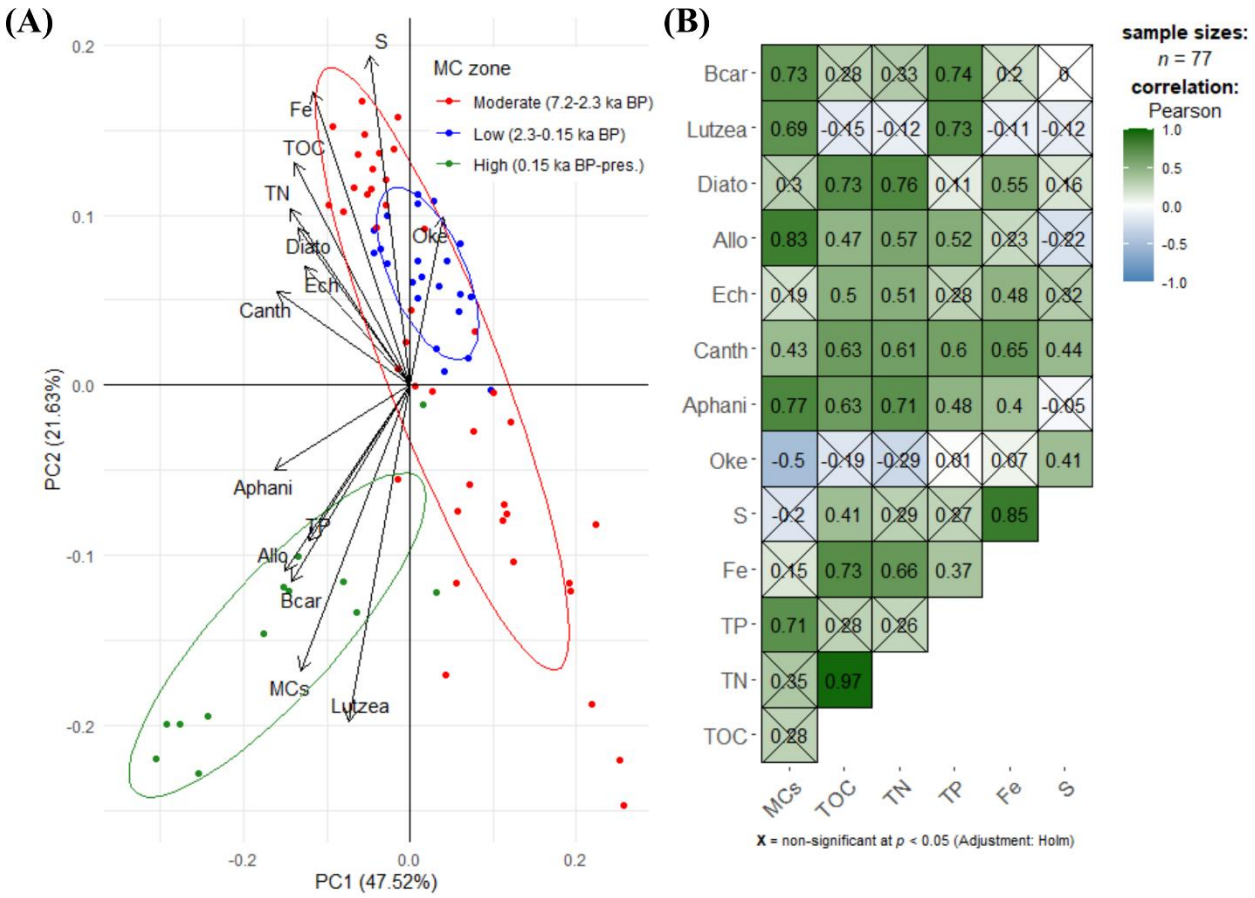

Figure 3.6 Data exploration of the LMA dataset through (A) Principal component analysis (PCA) and (B) Pearson correlation analysis. The photosynthetic pigments are beta-carotene (B-car), lutein+zeaxanthin (Lutzea), alloxanthin (Allo), diatoxanthin (Diato), echinenone (Ech), canthaxanthin (Canth), aphanizophyll (Aphani), and okenone (Oke). (A) Dimensionality reduction using PCA. The plot presents the variance in the dataset using PC1 (47.52%) and PC2 (21.63%) while grouping the data points into the three MCs-defined chronological zones (I, II, and III) with limnological conditions over the last 7.2 ka BP. The oval shapes represent 68% confidence intervals. (B) Correlation matrices with MCs, elements, and photosynthetic pigments with samples spanning the last 7.2 ka BP.

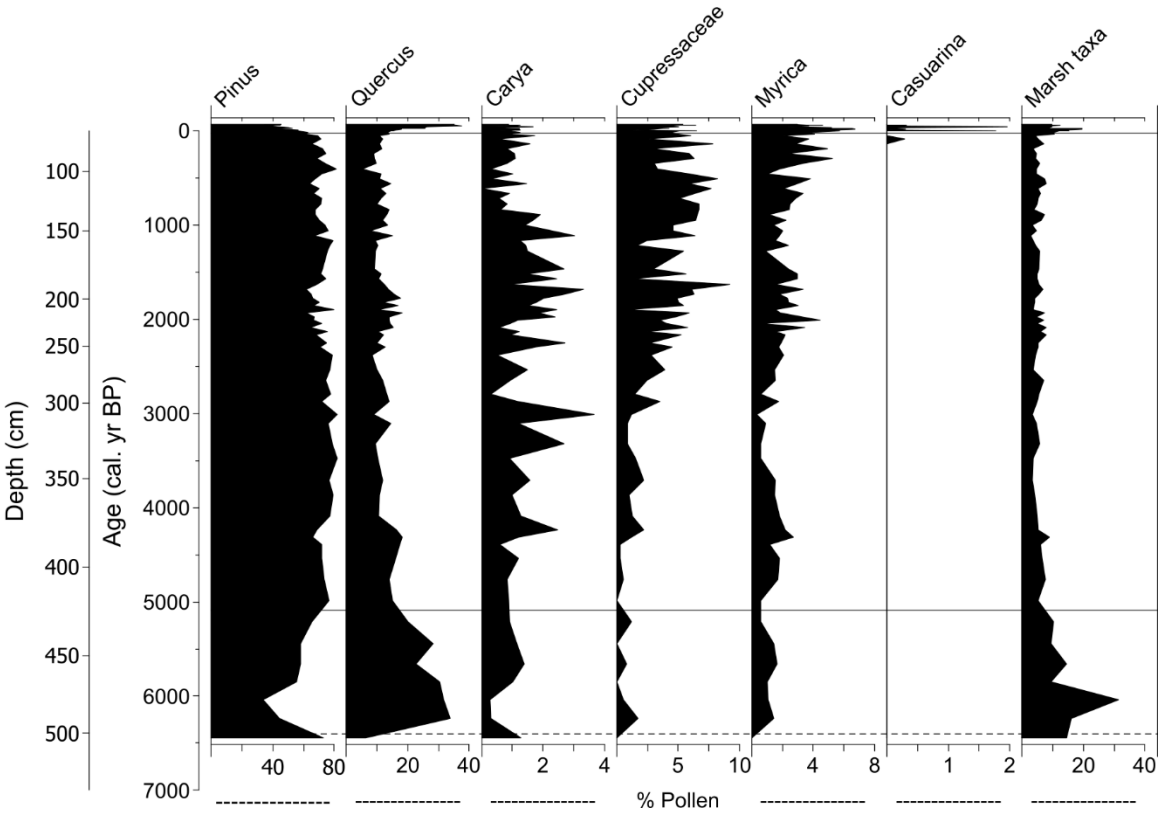

Figure 3.7 Pollen diagram of selected types in percentages for LDO. Marsh taxa include pollen from *Poaceae, Amaranthaceae, Asteraceae, Cyperaceae, Nymphaea, Sagittaria, Typha, Nuphar, Myriophyllum, Utricularia, and Orontium* (Fig. S3.13). The solid lines delineate the MC concentration zones. The dashed line delineates the initiation of continuous limnological conditions.

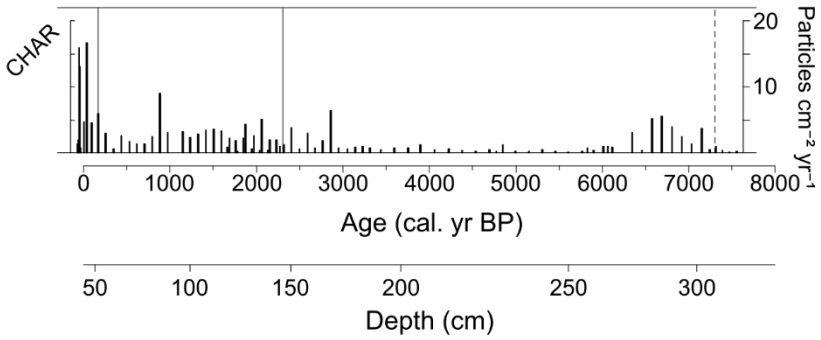

Figure 3.8 Charcoal accumulation rate (CHAR) for LMA. The solid lines delineate the MC concentration zones. The dashed line delineates the initiation of continuous limnological conditions.

3.10 Supplemental Tables

Table S3.1 Location and setting characteristics.

Lake	Latitude (decimal degrees)	Longitude (decimal degrees)	Elevation (m a.s.l.)	Surface area (km^2)	Mean depth (max) (m)	Geology	Land cover
Dora	28.79	-81.69	17	18.1	2.4 (4.2)	Holocene sediments undifferentiated sediments from the Pleistocene and Holocene epochs	developed agriculture
Marian	27.88	-81.11	17	23.2	4.3 (4.6)		

Table S3.2 Monitoring period and water conditions adapted from Florida Lakewatch county reports (2023). Cyanobacteria pigments and cyanotoxin measurements adapted from Lamb (2021).

Lake	Monitoring period	Mean Secchi depth (m)	Mean chlorophyll (µg L^{-1})	Mean TN (µg L^{-1})	Mean TP (µg L^{-1})	Sedimentary pigments (cyanobacteria)	Sediment microcystins (ng g^{-1} org)
Dora	1990-2022	0.4	101	2,787	54	myxoxanthophyll, aphanizophyll	64.2
Marian	2007-2017	0.5	104	2,366	122	canthaxanthin, aphanizophyll	674.1

Table S3.3 Radiocarbon-dated samples from LDO and LMA.

Laboratory no.	Depth (cm)	Material	Age ^{14}C BP	Calibrated years BP (2 sigma median)
		Lake Dora		
OS-170570	200	charcoal	1,970 ± 55	1,897
OS-171790	250	charcoal	2,050 ± 55	2,001
OS-170572	288	charcoal	2,640 ± 45	2,760
OS-171791	320	charcoal	2,790 ± 45	2,891
OS-170571	364	charcoal	3,630 ± 65	3,949
OS-171792	456	charcoal	4,980 ± 110	5,727
OS-170573	492	charcoal	5,400 ± 35	6,223
		Lake Marian		
OS-173620	190	charcoal	2,320 ± 85	2,347
OS-171793	258	charcoal	5,190 ± 25	5,947
OS-171794	302	charcoal	6,320 ± 50	7,240
OS-170351	322	bulk sediment	21,900 ± 180	26,160

Table S3.4 The analysis of variance (ANOVA) indicated significant differences between the MC zones (p<2e-16) in LDO, and ANOVA was followed by Tukey's post-hoc test to determine the significance between the successive zones.

MC	Difference	Lower bound	Upper bound	Adjusted p-value
Moderate – Low	0.2444396	0.1322512	0.3566280	2.7e-06
Low – High	-1.3482334	-1.4762138	-1.2202530	0.0e+00

Table S3.5 The analysis of variance (ANOVA) indicated significant differences between the MC zones (p<2e-16) in LMA, and ANOVA was followed by Tukey's post-hoc test to determine the significance between the successive zones.

MC	Difference	Lower bound	Upper bound	Adjusted p-value
Moderate – Low	0.2635127	0.09553592	0.4314895	0.0009991
Low – High	-2.2384419	-2.46217533	-2.0147085	0.0000000

Table S3.6 List of photosynthetic pigments, their preservation ranging from high (1) to low (3), and their role as markers of aquatic community composition. The table is adapted from Leavitt and Hodgson (2001), Waters (2016), and Rastogi et al. (2015).

Photosynthetic pigment	Abbreviation	Preservation	Aquatic marker
Beta-carotene	B-car	1	Total primary producer abundance
Chlorophyll-a	Chl-a	3	Total primary producer abundance
Pheophytin-a	Pheo-a	1	Chl-a derivative
Alloxanthin	Allo	1	Cryptophyta
Diatoxanthin	Diato	2	Diatoms
Lutein + zeaxanthin	Lut+zea	1	Green algae and cyanobacteria
Aphanizophyll	Aphani	2	N_2-fixing cyanobacteria
Echinenone	Ech	1	Cyanobacteria
Oscillaxanthin	Osc	2	Cyanobacteria
Canthaxanthin	Canth	1	Colonial cyanobacteria
Myxoxanthophyll	Myxo	2	Colonial cyanobacteria
Scytonemin	Scyto	1	Colonial cyanobacteria
Cyanobacterium #1	Cyano 12.7	-	Unknown cyanobacterium
Cyanobacterium #2	Cyano 20.7	-	Unknown cyanobacterium
Okenone	Oke	1	Purple-sulfur bacteria

Table S3.7 Average concentrations and standard deviations for the analyzed variables in LDO (Fig. S3.7) distributed in the three chronologically sorted MC zones.

Variable	Unit	6.4-5.1 ka BP (n=21)	5.1-0.02 ka BP (n=89)	1930 CE to pres. (n=17)
MC Zone		Moderate	Low	High
Bulk density	gm cc^{-1}	0.21 (±0.26)	0.06 (±0.01)	0.03 (±0.01)
LOI	%	29.56 (±11.69)	65.21 (±4.63)	62.49 (±11.69)
Lut+zea	nmol g^{-1} org	154.21 (±70.77)	55.76 (±25.35)	543.83 (±211.63)
Osc	nmol g^{-1} org	1.96 (±0.88)	0.43 (±0.68)	14.19 (±10.74)
Aphani	nmol g^{-1} org	-	0.04 (±0.09)	11.62 (±7.22)
Myxo	nmol g^{-1} org	0.23 (±0.49)	0.09 (±0.12)	3.34 (±1.71)
Cyano 12.7	nmol g^{-1} org	1.56 (±0.9)	1.97 (±1.33)	3.12 (±3.09)
Cyano 20.7	nmol g^{-1} org	16.2 (±6.57)	6.39 (±3.26)	-

Table S3.8 Average concentrations and standard deviations for the analyzed variables in LMA (Fig. S3.8) distributed in the three chronologically sorted MC zones.

Variable	Unit	7.2-2.3 ka BP (n=42)	2.3-0.15 ka BP (n=23)	1800 CE to pres. (n=13)
MC Zone		Moderate	Low	High
Bulk density	gm cc^{-1}	0.18 (±0.17)	0.1 (±0.02)	0.05 (±0.04)
LOI	%	29.01 (±17.67)	42.36 (±8.18)	54.08 (±13.21)
Lut+zea	nmol g^{-1} org	201.18 (±164.29)	71.51 (±16.01)	517.33 (±354.02)
Osc	nmol g^{-1} org	24.79 (±21.92)	30.62 (±11.84)	89.08 (±63.4)
Aphani	nmol g^{-1} org	0.88 (±1.17)	1.11 (±0.87)	9.36 (±5.55)
Myxo	nmol g^{-1} org	0.29 (±0.94)	0.14 (±0.13)	0.36 (±0.3)
Scyto	nmol g^{-1} org	2.02 (±4.68)	0.2 (±0.11)	3.3 (±5.48)
Cyano 12.7	nmol g^{-1} org	6.59 (±6.4)	13.14 (±3.96)	3.16 (±5.11)
Cyano 20.7	nmol g^{-1} org	11.76 (±7.43)	7.56 (±2.6)	17.27 (±11.09)

3.11 Supplemental Figures

Figure S3.1 Horses and other livestock animals were observed along the coast of LMA. The photograph was taken on January 7th, 2022.

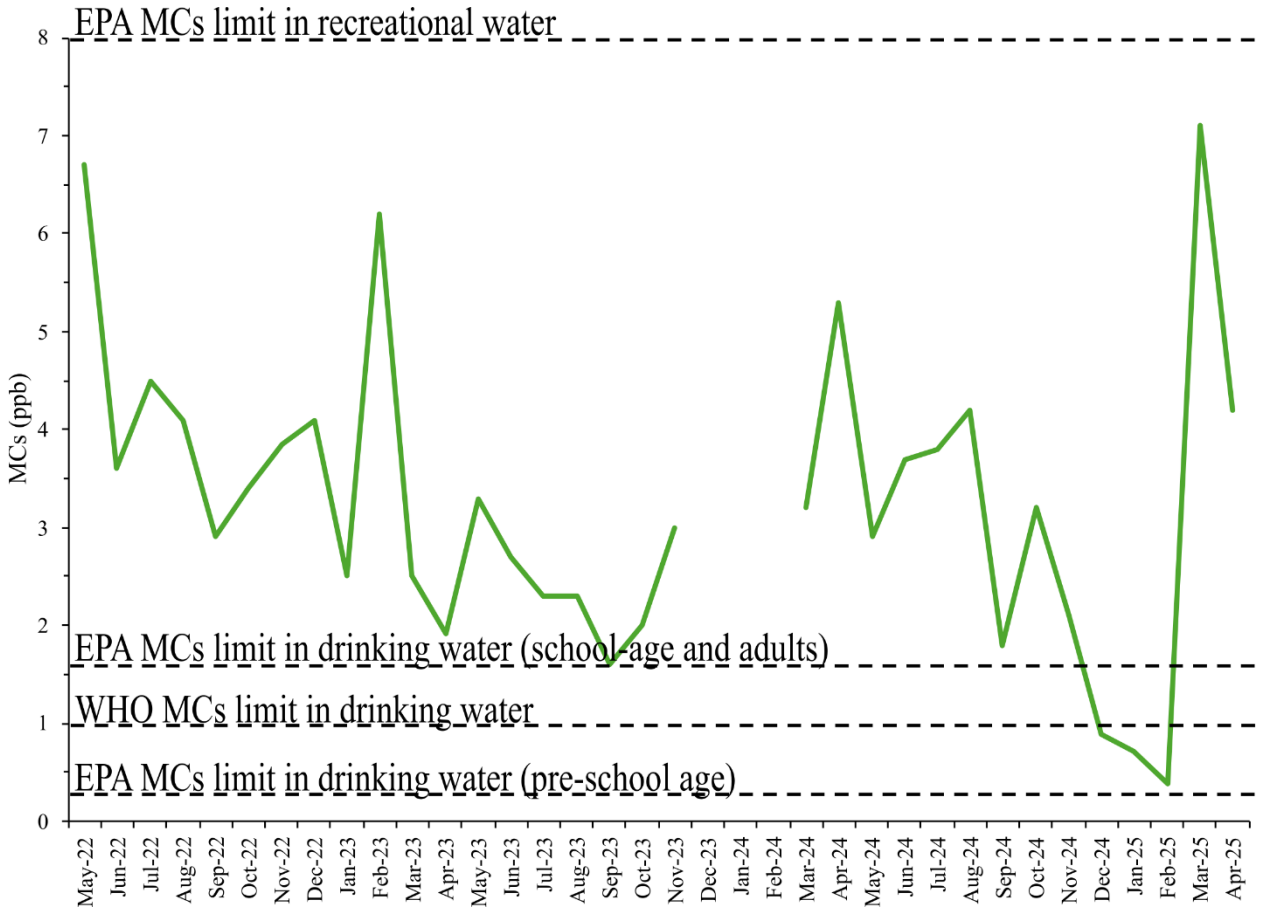

Figure S3.2 Microcystin measurements in the water of LMA from May 2022 to April 2025, as reported by the Florida Department of Environmental Protection in their blue-green algal bloom weekly update. Data source: https://floridadep.gov/.

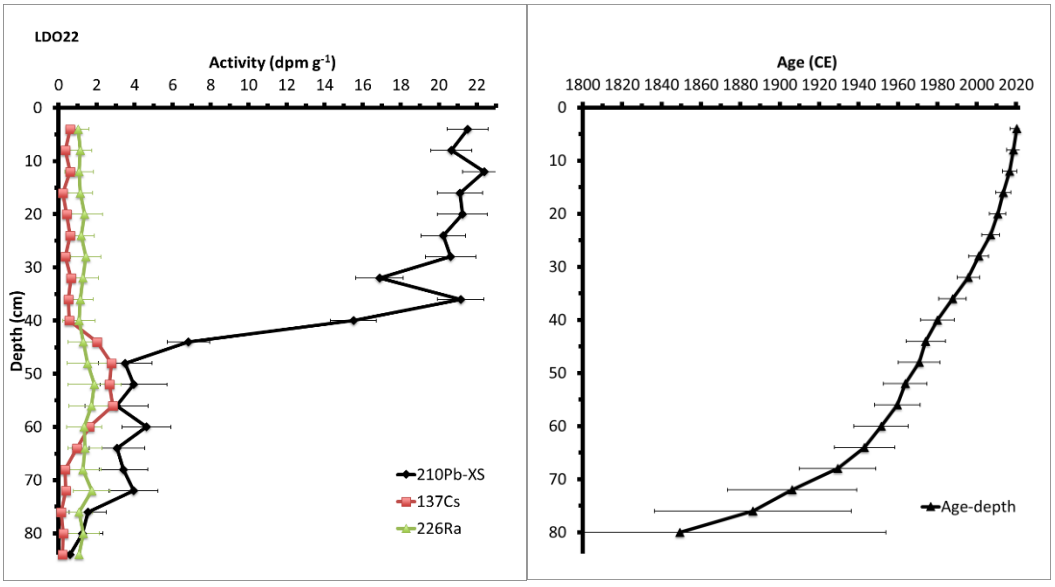

Figure S3.3 Excess ^{210}Pb, ^{137}Cs, and ^{226}Ra activities (left) and age-depth relationship determined by the CRS model (right) for LDO.

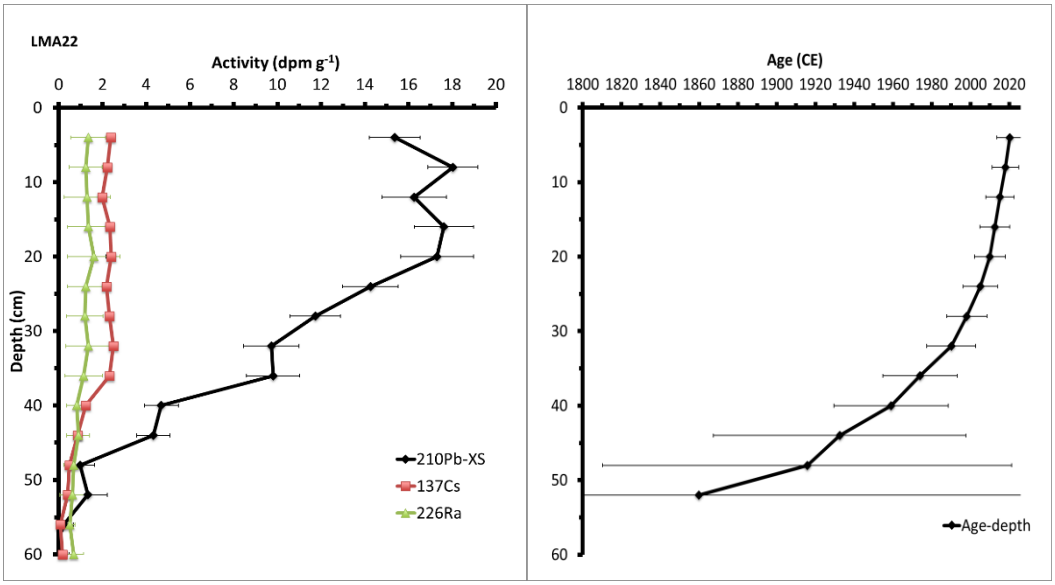

Figure S3.4 Excess ^{210}Pb, ^{137}Cs, and ^{226}Ra activities (left) and age-depth relationship determined by the CRS model (right) for LMA.

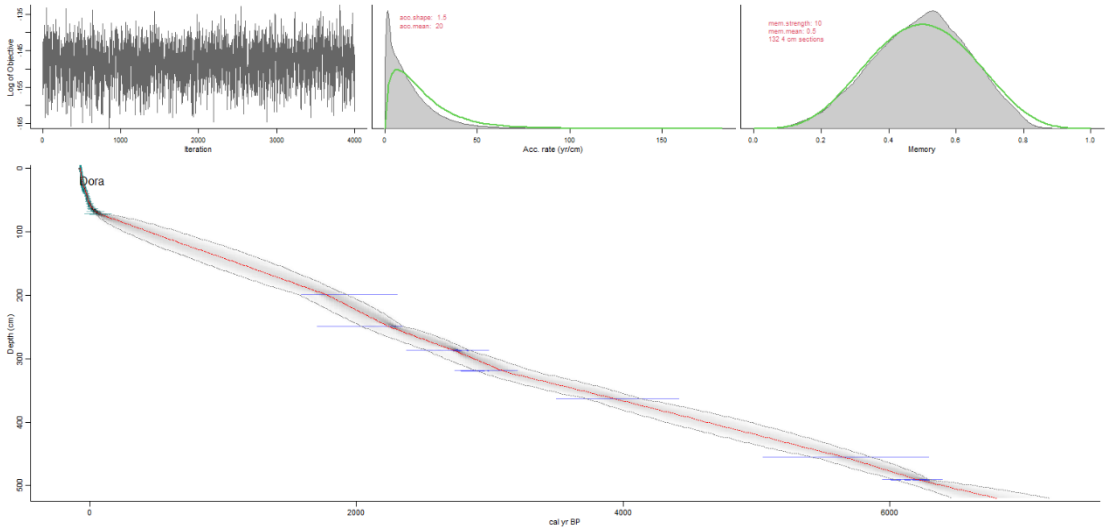

Figure S3.5 The age-depth model used for LDO includes the ^{210}Pb record and the radiocarbon-dated samples.

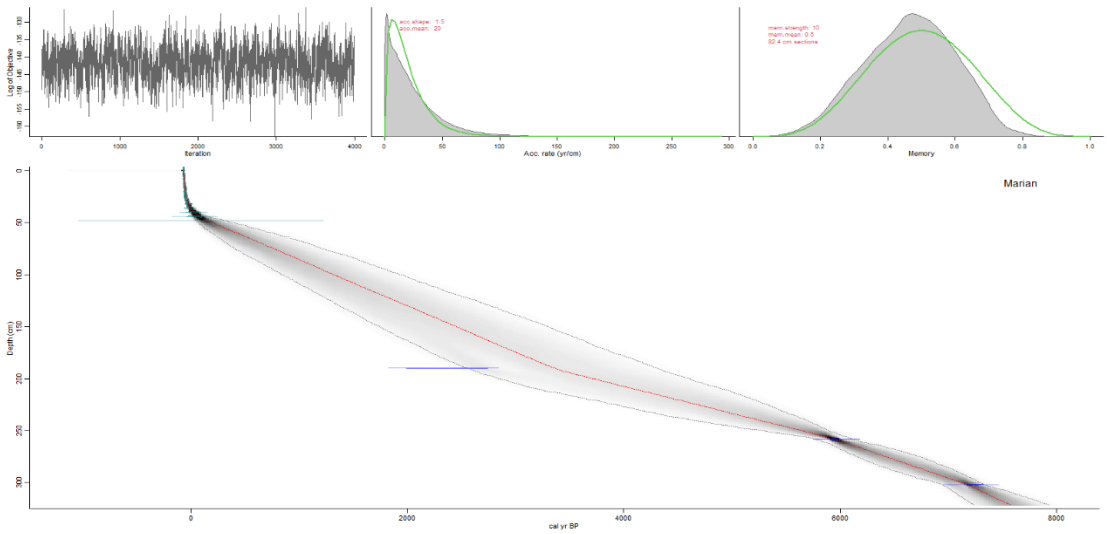

Figure S3.6 The age-depth model used for LMA includes the ^{210}Pb record and the radiocarbon-dated samples. The bottom date at 322 cm was excluded from the model.

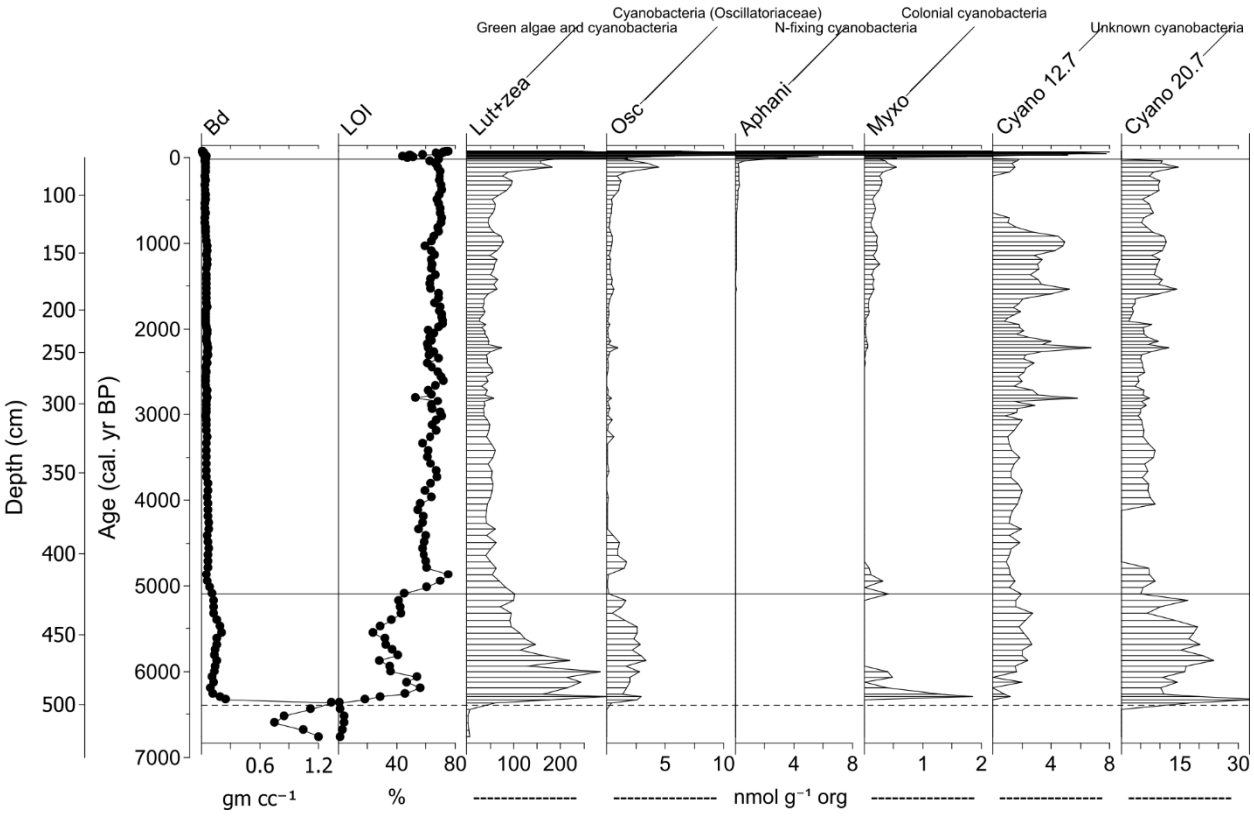

Figure S3.7 Summary time plot of bulk density (Bd), loss-on-ignition (LOI), and photosynthetic pigments for LDO. The solid lines delineate the MC concentration zones. The dashed line delineates the initiation of continuous limnological conditions. The photosynthetic pigments are lutein+zeaxanthin (Lut+zea), oscilloxanthin (Osc), aphanizophyll (Aphani), myxoxanthophyll (Myxo), unknown cyanobacteria 12.7 (Cyano 12.7), and unknown cyanobacteria 20.7 (Cyano 20.7). An analytical description of each photosynthetic pigment is presented in Table S3.4. The abundances of all photosynthetic pigments but cyano 12.7 and 20.7 have been truncated in the top MC zone.

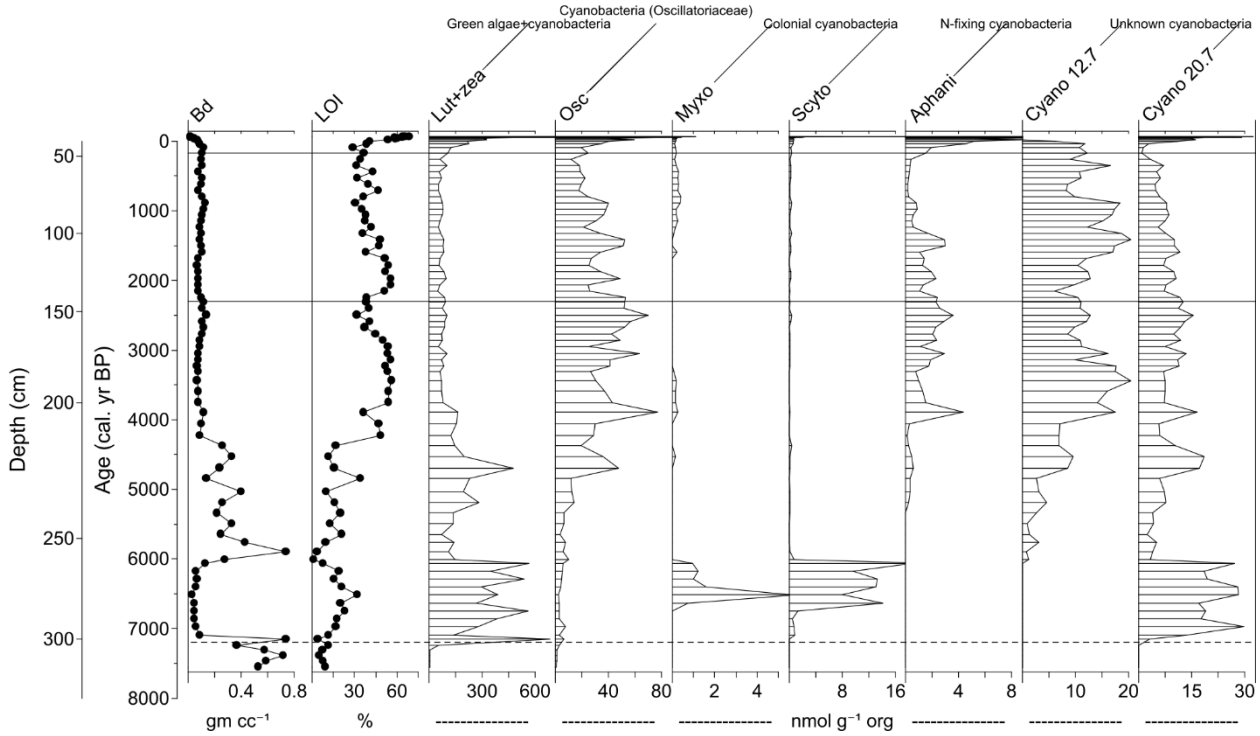

Figure S3.8 Summary time plot of bulk density (Bd), loss-on-ignition (LOI), and photosynthetic pigments for LMA. The solid lines delineate the MC concentration zones. The dashed line delineates the initiation of continuous limnological conditions. The photosynthetic pigments are lutein+zeaxanthin (Lut+zea), oscilloxanthin (Osc), scytonemin (Scyto), aphanizophyll (Aphani), myxoxanthophyll (Myxo), unknown cyanobacteria 12.7 (Cyano 12.7), and unknown cyanobacteria 20.7 (Cyano 20.7). An analytical description of each photosynthetic pigment is presented in Table S3.5. The abundances of all photosynthetic pigments, but cyano 12.7, over the period with increased pigment preservation (high chl-a / pheo-a over the last ~10 years) have been truncated.

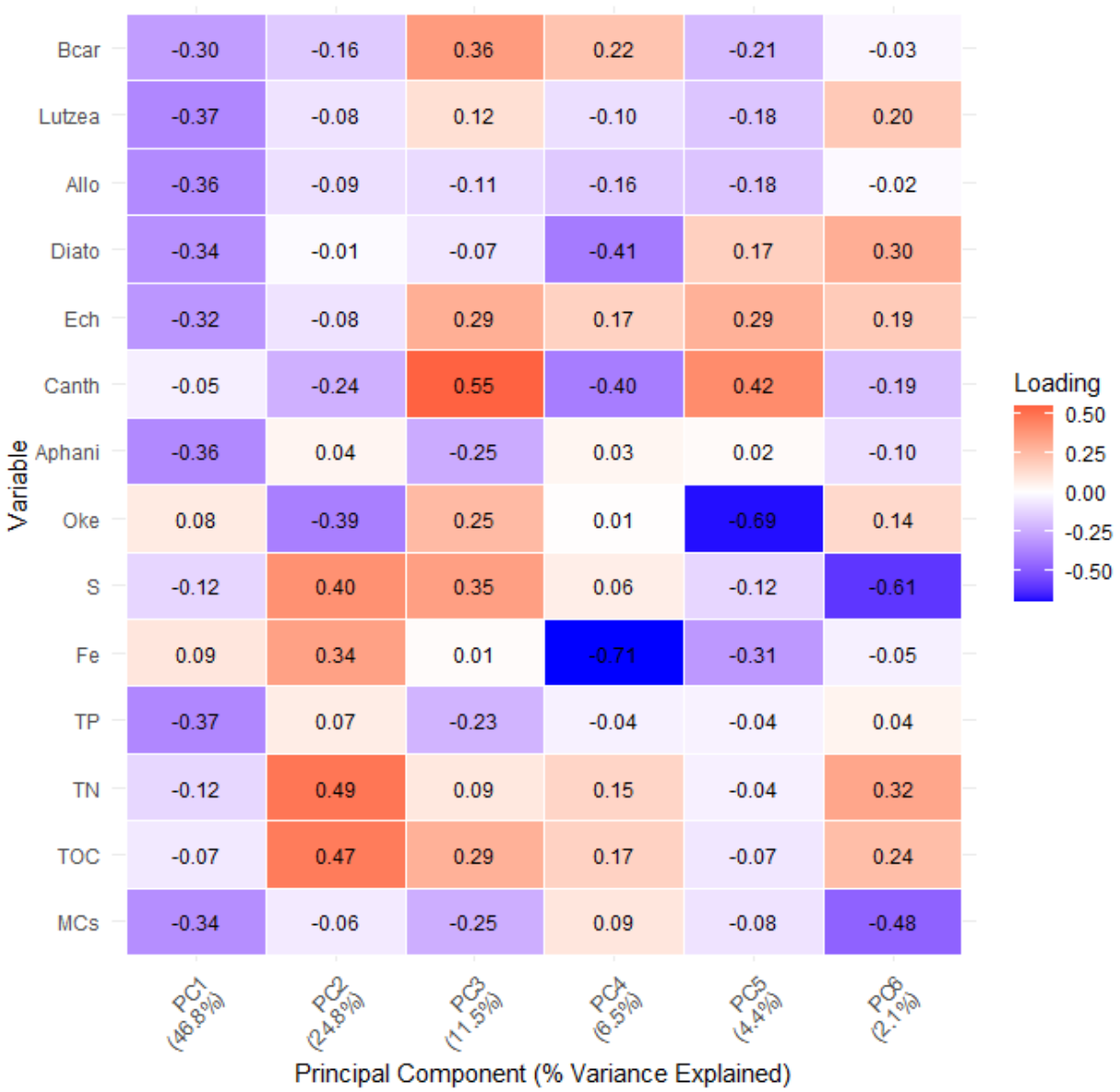

Figure S3.9 Heatmap of the principal components (PC1-6) derived from the analyzed paleolimnological variables. Each value in the heatmap represents the loading of the variable for the respective PC. The percentage of variance explained by each PC is shown in parentheses. Microcystins have the greatest contribution in PC1, 3, and 6.

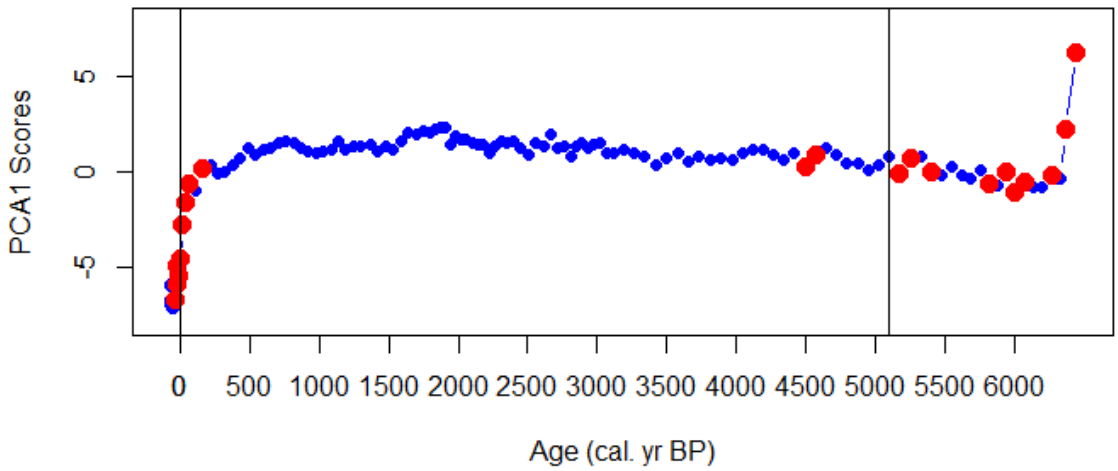

Figure S3.10 PCA1 scores for LDO plotted with time. The vertical solid lines delineate the established chronological zones (I, II, and III from right to left) based on MCs concentration. The red dots depict data points that the sequential t-test estimated significant ($p<0.05$) t-statistic value changes ($-2>t\text{-stat}>2$).

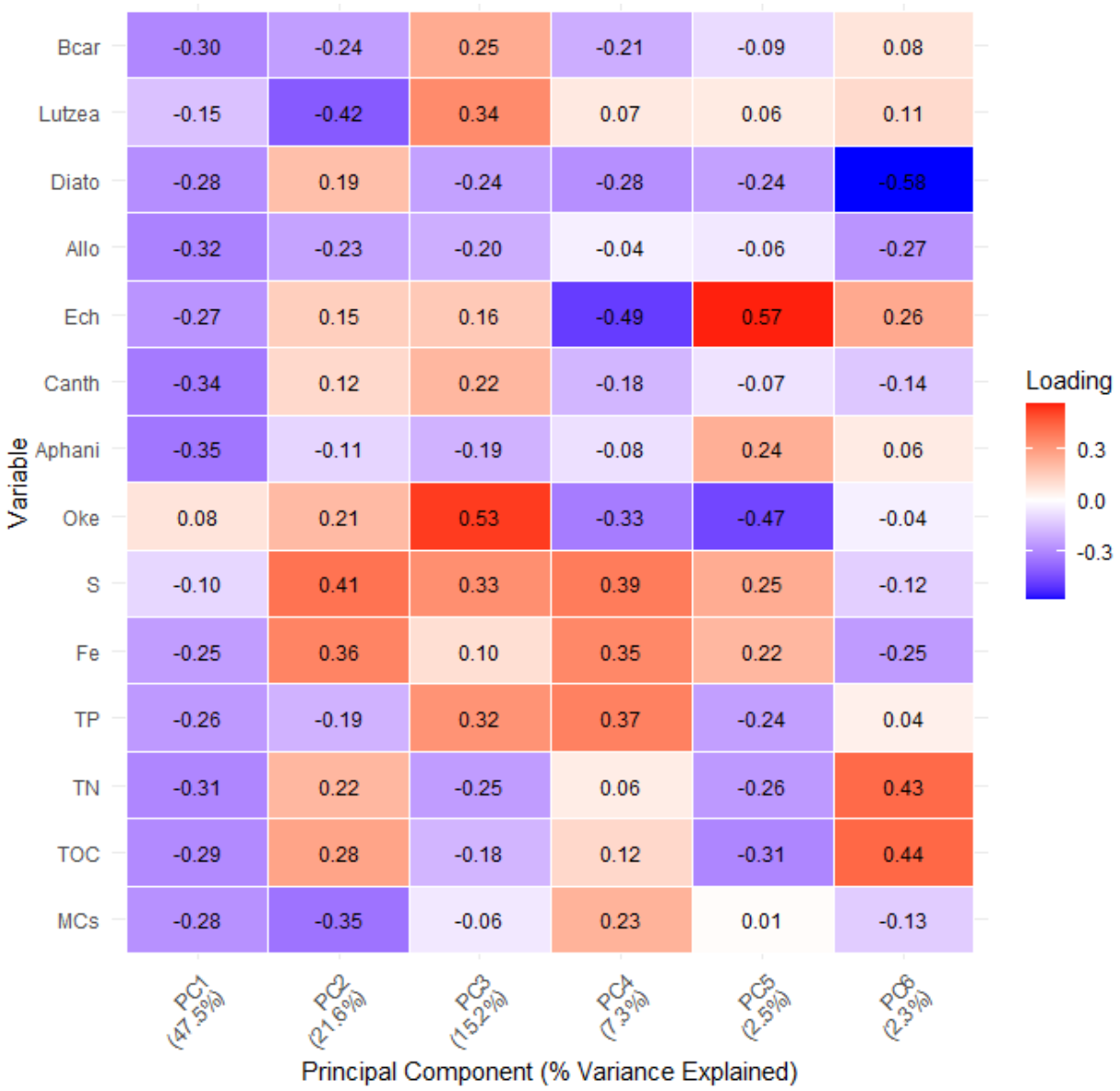

Figure S3.11 Heatmap of the principal components (PC1-6) derived from the analyzed paleolimnological variables. Each value in the heatmap represents the loading of the variable for the respective PC. The percentage of variance explained by each PC is shown in parentheses. Microcystins have the greatest contribution in PC1, 2, and 4.

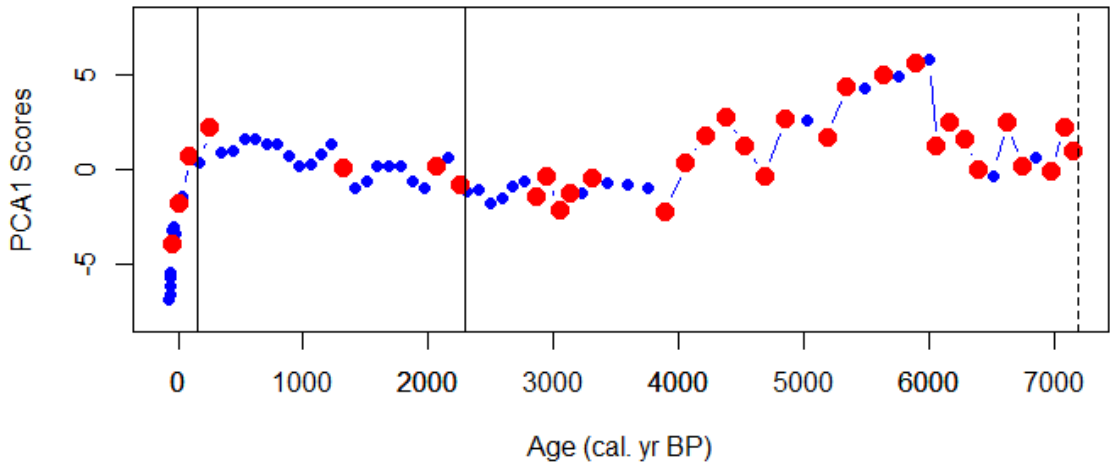

Figure S3.12 PCA1 scores for LMA plotted with time. The solid lines delineate the established chronological zones (I, II, and III from right to left) based on MCs concentration. The dashed line delineates the initiation of continuous limnological conditions. The red dots depict data points that the sequential t-test estimated significant ($p<0.05$) t-statistic value changes ($-2>t\text{-stat}>2$).

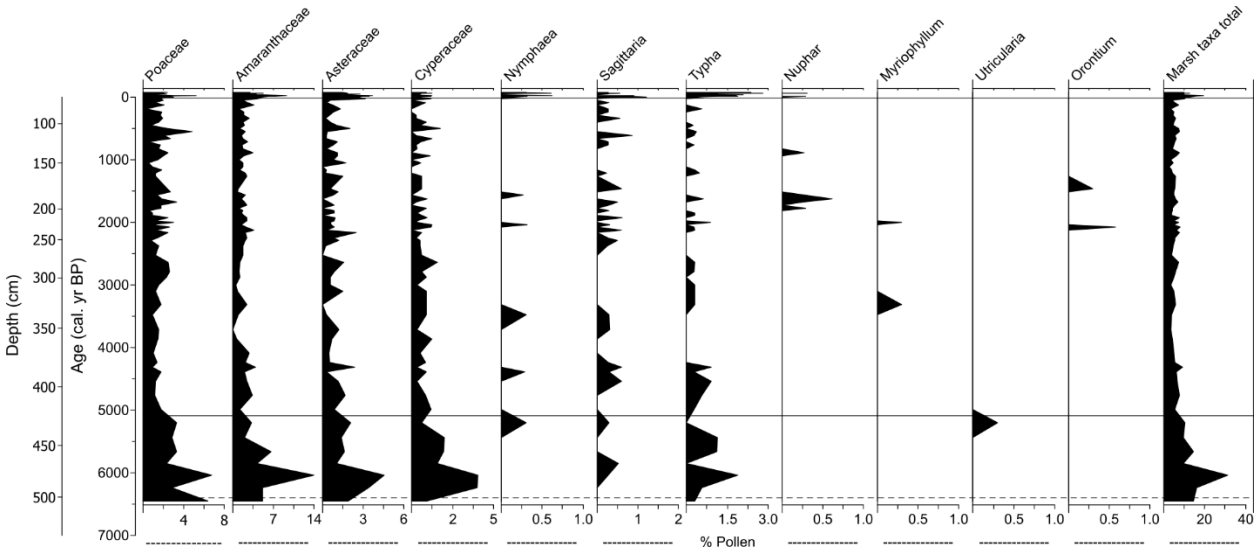

Figure S3.13 Pollen diagram of marsh taxa in percentages for LDO. The solid lines delineate the MC concentration zones. The dashed line delineates the initiation of continuous limnological conditions.

Chapter 4: Abrupt Earth, Water, and Fire Transitions and Sustained Cyanobacteria Dominance over the last 27,500 Years in the North American Subtropics

4.1 Abstract

The Carolina Bays are a unique lake type in the subtropical region of North Carolina, USA, and, having maintained ice-free conditions, they have produced paleolimnological records spanning well into the last glacial period. Likewise, Lake Waccamaw, the largest inundated Carolina Bay, holds high ecological value due to its rich assemblage of endemic and endangered species. Here, we analyzed a sediment core spanning more than 27,500 years BP for aquatic proxies of nutrients, photosynthetic pigments, cyanotoxins, and carbon stable isotopes and terrestrial proxies of pollen and charcoal morphotypes and abundance. The objective of the study was to investigate paleolimnological changes in the aquatic environment linked to terrestrial changes and known climate periods during the Late Quaternary in the southeastern Atlantic Coastal Plain of the United States. Results show that the elevated colonial cyanobacteria abundance at present is concerning, but past conditions featured even higher abundances of cyanobacteria, other primary producers, and cyanotoxins under natural climate variability. Likewise, synchronous and abrupt ecosystem responses to increasing trophic conditions during Interstadial 3 (26.4–27.8 ka BP) and the early Holocene (7–11.4 ka BP) were marked by increased primary producer abundance, deciduous vegetation expansion, and heightened fire activity. Cyanobacteria dominated throughout the record and since the early Holocene, colonial forms prevail. Increases in pigment concentrations generally coincided with *Quercus* dominance and were more strongly influenced by hydroclimatic variability and nutrient stoichiometry than by temperature. Transitions between *Pinus* and *Quercus* pollen corresponded with stadials and interstadials in the $\delta^{18}O$ record of the North Greenland Ice Core Project (NGRIP), respectively. This study emphasizes the need for more multi-proxy paleolimnological records that extend into the Late Pleistocene for deciphering aquatic ecosystem response to various climatic conditions.

4.2 Introduction

Identifying aquatic ecosystem responses to millennial-scale environmental changes is essential for contextualizing modern ecosystem degradation from the rise of harmful algal blooms (HABs), human-driven nutrient enrichment, and climate change (Feng et al., 2024; Hou et al., 2022; Paerl and Huisman, 2009). Whereas short-term paleolimnological records (~150 years) can offer valuable insights into past ecosystems and inform our understanding of the Earth

system, long-term aquatic reconstructions on the millennial scale remain scarce, particularly in subtropical environments (Waters, 2016). Climate affects lakes both directly, by regulating energy balance and hydrologic inputs, and indirectly, through its influence on terrestrial processes that govern the transport of nutrients and other materials into aquatic systems (Ball et al., 2010; Grimm et al., 2013; Leavitt et al., 2009). However, multi-proxy lake sediment records combining both aquatic and terrestrial proxies are rare, leaving a critical gap in our understanding of aquatic primary producer response to past landscape changes.

Cyanobacteria have adapted to extreme conditions across various latitudes (Nienaber and Steinitz-Kannan, 2018) and global warming establishes optimal conditions for their growth (Paerl and Huisman, 2008; Paerl and Scott, 2010; Moss et al., 2011; Havens and Paerl, 2015; Meerhoff et al., 2022). While cyanobacteria are often associated with cultural eutrophication, paleolimnological studies have also linked cyanobacteria dominance in primary producer communities before increased human presence (McGowan et al., 1999; Ryves et al., 1996; Tu et al., 2021; Waters et al., 2012). Most of these studies utilize the measurement of fossil photosynthetic pigments (chlorophylls and carotenoids) as diagnostic tools for phytoplankton abundance as well as community structure (Leavitt and Hodgson, 2001; Waters et al., 2015). However, the role of climate-driven terrestrial changes in shaping cyanobacteria dynamics and primary producer communities have seldom been studied in relation to climate patterns and changes in terrestrial landscapes, especially beyond the last few thousand years of the Holocene Epoch. Despite the ability of photosynthetic pigments to reconstruct primary producer community composition over periods exceeding over 10,000 years, they have sparingly been applied over such timescales and especially in warm tropical or subtropical areas (Hodgson et al., 2005; Vuillemin et al., 2016).

The Carolina Bays are a group of thousands of lakes featuring unique geomorphological characteristics found on the Atlantic Coastal Plain, stretching from North Florida to New Jersey in the USA (Lundine and Trembanis, 2021; Piovan and Hodgson, 2017). These bays are identified by their elliptical depressions that form lakes or wetlands, typically oriented NW-SE, with a sandy rim along the SE edge (Kaczorowski, 1977; Lide, 1997). While the origin of Carolina Bays remains unresolved (Pinter and Ishman, 2008; Pinter et al., 2011), several of their geomorphological characteristics appear to be shaped by wind and wave action along with water level fluctuations (Lundine and Trembanis, 2025). Paleolimnological research has shown that

several Carolina Bays contain sediments dating back to at least ~6.5 ka BP (Rodriguez et al., 2012), ~50 ka BP (Spencer et al., 2017), or potentially older (Brooks et al., 2010). Some of these lakes possess long paleo records that shed light on environmental transformations during the Late Quaternary period to present (Lundine and Trembanis, 2025). Previous studies have used these records to investigate regional climate shifts and their influence on terrestrial vegetation (Frey, 1953; Krause et al., 2019; Lane et al., 2018; Spencer et al., 2017), as well as the geomorphological history of the region (Leigh, 2008; Suther et al., 2018), but limnological ontogeny and change has rarely been considered.

While many Carolina Bays are infilled with peat and transitioned into wetland or terrestrial systems, several of the Bays have also remained lentic. The current trophic state of some of the inundated basins in North Carolina varies from dystrophic in Pungo Lake (Waters et al., 2012) to meso-eutrophic in Lake Waccamaw (EPA, 1975) and hypereutrophic in Lake Mattamuskeet (Waters et al., 2009). A few studies have investigated the trophic history of the lakes in the region, with some suggesting a eutrophic past predating human settlement (Stager and Cahoon, 1987; Waters et al., 2009, 2012). However, these studies have primarily focused on limnological changes during the Holocene. While Late Pleistocene sediments have been recovered (Stager and Cahoon, 1987; Leigh, 2008; Spencer et al., 2017; Lane et al., 2018; Krause et al., 2019), modern paleolimnological techniques have neither targeted the reconstruction of primary producer assemblages and dynamics nor the links between climate-driven vegetation changes and aquatic productivity over stadial and interstadial periods.

This study investigates aquatic ecosystem responses in Lake Waccamaw, Columbus County, NC, USA (Fig. 4.1) over the Late Pleistocene and Holocene periods to both the direct hydroclimatic forcing and indirect influences from terrestrial vegetation and fire regime shifts on primary producer communities. Lake Waccamaw is a large, shallow lake underlain by phosphorus-rich geology (Cahoon et al., 1990). The lake has a sediment record that extends beyond the Holocene and has a history of high natural productivity (Stager and Cahoon, 1987). We analyzed a sediment core using multiproxy paleolimnological techniques, including nutrients, photosynthetic pigments, cyanotoxins, charcoal and pollen to connect drivers of material inputs into the lake issued water quality responses such as primary producer abundance, cyanobacteria dominance, phytoplankton community structure and cyanotoxin production. The objectives of the study were to: 1) identify primary producer histories in response to rapid Late

Quaternary climate changes, 2) determine if primary producers maintained constant conditions during the early Holocene, and 3) investigate the development of modern eutrophic conditions during the Late Holocene. We hypothesized that major vegetation successions on the terrestrial landscape, such as transitions between coniferous and deciduous taxa, would align with changes in fire regime, and aquatic biogeochemistry and ecology. We expected warm and wet periods to enhance nutrient delivery and support cyanobacteria dominance and cyanotoxin production in the lake. By reconstructing these coupled terrestrial-aquatic responses over the last 27,500 years, our study provides a novel eco-climatic history of the region and contributes to understanding modern ecosystem responses to human impacts and climate change.

4.3 Material and Methods

4.3.1 Study Site

Lake Waccamaw (34°17'14" N, 78°30'39" W) is a large (36.2 km^2) and shallow (~2.3 m mean depth and ~3.4 m max depth) subtropical lake located near the town of Lake Waccamaw in Columbus County in North Carolina, USA (Fig. 4.1). It is one of the largest of the currently inundated Carolina Bay lakes (Casterlin et al., 1984; Cahoon et al., 1990). The lake is on a flat terrain (13 m a.s.l.) with a gentle slope on the northwestern side. The geology of the area is characterized by the Pee Dee Formation, with calcareous and locally fossiliferous sands and clays from the Cretaceous period, as well as the more recent Waccamaw Formation, with limestone, fossiliferous sands, silts, and clays from the Tertiary period (NC Geological Survey, 1985).

The lake has a tributary, the Big Creek, on the northeast side and an outlet to the Waccamaw River on the southeast side, controlled by a small dam since 1943 (EPA, 1975; Stager and Cahoon, 1987). More than half of the lake's shore is built with residences, and the rest is the Lake Waccamaw State Park (Cahoon et al., 1990), however, beyond the shoreline strip of land, the area is covered by forested wetlands (cypress and gum swamps) (Stager and Cahoon, 1987). The lake's connection to adjacent wetlands with the limestone outcrops contributes to acidic and alkaline water inputs that create pH neutrality (Casterlin et al., 1984). Physical and chemical weathering of fossiliferous sediments increases the P loading to the lake, providing constant P inputs through time (Cahoon et al., 1993). The pristine nature of the lake and the surrounding environment offer refuge to several endemic and endangered aquatic species (Casterlin et al., 1984). The region has also been inhabited by Native American tribes for

millennia, and recently, a 1,000-year-old canoe was retrieved from the bottom of the lake (Yang, 2023). The lake is naturally mesotrophic to eutrophic, but recent cultural eutrophication may increase primary productivity and negatively impact water quality (Stager and Cahoon, 1987).

4.3.2 Fieldwork and Core Collection

A sediment core was collected in March 2023 during a sampling trip in North Carolina, USA, by the Auburn Paleoenvironmental Lab. The coring location was selected after a soft sediment survey was conducted to determine depositional areas of the lake (Whitmore et al., 1996; Waters et al., 2009) (Fig. S4.1). The uppermost sediments were collected with a piston corer (7 cm diameter tubes) designed to collect undisturbed mud/water interface sediments (Fisher et al., 1992), while deeper sediments were extruded using a modified Livingstone corer (5.5 cm diameter tubes). Each sediment core had an overlapping section with the previous core, allowing for core sections to be combined into one continuous record. The mud-water interface cores were subsampled in 2 cm sections in the field, packed in labeled Whirl-pak bags (VWR, USA), and stored in the refrigerator until subsampling. The more consolidated sections were kept in their labeled polycarbonate core barrels and transported to the laboratory on ice and in the dark. In the lab, the deeper core sections were cut in half lengthwise, photographed, and described. One half was stored as an archive, and the second was subsampled in 2 cm sections. After subsampling, the wet sediments were processed to estimate the organic matter content and bulk density and then freeze-dried, ground, and transferred to labeled scintillation vials for further analyses.

4.3.3 Laboratory Techniques and Core Collection

4.3.3.1 Loss on Ignition and Bulk Density

For estimating the bulk density, wet samples were weighed and put in the oven at 60°C for 24 h, and then, the dried samples were reweighed to estimate the dry mass per wet volume after dividing the dried sample by the empirically measured volume of the subsampled sediment, 4.929 cm^3 (for 5 mL scoops of sample). Bulk density is reported in g dry cm^{-3} wet. For loss on ignition (LOI), the dried samples were placed in a muffle furnace at 550°C for 3 h and then reweighed. LOI is a measurement of organic matter content, expressed as a percentage (Dean, 1974).

4.3.3.2 Geochemical Analysis

Samples for total organic carbon (TOC) and total nitrogen (TN) were measured using a Costech ECS 4010 elemental analyzer at Auburn University. The samples were weighed using the estimated carbon content based on organic matter measurements (LOI). The samples for TOC were weighed in silver capsules and fumigated in an acid bath with hydrochloric acid (HCl) for 24 h to remove inorganic C. The silver capsules were then folded and placed in tin capsules to achieve full combustion. Samples for TN were weighed in tin capsules. TOC/TN were also used to generate a molar ratio and determine organic matter origin (Meyers and Teranes, 2001). Other elements (P, K, Fe, Mn) were measured using the Inductively Coupled Plasma (ICP) Spectroscopy technique with 90-minute nitric acid digestion on a heated block (EPA 6010B) at Waters Agricultural Laboratories, Camilla, GA, USA. Carbon isotopic analysis ($\delta^{13}C$) was carried at the Light Stable Isotope Mass Spec Lab of the University of Florida with a Thermo Electron DeltaV Advantage isotope ratio mass spectrometer coupled with a ConFlo II interface linked to a Carlo Erba NA 1500 CNHS Elemental Analyzer.

4.3.3.3 Pigment Analysis

Photosynthetic pigment analysis was performed at Auburn University using High-Performance Liquid Chromatography (HPLC) following the methods for pigment extraction from sediments (Leavitt and Hodgson, 2001; Waters et al., 2012). Chlorophylls and carotenoids were extracted from dried sediment samples using a solvent mixture of 80% acetone, 15% methanol, and 5% HPLC-grade water containing an internal standard (Apocarotenal or trans-β-apo-8'-carotenal; Sigma-Aldrich Chemical Corp.). The samples were injected into a Shimadzu HPLC system with a Phenomenex Luna 3 μm C18 column (200 x 4.6 mm), following the mobile phase and the time sequence of Leavitt and Hodgson (2001). Carotenoids and chlorophylls were measured using a photodiode array detector coupled with a fluorescence detector, respectively. Pigment identification was performed using retention times and pigment-specific spectra of known standards (DHI Lab Products, Denmark). Pigment concentration was calculated by comparing peak areas against standards of known concentration and was expressed in nmol per gram of organic matter.

4.3.3.4 Cyanotoxin Analysis

Cyanotoxins were measured as total microcystins (MCs) using the microcystin/nodularin ADDA OH enzyme-linked immunosorbent assay (ELISA) kit by Abraxis, purchased from Gold Standard Diagnostics as described by Waters et al. (2021) and Paradeisis-Stathis and Waters (2025). The analysis was performed in 46 out of 65 total samples, and total MCs are reported as ng toxin per gram of organic matter.

4.3.3.5 Pollen Analysis

Pollen analysis was performed by Dr. Debra Willard and the Palynology Laboratory at the Florence Bascom Geoscience Center of the US Geological Survey. Each sample was dried and weighed before adding one Lycopodium marker tablet (batch 3862, 9666 ±212 spores/tablet) for the calculation of absolute pollen concentration (Stockmarr, 1971). Following standard techniques (Traverse, 2007; Willard et al., 2011), samples were demineralized with HCl and HF, acetolyzed using 1 part sulfuric acid to 9 parts acetic anhydride, treated with 10% KOH in a boiling water bath to remove humic material, and sieved with 150 µm and 10 µm mesh to remove sands and clays, respectively. After staining with Bismarck Brown, pollen residues were mounted on microscope slides with glycerin jelly. Residues are stored in ethanol and curated in the working collections of the U.S. Geological Survey Florence Bascom Geoscience Center in Reston, Virginia. At least 300 palynomorphs were counted from each slide using 400X magnification on a Nikon Eclipse microscope with Nomarski optics.

4.3.3.6 Charcoal Analysis

Charcoal analysis was performed on a cubic centimeter of wet sediment subsampled in 15 mL plastic tubes in a total of 65 samples by Dr. Richard Vachula's lab at the Department of Geosciences at Auburn University. The samples were treated with 5 mL of 1 M sodium hexametaphosphate ($Na_6[(PO_3)_6]$) and 5 mL of 3.75% bleach for 24 h. The samples were sieved through a 125 µm mesh, rinsed with DI water, and transferred into lined counting trays (Vachula et al., 2019). Charcoal particles were identified under a microscope attached to a Nikon DS-Fi3 camera. The free open-source Charcoal Quantification Tool (CharTool) in ImageJ was used to quantify and classify charcoal particles (Snitker, 2020). The identification of different charcoal morphotypes (D, F, M, P, S/B) was based on the scheme of Enache and Cumming (2006). Additional morphometric parameters collected by the CharTool, such as area to perimeter (A:P)

and length to width (L:W) were utilized to detect any relationships between charcoal morphology and vegetation type changes based on pollen (Nelle et al., 2010; Vachula et al., 2021). The charcoal accumulation rate (CHAR) was calculated for each sample in particles per cubic centimeter per year based on the volumetric concentration and the age-depth model following the formula of Vachula et al. (2019):

$$\text{CHAR} = \frac{\text{\# of Particles}}{\text{Volume}} \times \frac{(\text{Top Depth} - \text{Bottom Depth})}{(\text{Top Age} - \text{Bottom age})}$$

4.3.3.7 ^{210}Pb, ^{14}C Dating and Age-Depth Modeling

Continuous sediment intervals from the mud/water interface cores were dated at Auburn University using gamma spectroscopy with an ORTEC Intrinsic Germanium Detector connected to a 4096-channel multichannel analyzer. The samples were measured for ^{210}Pb total activity and ^{226}Ra (supported ^{210}Pb) to calculate the excess ^{210}Pb (Appleby et al., 1986; Schelske et al., 1994). The constant rate of supply (CRS) model was used to calculate excess ^{210}Pb, assuming a continuous supply rate (Appleby and Oldfield, 1983). Sediment intervals beneath the excess ^{210}Pb were ^{14}C-dated using the radiocarbon dating technique on six charcoal and one wood sample (Table S4.1) at the National Ocean Sciences Accelerator Mass Spectrometry (NOSAMS) facility of the Woods Hole Oceanographic Institution in Massachusetts, USA. Charcoal particles for ^{14}C-dating were subsampled from at least 5 mL of wet sediments and processed with 10 mL of 5% potassium hydroxide (KOH) overnight, and after removing the supernatant, with 10 mL of 5% hydrogen peroxide (H_2O_2) overnight. The samples were sieved through a 125 μm mesh sieve, and charcoal was collected from a petri dish under a microscope. The ^{14}C-dated ages were calibrated with the IntCal20 calibration curve (Reimer et al., 2020) using the rbacon package in R (Blaauw and Christen, 2011) and combined with the excess ^{210}Pb-calculated ages to create an age-depth model with 4 cm thickness sections and a 200 cm accumulation rate.

4.3.3.8 Data Visualization and Analysis

The location map for Lake Waccamaw was created in ESRI ArcGIS Pro v. 3.4.2 using an online service layer for basemap, land cover data from the North Carolina state National Land Cover Database (2019) (https://www.lib.ncsu.edu/gis/nlcd), and a digital elevation model based on USGS lidar data (2018-2020) from National Oceanic and Atmospheric Administration (NOAA) data access viewer (https://coast.noaa.gov/dataviewer/#/). Time plots with paleoenvironmental data were created in Tilia (version 3.0.3) (Williams et al., 2018). Principal

components analysis (PCA) was performed in R (version 4.4.1, R Core Team, 2024) using log-normalized datasets in the built-in prcomp function and the autoplot function in the ggfortify package (Tang and Li, 2016). Correlation plots were generated in R using the built-in cor and cor_pmat functions with the Pearson correlation method and the ggcorrplot package (Kassambara, 2023).

4.4 Results

4.4.1 Sediments, Chronology and Core Separation into Climate Periods

The lithology, bulk density, and organic matter content (LOI) demonstrated changes in sedimentary horizons (Fig. 4.2). At the bottom of the sequence, there was a narrow band of dark gyttja with low bulk density and approximately 10% organic matter. An abrupt transition occurred to a bright silty clay layer with very low organic matter (~1%), higher bulk density, and rich in macrofossils. At approximately 124 cm below the lakebed, there was a slight decrease in bulk density followed by a gradual transition to pale brown and grey gyttja sand. A narrow, dark-grey sandy gyttja layer, accompanied by a significant decrease in bulk density and an increase in LOI (~7%), occurred around 100 cm, and was followed by pale brown and grey gyttja sand up to about 76 cm below the lakebed. Subsequently, the lithology transitioned to dark, organic-rich gyttja with lower bulk density and considerably higher organic matter content (~20%), which persisted to the top of the core, apart from an interruption with sandy gyttja between 40 and 56 cm.

The excess ^{210}Pb activity decreased downcore, reaching supported levels at 24 cm in the sediments or 1884 CE as determined by the CRS model (Fig. S4.2). The sedimentation rate was slow up to 14 cm or ~1980 CE, followed by an increase to the top of the excess ^{210}Pb record. The radiocarbon dates of the charcoal material were mainly continuous (Table S4.1). However, one charcoal date from the 98-100 cm depth yielded an older date than the two deeper radiocarbon-dated samples, leading the rbacon model to exclude it from the calibration curve. Additionally, the dated macrofossil from 136-138 cm was determined to be radiocarbon dead. The CRS model dates, combined with the radiocarbon dates, produced an age-depth model exhibiting a slow sedimentation rate and two shorter periods of relatively increased sedimentation (Fig. S4.3). During the slow sedimentation periods from 11.4 to 26.4 ka BP and 0.5 to 6.7 ka BP, every 2-cm sampled section averaged ~850 years of paleolimnological activity. In contrast, during the periods with increased sedimentation from 26.4 to 27.8 ka BP and 7.4 to 11.2 ka BP, every 2-cm

sampled section averaged ~200 years of paleolimnological activity. While rbacon extrapolated the age-depth model below our last radiocarbon-dated sample 122-124 cm, yielding 27,760 ka BP, we exercise caution using the extrapolated relationship over such time scales.

The regional synchronicity between pollen records from the southeastern USA and $\delta^{18}O$ records from the North Atlantic has been shown in the work of Grimm et al. (1993, 2006) in Lake Tulane, Florida. Lake Waccamaw's sediment core was divided into distinct climate periods based on variations in the abundance of *Pinus* and *Quercus* pollen in comparison to fluctuations in the $\delta^{18}O$ record of the NGRIP ice core from Greenland (North Greenland Ice Core Project members, 2004) (Fig. 4.3). Additionally, the timing and sequence of the interstadials was compared to the global composite of speleothem records in Corrick et al. (2020) (Table 4.1). Although the matching of the two records indicated potential stadial and interstadial periods over the last ~33.6 ka, the age-depth uncertainty below ~27.5 ka BP limits chronological control. Therefore, the climate periods were identified with greater confidence after interstadial I3 (~27.8 - 26.4 ka BP), followed by the Last Glacial Maximum (LGM) (~26.4 - 24.4 ka BP), post-LGM (~24.4 - 18 ka BP), Oldest Dryas (OD) (~18 - 14.2 ka BP), Bølling–Allerød Interstadial (B-A) (~13.6 ka BP), Younger Dryas (YD) (~13 - 11.4 ka BP), and the Holocene (~11.4 ka BP - Present).

4.4.2 Sediment Geochemistry and Aquatic Primary Producers

The elemental and photosynthetic pigment profiles exhibited notable fluctuations relative to the established climate zones (Fig. 4.4). The period preceding the Holocene was characterized by a low accumulation of organic material (Fig. 4.2, 4.4A). Total OC and TN concentrations aligned with the lithological units, demonstrating primarily low values, except for the bottom sample and during the post-LGM period (Fig. 4.2). Although acid fumigation was insufficient for removing $CaCO_3$ and accurately measuring TOC and $\delta^{13}C$ for the entire record, based on the LOI values, the concentration of TOC remained consistently low at ~1% before the I3 interstadial. The C/N ratio briefly declined during the I3 interstadial before rising to ~20 until the beginning of the Holocene. Total P, K, and the Fe/Mn ratio displayed trends similar to TOC and TN. However, below the I3 interstadial, TP reached exceptionally high concentrations, comparable only to the second half of the Holocene Epoch (Fig. 4.4A). The N/P ratio was low and began a gradual increase after the I3 interstadial, and there was a relative enrichment in $\delta^{13}C$ until 18 ka BP, followed by a slight depletion during OD, B-A, and YD. The presence of

photosynthetic pigments and MCs was recorded throughout the core (Fig. 4.4B). The generalized pigment biomarkers beta-carotene and lutein+zeaxanthin maintained the highest concentrations, and from specific pigment markers, alloxanthin, diatoxanthin, echinenone, and canthaxanthin were recorded continuously. However, the consistent presence of many photosynthetic pigments commenced with an abrupt rise to high concentrations at the I3 interstadial, whereas previously, chlorophylls, beta-carotene, pyropheophorbide, echinenone, and canthaxanthin were only detectable in the bottom sample. Primary producer pigment concentrations rapidly declined during the LGM and largely maintained low values until the onset of the Holocene. Nonetheless, a slight increase was noted in canthaxanthin and okenone during the post-LGM period, while alloxanthin was high during the OD, B-A, and YD periods and MCs peaked during B-A.

The Holocene started around 11.4 ka BP with abrupt increases in nutrients and photosynthetic pigments, followed by a remarkable decrease from ~9.5 to 7.5 ka BP (Fig. 4.4). There was approximately an eight-fold increase in TOC, TN, TP, and K during the early Holocene compared to the end of the Late Pleistocene (YD, B-A, OD), an almost equal in magnitude drop from ~9.5 to 7.5 ka BP, and an increase after 7.5 ka BP. The C/N ratio decreased from ~20 to 17, while a further gradual decrease was initiated after ~7.5 ka BP. The N/P ratio gradually increased and peaked at ~7.5 ka BP, and then rapidly decreased. The Fe/Mn ratio abruptly increased from ~9.5 to 7.5 ka BP and rapidly decreased up core. The $\delta^{13}C$ values showed a slight depletion at 11.4 ka BP, followed by a more abrupt depletion at ~7.5 ka BP. The increase in most photosynthetic pigment concentration during the ~11.4 to 9.5 ka BP period was similar to the I3 interstadial, except for alloxanthin and cyanotoxin MCs, which decreased and remained low during the same period. While beta-carotene, lutein+zeaxanthin, diatoxanthin, echinenone, and okenone decreased abruptly around 9.5 ka BP, alloxanthin and canthaxanthin showed a slight increase, and there was a notable increase in MCs. From 7.5 ka BP to the present, diatoxanthin, alloxanthin, and canthaxanthin increased while the rest of the pigments and MCs maintained low concentrations.

4.4.3 Pollen and Charcoal Analysis

The palynological analysis revealed a high abundance of pollen from various species, with the highest percentages observed in *Pinus* and *Quercus* (Fig. 4.5A, S4.4). However, there were notable fluctuations in the percentages of other pollen types. In addition to the fluctuations in *Pinus* and *Quercus* (Fig. 4.3), stadial and interstadial periods were associated with changes in

the percentages of *Picea* and *Fagus* and *Ostrya/Carpinus*, respectively. The early terrestrial landscape was characterized by periods of increased abundance of *Carya* and *Liquidambar* (Fig. S4.4). Before the I3 interstadial, *Poaceae*, and *Cyperaceae* pollen increased in abundance and fluctuated, maintaining a relatively higher abundance. However, at the onset of the Holocene, *Pinus*, *Poaceae*, and *Cyperaceae* pollen decreased, while *Quercus*, *Fagus*, and *Ostrya/Carpinus* (Fig. 4.5A), along with other arboreal pollen such as *Ulmus* (Fig. S4.4), increased remarkably. Most of the pollen types, except *Quercus*, decreased around 9.5 ka BP, coinciding with a slight increase in *Cupressaceae*. The pollen record was dominated by *Quercus* at least until ~7 ka BP, when a shift occurred characterized by an increase in *Pinus* abundance. By 5.5 ka BP, *Pinus* had become the dominant species in the terrestrial landscape (Fig. 4.5A).

The charcoal analysis recorded a constant presence of charcoal particles throughout the sediment core (Fig. 4.5B). During the periods when CHAR values could be calculated, the highest values were observed during the I3 interstadial, LGM, the early to mid-Holocene, and over the past century. Conversely, the lowest CHAR values were recorded during the late deglaciation (OD, B-A, YD) and late Holocene. Throughout the record, the morphotypes of charcoal fluctuated. In the period preceding the LGM, there was a higher percentage of irregular geometric structured particles (M). However, the bottom of the core was dominated by elongated particles without ramifications (F) and geometric compacted and structured black/partially black particles (S/B). Although the area to perimeter ratio (A:P) showed minor fluctuations throughout the record, it reached its highest values at the bottom. After the LGM, the percentages of charcoal morphotypes increased, leading to greater diversity and more notable fluctuations. An increase in the length-to-width ratio (L:W) was also noted during the LGM, the deglaciation phase, and the early to mid-Holocene. Alongside the pronounced increase in CHAR during the early to mid-Holocene, there were increases in morphotypes F and S/B, as well as in the L:W ratio. However, in the mid-Holocene, the L:W ratio decreased, and morphotype M became dominant, while other morphotypes exhibited sporadic increases.

4.4.4 Synthesis of Aquatic and Terrestrial Changes

Although the Holocene Epoch is generally regarded as having a stable climate compared to the Late Pleistocene, the datasets presented (Fig. 4.4, 4.5) reveal notable changes from the early Holocene to both the latter part of the early Holocene and the mid-to-late Holocene. Hence, the period was divided into three zones to understand the environmental changes during the

Holocene Epoch. Additionally, due to a limited number of data points, the OD, B-A, and YD periods have been combined into a single phase referred to as late deglaciation.

The PCA of the photosynthetic pigment and element dataset produced PC1 (52.7%) and PC2 (27.8%), which accounted for 80.5% of the dataset variance (Fig. 4.6A), and an additional 17% was explained by PC3-PC6 (Fig. S4.5A). The eigenvectors of elements (TOC, TN, TP, K) were ordinated with canthaxanthin, diatoxanthin, and pyropheophorbide in PC1, while having an opposite ordination with echinenone, beta-carotene, lutein+zeaxanthin, and $\delta^{13}C$. In contrast, most photosynthetic pigments except alloxanthin aligned with TOC, TN, and K in PC2. Alloxanthin had the strongest alignment with PC3, explaining 9.1% of the dataset variance, and it was ordinated with diatoxanthin, beta-carotene, echinenone, and TP. Furthermore, diatoxanthin, canthaxanthin, and elemental data aligned more with the early and mid-to-late Holocene periods. In contrast, beta-carotene, lutein+zeaxanthin, echinenone, and $\delta^{13}C$ had a stronger alignment with the Late Pleistocene (preHolocene). The Pearson correlation analysis (r) showed significant ($p<0.05$) positive correlations of canthaxanthin, diatoxanthin, and pyropheophorbide with all nutrients (TOC, TN, TP) and alloxanthin with TP (Fig. 4.6B). However, several pigments (ech, b-car, lut+zea) had a negative correlation with those nutrients. Additionally, enriched $\delta^{13}C$ values had a positive correlation with echinenone, lutein+zeaxanthin, beta-carotene, and okenone, while depleted values corresponded to canthaxanthin, diatoxanthin, alloxanthin, and pyropheophorbide.

The PCA of the pollen and charcoal dataset produced PC1 (39.4%) and PC2 (14.8%), which accounted for 50.2% of the dataset variance (Fig. 4.7A), and an additional 29.9% was explained by PC3-PC6 (Fig. S4.5B). The eigenvectors of most pollen and charcoal types had a positive ordination in PC1, except for *Pinus*, *Cupressaceae*, and charcoal morphotype M, which had a negative ordination. The latter variables showed a stronger alignment with the mid-to-late Holocene period, while *Quercus*, *Fagus*, *Ostrya/Carpinus*, and most other charcoal variables aligned with the two zones associated with the early Holocene. Furthermore, *Picea*, *Poaceae*, and *Cyperaceae* aligned with the Late Pleistocene (preHolocene). The Pearson correlation analysis (r) showed significant ($p<0.05$) positive correlations of *Pinus* with charcoal morphotype M. At the same time, they had a negative correlation with *Quercus*, *Fagus*, *Ostrya/Carpinus* and most of the other charcoal morphotypes (Fig. 4.7B). Additionally, the number of charcoal

particles and L:W ratio had a strong positive correlation with *Quercus* and other associated pollen types and a negative correlation with *Pinus*.

4.5 Discussion

4.5.1 The Lake Waccamaw Sediment Record

Lake Waccamaw's paleolimnological record constitutes a unique archive of climate-driven environmental and limnological transitions over time scales exceeding 27,500 years BP in the subtropical southeastern USA. The site was outside the Pleistocene glaciation, so it remained ice-free, allowing continuous sedimentation from the Late Quaternary period to present. Additionally, unlike many sediment records from North America, the site remained inundated, allowing the preservation of paleoecological signals over timescales that have rarely been recorded. The lake recorded aquatic and terrestrial processes during the Late Pleistocene and the major transition to the Holocene Epoch. Contrary to other pollen records from the region that indicate a constant dominance of *Pinus* from ~30 to 18 ka BP (Krause et al., 2019; Spencer et al., 2017), Lake Waccamaw sediments recorded the approximate timing of stadials and interstadials with transitions between *Pinus* and *Quercus* (Fig. 4.3; Table 4.1). Many of these climate intervals were marked by synchronous, abrupt changes in nutrient dynamics, the composition of the aquatic primary producer community, the production of MCs, as well as the composition of terrestrial vegetation and fire regimes. This study represents one of the first attempts to employ a multiproxy approach that combines sediment geochemistry, photosynthetic pigments, cyanotoxins, pollen analysis, and the abundance and morphotypes of charcoal to describe shifts in both aquatic and terrestrial environments. Also, the application of photosynthetic pigments as a proxy for historical changes in aquatic community composition has rarely been extended into the Late Pleistocene before (Hodgson et al., 2005; Vuillemin et al., 2016). Additionally, this record marks what is believed to be the first successful attempt to reconstruct cyanotoxins (MCs) over time scales that precede the Holocene (Paradeisis-Stathis and Waters, 2025; Paradeisis-Stathis et al., In Prep; Waters, 2016; Waters et al., 2021).

4.5.2 Paleoenvironmental Transitions in the Late Pleistocene: Ecosystem Responses to Stadials and Interstadials

Lake Waccamaw's environmental conditions before I3 (27.8 ka BP) more closely resembled a dynamic wetland rather than a stable lentic system. The pigment preservation index (chl-a/pheo-a) and the geochemical signals (Fig. 4.4) indicate intermittent lacustrine conditions,

where fluctuating water levels likely exposed sediments to photochemical oxidation, thereby hindering preservation of more labile biomarkers (Leavitt, 1993). Climatic variability over the period was sufficient to drive broad-scale ecosystem changes. Apart from shifts in *Pinus* and *Quercus* pollen, stadials and interstadials were also accompanied by shifts in other pollen types, such as peaks in *Picea* and *Ostrya*/*Carpinus*, *Carya, Liquidambar, Ulmus*, and *Betula*, respectively (Fig. 4.5A, S4.4). Despite the diverse tree pollen assemblage, consistently low pollen concentrations in both Lake Waccamaw and other regional records (LaMoreaux et al., 2009) suggest an open, sparsely forested landscape. The charcoal record also reflected a sparsely forested landscape. While fire activity remained relatively stable from 27.8 to 33.6 ka BP (Fig. 4.5B), the dominant charcoal morphotypes M and high A:P ratios, have previously been linked to the burning of grasses and leaves (Mustaphi and Pisaric, 2014) under lower intensity fires, respectively (Feurdean et al., 2023). Such an open landscape, characterized by limited vegetation cover and unstable soils, was prone to erosion of local P-rich outcrops (Cahoon et al., 1993), creating nutrient-enriched conditions that facilitated the abundance of certain primary producers in the aquatic system during periods of inundation. Although cyanobacteria pigments were not deposited, cyanobacteria ecology is rooted in both soil and freshwater environments (Grettenberger et al., 2025) and their ability to produce MCs under diverse environmental conditions (Cirés et al., 2017) suggest that cyanobacteria may have played a role, even if not directly detectable in the sedimentary record.

The total primary producer abundance (b-car) exhibited a dramatic increase during the I3 period, spanning from 26.4 to 27.8 ka BP (Fig. 4.4B). This period showed the highest pigment and MC concentrations in the sediment record, including the warm Holocene Epoch. Photosynthetic pigment biomarkers of green algae and cyanobacteria (lut+zea), as well as diatoms (diato), cryptophytes (allo), and general cyanobacteria (ech), supported a diverse primary producer community with evidence of stratification due to the presence of purple-sulfur bacteria (oke) (Bjorndahl et al., 2022; Karmakar et al., 2015). Similar increases in primary producer pigment abundance have been previously recorded during the middle to late Holocene, in Pungo Lake, NC, USA (Waters et al., 2012) and other lakes in Florida, USA (Paradeisis-Stathis et al., In prep) when nutrient inputs increased in response to wetland inundation and lake expansion. The few pigment records extending into the pre-LGM are found in Patagonia,

Argentina, and Antarctica, and photosynthetic pigment abundance showed a less distinctive pattern during the same period (Hodgson et al., 2005; Vuillemin et al., 2016).

The remarkable decrease in the C/N ratio also indicates the shift from terrestrial to increased algal organic matter contribution during the I3 period (Meyers and Teranes, 2001). While primary producers typically respond to nutrient additions, apart from an increase in the N/P ratio (Fig. 4.4A), the deposited sediments exhibited no apparent increase in nutrients. This may indicate that the enhanced primary production and cyanobacteria blooms (Fig. 4.4B) were driven by more efficient nutrient cycling, potentially facilitated by dynamic stratification-mixing regimes and episodic disruptions of stratification during lake turnover or wind-driven mixing (Reinl et al., 2023). However, nutrient deprivation due to the overall higher abundance of primary producers was still evident, leading to increased MC production by cyanobacteria (Pimentel and Giani, 2014).

The pre-LGM climate in the southeastern United States was predominantly cold, dry, and windy (LaMoreaux et al., 2009), largely driven by a persistent high-pressure system over the Laurentide Ice Sheet, which displaced the jet stream southward (Lane et al., 2018). However, interstadial phases preceding deglaciation, such as the I3 interval, brought temporary climatic amelioration, with modest increases in temperature and precipitation that could enhance biological production (Spencer et al., 2017). A northern migration or weakening of the jet stream would allow the transfer of moisture from the Gulf of Mexico/America, the intertropical convergence zone, and the North Atlantic storm tracks to higher latitudes in North America (Broccoli et al., 2006; Joyce et al., 2019; Michels et al., 2007).

The aquatic ecosystem responded rapidly to the increased influx of energy from higher temperatures and increased precipitation during the I3. However, the proliferation of grasses, sedges, and flowering plants (Fig. 4.5A, S4.4), along with the still sparsely forested landscape, limited the indirect effects of energy influx and restricted mass transfer from the terrestrial landscape (Leavitt et al., 2009). The restricted terrestrial input is further supported by relatively low nutrient deposition and $\delta^{13}C$ enrichment in the sediments (Fig. 4.4A). Increased primary productivity can induce CO_2 limitation that often leads to $\delta^{13}C$ enrichment, as phytoplankton increasingly utilize the heavier ^{13}C from bicarbonate sources or isotopically heavier CO_2 produced as a byproduct of anoxygenic methanogenesis (Brenner et al., 1999). In parallel, increased transfer of atmospheric heat may have elevated fire activity in the landscape (Fig.

4.5B). While nutrient additions in Lake Waccamaw were typically simultaneous for TOC, TN, and TP, the beginning of the I3 was only associated with a momentary substantial increase in TP. Fires produce P-rich ash that could enhance atmospheric P delivery, leading to a sharp increase in primary producer abundance through pyroeutrophication (Waters et al., 2023). Although TP deposition declined and the N/P ratio rose for the remainder of the I3 period, primary producer abundance continued to increase, suggesting that P inputs from fires triggered a lasting aquatic response, potentially sustained by internal nutrient cycling.

The aquatic primary producer response during the I3 was unprecedented for the Late Pleistocene portion of the sediment record (Fig. 4.4B). In the subsequent periods, overall changes in the aquatic environment were less apparent (Fig. 4.4). Apart from the notable decrease in photosynthetic pigments during the LGM, other *Pinus*-dominated periods in the Late Pleistocene were also associated with slight decreases in pigment abundance. In contrast, *Quercus*-dominated periods were more closely related to increases or relative stability in primary producer abundance. Increased nutrient deposition during the *Quercus*-dominated post-LGM coincided with higher abundance and greater diversity of pollen from tree taxa (Fig. 4.5A, S4.4), indicating increased mass transfer from the terrestrial landscape (Leavitt et al., 2009). Surprisingly, post-LGM period had reduced content of sand (90-100 cm, Fig. 4.2), no apparent change in geochemical ratios indicative of organic matter sources (C/N, $\delta^{13}C$) (Fig. 4.4A), and only a slight increase in colonial cyanobacteria (canth) (Fig. 4.4B). Additionally, the onset of B-A brought a peak in MCs deposition and a slight increase in most primary producers, consistent with patterns observed in other globally distributed lakes such as Lake Victoria in Africa (Wienhues et al., 2024), Lake Lielais Svētiņu in Latvia (Tõnno et al., 2021), and Laguna Potrok Aike in Argentina (Vuillemin et al., 2016).

The subtle changes in the aquatic environment after the LGM may indicate a decoupling from terrestrial changes or containment by them. Nearby Pungo Lake exhibited a decrease in primary producers during periods of terrestrial organic matter inputs, suggesting light limitation due to dystrophic conditions (browning) (Waters et al., 2012). In addition to *Pinus*-*Quercus* transitions throughout the Late Pleistocene, other pollen taxa also responded, indicating the broader impact of climatic variations. Nevertheless, a gradual change was also occurring in vegetation composition, transitioning from an open landscape to one with denser tree cover. Despite the decrease in fire activity after the LGM (Fig. 4.5B), the charcoal record also suggests

a change in the regime of fires, with charcoal morphotypes (F, L:W) indicating that predominantly woody and needle material, as well as grasses, constituted the fuel for fires burning at higher temperatures (Feurdean et al., 2023; Vachula et al., 2024). These changes in vegetation and fire regime indicate differences between the pre-LGM and post-LGM terrestrial landscapes, as also supported by shifts in the migratory patterns of prehistoric mammals in the southeastern United States (Hoppe and Koch, 2007). Furthermore, likely in connection with hydroclimatic fluctuations, the southeastern Atlantic Coastal Plain has previously recorded notable paleochannel activity and dynamic surface flows (Leigh, 2008; Suther et al., 2018). Although the Lake Waccamaw sediment core lacked a typical flood stratigraphy, lithological shifts to an increased frequency of coarse sand deposition between ~27.5 and 7 ka BP (40–126 cm, Fig. 4.2) and decreased sedimentation during climate intervals after the LGM in the Late Pleistocene (post-LGM, OD, B-A, and YD) (80-100 cm, Fig. 4.2) could suggest alterations in energy regimes, possibly linked to regional hydroclimatic shifts, and changing surficial flows and lake-levels (Dearing, 1997).

4.5.3 Holocene Paleoenvironmental Dynamics: Abrupt Synchronous Changes in Water and Land

Dramatic changes in the aquatic and terrestrial ecosystems occurred after 11.4 ka BP, highlighting the profound influence of the transition from the glacial climate of the Late Pleistocene to the postglacial climate of the early Holocene (Birks and Ammann, 2000; Engels et al., 2018; Hanisch et al., 2009; Tõnno et al., 2021; Tu et al., 2021; Vuillemin et al., 2016; Zander et al., 2021). The aquatic system rapidly shifted to a eutrophic state, characterized by increases in generalized photosynthetic pigments biomarkers for total primary producer abundance (b-car) and algae and cyanobacteria (lut+zea), as well as diatoms (diato) and general cyanobacteria (ech). Additionally, increased abundance of purple-sulfur bacteria (oke), indicative of stratified conditions likely driven by sustained lake-level rise and longer hydroperiods (Rogozin et al., 2020). Unlike the I3 period, there was a notable increase in zooplankton grazing (pyro), while the cyanobacteria community became dominated by colonial forms (canth). In contrast, cryptophytes (allo) declined, and MC concentrations dropped to their lowest levels, suggesting that the aquatic community composition, and not just nutrients, trigger cyanotoxin ecology (Kaplan et al., 2012). Nevertheless, the major influx of nutrients (TOC, TN, TP) and a second notable increase in the TN:TP ratio seem to have supported the shift to increased autochthonous

production (C/N) (Meyers and Teranes, 2001). Similar nutrient enrichment has previously been recorded during the early Holocene in Lake Uddelermeer in the Netherlands, where they constituted the highest natural nutrient deposition conditions (Engels et al., 2018). The combined increases in nutrient loading, primary producer biomass, and stratification closely resemble those observed in modern lake eutrophication trajectories (Taranu et al., 2015; Waters et al., 2009).

The onset of the Holocene was also marked by denser forest cover and a pollen transition from the cold-adapted *Pinus* to more thermophilus taxa such as *Quercus*, *Fagus*, and *Ostrya*/*Carpinus* (Fig. 4.5A). Pollen-based temperature reconstructions for the southeastern United States remain inconclusive, showing both warming and cooling trends across sites (Krause et al., 2019; Spencer et al., 2017), while precipitation reconstructions indicate increasing precipitation since the B-A period (Spencer et al., 2017). Although transitions to *Quercus* dominance have been linked to a wide range of hydroclimatic conditions, including both wetter and drier regimes (Spencer et al., 2017), Lake Waccamaw seems to have sustained a positive evapotranspiration budget during the early Holocene. This is supported by elevated K concentrations (Fig. 4.4A), which likely reflect increased terrestrial runoff driven by higher precipitation (Kuhlmann et al., 2004), coinciding with rapid sea-level rise (Smith et al., 2011). Nevertheless, the increased fire activity and intensity based on charcoal accumulation rate and morphotypes (high F and L:W) (Fig. 4.5B), suggest a shift toward greater rainfall seasonality and potentially intensified summer droughts (Ruan et al., 2020). Moreover, the dramatic decrease in *Pinus* pollen, along with its strong negative correlation with charcoal particles and morphotypes (Fig. 4.7B), implies that fires acted as a stressor driving vegetation change. Although less clear in such timescales, increases in fire activity have also been suggested as a driver of nutrient enrichment and cyanobacteria blooms through lake pyroeutrophication (Waters et al., 2023).

Despite the sharp decline in nutrients and most primary producers after approximately 9.4 ka BP, colonial cyanobacteria persisted, and MC deposition increased (Fig. 4.4B), highlighting the versatile role of cyanotoxins in cyanobacteria ecology (Kaplan et al., 2012). Throughout Lake Waccamaw's history with lentic conditions, cyanotoxins have increased under low nutrient conditions, which contradicts modern observations (Clift and Waters, 2024; Paradeisis-Stathis and Waters, 2025; Paradeisis-Stathis et al., In prep; Waters, 2016; Waters et al., 2021) and indicates that it is not solely nutrient increases but nutrient stoichiometry under eutrophication that constitutes the primary driver of cyanotoxin production (Brandenburg et al., 2020).

The decline of many primary producers after 9.4 ka BP coincided with potentially climate-driven changes in the terrestrial landscape and increased allochthonous inputs to the lake (Fig. 4.4, 4.5). While primary producers exhibit a wide range of carbon isotope fractionation, the gradual depletion in $\delta^{13}C$ and slight increase in C/N (Fig. 4.4A) indicate that the source of organic matter entering the lake shifted in response to the growing influence of terrestrial vegetation (Hecky and Hesslein, 1995; Meyers and Teranes, 2001). This increase in allochthonous inputs occurred simultaneously with a decrease in several pollen taxa, including *Fagus* and *Ostrya*/*Carpinus* (Fig. 4.5A). Additionally, there is a decoupling between K deposition and Fe/Mn ratio (Fig. 4.4B). In the absence of minerogenic inputs (K), the Fe/Mn ratio acts as a proxy for bottom water anoxia (Davies et al., 2015), and without detectable purple-sulfur bacteria, the increase in Fe/Mn could suggest anoxia under increased light attenuation, potentially due to phytoplankton or increased terrestrial organic matter inputs (browning).

The aquatic and terrestrial ecosystem changes indicate a potential link to deteriorated climatic conditions. The timing of the decline in nutrients (TOC, TN, TP), photosynthetic pigments (b-car, lut+zea, diato, ech, oke, pyro), and several pollen taxa (*Fagus*, *Ostrya*/*Carpinus*) (Fig. 4.4, 4.5A), coincided with the 9.3 ka cold event, triggered by alterations in ocean circulation due to the rapid drainage of fresh water from Lake Superior into the Atlantic Ocean (Yu et al., 2010). While dynamic landscape changes during the early Holocene deglaciation rerouted fresh water in regions like Fennoscandia (Möller et al., 2022), the connection between ice-dammed lakes formed during the deglaciation of the Laurentide Ice Sheet and the North Atlantic Current through the Labrador Sea could lead to abrupt climate changes during freshwater outbursts (Törnqvist and Hijma, 2012). The 9.3 ka event may have caused a shift to relatively colder and drier conditions, potentially intensified by increased seasonality from summer maximum and winter minimum insolation (Krause et al., 2019).

The onset of modern environmental conditions at Lake Waccamaw began in the middle Holocene, after 6.6 ka BP, marking a period of long-term ecological stabilization. Since that time, TP deposition has shown a continuous increase, while TOC and TN peaked at 6.6 ka BP, then declined, and gradually increased over the last 2 ka (Fig. 4.4A). Although most primary producer pigment concentrations started to gradually decline after their mid-Holocene peak, colonial cyanobacteria (canth) have dominated the aquatic system (Fig. 4.4B), reflecting sustained eutrophic conditions under TP enrichment and stoichiometric imbalance with TN.

While other Carolina Bays in the region developed stable limnologic conditions in the mid-Holocene, which was much later than Lake Waccamaw, the currently dystrophic Pungo Lake has shown similar TP enrichment and changes in primary community structure over the last 4 ka BP (Waters et al., 2012).

This mid to late Holocene period also coincided with terrestrial shifts, including the *Quercus* to *Pinus* transition (Fig. 4.5A), and the expansion of wetlands, as indicated by increased *Cupressaceae* and *Nyssa* pollen (Fig. 4.5A, S4.4). Moreover, fire activity declined, and charcoal morphologies shifted toward more herbaceous fuels (M) and fewer woody sources (F) (Fig. 4.5B) (Mustaphi and Pisaric, 2014; Vachula et al., 2024). Despite the presence of Native Americans in the region, which includes potential evidence of fire use over the past millennium in nearby Jones and Singletary Lakes (Spencer et al., 2017) and the recent discovery of a ~1,000-year-old canoe in Lake Waccamaw (Yang, 2023), there was no significant increase in charcoal accumulation in the lake until the last century.

While the dominance of cyanobacteria has persisted throughout the mid to late Holocene and human-induced nutrient loading has intensified during the last century, the overall abundance of primary producers has yet to surpass the levels seen in the early Holocene. This suggests that, natural nutrient stoichiometry under hydroclimatic fluctuations has been a more significant factor than recent temperature warming and anthropogenic landscape and aquatic impacts. However, the future trajectory of the lake is more nuanced. While some lakes have taken on a dystrophic trajectory, characterized by low productivity and humic-rich waters, such as Pungo Lake (Waters et al., 2012), the modern persistence of colonial cyanobacteria, coupled with increased P and N deposition and climate-induced disturbance events, could be concerning for more eutrophic conditions (Paerl et al., 2011).

4.5.4 Cyanobacteria Dominance Preceding Human Impacts

The sediments of Lake Waccamaw capture the integrated response of aquatic and terrestrial ecosystems to varying climate intervals over a period exceeding 27,500 years (Fig, 4.4, 4.5). This long-term perspective offers a valuable baseline for interpreting primary producer community dynamics and conditions that drive cyanobacteria abundance and dominance in the absence of human disturbance. Multiproxy evidence utilizing aquatic geochemical proxies, photosynthetic pigments, pollen, and charcoal indicates increased primary producer abundance, cyanobacteria dominance, and elevated MC production under natural conditions preceding

anthropogenic impacts. During the Late Pleistocene and early Holocene, periods with increased *Quercus* pollen and other deciduous taxa (Fig. 4.5A) coincided with increased primary producer abundance dominated by general or colonial cyanobacteria (Fig. 4.4B), occasional increases in fire activity (Fig. 4.5B), and dynamic nutrient conditions (Fig. 4.4A). While the modern dominance of colonial cyanobacteria under an overall low primary producer abundance can be viewed as a human-influenced novel ecosystem, our paleolimnological record indicates that cyanobacteria dominance occurred naturally, even under varying aquatic and terrestrial conditions.

The aquatic environment was more likely to develop abrupt changes during intervals with synchronous terrestrial ecosystem changes. Although the aquatic response during the (I3) is difficult to compare directly with other records, the early Holocene reveals a striking coupling between aquatic and terrestrial proxies, a pattern also observed in European lakes (Birks and Ammann, 2000). While this period was marked by elevated temperatures and widespread ecological change, temperature itself was not the primary driver of increased primary producer abundance. Instead, shifts in nutrient stoichiometry (N/P) and hydroclimatic variability played the dominant role in shaping the aquatic community (Bjerring et al., 2013; Vuillemin et al., 2016).

Lake Waccamaw's sediment record is among the oldest paleolimnological archives of aquatic and terrestrial processes from a subtropical, non-glaciated environment. The absence of prolonged ice-cover and continuous inundation during the Late Pleistocene and Holocene periods offered a rare opportunity to study the interaction of multiple natural drivers, without the influence of anthropogenic activities. The aquatic environment responded to various drivers, such as hydroclimate, nutrient availability, and terrestrial changes in vegetation and fires, and showed that modern cyanobacteria dominance is neither necessarily an unprecedented phenomenon nor the worst water quality state for this system.

4.6 Conclusions

The sediment record of Lake Waccamaw constitutes an archive of paleoenvironmental changes during the Late Quaternary period to the present in the southeastern United States. The multiproxy analysis, including photosynthetic pigments, cyanotoxins, geochemical proxies, pollen, and charcoal data, revealed how both terrestrial and aquatic ecosystems responded to climate shifts over more than 30,000 years. The record indicates continuous lentic conditions

since the I3 interval, approximately 27,500 years BP. Periods dominated by *Pinus* and *Quercus* pollen corresponded with stadials and interstadials in the $\delta^{18}O$ record of NGRIP, respectively. Abrupt shifts in aquatic primary producer abundance occurred during I3 and the early Holocene, periods also marked by synchronous increases in deciduous pollen and fire activity. Throughout the record, cyanobacteria remained the dominant primary producers, with colonial forms becoming prevalent during most of the Holocene. Although nutrient inputs and human activities have intensified during the last century, the presence of cyanobacteria is not novel and past lake conditions under natural hydroclimatic fluctuations were characterized by higher primary producer abundance, including cyanobacteria and cyanotoxins. This study demonstrates the importance of paleolimnology in understanding the past and present of aquatic ecosystems. Paleolimnological records extending into the LGM are scarce and there is great need to understand how aquatic ecosystems have responded to a range of climatic conditions.

4.7 References

Appleby, P.G., Nolan, P.J., Gifford, D.W., Godfrey, M.J., Oldfield, F., Anderson, N.J., Battarbee, R.W., 1986. 210Pb dating by low background gamma counting. Hydrobiologia 143, 21-27. https://doi.org/10.1007/BF00026640.

Appleby, P.G., Oldfieldz, F., 1983. The assessment of 210Pb data from sites with varying sediment accumulation rates. Hydrobiologia 103, 29-35. https://doi.org/10.1007/BF00028424.

Ball, B.A., Kominoski, J.S., Adams, H.E., Jones, S.E., Kane, E.S., Loecke, T.D., Mahaney, W.M., Martina, J.P., Prather, C.M., Robinson, T.M.P., Solomon, C.T., 2010. Direct and terrestrial vegetation-mediated effects of environmental change on aquatic ecosystem processes. BioScience 60, 590-601. https://doi.org/10.1525/bio.2010.60.8.5.

Birks, H.H., Ammann, B., 2000. Two terrestrial records of rapid climatic change during the glacial–Holocene transition (14,000– 9,000 calendar years B.P.) from Europe. Proceedings of the National Academy of Sciences 97, 1390-1394. https://doi.org/10.1073/pnas.97.4.1390.

Bjerring, R., Olsen, J., Jeppesen, E., Buchardt, B., Heinemeier, J., McGowan, S., Leavitt, P.R., Enevold, R., Odgaard, B.V., 2013. Climate-driven changes in water level: a decadal scale multi-proxy study recording the 8.2-ka event and ecosystem responses in Lake Sarup (Denmark). Journal of Paleolimnology 49, 267-285. https://doi.org/10.1007/s10933-012-9673-7.

Bjorndahl, J.A., Gushulak, C.A.C., Mezzini, S., Simpson, G.L., Haig, H.A., Leavitt, P.R., Finlay, K., 2022. Abrupt changes in the physical and biological structure of endorheic upland lakes due to 8-m lake-level variation during the 20th century. Limnology and Oceanography 67, 1022-1039. https://doi.org/10.1002/lno.12054.

Blaauw, M., Christen, J.A., 2011. Flexible paleoclimate age-depth models using an autoregressive gamma process. Bayesian Analysis 6, 457-474, 418. https://doi.org/10.1214/11-BA618.

Brandenburg, K., Siebers, L., Keuskamp, J., Jephcott, T.G., Van de Waal, D.B., 2020. Effects of nutrient limitation on the synthesis of N-rich phytoplankton toxins: A meta-analysis. Toxins 12, 221. https://doi.org/10.3390/toxins12040221.

Brenner, M., Whitmore, T.J., Curtis, J.H., Hodell, D.A., Schelske, C.L., 1999. Stable isotope (δ13C and δ15N) signatures of sedimented organic matter as indicators of historic lake trophic state. Journal of Paleolimnology 22, 205-221. https://dx.doi.org/10.1023/a:1008078222806.

Broccoli, A.J., Dahl, K.A., Stouffer, R.J., 2006. Response of the ITCZ to Northern Hemisphere cooling. Geophysical Research Letters 33. https://doi.org/10.1029/2005GL024546.

Brooks, M.J., Taylor, B.E., Ivester, A.H., 2010. Carolina Bays: Time capsules of culture and climate change. Southeastern Archaeology 29, 146-163. https://doi.org/10.1179/sea.2010.29.1.010.

Cahoon, L.B., Kucklick, J.R., Kiefer, R.H., Willey, J.D., 1993. The effects of chemical weathering on limestone dissolution and phosphate release into Lake Waccamaw, North Carolina. Journal of the Elisha Mitchell Scientific Society 109, 123-134. http://www.jstor.org/stable/24335294.

Cahoon, L.B., Kucklick, J.R., Kiefer, R.H., Willey, J.D., 1993. The effects of chemical weathering on limestone dissolution and phosphate release into Lake Waccamaw, North Carolina. Journal of the Elisha Mitchell Scientific Society 109, 123-134. http://www.jstor.org/stable/24335294.

Cahoon, L.B., Kucklick, J.R., Stager, J.C., 1990. A natural phosphate source for Lake Waccamaw, North Carolina, USA. Internationale Revue der gesamten Hydrobiologie und Hydrographie 75, 339-351. https://doi.org/10.1002/iroh.19900750306.

Casterlin, M.E., Reynolds, W.W., Lindquist, D.G., Yarbrough, C.G., 1984. Algal and physicochemical indicators of eutrophication in a lake harboring endemic species: Lake Waccamaw, North Carolina. Journal of the Elisha Mitchell Scientific Society 100, 83-103. http://www.jstor.org/stable/24333406.

Cirés, S., Casero, M.C., Quesada, A., 2017. Toxicity at the edge of life: A review on cyanobacterial toxins from extreme environments. Marine Drugs 15, 233. https://doi.org/10.3390/md15070233.

Clift, T.L., Waters, M.N., 2024. Paleolimnological evidence for primary producer change linked to hydrologic connectivity and human impacts in Lake Carlton, Florida, USA. Journal of Paleolimnology 72, 35-48. https://doi.org/10.1007/s10933-024-00318-y.

Corrick, E.C., Drysdale, R.N., Hellstrom, J.C., Capron, E., Rasmussen, S.O., Zhang, X., Fleitmann, D., Couchoud, I., Wolff, E., 2020. Synchronous timing of abrupt climate changes during the last glacial period. Science 369, 963-969. https://doi.org/10.1126/science.aay5538.

Davies, S.J., Lamb, H.F., Roberts, S.J., 2015. Micro-XRF Core Scanning in Palaeolimnology: Recent Developments, in: Croudace, I.W., Rothwell, R.G. (Eds.), Micro-XRF Studies of Sediment Cores: Applications of a non-destructive tool for the environmental sciences. Springer Netherlands, Dordrecht, pp. 189-226. https://doi.org/10.1007/978-94-017-9849-5_7.

Dean, W.E., 1974. Determination of carbonate and organic matter in calcareous sediments and sedimentary rocks by loss on ignition; comparison with other methods. Journal of Sedimentary Research 44, 242-248. https://doi.org/10.1306/74D729D2-2B21-11D7-8648000102C1865D.

Dearing, J.A., 1997. Sedimentary indicators of lake-level changes in the humid temperate zone: a critical review. Journal of Paleolimnology 18, 1-14. https://doi.org/10.1023/A:1007916210820.

Enache, M.D., Cumming, B.F., 2006. Tracking recorded fires using charcoal morphology from the sedimentary sequence of Prosser Lake, British Columbia (Canada). Quaternary Research 65, 282-292. https://doi.org/10.1016/j.yqres.2005.09.003.

Engels, S., van Oostrom, R., Cherli, C., Dungait, J.A.J., Jansen, B., van Aken, J.M., van Geel, B., Visser, P.M., 2018. Natural and anthropogenic forcing of Holocene lake ecosystem development at Lake Uddelermeer (The Netherlands). Journal of Paleolimnology 59, 329-347. https://doi.org/10.1007/s10933-017-0012-x.

EPA, 1975. Lake Waccamaw Columbus County North Carolina, National Eutrophication Survey. US Environmental Protection Agency. https://nepis.epa.gov/Exe/ZyPDF.cgi?Dockey=9100D89A.PDF.

Feng, L., Wang, Y., Hou, X., Qin, B., Kutser, T., Qu, F., Chen, N., Paerl, H.W., Zheng, C., 2024. Harmful algal blooms in inland waters. Nature Reviews Earth & Environment 5, 631-644. https://doi.org/10.1038/s43017-024-00578-2.

Feurdean, A., Vachula, R.S., Hanganu, D., Stobbe, A., Gumnior, M., 2023. Charcoal morphologies and morphometrics of a Eurasian grass-dominated system for robust interpretation of past fuel and fire type. Biogeosciences 20, 5069-5085. https://doi.org/10.5194/bg-20-5069-2023.

Fisher, M.M., Brenner, M., Reddy, K.R., 1992. A simple, inexpensive piston corer for collecting undisturbed sediment/water interface profiles. Journal of Paleolimnology 7, 157-161. https://doi.org/10.1007/BF00196870.

Frey, D.G., 1953. Regional aspects of the late-glacial and post-glacial pollen succession of southeastern North Carolina. Ecological Monographs 23, 289-313. https://doi.org/10.2307/1943595.

Grettenberger, C., Gold, D.A., Brown, C.T., 2025. Distribution of early-branching Cyanobacteriia and the potential habitats that gave rise to the earliest oxygenic phototrophs. mSphere, e0101324. https://doi.org/10.1128/msphere.01013-24.

Grimm, E.C., Jacobson, G.L., Jr., Watts, W.A., Hansen, B.C., Maasch, K.A., 1993. A 50,000-year record of climate oscillations from Florida and its temporal correlation with the heinrich events. Science 261, 198-200. https://doi.org/10.1126/science.261.5118.19.

Grimm, E.C., Watts, W.A., Jacobson, G.L., Hansen, B.C.S., Almquist, H.R., Dieffenbacher-Krall, A.C., 2006. Evidence for warm wet Heinrich events in Florida. Quaternary Science Reviews 25, 2197-2211. https://doi.org/10.1016/j.quascirev.2006.04.008.

Grimm, N.B., Chapin III, F.S., Bierwagen, B., Gonzalez, P., Groffman, P.M., Luo, Y., Melton, F., Nadelhoffer, K., Pairis, A., Raymond, P.A., Schimel, J., Williamson, C.E., 2013. The impacts of climate change on ecosystem structure and function. Frontiers in Ecology and the Environment 11, 474-482. https://doi.org/10.1890/120282.

Hanisch, S., Wessels, M., Niessen, F., Schwalb, A., 2009. Late Quaternary lake response to climate change and anthropogenic impact: biomarker evidence from Lake Constance sediments. Journal of Paleolimnology 41, 393-406. https://doi.org/10.1007/s10933-008-9232-4.

Havens, K.E., Paerl, H.W., 2015. Climate change at a crossroad for control of harmful algal blooms. Environmental Science & Technology 49, 12605-12606. https://doi.org/10.1021/acs.est.5b03990.

Hecky, R.E., Hesslein, R.H., 1995. Contributions of benthic algae to lake food webs as revealed by stable isotope analysis. Journal of the North American Benthological Society 14, 631-653. https://doi.org/10.2307/1467546.

Hodgson, D.A., Vyverman, W., Verleyen, E., Leavitt, P.R., Sabbe, K., Squier, A.H., Keely, B.J., 2005. Late Pleistocene record of elevated UV radiation in an Antarctic lake. Earth and Planetary Science Letters 236, 765-772. https://doi.org/10.1016/j.epsl.2005.05.023.

Hoppe, K.A., Koch, P.L., 2007. Reconstructing the migration patterns of late Pleistocene mammals from northern Florida, USA. Quaternary Research 68, 347-352. https://doi.org/10.1016/j.yqres.2007.08.001.

Hou, X., Feng, L., Dai, Y., Hu, C., Gibson, L., Tang, J., Lee, Z., Wang, Y., Cai, X., Liu, J., Zheng, Y., Zheng, C., 2022. Global mapping reveals increase in lacustrine algal blooms over the past decade. Nature Geoscience 15, 130-134. https://doi.org/10.1038/s41561-021-00887-x.

Joyce, T.M., Kwon, Y.-O., Seo, H., Ummenhofer, C.C., 2019. Meridional Gulf Stream shifts can influence wintertime variability in the North Atlantic storm track and Greenland blocking. Geophysical Research Letters 46, 1702-1708. https://doi.org/10.1029/2018GL081087.

Kaczorowski, R.T., 1977. The Carolina Bays and their relationship to modern oriented lakes, Department of Geology. University of South Carolina. https://www.proquest.com/dissertations-theses/carolina-bays-their-relationship-modern-oriented/docview/302855857/se-2?accountid=8421.

Kaplan, A., Harel, M., Kaplan-Levy, R.N., Hadas, O., Sukenik, A., Dittmann, E., 2012. The languages spoken in the water body (or the biological role of cyanobacterial toxins). Frontiers in Microbiology 3, 138. https://doi.org/10.3389/fmicb.2012.00138.

Karmakar, M., Leavitt, P.R., Cumming, B.F., 2015. Enhanced algal abundance in northwest Ontario (Canada) lakes during the warmer early-to mid-Holocene period. Quaternary Science Reviews 123, 168-179. https://doi.org/10.1016/j.quascirev.2015.06.025.

Kassambara, A., 2023. ggcorrplot: Visualization of a Correlation Matrix using 'ggplot2'. R package version 0.1.4.999. https://github.com/kassambara/ggcorrplot.

Krause, T.R., Russell, J.M., Zhang, R., Williams, J.W., Jackson, S.T., 2019. Late Quaternary vegetation, climate, and fire history of the Southeast Atlantic Coastal Plain based on a 30,000-yr multi-proxy record from White Pond, South Carolina, USA. Quaternary Research. https://doi.org/10.1017/QUA.2018.95.

Kuhlmann, H., Meggers, H., Freudenthal, T., Wefer, G., 2004. The transition of the monsoonal and the N Atlantic climate system off NW Africa during the Holocene. Geophysical Research Letters 31. https://dx.doi.org/10.1029/2004gl021267.

LaMoreaux, H.K., Brook, G.A., Knox, J.A., 2009. Late Pleistocene and Holocene environments of the Southeastern United States from the stratigraphy and pollen content of a peat deposit on the Georgia Coastal Plain. Palaeogeography, Palaeoclimatology, Palaeoecology. https://doi.org/10.1016/J.PALAEO.2009.06.017.

Lane, C.S., Taylor, A.K., Spencer, J., Jones, K.B., 2018. Compound-specific isotope records of late-quaternary environmental change in southeastern North Carolina. Quaternary Science Reviews. https://doi.org/10.1016/J.QUASCIREV.2017.12.022.

Leavitt, P.R., 1993. A review of factors that regulate carotenoid and chlorophyll deposition and fossil pigment abundance. Journal of Paleolimnology 9, 109-127. https://doi.org/10.1007/BF00677513.

Leavitt, P.R., Fritz, S.C., Anderson, N.J., Baker, P.A., Blenckner, T., Bunting, L., Catalan, J., Conley, D.J., Hobbs, W.O., Jeppesen, E., Korhola, A., McGowan, S., RÜhland, K., Rusak, J.A., Simpson, G.L., Solovieva, N., Werne, J., 2009. Paleolimnological evidence of the effects on lakes of energy and mass transfer from climate and humans. Limnology and Oceanography 54, 2330-2348. https://doi.org/10.4319/lo.2009.54.6_part_2.2330.

Leavitt, P., Hodgson, D., 2001. Sedimentary pigments. In: Smol, J.P., Birks, H.J.B., Last, W.M., Bradley, R.S., Alverson, K. (eds), Tracking environmental change using lake sediments. Springer, pp. 295–325. https://doi.org/10.1007/0-306-47668-1_15.

Leigh, D.S., 2008. Late Quaternary climates and river channels of the Atlantic Coastal Plain, Southeastern USA. Geomorphology. https://doi.org/10.1016/J.GEOMORPH.2008.05.024.

Lide, R.F., 1997. When is a depression wetland a Carolina Bay? Southeastern Geographer 37, 90-98. http://www.jstor.org/stable/44370980.

Lundine, M.A., Trembanis, A.C., 2021. Using convolutional neural networks for detection and morphometric analysis of Carolina Bays from publicly available digital elevation models. Remote Sensing 13, 3770. https://doi.org/10.3390/rs13183770.

Lundine, M., Trembanis, A., 2025. Investigating the origin and dynamics of Carolina Bays. Marine Geology 480, 107449. https://doi.org/10.1016/j.margeo.2024.107449.

McGowan, S., Britton, G., Haworth, E., Moss, B., 1999. Ancient blue-green blooms. Limnology and Oceanography 44, 436-439. https://doi.org/10.4319/lo.1999.44.2.0436.

Meerhoff, M., Audet, J., Davidson, T.A., De Meester, L., Hilt, S., Kosten, S., Liu, Z., Mazzeo, N., Paerl, H., Scheffer, M., Jeppesen, E., 2022. Feedback between climate change and eutrophication: revisiting the allied attack concept and how to strike back. Inland Waters 12, 187-204. https://doi.org/10.1080/20442041.2022.2029317.

Meyers, P.A., Teranes, J.L., 2001. Sediment organic matter, in: Last, W.M., Smol, J.P. (Eds.), Tracking Environmental Change Using Lake Sediments: Physical and Geochemical Methods. Springer Netherlands, Dordrecht, pp. 239-269. https://doi.org/10.1007/0-306-47670-3_9.

Michels, A., Laird, K.R., Wilson, S.E., Thomson, D., Leavitt, P.R., Oglesby, R.J., Cumming, B.F., 2007. Multidecadal to millennial-scale shifts in drought conditions on the Canadian prairies over the past six millennia: implications for future drought assessment. Global Change Biology 13, 1295-1307. https://doi.org/10.1111/j.1365-2486.2007.01367.x.

Moss, B., Kosten, S., Meerhoff, M., Battarbee, R.W., Jeppesen, E., Mazzeo, N., Havens, K., Lacerot, G., Liu, Z., De Meester, L., Paerl, H., Scheffer, M., 2011. Allied attack: climate change and eutrophication. Inland Waters 1, 101-105. https://doi.org/10.5268/IW-1.2.359.

Mustaphi, C.J.C., Pisaric, M.F.J., 2014. A classification for macroscopic charcoal morphologies found in Holocene lacustrine sediments. Progress in Physical Geography: Earth and Environment 38, 734-754. https://doi.org/10.1177/0309133314548886.

Nelle, O., Dreibrodt, S., Dannath, Y., 2010. Combining pollen and charcoal: evaluating Holocene vegetation composition and dynamics. Journal of Archaeological Science 37, 2126-2135. https://doi.org/10.1016/j.jas.2010.02.010.

Nienaber, M.A., Steinitz-Kannan, M., 2018. A Guide to Cyanobacteria Identification and Impact. University Press of Kentucky. https://doi.org/10.2307/j.ctv8j70z.

NC Geological Survey, 1985. Geologic Map of North Carolina. Department of Environmental Quality Interactive Geological Maps. Accessed May 28, 2024, from https://experience.arcgis.com/experience/52e7e472f21444e794d6ef02a9b02121/

North Greenland Ice Core Project members, 2004. High-resolution record of Northern Hemisphere climate extending into the last interglacial period. Nature 431, 147-151. https://doi.org/10.1038/nature02805.

Paerl, H.W., Hall, N.S., Calandrino, E.S., 2011. Controlling harmful cyanobacterial blooms in a world experiencing anthropogenic and climatic-induced change. Science of The Total Environment 409, 1739-1745. https://doi.org/10.1016/j.scitotenv.2011.02.001.

Paerl, H.W., Huisman, J., 2008. Blooms Like It Hot. Science 320, 57-58. https://doi.org/10.1126/science.1155398.

Paerl, H.W., Huisman, J., 2009. Climate change: a catalyst for global expansion of harmful cyanobacterial blooms. Environ Microbiol Rep 1, 27-37. https://doi.org/10.1111/j.1758-2229.2008.00004.x.

Paerl, H.W., Scott, J.T., 2010. Throwing Fuel on the Fire: Synergistic Effects of Excessive Nitrogen Inputs and Global Warming on Harmful Algal Blooms. Environmental Science & Technology 44, 7756-7758. https://doi.org/10.1021/es102665e.

Paradeisis-Stathis, S., Waters, M.N., 2025. Linking phosphorus dynamics with hypereutrophic conditions on the millennial scale: The paleolimnology of shallow and subtropical Lake Wauberg, Florida, USA. Science of The Total Environment 982, 179625. https://doi.org/10.1016/j.scitotenv.2025.179625.

Paradeisis-Stathis, S., Waters, M.N., Willard, D.A., Foliano, S., Vachula, R.S., In Prep. Microcystin production on the millennial-scale: a paleolimnological investigation of two subtropical lakes in central Florida, USA.

Pimentel, J.S.M., Giani, A., 2014. Microcystin production and regulation under nutrient stress conditions in toxic *Microcystis* strains. Applied and Environmental Microbiology 80(18), 5836-5843. https://doi.org/10.1128/aem.01009-14.

Pinter, N., Ishman, S., 2008. Impacts, mega-tsunami, and other extraordinary claims. Gsa Today 18. https://doi.org/10.1130/GSAT01801GW.1.

Pinter, N., Scott, A.C., Daulton, T.L., Podoll, A., Koeberl, C., Anderson, R.S., Ishman, S.E., 2011. The Younger Dryas impact hypothesis: A requiem. Earth-Science Reviews 106, 247-264. https://doi.org/10.1016/j.earscirev.2011.02.005.

Piovan, S.E., Hodgson, M.E., 2017. How many Carolina bays? An analysis of Carolina bays from USGS topographic maps at different scales. Cartography and Geographic Information Science 44, 310-326. https://doi.org/10.1080/15230406.2016.1162670.

Reimer, P.J., Austin, W.E.N., Bard, E., Bayliss, A., Blackwell, P.G., Bronk Ramsey, C., Butzin, M., Cheng, H., Edwards, R.L., Friedrich, M., Grootes, P.M., Guilderson, T.P., Hajdas, I., Heaton, T.J., Hogg, A.G., Hughen, K.A.,

Kromer, B., Manning, S.W., Muscheler, R., Palmer, J.G., Pearson, C., van der Plicht, J., Reimer, R.W., Richards, D.A., Scott, E.M., Southon, J.R., Turney, C.S.M., Wacker, L., Adolphi, F., Büntgen, U., Capano, M., Fahrni, S.M., Fogtmann-Schulz, A., Friedrich, R., Köhler, P., Kudsk, S., Miyake, F., Olsen, J., Reinig, F., Sakamoto, M., Sookdeo, A., Talamo, S., 2020. The IntCal20 Northern Hemisphere Radiocarbon Age Calibration Curve (0–55 cal kBP). Radiocarbon 62, 725-757. https://doi.org/10.1017/RDC.2020.41.

Reinl, K.L., Harris, T.D., North, R.L., Almela, P., Berger, S.A., Bizic, M., Burnet, S.H., Grossart, H.-P., Ibelings, B.W., Jakobsson, E., Knoll, L.B., Lafrancois, B.M., McElarney, Y., Morales-Williams, A.M., Obertegger, U., Ogashawara, I., Paule-Mercado, M.C., Peierls, B.L., Rusak, J.A., Sarkar, S., Sharma, S., Trout-Haney, J.V., Urrutia-Cordero, P., Venkiteswaran, J.J., Wain, D.J., Warner, K., Weyhenmeyer, G.A., Yokota, K., 2023. Blooms also like it cold. Limnology and Oceanography Letters 8, 546-564. https://doi.org/10.1002/lol2.10316.

Rodriguez, A.B., Waters, M.N., Piehler, M.F., 2012. Burning peat and reworking loess contribute to the formation and evolution of a large Carolina-bay basin. Quaternary Research 77, 171-181. https://doi.org/10.1016/j.yqres.2011.11.004.

Rogozin, D.Y., Zykov, V.V., Bulkhin, A.O., Degermendzhi, A.G., 2020. Okenone in bottom sediments as a proxy for changes in the water level of a saline stratified lake. Doklady Earth Sciences 493, 565-568. https://doi.org/10.1134/S1028334X20070168.

Ruan, Y., Mohtadi, M., Dupont, L.M., Hebbeln, D., van der Kaars, S., Hopmans, E.C., Schouten, S., Hyer, E.J., Schefuß, E., 2020. Interaction of Fire, Vegetation, and Climate in Tropical Ecosystems: A Multiproxy Study Over the Past 22,000 Years. Global Biogeochemical Cycles 34, e2020GB006677. https://doi.org/10.1029/2020GB006677.

Ryves, D.B., Jones, V.J., Guilizzoni, P., Lami, A., Marchetto, A., Battarbee, R.W., Bettinetti, R., Devoy, E., 1996. Late Pleistocene and Holocene environmental changes at Lake Albano and Lake Nemi (central Itlay) as indicated by algal remains.

Schelske, C.L., Peplow, A., Brenner, M., Spencer, C.N., 1994. Low-background gamma counting: applications for 210Pb dating of sediments. Journal of Paleolimnology 10, 115-128. https://doi.org/10.1007/BF00682508.

Smith, D.E., Harrison, S., Firth, C.R., Jordan, J.T., 2011. The early Holocene sea level rise. Quaternary Science Reviews 30, 1846-1860. https://doi.org/10.1016/j.quascirev.2011.04.019.

Snitker, G., 2020. The Charcoal Quantification Tool (CharTool): A suite of open-source tools for quantifying charcoal fragments and sediment properties in archaeological and paleoecological analysis. Ethnobiology Letters 11(1). https://doi.org/10.14237/ebl.11.1.2020.1653.

Spencer, J., Jones, K.B., Gamble, D.W., Benedetti, M.M., Taylor, A.K., Lane, C.S., 2017. Late-Quaternary records of vegetation and fire in southeastern North Carolina from Jones Lake and Singletary Lake. Quaternary Science Reviews. https://doi.org/10.1016/J.QUASCIREV.2017.09.001.

Stager, J.C., Cahoon, L.B., 1987. The age and trophic history of Lake Waccamaw, North Carolina. Journal of the Elisha Mitchell Scientific Society 103, 1-13. http://www.jstor.org/stable/24333337.

Stockmarr, J., 1971. Tablets with Spores used in Absolute Pollen Analysis. Pollen et Spores 13, 615-621.
Tang Y, H.M., Li W, 2016. ggfortify: Unified interface to visualize statistical result of popular R packages. The R Journal 8(2), 474–485. https://doi.org/10.32614/RJ-2016-060.

Suther, B.E., Leigh, D.S., Brook, G.A., Yang, L., 2018. Mega-meander paleochannels of the southeastern Atlantic Coastal Plain, USA. Palaeogeography, Palaeoclimatology, Palaeoecology. https://doi.org/10.1016/J.PALAEO.2018.07.002.

Taranu, Z.E., Gregory-Eaves, I., Leavitt, P.R., Bunting, L., Buchaca, T., Catalan, J., Domaizon, I., Guilizzoni, P., Lami, A., McGowan, S., Moorhouse, H., Morabito, G., Pick, F.R., Stevenson, M.A., Thompson, P.L., Vinebrooke,

R.D., 2015. Acceleration of cyanobacterial dominance in north temperate-subarctic lakes during the Anthropocene. Ecology Letters 18, 375-384. https://doi.org/10.1111/ele.12420.

Tõnno, I., Talas, L., Freiberg, R., Kisand, A., Belle, S., Stivrins, N., Alliksaar, T., Heinsalu, A., Veski, S., Kisand, V., 2021. Environmental drivers and abrupt changes of phytoplankton community in temperate lake Lielais Svētiņu, Eastern Latvia, over the last Post-Glacial period from 14.5 kyr. Quaternary Science Reviews 263. https://doi.org/10.1016/j.quascirev.2021.107006.

Törnqvist, T.E., Hijma, M.P., 2012. Links between early Holocene ice-sheet decay, sea-level rise and abrupt climate change. Nature Geoscience 5, 601-606. https://doi.org/10.1038/ngeo1536.

Traverse, A., 2007. Paleopalynology, 2nd ed. Springer, Dordrecht.

Tu, L., Gilli, A., Lotter, A.F., Vogel, H., Moyle, M., Boyle, J.F., Grosjean, M., 2021. The nexus among long-term changes in lake primary productivity, deep-water anoxia, and internal phosphorus loading, explored through analysis of a 15,000-year varved sediment record. Global and Planetary Change 207, 103643. https://doi.org/10.1016/j.gloplacha.2021.103643.

Vachula, R.S., Cullen, T.M., Galinger, M.R., Welch, J.C., Battaglia, J., Smith, D., Waters, M.N., 2024. Morphometric characteristics of charcoal produced from plants native to the southeastern United States of America (USA). The Holocene 34, 1743-1751. https://doi.org/10.1177/09596836241274975.

Vachula, R.S., Russell, J.M., Huang, Y., 2019. Climate exceeded human management as the dominant control of fire at the regional scale in California's Sierra Nevada. Environmental Research Letters 14(10), 104011. https://dx.doi.org/10.1088/1748-9326/ab4669.

Vachula, R.S., Sae-Lim, J., Li, R., 2021. A critical appraisal of charcoal morphometry as a paleofire fuel type proxy. Quaternary Science Reviews 262, 106979. https://doi.org/10.1016/j.quascirev.2021.106979.

Vuillemin, A., Ariztegui, D., Leavitt, P.R., Bunting, L., the, P.S.T., 2016. Recording of climate and diagenesis through sedimentary DNA and fossil pigments at Laguna Potrok Aike, Argentina. Biogeosciences 13, 2475-2492. https://doi.org/10.5194/bg-13-2475-2016.

Waters, M.N., 2016. A 4700-year history of cyanobacteria toxin production in a shallow subtropical lake. Ecosystems 19, 426-436. https://doi.org/10.1007/s10021-015-9943-0.

Waters, M.N., Brenner, M., Curtis, J.H., Romero-Oliva, C.S., Dix, M., Cano, M., 2021. Harmful algal blooms and cyanotoxins in Lake Amatitlán, Guatemala, coincided with ancient Maya occupation in the watershed. Proceedings of the National Academy of Sciences 118, e2109919118. https://doi.org/10.1073/pnas.2109919118.

Waters, M.N., Piehler, M.F., Rodriguez, A.B., Smoak, J.M., Bianchi, T.S., 2009. Shallow lake trophic status linked to late Holocene climate and human impacts. Journal of Paleolimnology 42, 51-64. https://doi.org/10.1007/s10933-008-9247-x.

Waters, M.N., Piehler, M.F., Smoak, J.M., Bianchi, T.S., 2012. Algal community responses to shallow lake dystrophication. Canadian Journal of Fisheries and Aquatic Sciences, 69(8), 1433-1443. https://doi.org/10.1139/f2012-021.

Waters, M.N., Schelske, C.L., Brenner, M., 2015. Cyanobacterial dynamics in shallow Lake Apopka (Florida, U.S.A.) before and after the shift from a macrophyte-dominated to a phytoplankton-dominated state. Freshwater Biology 60, 1571-1580. https://doi.org/10.1111/fwb.12589.

Waters, M.N., Smoak, J.M., Vachula, R.S., 2023. Linking prescribed fire, nutrient deposition and cyanobacteria dominance through pyroeutrophication in a subtropical lake ecosystem from the mid Holocene to present. Anthropocene 44, 100420. https://doi.org/10.1016/j.ancene.2023.100420.

Wienhues, G., Lami, A., Bernasconi, S., Jaggi, M., Morlock, M.A., Vogel, H., Cohen, A.S., Courtney Mustaphi, C.J., Heiri, O., King, L., Kishe, M.A., Misra, P., Muschick, M., Ngoepe, N., Matthews, B., Seehausen, O., Temoltzin-Loranca, Y., Tinner, W., Grosjean, M., 2024. Latest Pleistocene and Holocene primary producer communities and hydroclimate in Lake Victoria, eastern Africa. Quaternary Science Reviews 330, 108599. https://doi.org/10.1016/j.quascirev.2024.108599.

Willard, D., Bernhardt, C., Brown, R., Landacre, B., Townsend, P., 2011. Development and application of a pollen-based paleohydrologic reconstruction from the Lower Roanoke River Basin, North Carolina, USA. The Holocene 21(2), 305-317. https://doi.org/10.1177/0959683610378876.

Whitmore, T.J., Brenner, M., Schelske, C.L., 1996. Highly variable sediment distribution in shallow, wind-stressed lakes: a case for sediment-mapping surveys in paleolimnological studies. Journal of Paleolimnology 15, 207-221. https://doi.org/10.1007/BF00213041.

Yang, M. (2023, April 21). 1,000-year-old Native American canoe retrieved from North Carolina lake. The Guardian. https://www.theguardian.com/us-news/2023/apr/21/north-carolina-lake-native-american-canoe

Yu, S.-Y., Colman, S.M., Lowell, T.V., Milne, G.A., Fisher, T.G., Breckenridge, A., Boyd, M., Teller, J.T., 2010. Freshwater outburst from Lake Superior as a trigger for the cold event 9300 years ago. Science 328, 1262-1266. https://doi.org/10.1126/science.1187860.

Zander, P.D., Żarczyński, M., Vogel, H., Tylmann, W., Wacnik, A., Sanchini, A., Grosjean, M., 2021. A high-resolution record of Holocene primary productivity and water-column mixing from the varved sediments of Lake Żabińskie, Poland. Science of The Total Environment 755, 143713. https://doi.org/10.1016/j.scitotenv.2020.143713.

4.8 Tables

Table 4.1 Paleoclimate periods represented in the pollen record of Lake Waccamaw and compared with the timing of the $\delta^{18}O$ record of NGRIP (North Greenland Ice Core Project members, 2004) (Fig. 4.3) and the timing of interstadials based on a global composite of speleothem records (Corrick et al., 2020).

Climate periods	**Pollen record of Lake Waccamaw (ka BP)***	**$\delta^{18}O$ record of NGRIP (ka BP)**	**Composite of speleothem records (ka BP)**
Holocene	Present – 11.4	Present – 11.4	-
Younger Dryas (YD)	11.4 – 13	11.4 – 13	-
Bølling–Allerød Interstadial (B-A)	13.6	13 – 14.5	14.65
Oldest Dryas (OD)	14.2 – 18	14.5 – 15.6	-
Post-Last Glacial Maximum (Post-LGM)	18 – 24.4	15.6 – 22.7	-
Last Glacial Maximum (LGM)	24.4 – 26.4	22.7 – 27.1	-
Interstadial 3 (I3)	26.4 – 27.8	27.1 – 27.4	27.8
Stadial*	27.8 – 28.5	27.4 – 28.2	-
Interstadial 4 (I4)*	28.5 – 29.9	28.2 – 28.5	29.1
Stadial*	29.9 – 31.4	28.5 – 31.8	-
Interstadial 5 (I5)*	31.4 – 33.6	31.8 – 32.2	31 / 32.5

*Dates below Interstadial 3 from the Lake Waccamaw sediment core are based on extrapolated dates from the Bacon model, and there were no measurable ^{14}C-dates (Table S4.1).

4.9 Figures

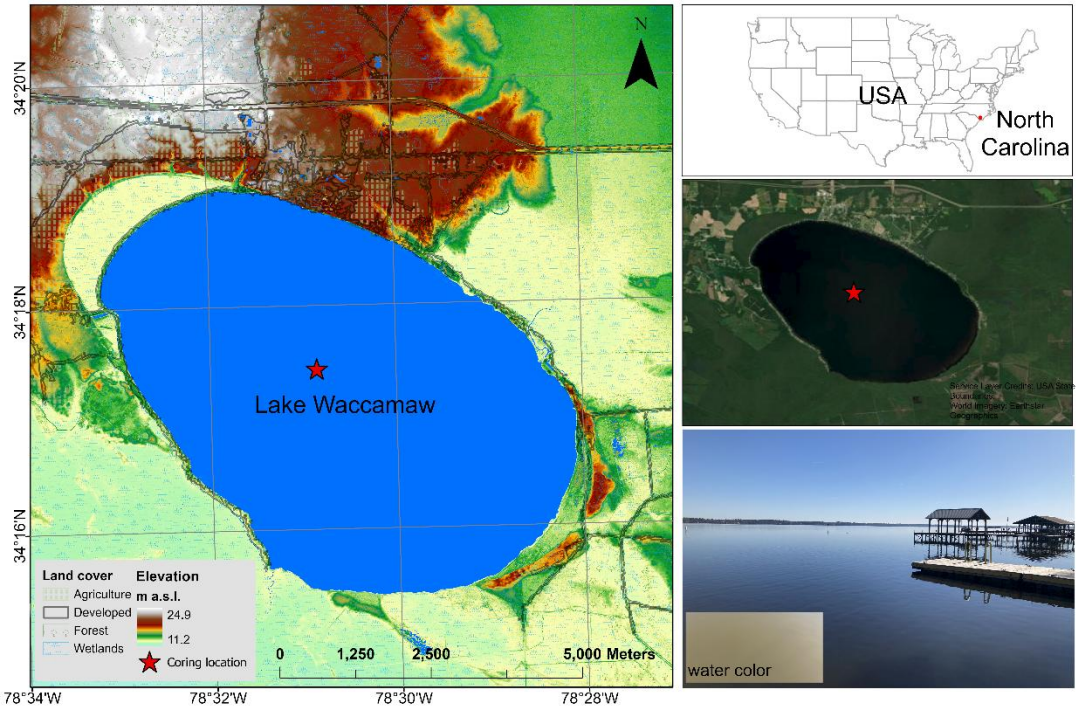

Figure 4.1 Location, elevation, and land use/cover maps of Lake Waccamaw, NC, USA. The landscape is low-elevated and dominated by forested wetlands. The rim structure found on the southeastern side of most Carolina Bays is notable. The town of Lake Waccamaw is situated on a coastal strip and the north shore, while I-76 runs north of the lake. The picture is from the main ramp to the lake. GIS layers source: NOAA/ NC NLCD /ESRI.

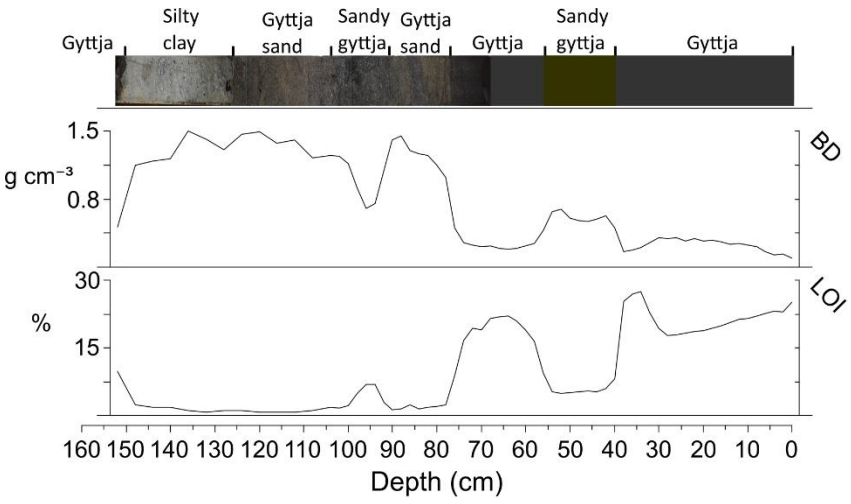

Figure 4.2 Visual representation (0 to 72 cm) and core photographs (72 to 154 cm) of the various stratigraphic units, along with bulk density and organic matter (LOI).

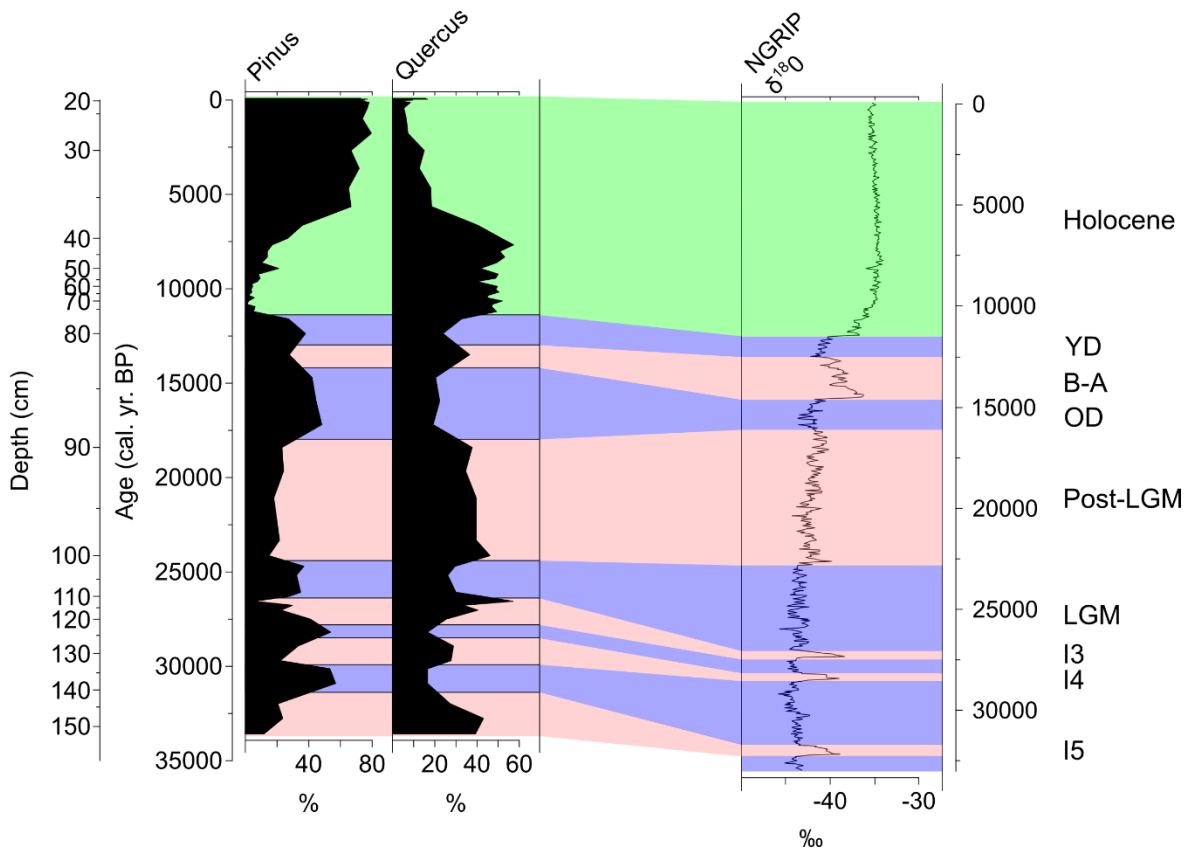

Figure 4.3 Matching of the *Pinus* and *Quercus* pollen record from this study with the $\delta^{18}O$ record of the NGRIP ice core from Greenland (North Greenland Ice Core Project members, 2004). The colors distinguish between *Pinus* (blue) and *Quercus* (light red) peaks, and the Holocene (green). The identified climate periods are the Holocene, Younger Dryas (YD), Bølling–Allerød interstadial (B-A), Older Dryas (OD), post-Last Glacial Maximum (Post-LGM), Last Glacial Maximum (LGM), and interstadial 3 (I3). Due to limited confidence in the age-depth model below ~27.5 ka BP, the stadials and interstadials (I4 and I5) below I3 are delineated tentatively. The exact chronological matching of the paleoclimate periods between the pollen and NGRIP records is in Table 4.1.

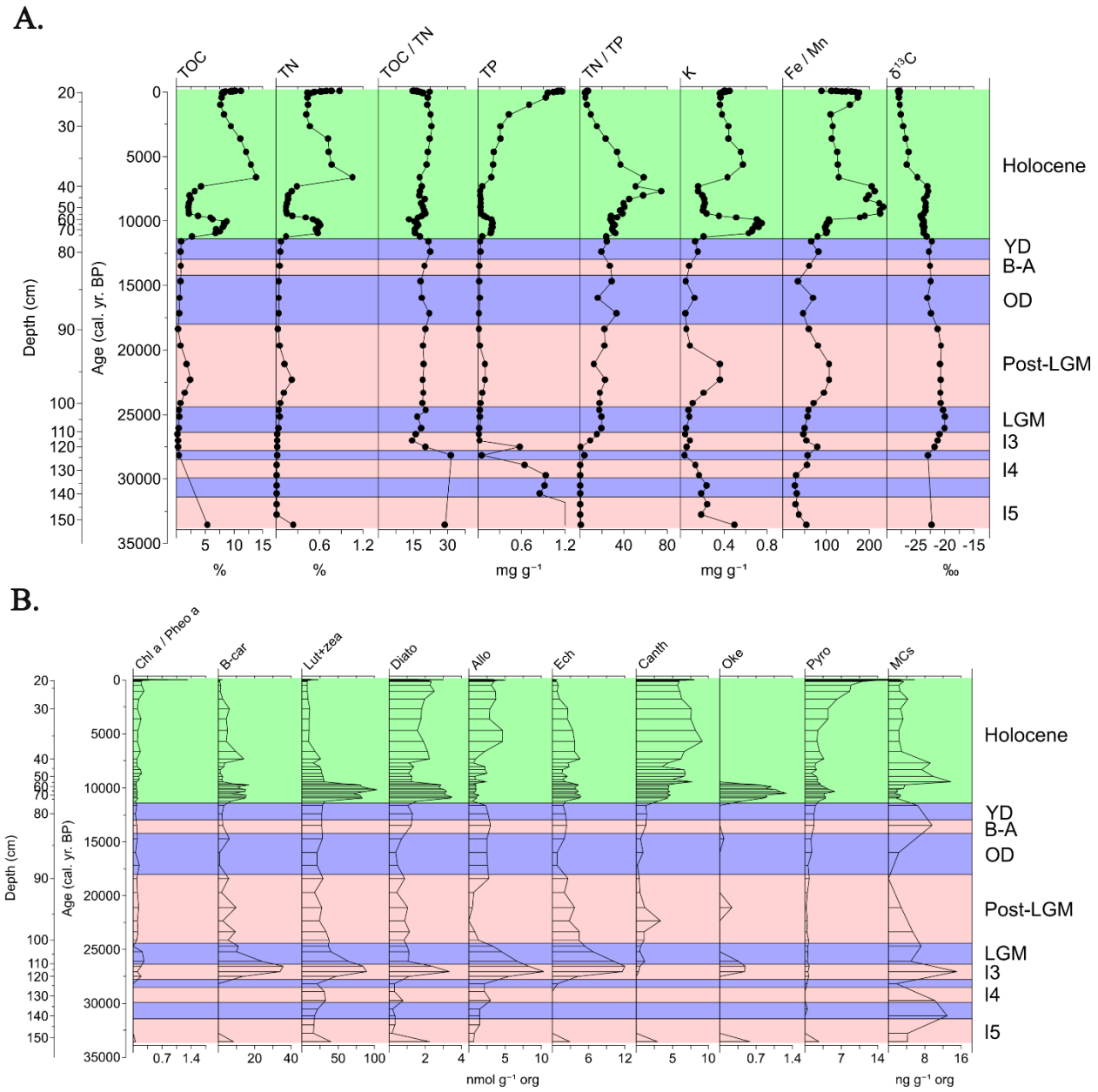

Figure 4.4 Plots with depth (cm) as primary axis and chronology (cal. yr. BP) as secondary. The colored boxes delineate the different climate periods based on Fig. 4.3 and Table 4.1. (A) Geochemical measurements of nutrients, elements, elemental ratios, and $\delta^{13}C$. Measurements of TOC, TOC/TN, and $\delta^{13}C$ were excluded from 128 to 150 cm because high $CaCO_3$ content prevented the accurate measurement of carbon. Based on the LOI measurements, the TOC content was close to 1% for that interval. The TP value of the bottom sample is 4.8 mg g^{-1}. (B) Photosynthetic pigments and cyanotoxins (microcystins, MCs). Microcystin was subsampled less regularly than the other indices. The chlorophyll-a (Chl-a) ratio to pheophytin-a (Pheo-a) is the pigment degradation index. The photosynthetic pigments are beta-carotene (B-car), lutein+zeaxanthin (Lut+zea), diatoxanthin (Diato), alloxanthin (Allo), echinenone (Ech), canthaxanthin (Canth), pyropheophorbide (pyro), and okenone (Oke). The precise pigment affinities are in Table S4.2.

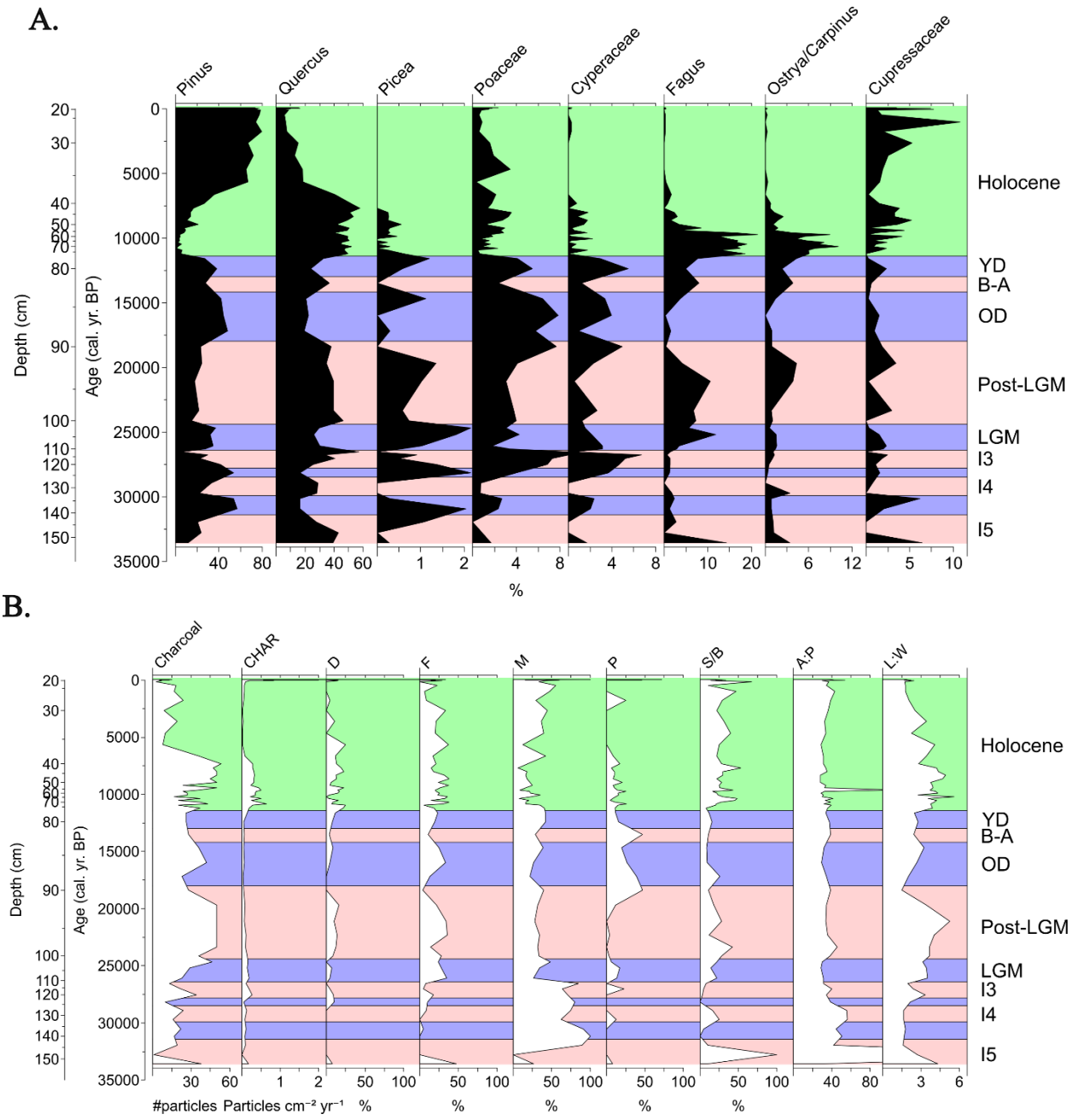

Figure 4.5 Plots of (A) pollen and (B) charcoal with depth (cm) as primary axis and chronology (cal. yr. BP) as secondary, delineated according to the different climate periods (Fig. 4.3, Table 4.1). Based on Enache and Cumming (2006), the charcoal morphotypes are geometric and elongated particles with ramifications (D) and without ramifications (F), irregular geometric structured (M) and unstructured particles (P), and geometric compacted and structured black/partially black particles (S/B). The ratios are area to perimeter (A:P) and length to width (L:W).

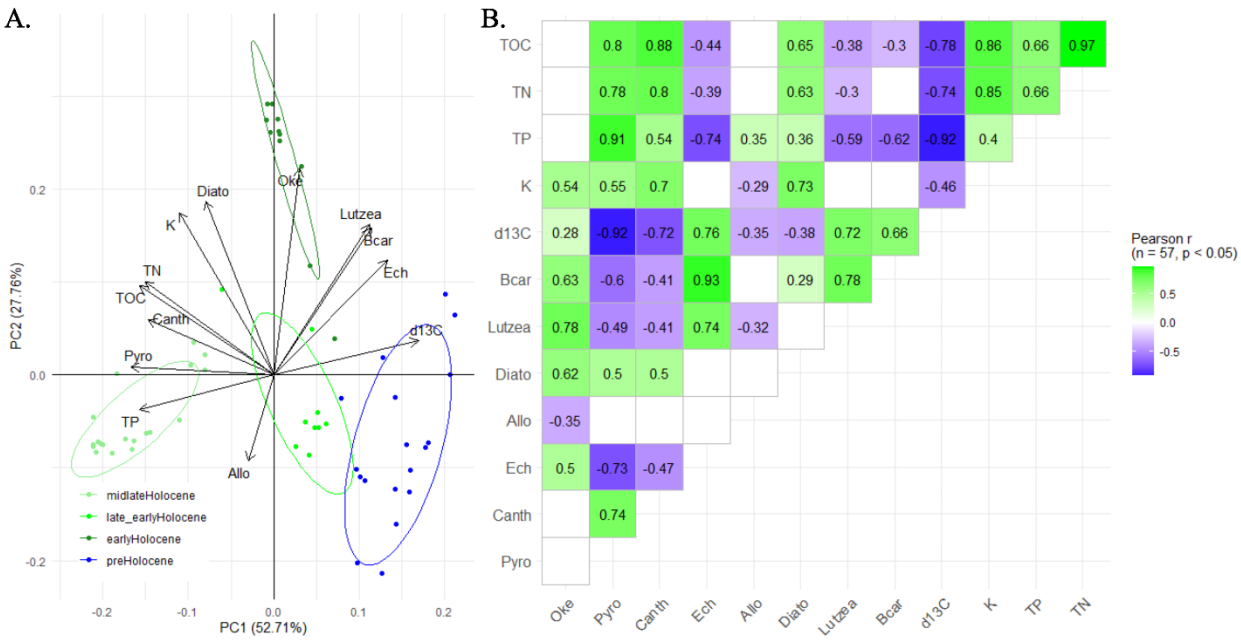

Figure 4.6 (A) Principal component analysis (PCA) of nutrients and photosynthetic pigments for the Lake Waccamaw sediment core. The plot presents the variance in the dataset using PC1 (49.79%) and PC2 (30.06%) while grouping the data points into different periods. The oval shapes represent 68% confidence intervals. (B) Pearson correlation matrices with photosynthetic pigments and elements with samples spanning the last ~27 ka BP (I3 interstadial to Holocene). The photosynthetic pigments are beta-carotene (B-car), lutein+zeaxanthin (Lutzea), alloxanthin (Allo), diatoxanthin (Diato), echinenone (Ech), canthaxanthin (Canth), pyropheophorbide (pyro), and okenone (Oke).

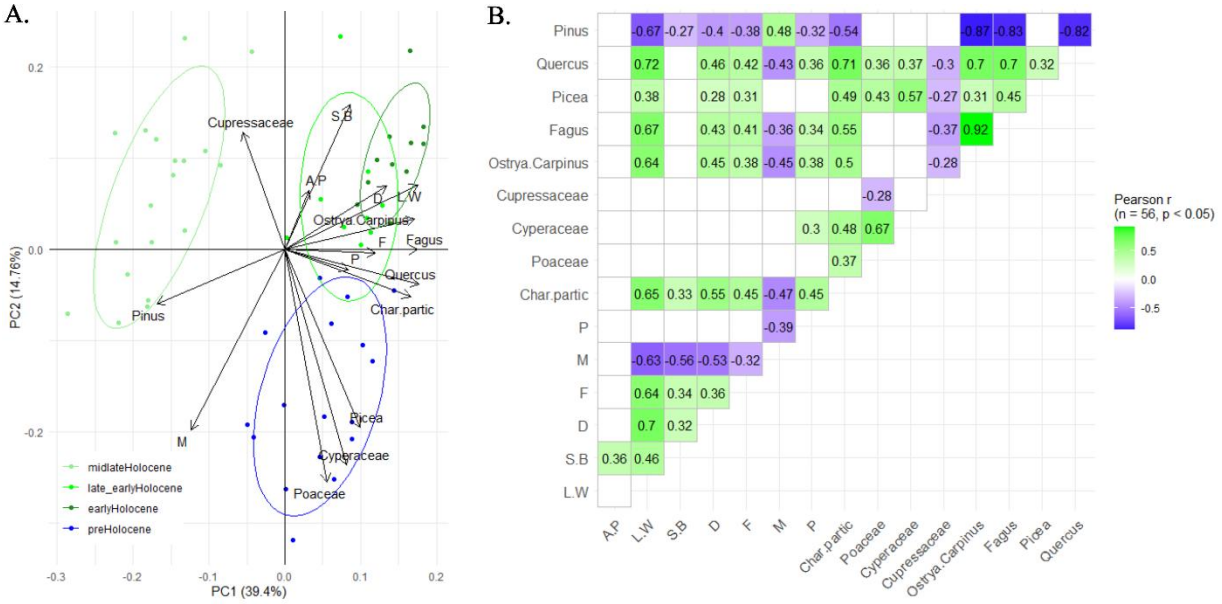

Figure 4.7 (A) Principal component analysis (PCA) of pollen and charcoal for the Lake Waccamaw sediment core. The plot presents the variance in the dataset using PC1 (39.4%) and PC2 (14.76%) while grouping the data points into different periods. The oval shapes represent 68% confidence intervals. (B) Pearson correlation matrices with photosynthetic pigments and elements samples spanning the last ~27 ka BP (I3 interstadial to Holocene).

5.1 Supplementary Tables

Table S4.1 Radiocarbon-dated samples from Lake Waccamaw.

Laboratory no.	Depth (cm)	Material	Age ^{14}C BP	Calibrated years BP (2 sigma median)
OS-175478	40-42	charcoal	6,500 ±120	7,397
OS-175479	54-56	charcoal	8,450 ±50	9,478
OS-173623	76-78	charcoal	9,790 ±50	11,216
OS-173624	98-100	charcoal	27,700 ±590	31,849
OS-175480	106-108	charcoal	21,700 ±350	26,001
OS-178007	122-124	charcoal	23,300 ±370	27,529
OS-173657	136-138	wood	>47,500	-

Table S4.2 List of photosynthetic pigments, their preservation ranging from high (1) to low (3), and their role as markers of aquatic community composition. The table is adapted from Leavitt and Hodgson (2001) and Waters (2016).

Photosynthetic pigment	Abbreviation	Preservation	Aquatic marker
Beta-carotene	B-car	1	Total primary producer abundance
Chlorophyll-a	Chl-a	3	Total primary producer abundance
Pheophytin-a	Pheo-a	1	Chl-a derivative
Pyropheophorbide	Pyro	2	Zooplankton grazing
Alloxanthin	Allo	1	Cryptophyta
Diatoxanthin	Diato	2	Diatoms
Lutein + zeaxanthin	Lut+zea	1	Green algae and cyanobacteria
Echinenone	Ech	1	Cyanobacteria
Canthaxanthin	Canth	1	Colonial cyanobacteria
Okenone	Oke	1	Purple-sulfur bacteria

7.1 Supplementary Figures

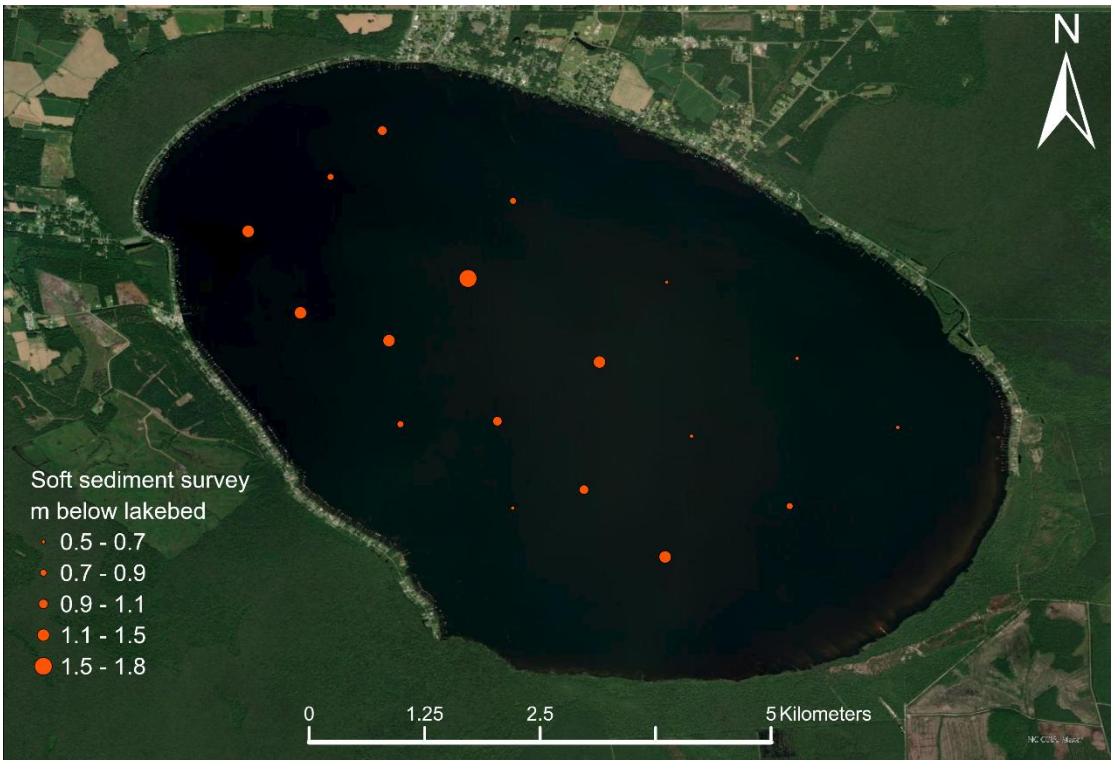

Figure S4.1 GPS locations of soft sediment thickness in Lake Waccamaw. The soft sediment survey was conducted before coring Lake Waccamaw. The coring location coincided with the thickest interval of soft sediment.

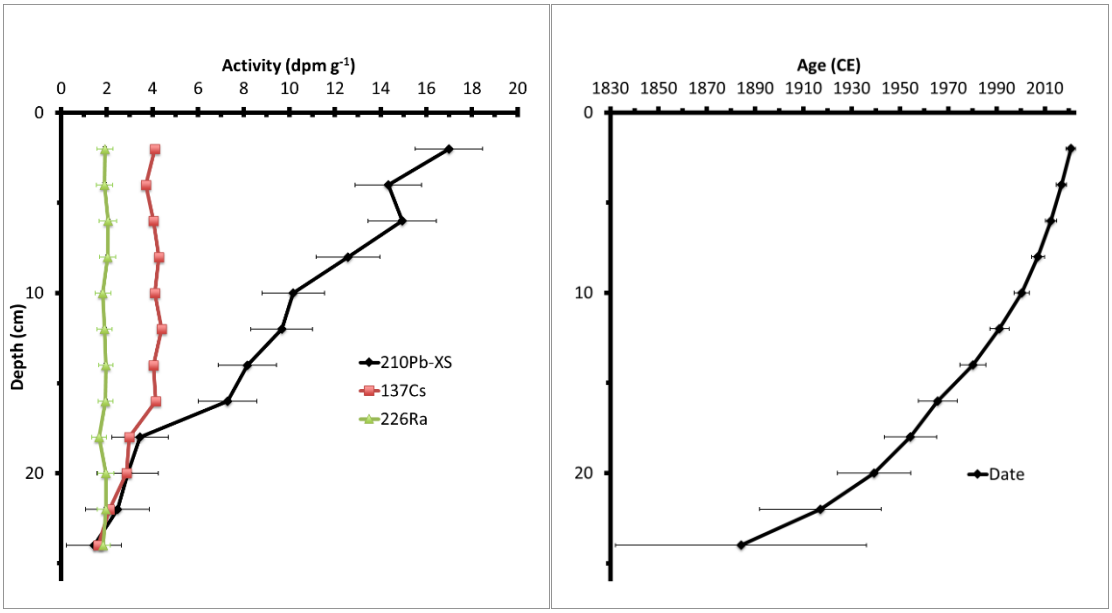

Figure S4.2 Excess ^{210}Pb, ^{226}Ra, and ^{137}Cs activity versus depth (left), and CRS-determined ages versus depth (right).

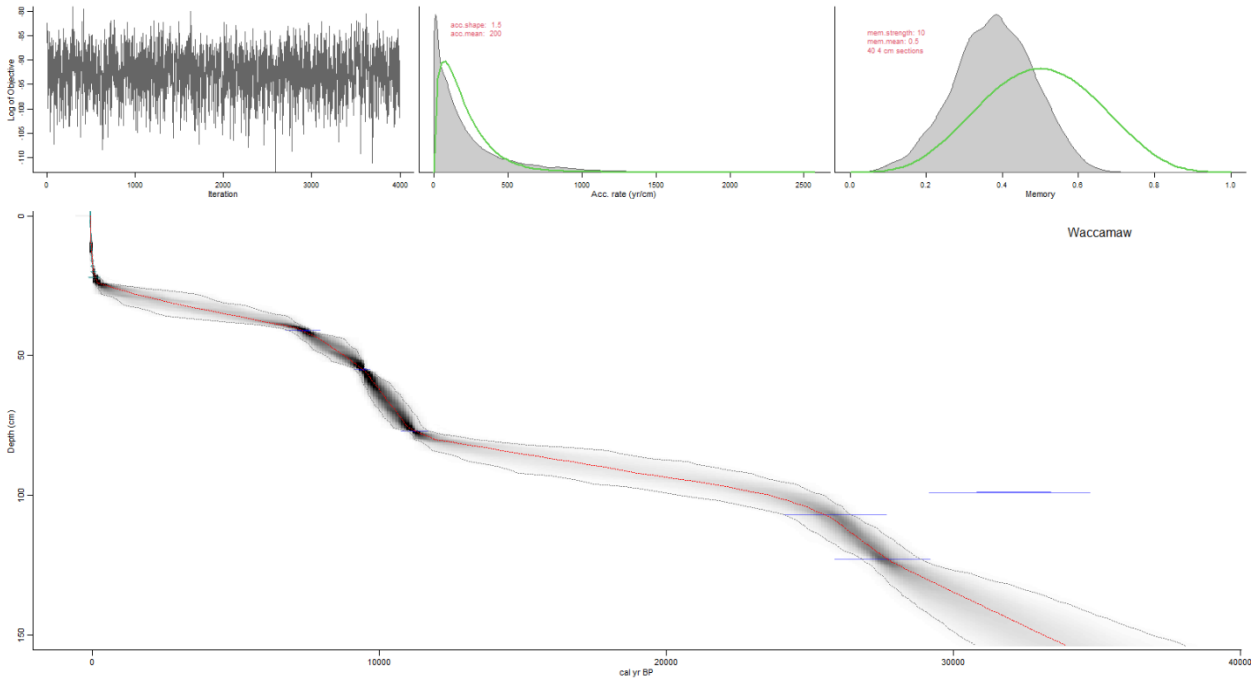

Figure S4.3 The age-depth model used for Lake Waccamaw was constructed by combining the ^{210}Pb and the ^{14}C-dated samples.

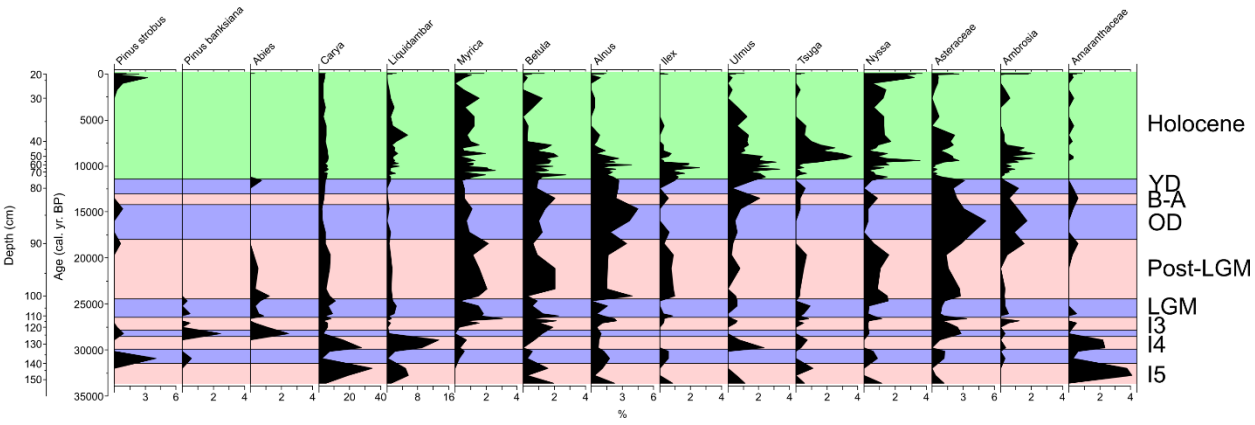

Figure S4.4 Complimentary pollen types in notable percentages.

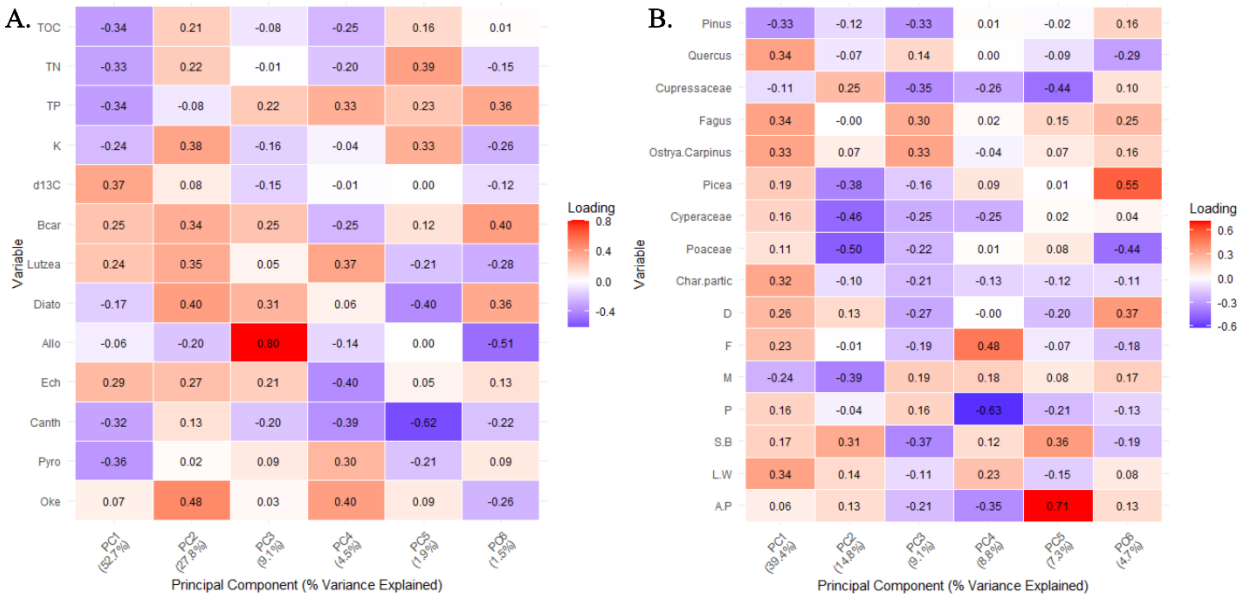

Figure S4.5 Heatmap of the principal components (PC1-6) derived from the analyzed paleolimnological variables. (A) Photosynthetic pigments, elements, and carbon stable isotopes. (B) Pollen and charcoal. Each value in the heatmaps represents the loading of the variable for the respective PC. The percentage of variance explained by each PC is shown in parentheses.